**FEDERAL UNIVERSITY OF SÃO CARLOS**
**CENTER OF EXACT SCIENCES AND TECHNOLOGY**
**GRADUATE PROGRAM IN MATERIALS SCIENCE AND ENGINEERING**

# DESIGN OF MULTICOMPONENT ALLOYS WITH SINGLE C14 LAVES PHASE FOR HYDROGEN STORAGE ASSISTED BY THERMODYNAMIC COMPUTATIONAL METHODS

Jéssica Bruna Ponsoni

SÃO CARLOS – SP
2024

**FEDERAL UNIVERSITY OF SÃO CARLOS**
**CENTER OF EXACT SCIENCES AND TECHNOLOGY**
**GRADUATE PROGRAM IN MATERIALS SCIENCE AND ENGINEERING**

# DESIGN OF MULTICOMPONENT ALLOYS WITH SINGLE C14 LAVES PHASE FOR HYDROGEN STORAGE ASSISTED BY THERMODYNAMIC COMPUTATIONAL METHODS

Jéssica Bruna Ponsoni

Thesis presented to Graduate Program in Materials Science and Engineering in partial fulfillment of the requirements for the DOCTOR DEGREE IN MATERIALS SCIENCE AND ENGINEERING

Supervisor: Prof. Dr. Guilherme Zepon
Grant Agency: Serrapilheira Institute – Process: 1709-17362
CNPq – Process: 381973/2023-9

SÃO CARLOS – SP
2024

## DEDICATION

*To my parents, Jair and Elizabete, and my sister Karla, with all love*

VITAE

Master in Materials Science and Engineering from the Federal University of São Carlos (2020), Bachelor in Materials Engineering from the Federal University of São Carlos (2018).

**UNIVERSIDADE FEDERAL DE SÃO CARLOS**

Centro de Ciências Exatas e de Tecnologia
Programa de Pós-Graduação em Ciência e Engenharia de Materiais

## Folha de Aprovação

Defesa de Tese de Doutorado da candidata Jéssica Bruna Ponsoni, realizada em 30/04/2024.

### Comissão Julgadora:

Prof. Dr. Guilherme Zepon (UFSCar)

Prof. Dr. Daniel Rodrigo Leiva (UFSCar)

Prof. Dr. Walter José Botta Filho (UFSCar)

Profa. Dra. Kátia Regina Cardoso (UNIFESP)

Prof. Dr. Marcelo Falcão de Oliveira (USP)

O Relatório de Defesa assinado pelos membros da Comissão Julgadora encontra-se arquivado junto ao Programa de Pós-Graduação em Ciência e Engenharia de Materiais.

## ACKNOWLEDGMENTS

I grateful to my beloved family, for being pillars of inspiration in my life. Their dedication, unconditional encouragement, and tireless prayers have been the guiding light through every moment of my life.

To Everton, for all the love, care and patience, which made this final and most important stage of my work, light and filled with happiness. Your love holds an immense significance.

To my friends for the countless conversations, laughter, and words of comfort and tenderness they have shared with me. Being surrounded by incredible people made everything better.

To Professor Guilherme Zepon, for all the opportunities, suggestions, discussions, countless contributions, and exceptional guidance. Your advices and encouraging words not only turned this journey into a significant professional achievement but an immense personal growth and development.

To Dr. Michael Felderhoff and Dr. Mateusz Balcerzak for all the suggestions, discussions, and contributions during my stay at Max-Planck-Institut für Kohlenforschung in Mülheim an der Ruhr - Germany.

To PPGCEM, DEMa, $LH_2M$, and LCE, for the excellent infrastructure and technical members, who contributed to the development of this work.

To the Max-Planck-Institut für Kohlenforschung in Mülheim an der Ruhr - Germany for scientific and financial support during my internship.

To the Serrapilheira Institute for financial support to carry out this work with a scholarship and to the internship abroad – Grant number Serra-1709-17362.

To the National Council for Scientific and Technological Development (CNPq) for financial support to carry out this work with a scholarship - Process no. 381973/2023-9.

This study was financed in part by the Coordenação de Aperfeiçoamento de Pessoal de Nível Superior - Brasil (CAPES) - Finance Code 001.

## ABSTRACT

Multicomponent alloys with C14 Laves phase structure hold great promise as hydrogen storage materials due to their capacity for reversible absorption of significant hydrogen amounts at room temperature with excellent kinetics. Design methodologies that incorporate predictive property modeling is essential for effectively navigating the vast compositional space of multicomponent alloys. The effectiveness of an alloy as a hydrogen storage media depends on its thermodynamic properties, often visualized through pressure-composition-temperature (PCT) diagrams. Therefore, the prediction of PCT diagrams for multicomponent alloys is a paramount factor to design alloys with optimized properties for hydrogen storage applications. This doctoral thesis introduces a strategy based on computational thermodynamics to design C14-type Laves phase alloys optimized for hydrogen storage. The design method employed to investigate the phase stability of alloys of the (Ti, Zr, or Nb)$_1$(V, Cr, Mn, Fe, Co, Ni, Cu, or Zn)$_2$ system, resulted in 440 alloys prone to solidify as C14 Laves phase structure. A thermodynamic model was developed to calculate the PCT diagrams of the C14 Laves phase alloys. It was possible to design compositions with equilibrium pressures in a wide range ($10^{-4}$ to $10^5$ bar). Based on this design approach, seven alloys with different equilibrium pressures were selected, produced, and experimentally characterized. Three alloys did not require activation procedures: $(Ti_{0.5}Zr_{0.5})_1(Mn_{0.5}Cr_{0.5})_2$, $(Ti_{0.5}Zr_{0.5})_1(Fe_{0.33}Mn_{0.33}Cr_{0.33})_2$, and $(Ti_{0.33}Zr_{0.33}Nb_{0.33})_1(Mn_{0.5}Cr_{0.5})_2$ alloys, and they reached hydrogen storage capacity close to H/M = 1 with fast kinetics. Moreover, the experimental PCIs were compared to the calculated ones. The order of magnitude of the equilibrium pressure for the tested alloys were well predicted by the model. These three compositions presented outstanding reversible hydrogen storage properties. Furthermore, the addition of a small fraction of Ce (0.4 wt.%) was proved to be an efficient strategy to allow activation of the alloys that were not able to be activated by thermal or hydrogenation treatments. The $(Ti_{0.5}Zr_{0.5})_1(Fe_{0.5}Mn_{0.5})_2$ + Ce alloy reversibly absorbed and desorbed the total amount of hydrogen (H/M = 0.9) at room temperature with excellent cycling stability.

**Keywords:** Multicomponent alloys; Hydrogen storage; C14 Laves phase; Computational thermodynamics; Thermodynamic model; Ce-addition.

## RESUMO


### Design de Ligas Multicomponentes Monofásicas Laves C14 para Armazenamento de Hidrogênio Assistido por Métodos Termodinâmicos Computacionais

Ligas multicomponentes com estrutura de fase C14 Laves são muito promissoras como materiais de armazenamento de hidrogênio devido à sua capacidade de absorção reversível de quantidades significativas de hidrogênio a temperatura ambiente, com excelente cinética. Metodologias de design que incorporam modelagem de propriedades preditivas são essenciais para navegar efetivamente no vasto espaço de composição das ligas multicomponentes. A eficácia de uma liga para armazenamento de hidrogênio depende de suas propriedades termodinâmicas, frequentemente visualizadas por meio de diagramas de pressão-composição-temperatura (PCT). Portanto, a previsão dos diagramas PCT para ligas multicomponentes é um fator crucial para projetar ligas com propriedades otimizadas para aplicações de armazenamento de hidrogênio. Esta tese de doutorado apresenta uma estratégia baseada em termodinâmica computacional para projetar ligas com a fase de Laves do tipo C14 para armazenamento de hidrogênio. O método de design empregado para investigar a estabilidade de fase de ligas do sistema (Ti, Zr ou Nb)$_1$(V, Cr, Mn, Fe, Co, Ni, Cu ou Zn)$_2$ resultou em 440 ligas com tendência a solidificar como estrutura da fase de Laves C14. Um modelo termodinâmico foi desenvolvido para calcular os diagramas PCT das ligas da fase C14 Laves. Foi possível projetar composições com pressões de equilíbrio em uma ampla faixa ($10^{-4}$ a $10^5$ bar). Com base nesta abordagem de design, foram selecionadas, produzidas e caracterizadas experimentalmente sete ligas com diferentes pressões de equilíbrio. Três ligas não necessitaram de procedimentos de ativação: $(Ti_{0,5}Zr_{0,5})_1(Mn_{0,5}Cr_{0,5})_2$, $(Ti_{0,5}Zr_{0,5})_1(Fe_{0,33}Mn_{0,33}Cr_{0,33})_2$ e $(Ti_{0,33}Zr_{0.33})_2$ e $(Ti_{0,33}Zr_{0.\ 33}Nb_{0,33})_1$ $(Mn_{0,5}Cr_{0,5})_2$, e atingiram capacidade de armazenamento de hidrogênio próxima à H/M = 1 com cinética rápida. Além disso, as PCIs experimentais foram comparadas com as calculadas. A ordem de grandeza da pressão de equilíbrio para as ligas testadas foi bem prevista pelo modelo. Estas três composições apresentaram excelentes propriedades reversíveis de armazenamento de hidrogênio. Além disso, a adição

de pequenos teores de Ce (0.4 %p.) mostrou-se uma opção eficiente para permitir a ativação de ligas que não foram possíveis serem ativadas por tratamentos térmicos ou por hidrogenação. A liga $(Ti_{0,5}Zr_{0,5})_1(Fe_{0,5}Mn_{0,5})_2$ + Ce absorveu e dessorveu reversivelmente a quantidade total de hidrogênio (H/M = 0,9) à temperatura ambiente com excelente estabilidade de ciclagem.

**Palavras-chave:** Ligas multicomponentes; Armazenamento de hidrogênio; Fase de Laves C14; Termodinâmica computacional; Modelamento termodinâmico; Adição de Ce.

## PUBLICATIONS

J. B. Ponsoni, V. Aranda, T. S. Nascimento, R. B. Strozi, W. J. Botta, G. Zepon, Design of multicomponent alloys with C14 Laves phase structure for hydrogen storage assisted by computational thermodynamic, Acta Materialia, 240 (2022) 118317. https://doi.org/10.1016/j.actamat.2022.118317.

J. B. Ponsoni, M. Balcerzak, W. J. Botta, M. Felderhoff, G. Zepon, A comprehensive investigation of the $(Ti_{0.5}Zr_{0.5})_1(Fe_{0.33}Mn_{0.33}Cr_{0.33})_2$ multicomponent alloy for room-temperature hydrogen storage designed by computational thermodynamic tools, Journal of Materials Chemistry A, 11 (2023) 14108-14118. https://doi.org/10.1039/D3TA02197A.

M. Balcerzak, J. B. Ponsoni, H. Petersen, C. Menéndez, J. Ternieden, L. Zhang, F. Winkelmann, K. F. A. Zinsou, M. Hirscher, M. Felderhoff, Hydrogen-stabilized ScYNdGd medium-entropy alloy for hydrogen storage, Journal of the American Chemical Society, Journal of the American Chemical Society, 146 (2024) 5283-5294. https://doi.org/10.1021/jacs.3c11943.

x

# TABLE OF CONTENTS

FOLHA DE APROVAÇÃO ..... i
ACKNOWLEDGMENTS ..... iii
ABSTRACT ..... v
RESUMO ..... vii
PUBLICATIONS ..... ix
TABLE OF CONTENTS ..... xi
LIST OF TABLES ..... xiii
LIST OF FIGURES ..... xv
1 INTRODUCTION ..... 1
2 OBJECTIVES ..... 5
3 LITERATURE REVIEW ..... 7
3.1 Thermodynamic of metal hydrides ..... 7
3.2 C14 Laves phase ..... 14
3.3 Hydrogen storage in C14 Laves phase ..... 20
3.4 Design strategy of alloys for hydrogen storage ..... 23
3.5 Activation methods for C14 Laves phase alloys ..... 28
4 MATERIALS AND METHODS ..... 31
4.1 Design methods ..... 31
4.1.1 Prediction of phase stability ..... 31
4.1.2 Thermodynamic model for PCT diagrams calculation ..... 32
4.2 Experimental methods ..... 33
4.2.1 Sample production ..... 33
4.2.2 Structural and chemical characterization ..... 35
4.2.3 Hydrogen storage properties ..... 36
4.2.4 Activation methodology ..... 37
5 RESULTS ..... 39
5.1 Design methods ..... 39
5.1.1 Prediction of phase stability ..... 39
5.1.2 Thermodynamic model for PCT diagrams calculation ..... 53
5.2 Alloy design for different hydrogen storage applications ..... 77

5.2.1 Selection of the compositions ..... 77
5.2.2 Structure characterization ..... 84
5.2.3 Hydrogen storage properties ..... 100
5.2.3.1 Kinetics measurements ..... 100
5.2.3.2 PCT measurements and cycling tests. ..... 103
5.2.3.2.1 PCT measurements and comparison ..... 104
5.2.3.2.2 Cycling tests ..... 113
5.3 Activation ..... 128
5.3.1 Activation procedure ..... 128
5.3.2 Ce addition ..... 131
5.3.3 Oxygen content ..... 147
6 DISCUSSIONS ..... 151
7 CONCLUSIONS ..... 155
8 SUGGESTIONS FOR FUTURE WORKS ..... 157
9 REFERENCES ..... 159
APPENDIX A ..... 167

## LIST OF TABLES

Table 3. 1 - Atomic positions of A and B elements. ..... 15
Table 3. 2 - Atomic radii (metallic bond) and VEC of the A and B elements. ..... 19
Table 3. 3 - Wyckoff positions and the coordinates of the interstitial sites. ..... 21
Table 3. 4 – Summary of the reported alloys with single C14 Laves phase and their characteristics. ..... 25
Table 4. 1 - Concentration atomic fraction of the elements and the factors VEC, $rArB$, δ, and calculated hydrogen equilibrium pressure ($PH2$) of the seven selected alloys. ..... 34
Table 5. 1 - Equiatomic compositions predicted to form C14 Laves phase alloys by CALPHAD calculations. The alloys were numbered from 1 to 86. For each composition, the atomic fraction of the elements and their $rArB$, VEC, and δ parameter are presented. ..... 42
Table 5. 2 - The chemical composition of the $(Ti_{0.5}Zr_{0.5})_1(Cr_{0.25}Mn_{0.25}Fe_{0.25}Ni_{0.25})_2$ alloy determined by SEM-EDX. ..... 52
Table 5. 3 - Hydrogen heat of hydrogen solution at infinite dilution of the A and B elements. ..... 56
Table 5. 4 - Atomic fraction of element $i$ in the sublattice A and sublattice B for each one of the 86 equiatomic alloys with tendency to form C14 Laves phase. For each composition are also presented the $hC14$, molar weight (M), maximum theoretical hydrogen content (considering H/M=1), and equilibrium pressure at $c_H$ = 0.5. ..... 59
Table 5. 5 - Calculated $hC14$in kJ/mol of H calculated for the tested alloys. ..... 70
Table 5. 6 - Atomic fraction of element $i$ in the sublattice A and sublattice B for the $(Ti_{0.5}Zr_{0.5})_1(Cr_{0.25}Mn_{0.25}Fe_{0.25}Ni_{0.25})_2$, $(Ti_{13}Zr_{20})_1(Nb_{2.5}Fe_{20}Ni_{7.5}Ti_{3.5})_2$, $(Ti_{0.5}Zr_{0.5})_1(V_{0.25}Ni_{0.55}Mn_{0.1}Fe_{0.1})_2$, and $Ti_1(Cr_{0.75}Mn_{0.25})_2$ alloys. ..... 71
Table 5. 7 - VEC, $rArB$, and δ values of the selected alloys. ..... 77
Table 5. 8 - Calculated hydrogen partial molar enthalpy of the phase ($hC14$) and hydrogen equilibrium pressure ($PH2$) at $cH$= 0.5 of the selected alloys. ..... 84
Table 5. 9 – Lattice parameters a and c obtained by the Rietveld refinement. . 88

Table 5. 10 - The chemical composition of the $(Ti_{0.5}Zr_{0.5})_1Mn_2$ alloy determined by SEM-EDX. ..... 90
Table 5. 11 - The chemical composition of the $(Ti_{0.5}Zr_{0.5})_1(Mn_{0.5}Cr_{0.5})_2$ alloy determined by SEM-EDX. ..... 92
Table 5. 12 - The chemical composition of the $(Ti_{0.5}Zr_{0.5})_1(Fe_{0.5}Mn_{0.5})_2$ alloy determined by SEM-EDX. ..... 93
Table 5. 13 - The chemical composition of the $(Ti_{0.5}Zr_{0.5})_1(Fe_{0.33}Mn_{0.33}Cr_{0.33})_2$ alloy determined by SEM-EDX. ..... 95
Table 5. 14 - The chemical composition of the $(Ti_{0.33}Zr_{0.33}Nb_{0.33})_1(Mn_{0.5}Cr_{0.5})_2$ alloy determined by SEM-EDX. ..... 96
Table 5. 15 - The chemical composition of the $(Ti_{0.33}Zr_{0.33}Nb_{0.33})_1(Fe_{0.5}Mn_{0.5})_2$ alloy determined by SEM-EDX. ..... 98
Table 5. 16 - The chemical composition of the $(Ti_{0.5}Nb_{0.5})_1(Fe_{0.5}Mn_{0.5})_2$ alloy determined by SEM-EDX. ..... 99
Table 5. 17 - Thermodynamic data determined by van´t Hoff analyses in absorption and desorption from the experimental PCI curves. The values of enthalpy and entropy are given in kJ/mol of H and J/K.mol of H, respectively, and correspond to a hydrogen concentration equal to $c_H = H/M = 0.5$. ..... 110
Table 5. 18 - The chemical composition of the $(Ti_{0.5}Zr_{0.5})_1(Fe_{0.5}Mn_{0.5})_2$+Ce alloy determined by SEM-EDX. ..... 134
Table 5. 19 - Oxygen content of the as-cast $(Ti_{0.5}Zr_{0.5})_1(Fe_{0.5}Mn_{0.5})_2$ and $(Ti_{0.5}Zr_{0.5})_1(Fe_{0.5}Mn_{0.5})_2$+Ce alloys. ..... 147
Table 5. 20 - Oxygen content of the as-cast alloys that absorbed hydrogen. . 148
Table 5. 21 - Oxygen content of the as-cast alloys that did not absorbed hydrogen. ..... 148

## LIST OF FIGURES

Figure 1. 1 - Schematic illustration of hydrogen economy cycle. ..... 1

Figure 3. 1 - Schematic illustration of the reaction of an $H_2$ molecule with a metal: (a) $H_2$ molecule approaching the metal surface, (b) Attractive interaction of the $H_2$ molecule by Van der Waals forces (physisorbed state), (c) Chemisorbed hydrogen after $H_2$ dissociation, and (d) Diffusion on the interstitial sites of the host metal lattice [19]. ..... 8

Figure 3. 2 - Schematic of potential energy curve of hydrogen in molecular and atomic form approaching the host metal. The hydrogen molecule is attracted by Van der Waals forces and forms a physisorbed state. Before diffusion into the bulk metal, the molecule has to dissociate, forming a chemisorbed state at the surface of the metal [5]. ..... 8

Figure 3. 3 - a) Gibbs free energy of α- and β-phase as a function of $cH$ for a hypothetical M-H system under PE condition for a given temperature and (b) its corresponding pressure-composition-isotherm diagram. Adapted from [18]. ... 10

Figure 3. 4 - Schematic illustration of the experimental method for determining the thermodynamic properties of hydride formation based on the van't Hoff equation. ..... 13

Figure 3. 5 - Schematic of (a) hexagonal C14 ($MgZn_2$-type), (b) cubic C15 ($MgCu_2$-type) and (c) hexagonal C36 ($MgNi_2$-type) crystal structures. Adapted from [26]. ..... 14

Figure 3. 6 - Unit cell of the hexagonal C14 Laves phase ($MgZn_2$-type). The red spheres represent the A positions, and the blue spheres represent the B positions (B positions are divided into two different crystallographic positions: B1 = dark blue and B2 = light blue)..... 15

Figure 3. 7 - (a) A and (b) B sublattices that form the (c) complete C14 Laves phase structure..... 16

Figure 3. 8 - Unit cell of the hexagonal C14 Laves phase (MgZn2-type) and the three types of tetrahedral interstices available: A2B2, AB3 and B4..... 16

Figure 3. 9 - Periodic table with the subdivision of the A- and B-type elements based on their binary hydride enthalpy of formation. A-type elements represented in shades of red, and B-type elements in shades of blue. Adapted from [7]..... 17
Figure 3. 10 - Interstitial sites per unit cell in the C14-type Laves phase (a) $A_2B_2$ sites: $6h_1$, $6h_2$, $12k_2$, and 24l (b) $AB_3$ sites: 4f and $12k_1$ and (c) $B_4$ sites: 4f..... 21
Figure 3. 11 - (a) Gibbs free energy of α-phase as function of $cH$ for a hypothetical system for a given temperature and (b) its corresponding pressure-composition-isotherm diagram. Adapted from [7]. ..... 22
Figure 3. 12 - Phase stability diagrams showing the stability ranges of Laves phase (a) as function of the $\Delta\chi\ Allen$ and δ for some selected HEAs (red dots correspond to solid solution HEAs and black dots HEAs with Laves phase, adapted from [17]) and (b) as function of the VEC and the atomic radius ratio for binary transition metal alloys (circles and triangles mark C14 and C15 structures, respectively; filled symbols indicate the existence of a temperature-dependent phase transition, adapted from [30]). ..... 24
Figure 3. 13 - Volume fraction of equilibrium phases as a function of temperature calculated by CALPHAD for the $(TiZr)_1(CrMnFeNi)_2$ alloy. Adapted from [10].. 26
Figure 3. 14 - Comparison between the calculated and experimental PCT diagrams of $(TiVNb)_{85}Cr_{15}$ alloy. Adapted from [18]. ..... 28
Figure 5. 1 - Results of the thermodynamic calculations by CALPHAD method from 854 equiatomic compositions and 354 non-equiatomic compositions displayed in a $rArB$ versus VEC chart. ..... 40
Figure 5. 2 - Amount of equilibrium phases as a function of temperature calculated for the $(Ti_{0.5}Zr_{0.5})_1(Fe_{0.33}Mn_{0.33}Co_{0.33})_2$, $(Ti_{0.5}Nb_{0.5})_1(Mn_{0.33}Ni_{0.33}Co_{0.33})_2$, $(Ti_{0.5}Nb_{0.5})_1(V_{0.5}Cr_{0.5})_2$, $(Ti_{0.5}Zr_{0.5})_1(Cr_{0.5}Co0.5)_2$, $(Ti_{0.5}Nb_{0.5})_1(Mn_{0.33}Cr_{0.33}Cu_{0.33})_2$, and $(Ti_{0.25}Nb_{0.75})_1(Mn_{0.49}Cr_{0.49}Cu_{0.02})_2$ compositions. ..... 47
Figure 5. 3 - Amount of equilibrium phases as a function of temperature calculated for the $(Ti_{0.5}Zr_{0.5})_1(Cr_{0.25}Mn_{0.25}Fe_{0.25}Ni_{0.25})_2$ alloy. ..... 50
Figure 5. 4 - Rietveld refinement of the XRD pattern of the as-cast $(Ti_{0.5}Zr_{0.5})_1(Cr_{0.25}Mn_{0.25}Fe_{0.25}Ni_{0.25})_2$ alloy indicating that the sample formed C14 Laves phase structure and a very small amount of TiNi phase. (Measured with KαCu radiation). ..... 51

Figure 5. 5 - SEM (SE and BSE) images and corresponding EDX elemental maps of the as-cast $(Ti_{0.5}Zr_{0.5})_1(Cr_{0.25}Mn_{0.25}Fe_{0.25}Ni_{0.25})_2$ alloy. ..... 52
Figure 5. 6 - $A_2B_2$ sites formed by a tetrahedron having 2 bonds with energy $\varepsilon A - H$ and 2 bonds with energy $\varepsilon B - H$. ..... 56
Figure 5. 7 - Hydrogen equilibrium pressure as a function of the hydrogen content in the C14 Laves phase for a hypothetical system at a constant temperature. 58
Figure 5. 8 - Calculated PCI diagrams at room temperature for 86 equiatomic C14 Laves phase alloys. ..... 65
Figure 5. 9 - Calculated PCI diagrams at room temperature for the non-equiatomic C14 Laves phase alloys (alloys number 87 to 263). ..... 66
Figure 5. 10 - Calculated PCI diagrams at room temperature for the non-equiatomic C14 Laves phase alloys (alloys number 264 to 440). ..... 67
Figure 5. 11 - Chart of the hydrogen equilibrium pressure values (alloys having $cH$ = 0.5) versus the maximum theoretical hydrogen content in weight percent of H considering $cH,max$= 1. Some compositions (alloy number shown in Table 5.1 and A1) are indicated inside the three regions of potential applications. ..... 68
Figure 5. 12 - Experimental absorption PCIs of the $(Ti_{0.5}Zr_{0.5})_1(Cr_{0.25}Mn_{0.25}Fe_{0.25}Ni_{0.25})_2$ (experimental data taken from [10]), $(Ti_{0.4}Zr_{0.6})_1(Nb_{0.1}Fe_{0.6}Ni_{0.2}Ti_{0.1})_2$ (experimental data taken from [11]), $(Ti_{0.5}Zr_{0.5})_1(V_{0.25}Ni_{0.55}Mn_{0.1}Fe_{0.1})_2$ (experimental data taken from [12]), $(Ti)_1(Cr_{0.75}Mn_{0.25})_2$ (experimental data taken from [13]) alloys compared with the calculated PCIs using the thermodynamic model proposed in this study. ..... 70
Figure 5. 13 - Experimental absorption and desorption PCT at 30 °C, 60 °C and 90 °C of the $(Ti_{0.5}Zr_{0.5})_1(Cr_{0.25}Mn_{0.25}Fe_{0.25}Ni_{0.25})_2$ alloy compared with the calculated PCI using the thermodynamic model proposed. ..... 74
Figure 5. 14 - Van´t Hoff plot for the absorption and desorption pressures at $cH$ = H/M = 0.5 for the $(Ti_{0.5}Zr_{0.5})_1(Cr_{0.25}Mn_{0.25}Fe_{0.25}Ni_{0.25})_2$ alloy. ..... 76
Figure 5. 15 - Amount of equilibrium phases as a function of temperature calculated for the $(Ti_{0.5}Zr_{0.5})_1Mn_2$ composition. ..... 78
Figure 5. 16 - Amount of equilibrium phases as a function of temperature calculated for the $(Ti_{0.5}Zr_{0.5})_1(Mn_{0.5}Cr_{0.5})_2$ composition. ..... 79

Figure 5. 17 - Amount of equilibrium phases as a function of temperature calculated for the $(Ti_{0.5}Zr_{0.5})_1(Fe_{0.5}Mn_{0.5})_2$ composition. ..... 80
Figure 5. 18 - Amount of equilibrium phases as a function of temperature calculated for the $(Ti_{0.5}Zr_{0.5})_1(Fe_{0.33}Mn_{0.33}Cr_{0.33})_2$ composition. ..... 80
Figure 5. 19 - Amount of equilibrium phases as a function of temperature calculated for the $(Ti_{0.33}Zr_{0.33}Nb_{0.33})_1(Mn_{0.5}Cr_{0.5})_2$ composition. ..... 81
Figure 5. 20 - Amount of equilibrium phases as a function of temperature calculated for the $(Ti_{0.33}Zr_{0.33}Nb_{0.33})_1(Fe_{0.5}Mn_{0.5})_2$ composition. ..... 82
Figure 5. 21 - Amount of equilibrium phases as a function of temperature calculated for the $(Ti_{0.5}Nb_{0.5})_1(Fe_{0.5}Mn_{0.5})_2$ composition. ..... 82
Figure 5. 22 - Calculated PCI curves for the selected alloys at 25 °C. ..... 83
Figure 5. 23 - Rietveld refinement of the XRD pattern of the as-cast $(Ti_{0.5}Zr_{0.5})_1Mn_2$ alloy indicating that the sample formed C14 Laves phase structure (measured with KαCu radiation). ..... 85
Figure 5. 24 - Rietveld refinement of the XRD pattern of the as-cast $(Ti_{0.5}Zr_{0.5})_1(Mn_{0.5}Cr_{0.5})_2$ alloy indicating that the sample formed C14 Laves phase structure (measured with KαCu radiation). ..... 85
Figure 5. 25 - Rietveld refinement of the XRD pattern of the as-cast $(Ti_{0.5}Zr_{0.5})_1(Fe_{0.5}Mn_{0.5})_2$ alloy indicating that the sample formed C14 Laves phase structure (measured with KαCu radiation). ..... 86
Figure 5. 26 - Rietveld refinement of the XRD pattern of the as-cast $(Ti_{0.5}Zr_{0.5})_1(Fe_{0.33}Mn_{0.33}Cr_{0.33})_2$ alloy indicating that the sample formed C14 Laves phase structure (measured with KαCu radiation). ..... 86
Figure 5. 27 - Rietveld refinement of the XRD pattern of the as-cast $(Ti_{0.33}Zr_{0.33}Nb_{0.33})_1(Mn_{0.5}Cr_{0.5})_2$ alloy indicating that the sample formed C14 Laves phase structure (measured with KαCu radiation). ..... 87
Figure 5. 28 - Rietveld refinement of the XRD pattern of the as-cast $(Ti_{0.33}Zr_{0.33}Nb_{0.33})_1(Fe_{0.5}Mn_{0.5})_2$ alloy indicating that the sample formed C14 Laves phase structure (measured with KαCu radiation). ..... 87
Figure 5. 29 - Rietveld refinement of the XRD pattern of the as-cast $(Ti_{0.5}Nb_{0.5})_1(Fe_{0.5}Mn_{0.5})_2$ alloy indicating that the sample formed C14 Laves phase structure (measured with KαCu radiation). ..... 88

Figure 5. 30 - SEM-BSE image and corresponding EDX elemental maps of the ..... 90
Figure 5. 31 - SEM-BSE image and corresponding EDX elemental maps of the ..... 91
Figure 5. 32 - SEM-BSE image and corresponding EDX elemental maps of the ..... 93
Figure 5. 33 - SEM-BSE image and corresponding EDX elemental maps of the ..... 94
Figure 5. 34 - SEM-BSE image and corresponding EDX elemental maps of the ..... 96
Figure 5. 35 - SEM-BSE image and corresponding EDX elemental maps of the ..... 97
Figure 5. 36 - SEM-BSE image and corresponding EDX elemental maps of the ..... 99
Figure 5. 37 - Measurement of hydrogen absorption kinetics at 25 °C in H/M of the $(Ti_{0.5}Zr_{0.5})_1(Mn_{0.5}Cr_{0.5})_2$ alloy under an initial hydrogen pressure $Pi$ = 25 bar (1st kinetic – black curve) and $Pi$ = 21 bar (2nd kinetic – red curve). ..... 100
Figure 5. 38 - Measurement of hydrogen absorption kinetics at 30 °C in H/M of the $(Ti_{0.5}Zr_{0.5})_1(Fe_{0.33}Mn_{0.33}Cr_{0.33})_2$ alloy under an initial hydrogen pressure $Pi$ = 52 bar. ..... 101
Figure 5. 39 - Measurement of hydrogen absorption kinetics at 25 °C in H/M of the $(Ti_{0.33}Zr_{0.33}Nb_{0.33})_1(Mn_{0.5}Cr_{0.5})_2$ alloy under an initial hydrogen pressure $Pi$ = 38 bar (1st kinetic – black curve) and $Pi$ = 36 bar (2nd kinetic – red curve). .... 102
Figure 5. 40 - Comparison between calculated and experimental PCIs of the $(Ti_{0.5}Zr_{0.5})_1(Mn_{0.5}Cr_{0.5})_2$ alloy with $c_H$ = H/M = 0.5 at 30 °C, 60 °C, and 90 °C. 104
Figure 5. 41 - Comparison between calculated and experimental PCIs of the $(Ti_{0.5}Zr_{0.5})_1(Fe_{0.33}Mn_{0.33}Cr_{0.33})_2$ alloy with $c_H$ = H/M = 0.5 at 30 °C, 60 °C, 90 °C and 130 °C. ..... 105
Figure 5. 42 - Comparison between calculated and experimental PCIs of the $(Ti_{0.33}Zr_{0.33}Nb_{0.33})_1(Mn_{0.5}Cr_{0.5})_2$ alloy with $c_H$ = H/M = 0.5 at 30 °C, 50 °C, and 70 °C. For the calculated PCIs curves the overall composition measured by EDS was used (Table 5.14). ..... 107

Figure 5. 43 - Van´t Hoff plot for the absorption and desorption pressure at $c_H$ = H/M = 0.5 for the (a) $(Ti_{0.5}Zr_{0.5})_1(Mn_{0.5}Cr_{0.5})_2$, (b) $(Ti_{0.5}Zr_{0.5})_1(Fe_{0.33}Mn_{0.33}Cr_{0.33})_2$, and (c) $(Ti_{0.33}Zr_{0.33}Nb_{0.33})_1(Mn_{0.5}Cr_{0.5})_2$ alloys. ..... 109
Figure 5. 44 - Comparison between calculated and experimental (measured in absorption) equilibrium pressure for the $(Ti_{0.5}Zr_{0.5})_1(Mn_{0.5}Cr_{0.5})_2$ (square), $(Ti_{0.5}Zr_{0.5})_1(Fe_{0.33}Mn_{0.33}Cr_{0.33})_2$ (circle), and $(Ti_{0.33}Zr_{0.33}Nb_{0.33})_1(Mn_{0.5}Cr_{0.5})_2$ (triangle) alloys with $c_H$ = H/M = 0.5. The temperatures are indicated by colors. ..... 112
Figure 5. 45 - Hydrogen absorption capacity in H/M of the $(Ti_{0.5}Zr_{0.5})_1(Mn_{0.5}Cr_{0.5})_2$ alloy over the 20$^{th}$ cycles of absorption and desorption at 30 °C. During the absorption cycles, the initial hydrogen pressure was 21 bar, and the final pressure was 16 bar, approximately; the desorption was carried without vacuum exposure. ..... 113
Figure 5. 46 - Hydrogen absorption capacity in H/M of the $(Ti_{0.5}Zr_{0.5})_1(Mn_{0.5}Cr_{0.5})_2$ alloy. (a) Over the 20$^{th}$ cycles of absorption at 30 °C. During the absorption cycles, the initial hydrogen pressure was 21 bar, and the final pressure was 16 bar; the desorption was carried out under dynamic vacuum. (b) Over 10$^{th}$ cycles of absorption and desorption. During the absorption cycles the temperature was at 30 °C and the initial hydrogen pressure was 21 bar, and the final pressure was 16 bar, approximately; the desorption was carried without vacuum exposure at 90 °C under an initial pressure of 0.2 bar. ..... 115
Figure 5. 47 - Pressure and capacity ranges observed during cycling tests of the $(Ti_{0.5}Zr_{0.5})_1(Mn_{0.5}Cr_{0.5})_2$ alloy. The red-colored rectangle highlights the cycling range showed in Figure 5.46 and the red- plus green-colored the cycling test showed in Figure 5.46 (b). ..... 117
Figure 5. 48 - Hydrogen absorption capacity in H/M of the $(Ti_{0.5}Zr_{0.5})_1(Fe_{0.33}Mn_{0.33}Cr_{0.33})_2$ alloy over the 1$^{st}$, 2$^{nd}$, 10$^{th}$, 20$^{th}$, 30$^{th}$, 40$^{th}$, and 50$^{th}$ cycles of absorption and desorption at 30 °C. During the absorption cycles, the initial hydrogen pressure was 52 bar, and the final pressure was 48 bar, approximately; the desorption was carried without vacuum exposure. ..... 118

Figure 5. 49 - Pressure and capacity range observed during cycling test of the $(Ti_{0.5}Zr_{0.5})_1(Fe_{0.33}Mn_{0.33}Cr_{0.33})_2$ alloy. The red-colored rectangle highlights the cycling range showed in Figure 5.48. ..... 119
Figure 5. 50 - Hydrogen absorption capacity in H/M of the $(Ti_{0.33}Zr_{0.33}Nb_{0.33})_1(Mn_{0.5}Cr_{0.5})_2$ alloy over the (a) 1st, 2nd, 10th, 20th, 30th, 40th, and 50th cycles of absorption and desorption. During the absorption cycles, the initial hydrogen pressure was 35 bar, and the final pressure was 33 bar, approximately; the desorption was carried without vacuum exposure. ..... 120
Figure 5. 51 - Pressure and capacity range observed during cycling test of the $(Ti_{0.33}Zr_{0.33}Nb_{0.33})_1(Mn_{0.5}Cr_{0.5})_2$ alloy. The red-colored rectangle highlights the cycling range showed in Figure 5.48. ..... 121
Figure 5. 52 - XRD patterns of the $(Ti_{0.5}Zr_{0.5})_1(Mn_{0.5}Cr_{0.5})_2$ alloy. (a) as-cast, (b) after one absorption cycle, and (c) after forty absorption/desorption cycles (measured with KαCu radiation). ..... 122
Figure 5. 53 - XRD patterns of the $(Ti_{0.5}Zr_{0.5})_1(Fe_{0.33}Mn_{0.33}Cr_{0.33})_2$ alloy. (a) as-cast, (b) after one absorption/desorption cycle, and (c) after fifty absorption/desorption cycles (measured with KαMo radiation). ..... 124
Figure 5. 54 - XRD patterns of the $(Ti_{0.33}Zr_{0.33}Nb_{0.33})_1(Mn_{0.5}Cr_{0.5})_2$ alloy. (a) as-cast, (b) after one absorption/desorption cycle, and (c) after fifty absorption/desorption cycles (measured with KαCu radiation). ..... 125
Figure 5. 55 - SEM images of the $(Ti_{0.5}Zr_{0.5})_1(Mn_{0.5}Cr_{0.5})_2$ alloy in as cast (a) and (c), and after 40th cycles of hydrogenation/dehydrogenation (b) and (d). ..... 126
Figure 5. 56 - SEM images of the $(Ti_{0.5}Zr_{0.5})_1(Fe_{0.33}Mn_{0.33}Cr_{0.33})_2$ alloy in as cast (a) and (c), and after 50th cycles of hydrogenation/dehydrogenation (b) and (d). ..... 127
Figure 5. 57 - SEM images of the $(Ti_{0.33}Zr_{0.33}Nb_{0.33})_1(Mn_{0.5}Cr_{0.5})_2$ alloy in as cast (a) and (c), and after 50th cycles of hydrogenation/dehydrogenation (b) and (d). ..... 127
Figure 5. 58 - Schematic illustration of the activation procedures in terms of time, temperature and atmosphere. The procedures consisted of (a) exposing the sample to dynamic vacuum for one hour at RT, (b) heating the sample to 390 °C under dynamic vacuum for 12 h and subsequently cool it to RT, and (c) exposing

the sample to a hydrogen pressure at RT for 1 h, then heat it to 390 °C for 1 h under hydrogen pressure, then cool it to RT while still under hydrogen pressure and finally exposed to a dynamic vacuum before absorption measurements. 129
Figure 5. 59 - Ellingham diagram for several metals giving the free energy of formation of metal oxides. Ce is highlighted in blue color. ..... 130
Figure 5. 60 - Measurement of hydrogen absorption kinetics at 25 °C in H/M of the $(Ti_{0.5}Zr_{0.5})_1(Fe_{0.5}Mn_{0.5})_2$+Ce alloy under an initial hydrogen pressure Pi = 33 bar. ..... 131
Figure 5. 61 - Rietveld refinement of the XRD pattern of the as-cast $(Ti_{0.5}Zr_{0.5})_1(Fe_{0.5}Mn_{0.5})_2$+Ce alloy indicating that the sample formed C14 Laves phase structure (measured with KαCu radiation). ..... 132
Figure 5. 62 - SEM-BSE image and corresponding EDX elemental maps of the ..... 133
Figure 5. 63 - SEM-BSE image and corresponding EDX elemental maps of the as-cast $(Ti_{0.5}Zr_{0.5})_1(Fe_{0.5}Mn_{0.5})_2$ alloy (left side) compared with the $(Ti_{0.5}Zr_{0.5})_1(Fe_{0.5}Mn_{0.5})_2$+Ce alloy (right side). ..... 135
Figure 5. 64 - (a) SEM-BSE image and corresponding EDX elemental (b) Ce and (c) Oxygen maps of the as-cast $(Ti_{0.5}Zr_{0.5})_1(Fe_{0.5}Mn_{0.5})_2$+Ce alloy. ..... 136
Figure 5. 65 - (a) SEM-BSE image and (b) corresponding line mapping measurement of the as-cast $(Ti_{0.5}Zr_{0.5})_1(Fe_{0.5}Mn_{0.5})_2$+Ce alloy. (c) Line mapping and the (d) corresponding graph with the count of elements in the line region. ..... 137
Figure 5. 66 - Measurement of hydrogen absorption kinetics at 25 °C in H/M of the $(Ti_{0.5}Zr_{0.5})_1(Fe_{0.5}Mn_{0.5})_2$+Ce alloy under an initial hydrogen pressure $Pi$ = 25 bar (1st kinetic – black curve), $Pi$ = 24 bar (2nd kinetic – grey curve), $Pi$ = 24 bar (3rd kinetic – blue curve), and $Pi$ = 37 bar (4th kinetic – red curve). ..... 138
Figure 5. 67 - PCIs of the $(Ti_{0.5}Zr_{0.5})_1(Fe_{0.5}Mn_{0.5})_2$+Ce alloy at 30 °C (a) with x-axis in logarithmic scale and (b) in linear scale. ..... 140
Figure 5. 68 - PCIs of the $(Ti_{0.5}Zr_{0.5})_1(Fe_{0.5}Mn_{0.5})_2$+Ce alloy at 30 °C compared to the calculated PCI for the base composition without Ce ($(Ti_{0.5}Zr_{0.5})_1(Fe_{0.5}Mn_{0.5})_2$). ..... 142

Figure 5. 69 – Hydrogen absorption capacity in H/M of the $(Ti_{0.5}Zr_{0.5})_1(Fe_{0.5}Mn_{0.5})_2$+Ce alloy over the 20th cycles of absorption and desorption at 30 °C. (a) During the absorption cycles, the initial hydrogen pressure was 37 bar, and the final pressure was 33 bar, approximately. (b) During the absorption cycles, the initial hydrogen pressure was 50 bar, and the final pressure was 49 bar, approximately. The desorption was carried out without vacuum exposure. ..... 143
Figure 5. 70 - XRD patterns of the $(Ti_{0.5}Zr_{0.5})_1(Fe_{0.5}Mn_{0.5})_2$+Ce alloy. (a) as-cast, (b) after one absorption/desorption cycle, and (c) after forty absorption/desorption cycles (measured with KαCu radiation). ..... 145
Figure 5. 71 - SEM images of the $(Ti_{0.5}Zr_{0.5})_1(Fe_{0.5}Mn_{0.5})_2$+Ce alloy in as cast (a) and (c), and after 40th cycles of hydrogenation/dehydrogenation (b) and (d). 146
Figure 5. 72 - Oxygen content of the as-cast samples of the alloys. ..... 149

## 1 INTRODUCTION

Among the renewable energy resources in focus on the current climate change scenario, hydrogen energy is expected to play an important role in a future sustainable energy economy. Hydrogen is an efficient energy vector for energies produced from renewable and environmentally clean sources, such as solar energy and wind power. The principal strength points are its high energy density (120 MJ/kg compared to 45 MJ/kg for gasoline), abundance, efficient production from water electrolysis, and generating only water as a byproduct after conversion and use [1,2]. Figure 1 shows a schematic illustration of the hydrogen economy cycle.

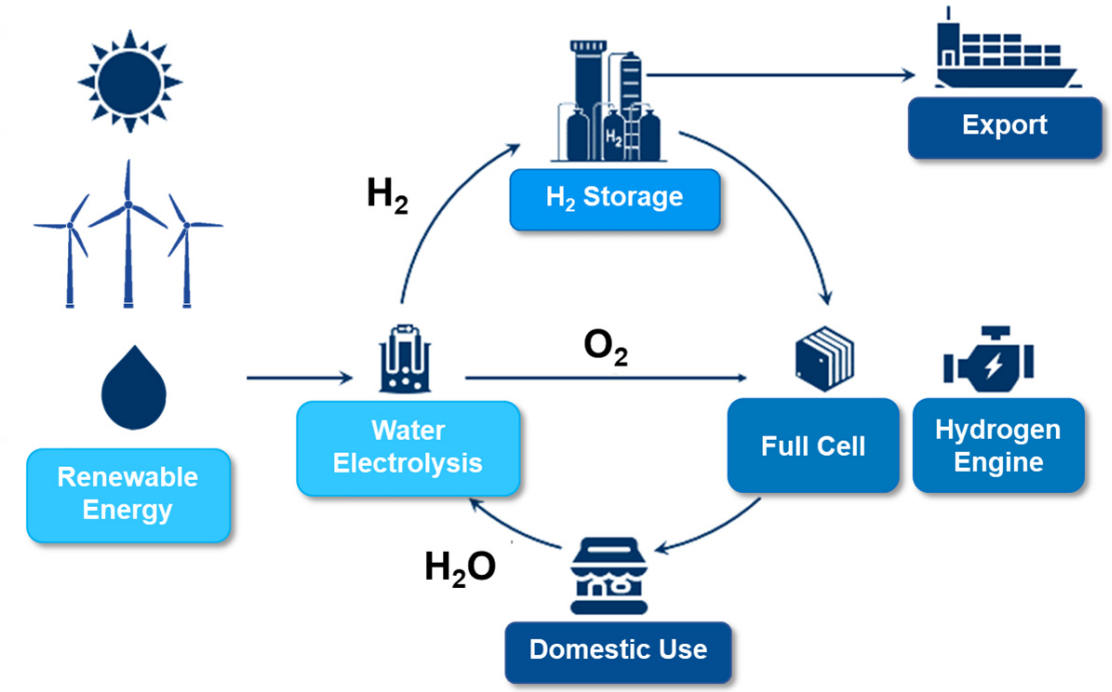


Figure 1. 1 - Schematic illustration of hydrogen economy cycle.

Despite the hydrogen economy holding a promising prospect for a more environmentally friendly energy sector, the safe, effective, and economically viable transition to the hydrogen-based economy is highly dependent on hydrogen storage. The low hydrogen energy density at ambient pressure and temperature (10 MJ/Nm$^3$) represents a significant drawback for practical use, demanding to be stored in compact form. For example, 4 kg of hydrogen as a

molecular gas at ambient pressure and temperature occupies a volume of 45 $m^3$, hardly a practical solution for a vehicle [2,3]. This amount of hydrogen is required for an electric car with a fuel cell to travel a total of 400 km. Whereas a car with a combustion engine version demands 8 kg of hydrogen to cover the same range. Meanwhile, a total of 24 kg of petrol (0.032 $m^3$) is burned to travel the same distance [3].

The main hydrogen storage methods currently investigated are high-pressure gas vessels (> 200 bar), liquid hydrogen in cryogenic tanks due to the low boiling point at ambient pressure (-252 °C), physisorption on materials with a very large specific surface area, and absorption in interstitial sites of a host metal forming a metal hydride (MH). The two first conventional methods are characterized for requiring large volumes tanks, investment costs, and presenting many safety problems. The physisorption method is based on Van der Waals interactions of gas molecules onto the surface of solids with a large specific surface area like activated or nanostructured carbon and carbon nanotubes. This method is characterized by low operating pressure and simple design of the storage system, however, the small gravimetric and volumetric hydrogen density on carbon, associated with the low temperatures required, are significant drawbacks [2–5]. Lastly, MHs have been considered as a great alternative for solid-state hydrogen storage, providing reversibility, safety, and high volumetric densities. MHs might enable the use of hydrogen energy in various stationary and mobile applications, such as tanks for solid-state hydrogen storage, heat storage systems, fuel cells, and batteries [2,3].

Each one of these applications demands a different set of properties and, therefore, different MHs. The hydrogen storage properties of MHs, such as the storage capacity, operation temperature-pressure, and cycling stability are highly dependent on the MH composition [6]. In this scenario, high entropy alloys (HEA), multi-principal element alloys (MPEA), complex concentrated alloys (CCA) or, more generally, multicomponent alloys have been investigated for hydrogen storage since their vast compositional space allows the tuning of hydrogen storage properties of MHs. Multicomponent alloys for hydrogen storage

application can be divided into three main groups: body-centered cubic (BCC), lightweight, and intermetallic multicomponent alloys [7].

Laves phase has been identified as the most common intermetallic phase among the intermetallic multicomponent alloys, and several times these alloys were constituted by a single Laves phase structure [8]. Furthermore, Laves phases are known to reversibly absorb considerable amounts of hydrogen at moderate conditions of temperature and pressure, with good kinetics and sometimes without any activation treatment [9–14]. Laves phases are classified according to their crystal structures, namely, C14 ($MgZn_2$-type), C15 ($MgCu_2$-type), and C36 ($MgNi_2$-type) [15]. For hydrogen storage, Laves phases are described as $AB_2$ compounds, being A strong hydride former elements and B elements with low affinity with hydrogen. The classification of A- and B-type elements are based on their binary hydride enthalpy of formation. A-type elements have lower values of enthalpy of hydride formation and B-type elements have higher values of enthalpy of hydride formation [7,16]. Most of the Laves phase multicomponent alloys for hydrogen storage reported so far are equiatomic, although non-equiatomic compositions within the same alloy system have been studied since it could improve the hydrogen storage behavior [11,12].

The development of effective methods to access the vast field of multicomponent alloys, enabling the design and prediction of phase formation, stability, and properties, is paramount for designing new alloys for hydrogen storage for all kinds of applications. The design of single-phase alloys for hydrogen storage is preferable since the effect (either beneficial or detrimental) of secondary phases on the hydrogen storage properties is not clear yet. In this way, few methods for obtaining single-phase alloys have been proposed, and they are classified into empirical, thermodynamic, and atomistic models, as reported by Marques et al. [7]. The empirical model considers geometrical and electronic factors based on the chemical alloy composition, such as the valence electron concentration (VEC), atomic radius ratio between A- and B-type elements ($r_A/r_B$), atomic size mismatch ($\delta$), and differences in electronegativity ($\delta_x$) [6,17]. The calculation Phase Diagrams (CALPHAD) method has been reported as a powerful and consolidated thermodynamic-based tool to predict

phase formation and stability of multicomponent alloys [7,10,11]. Therefore, CALPHAD can be helpful as a first approach to exploring the vast compositional space of multicomponent alloys. The atomistic models, such as *ab initio* calculations, are suited as complementary analysis to investigate narrow composition ranges previously selected by other screening techniques to reaffirm predictions that have been found as interesting.

The applicability of a MH for a specific hydrogen storage device is intrinsically related to its pressure-composition-temperature (PCT) diagram, which determines both the maximum hydrogen storage capacity and pressure-temperature operation condition. However, data collection of PCT diagrams is very time-consuming, and experimental investigation of a large number of compositions within the multicomponent field is unpractical. Thus, computational tools that allow the prediction of the thermodynamic properties of multicomponent alloys-hydrogen systems can be extremely helpful to navigate a large compositional field and to boost the discovery of new alloys with optimized properties for any specific application [18].

Therefore, the present doctoral thesis project aimed to present a comprehensive strategy to design single C14 Laves phase alloys for hydrogen storage using high-throughput calculation of electronic and geometrical parameters combined with CALPHAD calculations; to develop a thermodynamic model to calculate PCT diagrams of multicomponent C14-type Laves phase alloys; and consequently, to select alloys in a wide range of equilibrium pressures. The design and the models were compared with experimental data of alloys with suitable properties for different hydrogen storage applications.

## 2 OBJECTIVES

This doctoral thesis project aims to develop and validate a method based on computational thermodynamics to design multicomponent alloys with C14 Laves phase from the (Ti, Zr or Nb)$_1$(V, Cr, Mn, Fe, Co, Ni, Cu or Zn)$_2$ system for different hydrogen storage applications.

The design method must be able to predict phase stability of multicomponent alloys allowing the selection of compositions prone to form single C14-type Laves phase alloys. In addition, the method must allow the calculation of PCT diagrams of single C14-type Laves phase multicomponent alloys, allowing the selection of alloys with hydrogen storage properties tailored for any desirable application.

# 3 LITERATURE REVIEW

## 3.1 Thermodynamic of metal hydrides

Hydrogen reacts reversibly with many metals, their alloys, and intermetallic compounds, to form metal hydrides according to the reaction 3.1:

$$M + \frac{x}{2} H_2 \leftrightarrow MH_x \quad (3.1)$$

where $M$ is a metal, an alloy, or an intermetallic compound, $MH_x$ is the respective hydride and $x$ the ratio of hydrogen to metal, $x = H/M$. The hydride formation is an exothermic reaction and hydrogen release reaction is endothermic since the enthalpy of the hydride is lower in comparison to the metal and the gaseous hydrogen phase [19].

The reaction of the hydrogen gas with the metal (absorption process) is schematically illustrated in Figure 3.1 and can be described in terms of a potential energy curve (Figure 3.2), as reported by Züttel [5]. Firstly, far from the surface of the metal, the hydrogen molecules are in their gaseous form (Figure 3.1(a)), and the first attractive interaction of an approaching hydrogen molecule to the metal surface is a Van der Waals force leading to the physisorbed state (Figure 3.1(b)). In the next step of the hydrogen-metal interaction, the hydrogen has overcome an activation barrier for the dissociation and formation of the hydrogen-metal bond (Figure 3.1(c)). This process is named dissociation and chemisorption, and the magnitude of the activation barrier depends on the surface elements involved. After dissociation on the metal surface, the chemisorbed hydrogen atom can finally diffuse in the interstitial sites through the host metal lattice to form an M-H solid solution commonly referred to as α-phase (Figure 3.1(d)) [5,19]. In the solid solution phase, the crystalline structure of the host metal remains unchanged, however, the metal lattice expands proportional to the hydrogen concentration by approximately 2 to 3 Å$^3$ per hydrogen atom. At higher hydrogen concentrations in the host metal, hydride phases commonly referred to as β-phase, nucleate and grow. The concentration of hydrogen in the hydride phase is often reported to be between H/M = 1 and H/M = 2, and it may correspond to a volume expansion of 10 to 20% of the metal lattice. This expansion generates a high level of internal stress concentration in the host metal

and often leads to the embrittlement of the host metal after absorption, consequently, the final hydride is a powder with a particle size of 10 to 100 µm [5,19].

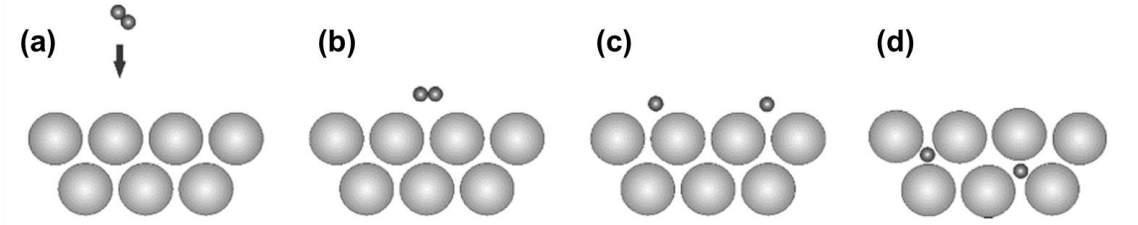


Figure 3. 1 - Schematic illustration of the reaction of an $H_2$ molecule with a metal: (a) $H_2$ molecule approaching the metal surface, (b) Attractive interaction of the $H_2$ molecule by Van der Waals forces (physisorbed state), (c) Chemisorbed hydrogen after $H_2$ dissociation, and (d) Diffusion on the interstitial sites of the host metal lattice [19].

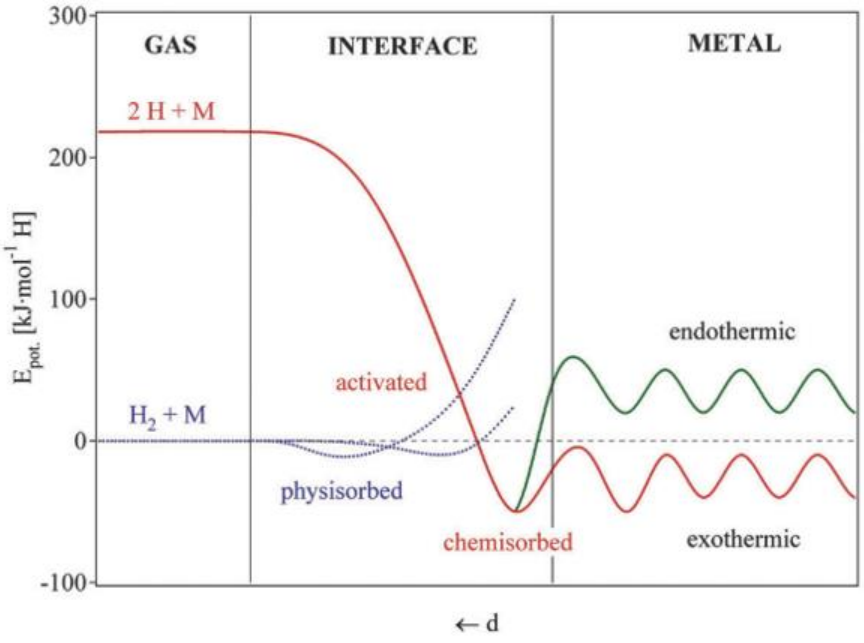


Figure 3. 2 - Schematic of potential energy curve of hydrogen in molecular and atomic form approaching the host metal. The hydrogen molecule is attracted by Van der Waals forces and forms a physisorbed state. Before diffusion into the bulk metal, the molecule has to dissociate, forming a chemisorbed state at the surface of the metal [5].

The hydride formation from gaseous hydrogen is also studied from thermodynamic aspects. The thermodynamic properties determine whether an alloy can absorb hydrogen at a given temperature and pressure and the amount of hydrogen in equilibrium within the alloy structure in such conditions. Besides, the thermodynamic properties of an alloy are directly dependent on the composition. The equilibrium condition for a metallurgic system is achieved when the chemical potential of all elements in the system is the same in all coexisting phases, resulting in the minimum free energy of the system. There are different degrees of equilibrium possible during the reaction of the hydrogen with a metal and, consequently, in the two-phase coexistence region of metal hydride systems. The para-equilibrium (PE) condition is a type of thermodynamic equilibrium observed in most hydrogen storage applications, which occurs at low or moderate temperatures. In this condition, the mobility of the metals atoms is limited, and it can be assumed that the metal atoms are “frozen” while only the hydrogen atoms are mobile. In this situation, an equilibrium condition is attained because hydrogen mobility allows the chemical potential of hydrogen to be the same in all the co-existing phases, resulting in the minimum free energy of the system. In contrast, the complete equilibrium (CE) condition is achieved when all atoms of the system have sufficient mobility, usually at high temperatures, so the chemical compositions of the phase can be adjusted to minimize the Gibbs free energy of the system [20].

For thermodynamic equilibrium studies of single-phase alloy at a given temperature (T) and a given hydrogen pressure ($P_{H_2}$), the chemical composition can be defined by the atomic fraction of a metal element $i$, then $\sum c_i = 1$, and due to the PE condition, differences in the chemical composition of the different phases are because the hydrogen content in these phases. The amount of hydrogen in the phase is determined as:

$$c_H = \frac{n_H}{n_M} \quad (3.2)$$

where $n_H$ and $n_M$ are the number of mols of hydrogen and metal atoms in the phase, respectively.

Therefore, the Gibbs free energy of the phases in the hypothetical system will depend only on $c_H$ as shown in Figure 3.3(a). These Gibbs free energy curves can be defined as the Gibbs free energy of hydrogen mixing in the α- and β-phase, as given by Equation 3.3.

$$\Delta G_m(c_H) = \Delta H_m(c_H) - T\Delta S_m(c_H) \quad (3.3)$$

where $\Delta G_m(c_H)$ describe the change in the Gibbs free energy between the α- or β-phase having composition $c_H$ and the reference state. For thermodynamic studies of metal-hydrogen (M-H) systems, the reference state is usually the hydrogen gas in its standard condition, $P^0 = 1$ atm, and the alloy in its stable form (BCC, FCC, HCP, C14, etc.).

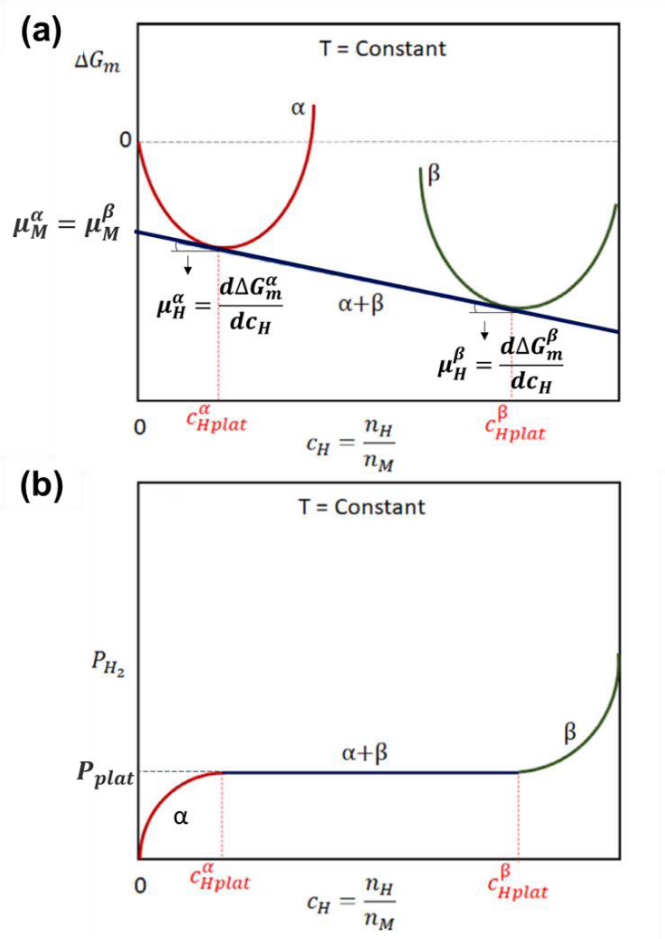


Figure 3. 3 - a) Gibbs free energy of α- and β-phase as a function of $c_H$ for a hypothetical M-H system under PE condition for a given temperature and (b) its corresponding pressure-composition-isotherm diagram. Adapted from [18].

The entropy and enthalpy of hydrogen mixing for any phase (α- or β-phase) are given by Equations 3.4 and 3.5, respectively.

$$\Delta S_m(c_H) = S\left(MH_{c_H}\right) - S(M^{ref}) - \frac{c_H}{2}S^0(H_2) \quad (3.4)$$

$$\Delta H_m(c_H) = H\left(MH_{c_H}\right) - H(M^{ref}) - \frac{c_H}{2}H^0(H_2) \quad (3.5)$$

where $S(M^{ref})$ and $H(M^{ref})$ are the entropy and enthalpy of the alloy in its reference state, $S\left(MH_{c_H}\right)$ and $H\left(MH_{c_H}\right)$ are the entropy and enthalpy of the α- or β-phase having composition $c_H$, and $S^0(H_2)$ and $H^0(H_2)$ are the standard entropy and enthalpy of the hydrogen gas ($P_{H_2}$ = 1 atm). $S^0(H_2)$ is given by Equation 3.6 according to [21]. It is worth mentioning that this equation is valid only between 298 K and 1000 K.

$$S°(H_2) = Aln(t) + Bt + \frac{Ct^2}{2} + \frac{Dt^3}{3} + \frac{Et^{-2}}{2} + G\left[\frac{J}{mol\ of\ H_2}\right] \quad (3.6)$$

where $t = T(K)/1000$, $A$ = 33.066178, $B$ = −11.363417, $C$ = 11.432816, $D$ = −2.772874, $E$ = −0.158558, and $G$ = 172.707974.

The hydrogen chemical potential of the hydrogen gas per mol of hydrogen atom is given by Equation 3.7, while the hydrogen chemical potential of the α- and β-phase are given by Equations 3.8 and 3.9, respectively. Besides, the chemical potential of the metal atoms in the α- and β-phase are given by Equations 3.10 and 3.11. Because of the PE condition, the compositions of both phases in terms of $c_i$ are the same, then the chemical potential is a function of $c_H$.

$$\mu_H^{H_2} = \frac{1}{2}RTln\left(\frac{P_{H_2}}{p^0}\right) \quad (3.7)$$

$$\mu_H^{\alpha}(c_H) = \frac{d\Delta G_m^{\alpha}(c_H)}{dc_H} \quad (3.8)$$

$$\mu_H^{\beta}(c_H) = \frac{d\Delta G_m^{\beta}(c_H)}{dc_H} \quad (3.9)$$

$$\mu_M^{\alpha}(c_H) = \Delta G_m^{\alpha}(c_H) - c_H\mu_H^{\alpha}(c_H) \quad (3.10)$$

$$\mu_M^{\beta}(c_H) = \Delta G_m^{\beta}(c_H) - c_H\mu_H^{\beta}(c_H) \quad (3.11)$$

Phases are in equilibrium when their chemical potential of hydrogen and chemical potential of the metal atoms are the same. Therefore, since $\mu_H^{H_2}$

depends on $P_{H_2}$, there is only a $P_{H_2}$ value in which the phase α, β, and $H_2$ will coexist in equilibrium: $\mu_H^{H_2} = \mu_H^{\propto}(c_{H\,plat}^{\propto}) = \mu_H^{\beta}(c_{H\,plat}^{\beta})$ and $\mu_M^{\propto}(c_{H\,plat}^{\propto}) = \mu_M^{\beta}(c_{H\,plat}^{\beta})$. Figure 3.3(a) shows the equilibrium condition between the α- and β-phase with composition $c_{H\,plat}^{\propto}$ and $c_{H\,plat}^{\beta}$, respectively, given by the common tangent of the Gibbs free energy curves (blue line). The respective pressure-composition-isotherm (PCI) diagram of this hypothetical system is schematic represented in Figure 3.3(b). Below the $P_{plat}$, only the α-phase is in equilibrium with the hydrogen gas, and the hydrogen content of the α phase depends on the hydrogen pressure. At the $P_{plat}$, the α phase with $c_{H\,plat}^{\propto}$ composition and β-phase with $c_{H\,plat}^{\beta}$ composition co-exist in equilibrium with the hydrogen gas. Above $P_{plat}$ only the β-phase is in equilibrium with the hydrogen gas, and its hydrogen content depends on the hydrogen pressure. The $P_{plat}$ is given by Equation 3.12.

$$\frac{1}{2}RTln\left(\frac{P_{plat}}{p^0}\right) = \frac{\Delta G_m^{\beta}\left(c_{H\,plat}^{\beta}\right) - \Delta G_m^{\alpha}\left(c_{H\,plat}^{\alpha}\right)}{c_{H\,plat}^{\beta} - c_{H\,plat}^{\propto}} \quad (3.12)$$

In a simplified way, the second part of equation 3.12 is often associated with a variation in the Gibbs free energy of the plateau ($\Delta G_{plat}$), and using the relationship $\Delta G_{plat} = \Delta H_{plat} - T\Delta S_{plat}$ we obtain the Van't Hoff equation (Equation 3.13).

$$\frac{1}{2}\ln\left(\frac{p_{Plat}}{p_o}\right) = \frac{\Delta H_{Plat}}{R}.\frac{1}{T} - \frac{\Delta S_{Plat}}{R} \quad (3.13)$$

In this case, it is assumed that $\Delta H_{plat}$ and $\Delta S_{plat}$ are constant over temperature and, therefore, these quantities can be found directly by the linearization of $\frac{1}{2}ln(P_{plat})$ vs $1/T$, as schematic illustrated in Figure 3.4. This consideration is only experimentally consistent since the variation of $\Delta H_{plat}$ and $\Delta S_{plat}$ with temperature is generally small. Therefore, the values obtained experimentally reflect a good approximation of the real values of enthalpy and entropy of the plateau.

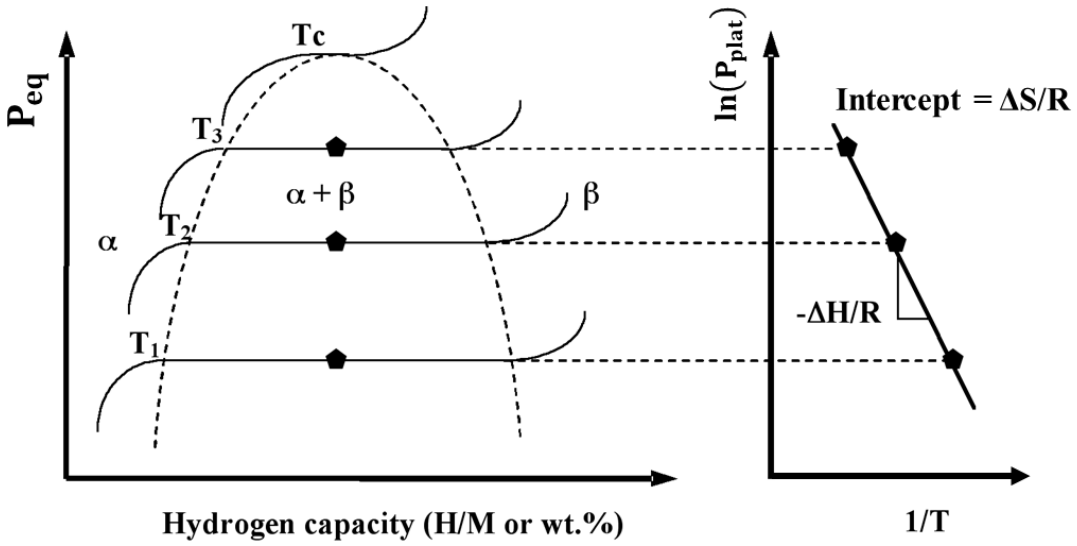


Figure 3. 4 - Schematic illustration of the experimental method for determining the thermodynamic properties of hydride formation based on the van't Hoff equation.

It is worth noting that some materials can present a formation of intermediate hydrides during the reaction with the hydrogen gas, which generates PCI diagrams with multiple plateaus. A difference in stability of the intermediate hydrides could be a problem in terms of the practical application of this material due to the substantial difference in the equilibrium pressures of these plateaus [7,19].

The length of the plateau pressure determines the hydrogen storage capacity of the material at a given temperature. Thus, the greater the length of the plateau, the greater the reversible storage capacity [5,19]. However, it is important to emphasize that problems in obtaining accurate thermodynamic data may occur due to some factors such as hysteresis, not well-defined or sloping plateaus, activation heat treatments, phase decomposition, and amorphization. These factors can eventually produce deviations in the thermodynamic behavior of the hydrides concerning the theoretical behavior, and lead to an erroneous conclusion of the thermodynamic properties [22].

### 3.2 C14 Laves phase

The main conventional metal hydrides reported over the years are the binary and ternary systems based on Mg, intermetallic systems of $AB_5$, $AB_2$, $A_2B$, and AB-type, complex hydrides, and BCC solid solutions [1,5,7,23,24].

Laves phase, which forms the largest group of intermetallics, has the ideal composition $AB_2$. The Laves phase crystallize in three structure prototypes: hexagonal C14 ($MgZn_2$-type), cubic C15 ($MgCu_2$-type) and hexagonal C36 ($MgNi_2$-type) [16]. The crystallographic structures of the three polytypes are shown in Figure 3.5. The original work on these compounds was performed by Friauf and Laves, from whom they derive their name: Friauf-Laves or, more commonly Laves phases [25]. These phases are classified as tetrahedrally close-packed, and constitute a subset of Frank-Kasper phases, because all the interstitial sites are tetrahedral, differently from the traditional close-packed structures such as face centered cubic (FCC) and hexagonal close packed (HCP), where both tetrahedral and octahedral interstices are present [16].

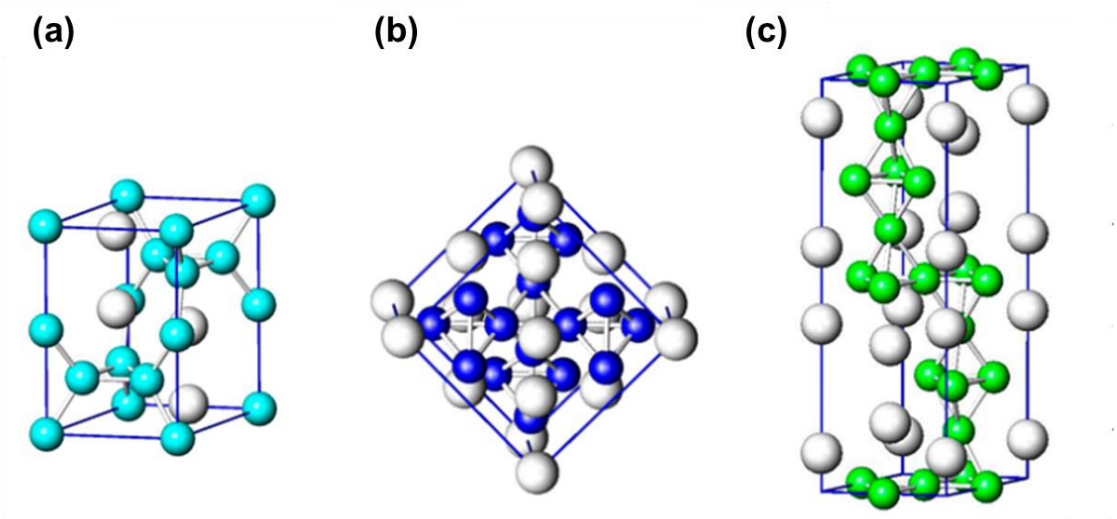


Figure 3. 5 - Schematic of (a) hexagonal C14 ($MgZn_2$-type), (b) cubic C15 ($MgCu_2$-type) and (c) hexagonal C36 ($MgNi_2$-type) crystal structures. Adapted from [26].

For more details, the crystal structure of the $AB_2$ C14 Laves phase is schematic illustrated in Figure 3.6 (structure drawn using VESTA). The C14

Laves phase is a hexagonal structure with space group $P6_3/mmc$ (space group number 194). The structure contains twelve atoms and four formula units per unit cell. The A and B atomic positions are described in Table 3.1. Depending on the parameters x and z in the atom positions of the C14 crystal structure as presented in Table 3.1, the $c/a$ ratio can vary around the ideal value, which from geometrical considerations is $c/a = \sqrt{8/3} \approx 1.633$.

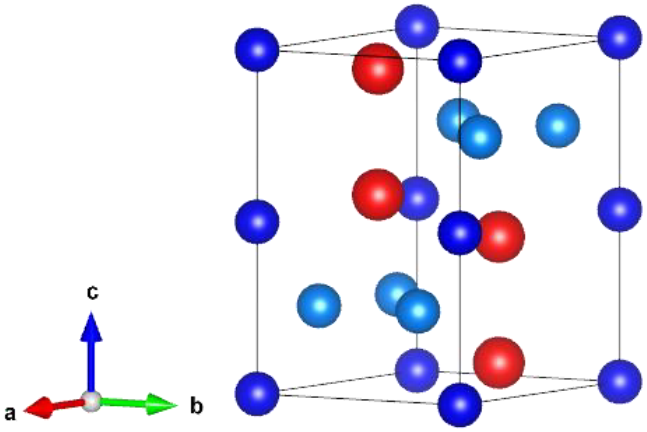


Figure 3. 6 - Unit cell of the hexagonal C14 Laves phase ($MgZn_2$-type). The red spheres represent the A positions, and the blue spheres represent the B positions (B positions are divided into two different crystallographic positions: B1 = dark blue and B2 = light blue). Structure drawn using software VESTA.

Table 3. 1 - Atomic positions of A and B elements.

| | | Atomic positions | | |
|---|---|---|---|---|
| **Element** | **Label** | **Wyckoff positions** | **Coordinates** | **Occupancy factor** |
| **A** | A1 | 4f | $\frac{1}{3},\frac{2}{3},z$ | 1 |
| **B** | B1 | 2a | 0,0,0 | 1 |
| **B** | B2 | 6h | $x,2x,\frac{1}{4}$ | 1 |

Figure 3.7 shows the A and B sublattices that form the C14 structure. The A sublattice defines a hexagonal diamond net, while the B sublattice is composed of $B_4$ tetrahedra alternatively sharing vertices and faces along the c axis as illustrated by Johnston and Hoffmann in their study about Laves phases [25].

These two sublattices merge by vertex sharing in the ab plane to form the C14 Laves phase structure. Therefore, the A positions are situated in the interstitial sites of the B sublattice.

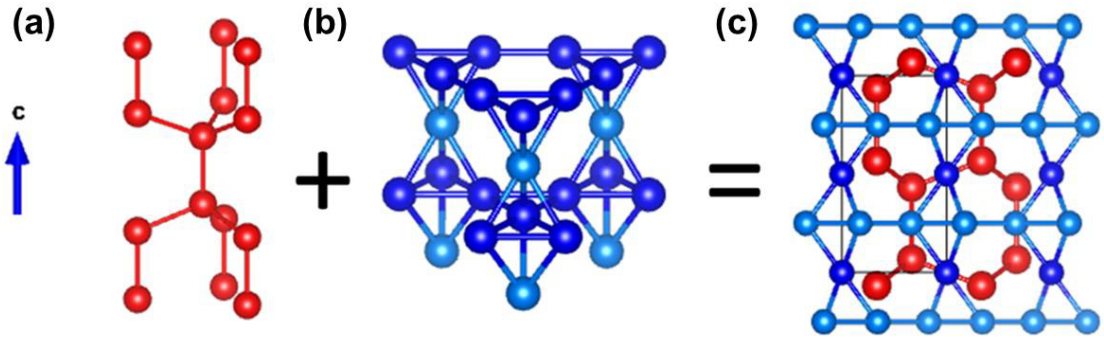


Figure 3. 7 - (a) A and (b) B sublattices that form the (c) complete C14 Laves phase structure. Structure drawn using software VESTA.

There are three types of tetrahedral interstitial sites in the C14-type Laves phase: $A_2B_2$, $AB_3$, and $B_4$, as illustrated in Figure 3.8. The C14 structure has 12 equivalent $A_2B_2$ sites, 4 equivalent $AB_3$ sites, and 1 $B_4$ site per formula unit [16].

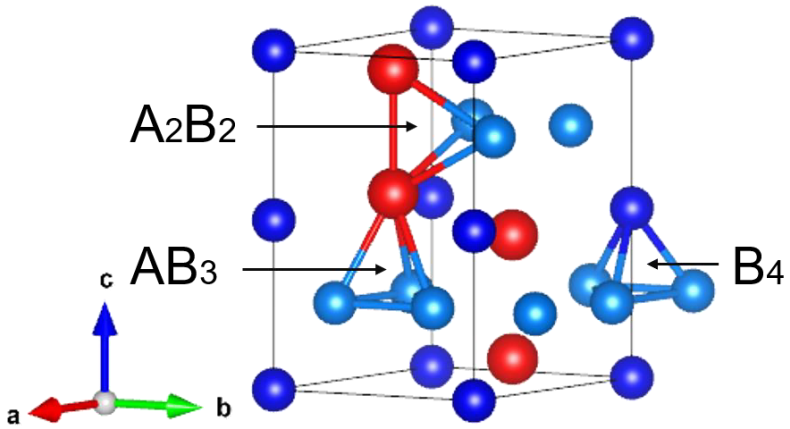


Figure 3. 8 - Unit cell of the hexagonal C14 Laves phase ($MgZn_2$-type) and the three types of tetrahedral interstices available: $A_2B_2$, $AB_3$ and $B_4$. Structure drawn using software VESTA.

In addition to the classification of atomic positions into A and B, the elements that occupy these positions also receive the same classification. In the

other words, the A-type elements occupy A positions and B-type elements occupy B positions in the unit cell of the C14 Laves phase. The atoms occupying the A sites typically have larger atomic radii (for example $r_{Zr} = 1.60$ Å), whereas those in the B sites are smaller (for example $r_{Fe} = 1.27$ Å). Moreover, A-type elements tend to be strong hydride formers, while B-type elements exhibit low affinity with hydrogen. The classification of A- and B-type elements are based on their binary hydride enthalpy of formation. A-type elements have lower values of enthalpy of hydride formation (lower than -20 kJ/mol of H or -40 kJ/mol of $H_2$) and B-type elements have higher values of enthalpy of hydride formation (higher than -10 kJ/mol de H or -20 kJ/mol de $H_2$), as illustrated in Figure 3.9 [7,16]. Nevertheless, there are exceptions, such as V, which shows a tendency for forming hydrides and can effectively occupy the B sites in the C14 structure due to its relatively small atomic radius ($r_V = 1.35$ Å).

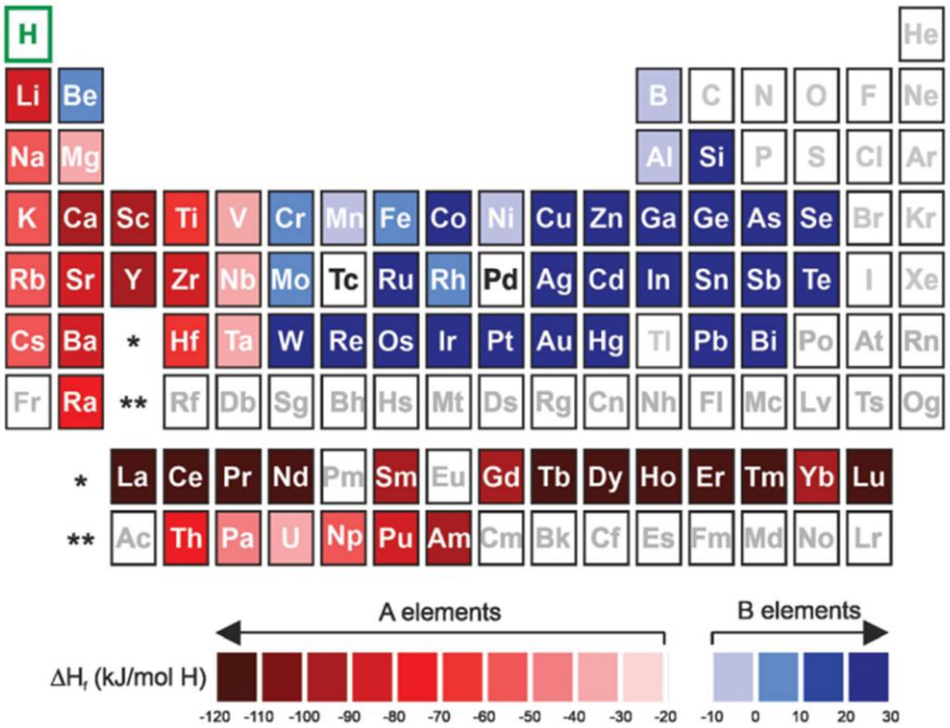


Figure 3. 9 - Periodic table with the subdivision of the A- and B-type elements based on their binary hydride enthalpy of formation. A-type elements represented in shades of red, and B-type elements in shades of blue. Adapted from [7].

Some geometric, electronic and thermodynamic factors based on the chemical alloy composition are well known to influence the formation and stability of a Laves phase [6,17]. Some of these structure-controlling factors are the atomic size parameters: atomic radius ratio between A- and B-type elements ($r_A/r_B$), atomic size mismatch (δ); electronegativity parameters: valence electron concentration (VEC), number of itinerant electrons (e/a), Pauling electronegativity difference ($\Delta\chi_{Pauling}$), and Allen electronegativity difference ($\Delta\chi_{Allen}$); and entropy of mixing ($\Delta S_{mix}$), enthalpy of mixing ($\Delta H_{mix}$), and Ω parameter. The most relevant parameters considered in this work are the valence electron concentration (VEC), atomic radius ratio between A- and B-type elements ($r_A/r_B$), and atomic size mismatch (δ).

The VEC of an alloy is calculated by Equation 3.14:

$$VEC = \sum c_i VEC_i \quad (3.14)$$

where $c_i$ is the atomic fraction and $VEC_i$ is the valence electron concentration of element $i$. $VEC_i$ is determined by considering the outer electron shell of the individual element. The total number of outer shell electrons for the A and B elements considered in the present study are Ti = 4 ($3d^2 4s^2$), Zr = 4 ($4d^2 5s^2$), Nb = 5 ($4d^4 5s^1$), V = 5 ($3d^2 4s^2$), Cr = 6 ($3d^5 4s^1$), Mn = 7 ($3d^5 4s^2$), Fe = 8 ($3d^6 4s^2$), Co = 9 ($3d^7 4s^2$), Ni = 10 ($3d^8 4s^2$), Cu = 11 ($3d^{10} 4s^1$), and Zn = 12 ($3d^{10} 4s^2$), as summarized in Table 3.2.

$r_A/r_B$ is calculated by Equation 3.15:

$$\frac{r_A}{r_B} = \frac{\sum_i c_i^A . r_i}{\sum_i c_i^B . r_i} \quad (3.15)$$

where $c_i^A$ and $c_i^B$ are the atomic fraction of element $i$ in the sublattices A and B, respectively (i.e., $\sum_i c_i^A = \sum_i c_i^B = 1$) and $r_i$ is atomic radius of element $i$.

δ is calculated by Equation 3.16:

$$\delta = \sqrt{\sum c_i \left(1 - \frac{r_i}{\bar{r}}\right)^2} \; x \; 100 \quad (3.16)$$

where $c_i$ and $r_i$ are the atomic fraction $i$ and $\bar{r} = \sum c_i r_i$ is the mean atomic radius of all elements in the alloy. In this work, we considered the atomic radius of the

pure elements reported by Guo et al [27]. The values of atomic radii of the elements considered in this work are displayed in Table 3.2.

Table 3. 2 - Atomic radii (metallic bond) and VEC of the A and B elements.

| Elements | | r [Å] [27] | VEC$_i$ |
|---|---|---|---|
| A | **Ti** | 1.46 | 4 |
| | **Zr** | 1.60 | 4 |
| | **Nb** | 1.47 | 5 |
| B | **Fe** | 1.27 | 8 |
| | **Mn** | 1.26 | 7 |
| | **Cr** | 1.28 | 6 |
| | **V** | 1.35 | 5 |
| | **Ni** | 1.25 | 10 |
| | **Co** | 1.25 | 9 |
| | **Zn** | 1.39 | 12 |
| | **Cu** | 1.28 | 11 |

Gorban et al. [28] in their study comprising the analysis of more than 200 high entropy alloys reported that the C14 Laves phase is typically formed in multicomponent alloys having VEC within the range of 4.4 – 8.1, but emphasized that single C14 Laves phase is formed in a range of 6.4 – 6.7. Zhu et al. [29] studied a series of transition metal Laves phases and reported that the C14 structure is stabilized in a range of 5.88 – 7.53.

Laves in his early studies showed that these structures can exist only at a particular value of $r_A/r_B$ = 1.225. Later, after years of investigation, studies reported that C14 Laves phase can be formed for $r_A/r_B$ ranging from 1.05 to 1.68 [28–31]. Yurchenko et al. [17] showed that Laves phase formation is observed when δ > 5%. In turn, the derived value δ > 5.0% for Laves phase formation in multicomponent alloys corresponds to the value of $r_A/r_B$ > 1.11. However, Gorban et al. [28] emphasize that the atomic radius ratio of the elements does not exceed 1.49.

### 3.3 Hydrogen storage in C14 Laves phase

In the C14 Laves phase, there are 17 interstitial sites per unit formula: 12 equivalent $A_2B_2$ sites, 4 equivalent $AB_3$ sites, and 1 $B_4$ site. All three types of interstitial sites are formed by tetrahedrons. As a result, the hydrogen absorption by these Laves phases increases the size of the unit cell continuously without changing the host structure. This behavior makes these Laves phase an attractive phase for structural investigation of hydrogen sorption. Although not all interstitial sites can be simultaneously occupied by hydrogen, this high variety of interstitial sites makes the $AB_2$ Laves phases exhibit excellent hydrogen absorption properties.

The Laves phase has attracted extensive attention on hydrogen storage properties due to their fast kinetics and high storage capacity at room temperature, sometimes without any activation treatment needed, and good structural stability. Theoretically, the C14-type Laves phase can form hydrides as rich as $AB_2H_{17}$, but the electrostatic forces between H neighbors as well as the large volume expansion are limitation factors, reducing the maximum number of six hydrogen atoms per $AB_2$ motif ($AB_2H_6$) such as for $YMn_2$. However, $YMn_2$ cannot be used for practical applications because its high stability [16,32–35]. As reported by Marques et al. [7] in their review on high-entropy alloys for hydrogen storage, the maximum hydrogen storage capacity of the alloys with single C14 Laves phase reported so far is in the range of 0.03 to 2.23 wt.% $H_2$. In terms of H/M, the reported values are between 0.02 and 1.17.

In studies of the hydrogen occupation of single C14 Laves phase alloys using Density functional theory (DFT) calculations and neutron diffraction measurements of deuterides [16,32–39], it was shown that hydrogen atoms prefer to occupy the $A_2B_2$- and $AB_3$-type interstitial sites, while $B_4$-type are never occupied. Further, in most of the Laves phase hydrides $AB_2H_x$, hydrogen atoms occupy only the $A_2B_2$ sites at low and intermediate hydrogen concentrations (up to $x \approx 2.5$) [38].

The $A_2B_2$ sites are preferentially occupied since their absolute value of the binding energy is substantially greater and consequently more energetically stable than $AB_3$ and $B_4$ sites. Moreover, their occupancy preference is related to

the trend for hydrogen to fill the tetrahedron constituted by two A atoms with a high hydrogen affinity as shown by Gesari et al. [16] and Merlino et al. [36] using density functional theory (DFT) calculations. Furthermore, previous experimental studies reported that the $AB_2$ C14 Laves phase produces a Laves phase hydrides with the composition $AB_2H_3$ which results in H/M = 1 [9,11,12,19].

Figure 3.10 shows all the 68 interstitial sites per unit cell (4 formula units per unit cell and 17 interstitial sites per formula unit). Table 3.3 shows the Wyckoff positions and the coordinates of the sites.

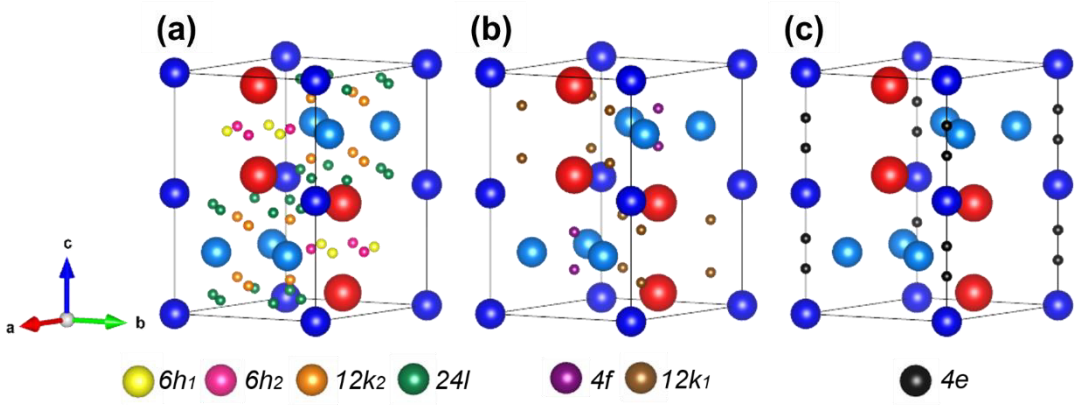


Figure 3. 10 - Interstitial sites per unit cell in the C14-type Laves phase (a) $A_2B_2$ sites: $6h_1$, $6h_2$, $12k_2$, and 24l (b) $AB_3$ sites: 4f and $12k_1$ and (c) $B_4$ sites: 4f. Structure drawn using software VESTA.

Table 3. 3 - Wyckoff positions and the coordinates of the interstitial sites.

| Sites | Wyckoff positions | Coordinates |
|---|---|---|
| **$A_2B_2$** | $6h_1$ | $x,2x,\frac{1}{4}$ |
| | $6h_2$ | $x,2x,\frac{1}{4}$ |
| | $12k_2$ | x, 2x, z |
| | 24l | x, y, z |
| **$AB_3$** | 4f | $\frac{1}{3},\frac{2}{3}$, z |
| | $12k_1$ | x,2x,z |
| **$B_4$** | 4e | 0,0,z |

Considering that the C14 Laves phase absorbs hydrogen only by solid solution, no equilibrium between two solid phases, i.e., a diluted hydrogen solid solution and a high concentration hydride, is considered. This condition results in an important characteristic of the PCT diagram, which is the absence of a well-defined plateau pressure. This behavior was reported for $Ti_{20}Zr_{20}Nb_5Fe_{40}Ni_{15}$ [11], $Ti_{0.5}Zr_{0.5}V_{0.5}Ni_{1.1}Mn_{0.2}Fe_{0.2}$ [12], and $Cr_uFe_vMn_wTi_xV_yZr_z$ [14] alloys with the predominant presence of C14 Laves phase.

However, experimental PCI diagrams of some C14 Laves phase presented a flat plateau, such as the $(TiZr)_1(CrMnFeNi)_2$ [10] and $Ti_1(Cr_{1.5}Mn_{0.5})_2$ [13] alloys. Which may suggest that a phase separation between a low hydrogen content solid solution and high hydrogen content hydride might occur for these alloys. This phase separation might be understood as a hydrogen miscibility gap in C14 Laves phase alloy. A miscibility gap means that there are two minimums in the $\Delta G_m(c_H)$ curve, which could result from a non-linear behavior of $\Delta \mathrm{H}_m(c_H)$ or for occupancy of preferential interstitial sites, which could affect $\Delta S_m(c_H)$.

Accordingly, the absorption only by solid solution results from the absence of two minimums in the $\Delta G_m(c_H)$ curve as illustrated in Figure 3.11(a), as reported by Marques et al. [7] for an α-phase for a hypothetical system. The schematic representation of the hydrogen equilibrium pressure as a function of the hydrogen content (PCI diagram) for this phase, without a well-defined plateau pressure, is illustrated in Figure 3.11(b).

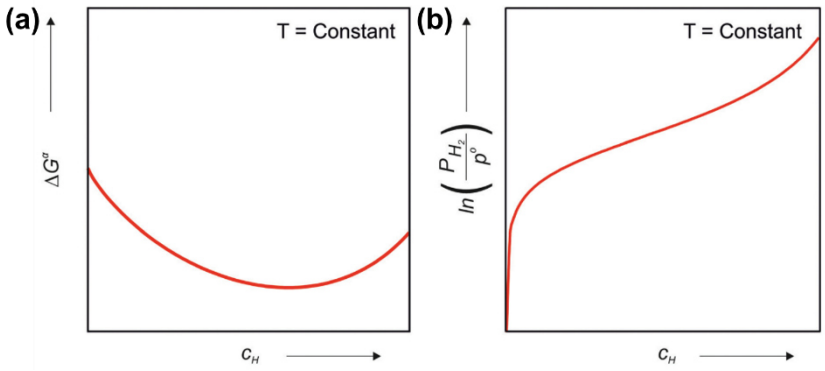


Figure 3. 11 - (a) Gibbs free energy of α-phase as function of $c_H$ for a hypothetical system for a given temperature and (b) its corresponding pressure-composition-isotherm diagram. Adapted from [7].

### 3.4 Design strategy of alloys for hydrogen storage

Among the models for multicomponent alloys design, the hydrogen storage studies are mainly relied on empirical and CALPHAD methods. Due to its simplicity, the empirical method allows the analytical screening of many systems; however, its predictive capacity is limited. The usefulness of this method in finding new promising systems could be improved by using more thermodynamically consistent approaches [7].

The empirical approach is fundamentally influenced by the Hume-Rothery rules for obtaining solid solution alloys. These rules state that extended solid solutions are favored in alloys whose elements have similar atom sizes, crystal structures, electronegativities and valences. To apply these concepts to predict the phase formation in complex alloys, the HEA community has developed composition-weighted terms, such as VEC and δ, as presented in Section 3.2. It is also worth mentioning the parameter $r_A/r_B$, often mentioned in studies of alloys with the ordered Laves phase. The appealing aspect of the empirical approach is its relative simplicity. Based on parameter calculations, many compositions can be evaluated enabling the construction of phase stability diagrams [6,7,17]. Some studies have focused on applying these empirical parameters to evaluate the parameters range of Laves phase formation, which is an important tool since Laves phase present significant potential for structural and functional applications, such as hydrogen storage [7,17,31].

Figure 3.12 shows some examples of phase stability diagrams or so-called structure maps, where the stable structure is given as function of the structure-controlling factors, such as the electronic and geometric parameters. Figure 3.12(a) shows the relationship between the parameters $\Delta\chi_{Allen}$ and δ for some selected HEAs. $\Delta\chi_{Allen}$ is calculated by Equation 3.17:

$$\Delta\chi_{Allen} = \sqrt{\sum c_i \left(1 - \frac{\chi_i^{Allen}}{\chi_a}\right)^2} \quad (3.17)$$

where $\chi_i^{Allen}$ is the Allen electronegativity of the element and $\chi_a = \sum c_i \chi_i^{Allen}$.

As can be seen, the Laves phases tend to form when the $\Delta\chi_{Allen}$ and δ values are higher (δ > 5.0% and $\Delta\chi_{Allen}$ > 7.0%), otherwise only solid solutions are found. This criterion correctly predicts Laves-phase formation in the

$AlCr_xNbTiV$ and $Al_xCrNbTiVZr$ alloys, as observed by Yurchenko et al. [17]. Figure 3.12(b) demonstrates the relationship between the parameters VEC and atomic radius ratio for some binary Laves phases with transition metals (circles and triangles mark C14 and C15 structures, respectively). As observed, the C14 Laves phase are stable within a restricted range of VEC and atomic radius ratio values [30].

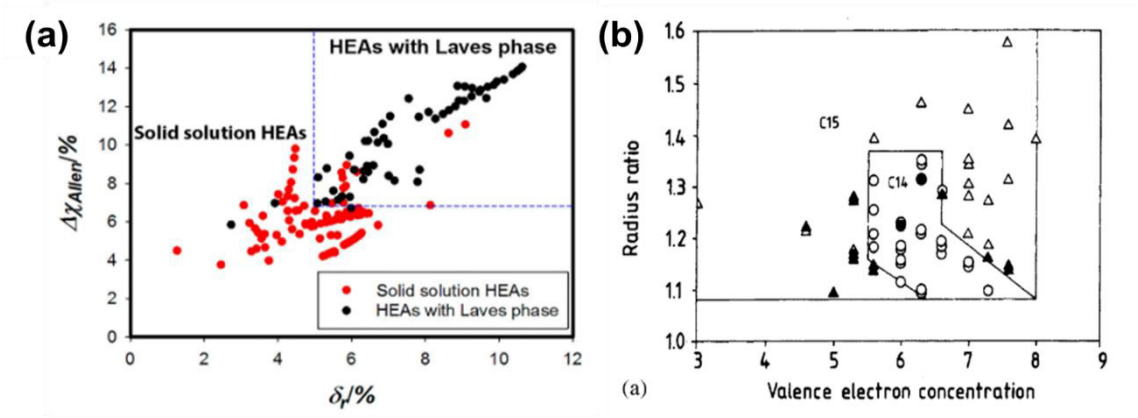


Figure 3. 12 - Phase stability diagrams showing the stability ranges of Laves phase (a) as function of the $\Delta\chi_{Allen}$ and δ for some selected HEAs (red dots correspond to solid solution HEAs and black dots HEAs with Laves phase, adapted from [17]) and (b) as function of the VEC and the atomic radius ratio for binary transition metal alloys (circles and triangles mark C14 and C15 structures, respectively; filled symbols indicate the existence of a temperature-dependent phase transition, adapted from [30]).

Table 3.4 shows a summary of characteristics including VEC, $r_A/r_B$, and δ parameters of some alloys with single C14 Laves phase reported in the literature. As observed, the values of these parameters are in accordance with the ideal range values described in Section 3.2. Table 3.4 shows some reported alloys with a single C14 Laves phase. This intermetallic compound for hydrogen storage is formed by combining a stable hydride forming element (A-type elements) with a nonstable hydride forming one (B-type elements), as mentioned above. The most prominent alloys from this group are those with Ti, Zr, and Nb on the A site and other transition metals on the B site, such as V, Cr, Mn, Fe, and Co.

Table 3. 4 – Summary of the reported alloys with single C14 Laves phase and their characteristics.

| Composition | Synthesis method | VEC | $r_A/r_B$ [c] | δ [d] | Maximum storage capacity [wt.% $H_2$] | Maximum storage capacity [H/M] | Ref. |
|---|---|---|---|---|---|---|---|
| **ZrTiVCrFeNi** | LENS[a] | 6.17[b] | 1.188 | 9.1 | 1.81 | 1.08[e] | [40] |
| **$(TiZr)_1(CrMnFeNi)_2$** | Arc melting | 6.4 | 1.209 | 9.7 | 1.70 | 1.00 | [10] |
| **$Ti_{20}Zr_{20}Nb_5Fe_{40}Ni_{15}$** | Arc melting | 6.5 | 1.198 | 9.9 | 1.38 | 0.95 | [11] |
| **$Zr_{19.4}Ti_{14.6}V_{8.6}Cr_{5.1}Mn_{7.5}Co_{6.4}Ni_{38.3}Sn_{0.1}$** | Arc melting | 6.46 | 1.197 | 13.8 | 1.45 | 0.91[e] | [41] |
| **$Ti_{0.5}Zr_{0.5}(V_{0.5}Ni_{1.1}Mn_{0.2}Fe_{0.2})_2$** | Arc melting | 6.83[b] | 1.193 | 9.5 | 1.64[e] | 1.00 | [12] |
| **$Ti_{0.9}Zr_{0.1}Mn_{1.4}V_{0.2}Cr_{0.4}$** | Arc melting | 5.73[b] | 1.180 | 7.4 | 2.03[e] | 1.10 | [42] |
| **$TiCr_{1.5}Mn_{0.5}$** | Arc melting | 5.50 | 1.150 | 6.5 | 1.91 | 0.99 | [13] |
| **CoFeMnTiVZr** | Arc melting | 6.78[b] | 1.167 | 8.6 | 1.70 | 1.00[e] | [43] |
| **$Cr_uFe_vMn_wTi_xV_yZr_z$ $0 \leq u, v, w, x, y, z \leq 2$** | Arc melting | 5.78-6.44[b] | 1.021-1.205 | 5.4-10.1 | 0.55-2.23 | 0.30-1.28[e] | [14] |
| **$(Ti_{0.8}Zr_{0.2})_{1.1}MnCr$** | Arc melting | 5.7[b] | 1.205[c] | 8.1[d] | 1.83 | 1.01[e] | [44] |
| **$Ti_{0.8}Zr_{0.2}Cr_{0.75}Mn_{1.25}Ce_{0.02}$** | Arc melting | 5.6[b] | 1.208[c] | 7.9[d] | 1.89 | 1.09[e] | [45] |

[a] LENS: laser engineered net shaping [b] VEC calculation based on Equation 13 [c] $r_A/r_B$ calculation based on Equation 14 [d] δ calculation based on Equation 15 [e] H/M or Wt.% calculation based on: $\frac{H}{M} = \frac{wt.\% * MM}{101 - 1.01 * wt.\%}$ and $wt.\% = \frac{\frac{H}{M} * 101}{MM + 1.01 * \frac{H}{M}}$ where MM= molar mass of the alloy (g/mol).

CALPHAD is a thermodynamic-based method that applies computational tools to calculate phase diagrams. The phase diagrams are obtained by using thermodynamic models that analytically assess the Gibbs–Helmholtz free energy for all expected competing phases. They give essential information for a given alloy composition and temperature, including the stable phases, their compositions, volume fractions, and transformation temperatures. The Redlich-Kistler functions, in polynomial form, constitute the thermodynamic models. Databases formed by experimental and theoretical data are used to fit the parameters of the polynomials [6,7].

It is a common practice in HEAs studies to investigate the predicted phases by CALPHAD at high temperatures (below the solidus temperature). This region usually favors the stability of solid solutions due to temperature contribution in the entropic term of the free energy [7]. Edalati et al. [10] and Floriano et al. [11] reported in their studies that these high-temperature phases are still present at room temperature, as verified by X-ray diffraction (XRD). The latter two works are related to single C14 Laves phase alloys. Therefore, the CALPHAD method can be helpful as a first approach to exploring the vast compositional space of multicomponent alloys. Figure 3.13 shows the phase diagram reported by Edalati et al. [10] for the $(TiZr)_1(CrMnFeNi)_2$ alloy.

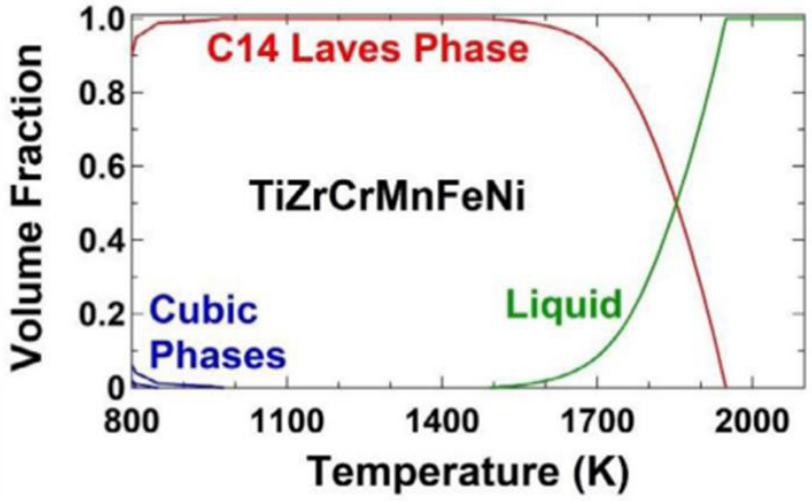


Figure 3. 13 - Volume fraction of equilibrium phases as a function of temperature calculated by CALPHAD for the $(TiZr)_1(CrMnFeNi)_2$ alloy. Adapted from [10].

As described above, the empirical and CALPHAD methods have been cited as methods that guided the design of the C14 Laves phase alloys. Most of the multicomponent alloys with Laves phase structure for hydrogen storage reported so far are equiatomic, although non-equiatomic compositions within the same alloy system has been studied since it could improve the hydrogen storage behavior as reported in [10,11].

The applicability of a MH in a specific hydrogen storage device is intrinsically related to its PCT diagram, which determines both the maximum hydrogen storage capacity and pressure-temperature operation condition. However, data collection of PCT diagrams is very time-consuming and experimental investigation of a large number of compositions within the multicomponent field is unpractical. Thus, computational tools that allows the prediction of the thermodynamic properties of multicomponent alloys-hydrogen systems are extremely helpful to navigate a large compositional field and to boost the discovery of new alloys with optimized properties for any specific application.

Recently, Zepon et al. [18] developed a thermodynamic model for calculating the PCT diagram for BCC multicomponent alloys, which yields relatively accurate predictions of PCT diagrams for different alloy compositions. In this model, three phases typically observed during the hydrogenation of BCC alloys were considered: the interstitial BCC solid solution (α-phase), the intermediate hydride with either BCC or BCT structure (β-phase), and the FCC hydride (δ-phase). The modeling considers the hydrogen-multicomponent alloy system under PE conditions. In these circumstances, an equilibrium condition is attained because hydrogen mobility allows the chemical potential of hydrogen to be the same in all the co-existing phases, resulting in a minimum free energy of the system ($\Delta G_m(c_H)$). The model estimates the enthalpy and entropy of hydrogen solution in the BCC phase by applying the necessary considerations regarding the phase structure and available interstitial sites for hydrogen absorption. The authors considered that the enthalpy of the phase ($\Delta H$) varies linearly with the hydrogen content and the coefficients of the linear function to describe the $\Delta H$ of each phase were determined using experimental data of binary hydrides (for α- and β- phases) and total energy calculation by DFT (for

the δ phase). The hydrogen partial molar enthalpy of a multicomponent phase was approximated by a mixture rule of the hydrogen partial molar enthalpy of the alloy components having the same structure as the considered phase. The entropy variation as a function of the hydrogen content was determined by applying the modeling proposed by Garcés [46] to describe the interstitial solid solution with site blocking effect (SBE).

Figure 3.14 illustrates the calculated PCT diagram using the thermodynamic model proposed by Zepon et al. [18] for the $(TiVNb)_{85}Cr_{15}$ alloy. The figure also presents the comparison of the calculated and experimental PCT diagrams for this alloy, and a good agreement is observed for all the evaluated temperatures.

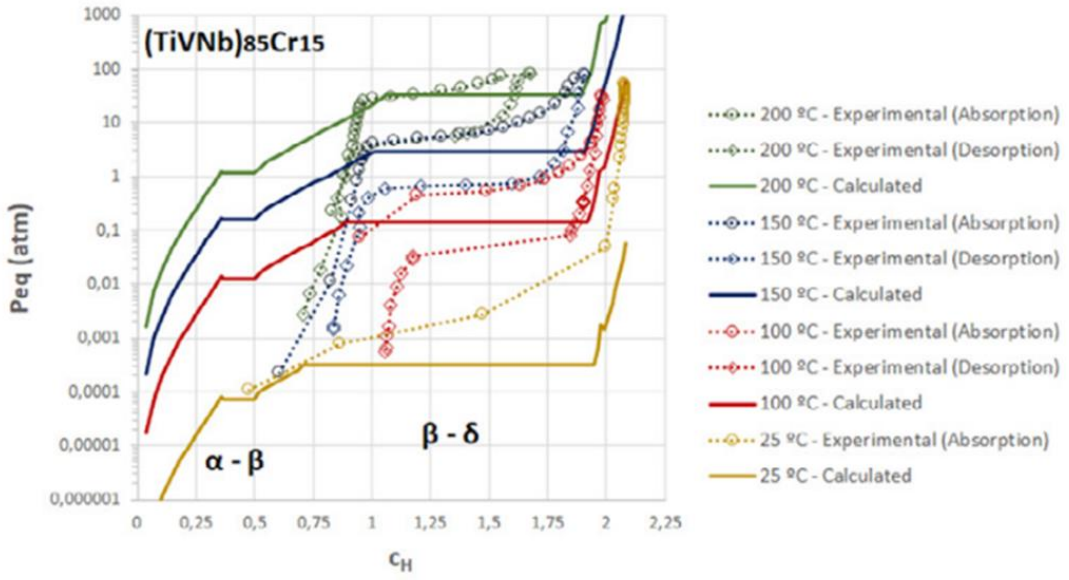


Figure 3. 14 - Comparison between the calculated and experimental PCT diagrams of $(TiVNb)_{85}Cr_{15}$ alloy. Adapted from [18].

### 3.5 Activation methods for C14 Laves phase alloys

The activation process is an important issue for hydrogen absorption alloys. In general, the authors report that activation treatments are necessary to make the alloys able to absorb hydrogen, i.e., the alloys can hardly absorb hydrogen when they are first exposed to hydrogen. This behavior has been reported for alloys with BCC structure, intermetallics and Mg-alloys, and the

conditions required for activation are usually high hydrogen pressure, high temperature, or long exposure time to vacuum [47–50].

Generally, the activation methodology for hydrogen absorption alloys is related to the surface state of the sample. The oxygen concentration in alloys designated for hydrogen absorption tests is considered a critical factor for proper absorption, and for most of these alloys, the surface can be easily contaminated by oxides formation when exposed to air. The surface oxide layer is considered as the main barrier for the hydrogen absorption by preventing the dissociation of hydrogen molecules into atoms and the penetration of hydrogen atoms into the bulk. Some authors suggested that the activation process occurs due to the formation of cracks in the surface layer of oxides, the dissociation of oxides into metals or suboxides, or the formation of new phases on the surface [48].

Regarding multicomponent alloys with the Laves C14 phase, the most commonly used activation process is to expose the alloy to an activation treatment by heating to 350 - 400 °C under dynamic vacuum for 1 - 2 h [7,13,51–53]. Nevertheless, very promising results have already been reported in terms of compositions that presented good hydrogen storage capacity without the need for an activation process [10,11].

Although many works have reported alloys with promising hydrogen storage properties after activation, only a few recent studies have focused on their activation procedures explanation [45,54–56]. Patel et al. [54] reported an alternative to the complicated activation of FeTi, which is usually conducted at relatively high temperature and pressure. The process is named self-shearing reactive milling (SSRM) and leads to the full hydrogenation of FeTi alloys. The process consists of the intense movement of the powder or even pieces of alloy under hydrogen pressure without any additional grinding media. The wear of particles, which is caused by their movement, causes the exposure of a fresh active alloy surface that is active enough to absorb hydrogen without any thermal treatment or evacuation.

Silva et al. [55] reported the use of process based on a nanosecond pulsed laser technique, named Pulsed Laser Activation (PLA) to activate hydrogen storage alloys. In their work, the $Ti_{11}V_{30}Nb_{28}Cr_{31}$ BCC alloy, which has been

previously exposed to air for 30 days, recovered the ability to absorb hydrogen reversibly after the PLA method. The authors consider that surface re-melting, the formation of oxide layers, and crack formation are the main factors that contributed to the activation of the alloy via PLA.

Small modifications in the alloy composition are also a methodology used to overcome complex or time-consuming activation procedures. Liu et al. [56] investigates the activation of TiFe alloys with different Ti/Fe ratios. Results shows that the $TiFe_{0.90}$ alloy can be activated at room temperature and moderate hydrogen pressure, in comparison with the poor activation kinetics of equimolar TiFe alloy. Furthermore, the authors described the activation behavior in four steps: first the hydrogen absorption by the $Ti_4Fe_2O_{1-x}$ oxide on the surfaces of the TiFe matrix; in the sequence the $Ti_4Fe_2O_{1-x}$ cracks; next the cracks extend into the TiFe matrix; and finally, the TiFe absorbs hydrogen.

In addition to small changes in the alloy composition, doping with specific elements can contribute to the activation or improvement of the hydrogen storage capacity of the alloys. Zhou et al. [45] demonstrated that the Ce-doping in the TiZrMnCr alloy improved the activation of the alloy at room temperature and enhanced the cyclic performance during the hydrogenation and dehydrogenation. The authors demonstrated that the Ce addition in the alloy slightly increased the lattice parameters of the major phase structure of Laves C14 and resulted in the formation of a $CeO_2$ phase.

# 4 MATERIALS AND METHODS

## 4.1 Design methods

### 4.1.1 Prediction of phase stability

The design strategy proposed in this work to find C14 Laves phase alloys comprises two steps: i) high-throughput calculation of electronic and geometrical factors to screen the alloys compositions prone to form C14 Laves phase; ii) CALPHAD calculations of these alloys to select only those predicted to solidify as single C14 Laves phase structure.

The first step consisted of the selection of the $AB_2$-type systems since the Laves phase presents this stoichiometry. The A elements considered in the designing process are Ti, Zr, and Nb, and the B elements are V, Cr, Mn, Fe, Co, Ni, Cu, and Zn. The designed alloys were divided into ten equiatomic systems (from binary to senary): $(A_1)(B_1)_2$, $(A_1A_2)(B_1)_2$, $(A_1)(B_1B_2)_2$, $(A_1A_2)(B_1B_2)_2$, $(A_1A_2A_3)(B_1)_2$, $(A_1)(B_1B_2B_3)_2$, $(A_1A_2)(B_1B_2B_3)_2$, $(A_1A_2A_3)(B_1B_2)_2$, $(A_1A_2A_3)(B_1B_2B_3)_2$ and $(A_1A_2)(B_1B_2B_3B_4)_2$. Considering all the possible permutations between the defined A- and B-type elements, we find 854 different alloy compositions that were evaluated by their VEC, $r_A/r_B$ , and δ values. For the sake of clarity, alloy compositions presenting equal atomic fractions of the elements in A and B sublattices will be referred to as “equiatomic”. On the other hand, “non-equiatomic compositions” are defined as those having A and B sublattices with different atomic fractions.

VEC, $r_A/r_B$, and δ parameters have been calculated. The $r_A/r_B$ values vary in the range from 1.05 to 1.28 for the 854 compositions. These values satisfied the geometrical factor required to obtain the C14-type Laves phase. Besides, the δ values for most of the alloys (except 10 compositions) also satisfied the geometrical factor required for the formation of the C14 Laves phase, as presented in the literature review in Section 3.2. Thereby, since the geometric factors $r_A/r_B$ and δ were favorable for most of the alloys, the electronic factor VEC became significant. In this way, all the compositions had the phase stability investigated by CALPHAD calculation to determine the range of VEC values of the compositions predicted to form the C14 Laves phase. Therefore, the equiatomic compositions were classified into three classes according to the

stable phases presented at high temperatures: i) C14 Laves phase alloys: the alloy was considered as C14 Laves phase when the CALPHAD calculation predicted solidification of the C14 Laves phase as major phase (> 95%); ii) multi-phase alloys: the alloy was considered a multiphase when it solidifies as multiple phases (BCC, FCC, C14 Laves, C15 Laves, etc.); and iii) C15 Laves phase alloys: the alloy was considered as C15 Laves phase when the CALPHAD calculation predicted solidification of the C15 Laves phase as major phase (> 95%). Among the multi-phase equiatomic compositions, some of them presented a fraction of the C14 Laves phase. The compositions related to these fractions were non-equiatomic $AB_2$ compositions and were investigated by CALPHAD resulting in new C14 Laves phase alloys. 354 non-equiatomic C14 Laves phase were identified.

Despite not being the phase of interest in this work, the C15 Laves phase was highlighted among the compositions calculated by CALPHAD since C15 Laves phase compositions appeared with a certain frequency (41 compositions) and it is also an attractive phase for hydrogen storage studies [57].

The amount of equilibrium phase as a function of temperature calculated by CALPHAD method was performed using the Thermo-Calc$^{TM}$ software and TCHEA5 database.

### 4.1.2 Thermodynamic model for PCT diagrams calculation

The thermodynamic model to calculate PCT diagrams of multicomponent C14-type Laves phase alloys proposed in this project was based on the model reported by Zepon et al. [18], who proposed a thermodynamic model for BCC multicomponent alloy systems under PE conditions. Thus, the present project proposes a first thermodynamic model for estimating the enthalpy and entropy of hydrogen solution in the C14 Laves phase alloys under PE, applying the necessary considerations regarding the C14 Laves phase structure and available interstitial sites for hydrogen absorption.

In this work, it was considered that the A-type elements (Ti, Zr, and Nb) will occupy the A positions and that the B-type elements (V, Cr, Mn, Fe, Co, Ni, Cu, and Zn) will occupy the B positions. In other words, there will be solid solution

formation of the A-type elements at the A sites and B-type elements at the B sites. It is worth noting that depending on the alloy composition (especially non-equiatomic alloys) A-type elements can partially occupy B sites and vice-versa.

Another consideration of this project is that the C14 Laves phase will absorb hydrogen only by solid solution, meaning that no equilibrium between two solid phases (a diluted hydrogen solid solution and a high concentration hydride, for example) will be considered. This condition results in an important characteristic of the PCT diagram, which is the absence of a well-defined plateau pressure. Furthermore, as a first approximation, this thermodynamic model will consider that hydrogen atoms will form an interstitial solid solution only in 12 $A_2B_2$ interstitial sites. All the considerations will be discussed in Section 5.1.2.

Applying these considerations related to C14 Laves phase structure, and experimental values from the literature, the thermodynamic equations presented in Section 3.1 for the general metal-hydrogen systems become specific to C14 Laves phase, as will be presented and discussed in the results section.

## 4.2 Experimental methods

### 4.2.1 Sample production

To verify the prediction capability of the design strategy and thermodynamic model proposed, seven compositions predicted to form single C14 Laves phase structure, namely $(Ti_{0.5}Zr_{0.5})_1Mn_2$, $(Ti_{0.5}Zr_{0.5})_1(Mn_{0.5}Cr_{0.5})_2$, $(Ti_{0.5}Zr_{0.5})_1(Fe_{0.5}Mn_{0.5})_2$, $(Ti_{0.5}Zr_{0.5})_1(Fe_{0.33}Mn_{0.33}Cr_{0.33})_2$, $(Ti_{0.33}Zr_{0.33}Nb_{0.33})_1(Mn_{0.5}Cr_{0.5})_2$, $(Ti_{0.33}Zr_{0.33}Nb_{0.33})_1(Fe_{0.5}Mn_{0.5})_2$, and $(Ti_{0.5}Nb_{0.5})_1(Fe_{0.5}Mn_{0.5})_2$ were selected, synthesized and characterized. Table 4.1 shows the chemical composition in atomic fraction, and the values of VEC, $r_A/r_B$, δ, and calculated hydrogen equilibrium pressure ($P_{H_2}$) for each of the seven alloys.

The alloys were selected in a wide range of equilibrium pressures (from approximately 0.01 to 68 bar) aiming to study C14 Laves phase alloys for different hydrogen storage applications.

Table 4. 1 - Concentration atomic fraction of the elements and the factors VEC, $r_A/r_B$, δ, and calculated hydrogen equilibrium pressure $(P_{H_2})$ of the seven selected alloys.

| Alloy | Concentration atomic fraction | | | | | | $r_A/r_B$ | VEC | δ | $P_{H_2}$ [bar] |
|---|---|---|---|---|---|---|---|---|---|---|
| | Ti | Zr | Nb | Fe | Mn | Cr | | | | |
| **$(TiZr)_1Mn_2$** | 16.67 | 16.67 | | | 66.67 | | 1.214 | 6.0 | 9.9 | 0.01 |
| **$(TiZr)_1(MnCr)_2$** | 16.67 | 16.67 | | | 33.33 | 33.33 | 1.205 | 5.7 | 9.5 | 1.81 |
| **$(TiZr)_1(FeMn)_2$** | 16.67 | 16.67 | | 33.33 | 33.33 | | 1.209 | 6.3 | 9.7 | 2.22 |
| **$(TiZr)_1(FeMnCr)_2$** | 16.67 | 16.67 | | 22.22 | 22.22 | 22.22 | 1.205 | 6.0 | 9.5 | 12.74 |
| **$(TiZrNb)_1(MnCr)_2$** | 11.11 | 11.11 | 11.11 | | 33.33 | 33.33 | 1.189 | 5.8 | 8.8 | 17.83 |
| **$(TiZrNb)_1(FeMn)_2$** | 11.11 | 11.11 | 11.11 | 33.33 | 33.33 | | 1.194 | 6.4 | 9.0 | 21.81 |
| **$(TiNb)_1(FeMn)_2$** | 16.67 | | 16.67 | 33.33 | 33.33 | | 1.158 | 6.5 | 7.1 | 68.45 |

The alloys were produced by arc-melting under an inert argon atmosphere, in electric arc furnaces (Arc Melter LSG 400 and MAM 1 from Edmund Buehler GmbH) available at the Laboratory of Amorphous and Nanocrystalline Metals (LabNano) at Department of Materials Engineering (DEMa/UFSCar). Samples weighting approximately 10 g were produced from pure elements (purity > 99%). In order to enhance the purity of the elements, the easily oxidizable Mn was subjected to a chemical cleaning procedure. This involved two cleaning solutions: initially, the Mn was immersed in a 5% HCl solution in distilled water for 1 minute, followed by washing with isopropyl alcohol. Subsequently, it was immersed in a solution of 1% $HNO_3$ in acetone for 2 minutes and then washed again with isopropyl alcohol. Before the arc-melting process, all elements were subjected to an ultrasonic bath in isopropyl alcohol and were subsequently dried.

As will be discussed in topic 4.2.4, four of the selected alloys did not absorb without activation treatment, namely $(Ti_{0.5}Zr_{0.5})_1Mn_2$, $(Ti_{0.5}Zr_{0.5})_1(Fe_{0.5}Mn_{0.5})_2$, $(Ti_{0.33}Zr_{0.33}Nb_{0.33})_1(Fe_{0.5}Mn_{0.5})_2$, $(Ti_{0.5}Nb_{0.5})_1(Fe_{0.5}Mn_{0.5})_2$. And one of these compositions, the $(Ti_{0.5}Zr_{0.5})_1(Fe_{0.5}Mn_{0.5})_2$ alloy, was produced with the addition of 0.4 wt.% of Ce. The high-purity Ce (purity > 99%) was stored submerged in vegetable oil to prevent oxidation. Prior to use, the Ce was careful cleaned using

a steel bristle brush followed by an ultrasonic bath in isopropyl alcohol. It remained immersed in isopropyl alcohol until transferred to the melting chamber.

All samples were melted following the same protocol. Titanium getters were melted before than the alloys to reduce the oxygen content in the melting chamber. To ensure chemical homogeneity, the samples were turned over and re-melted three times. The as-cast ingot samples were stored inside argon filled MBRAUM glovebox ($H_2O$ and $O_2$ levels below 0.1 ppm).

### 4.2.2 Structural and chemical characterization

The structural characterization was conducted via x-ray diffraction (XRD) using a Bruker D8 Advance Eco diffractometer with CuKα radiation (1.5406 Å) and an STOE STADI P transmission diffractometer with MoKα radiation (0.7093 Å) available at the Laboratory of Structural Characterization (LCE) at Department of Materials Engineering (DEMa/UFSCar) and Department of Heterogenous Catalysis at Max-Planck-Institut für kohlenforschung, respectively. For the XRD measurements using CuKα the data were collected in the 2θ range between 15° and 90° with a step width of 0.02°. For the XRD measurements using MoKα the data were collected in the 2θ range between 5° and 50° with a step width of 0.015°, and the samples were filled into 0.3 mm diameter borosilicate glass capillaries for the XRD analysis. The XRD profiles were analyzed by Rietveld refinement method using the GSAS-II software to determine lattice parameters and phase fraction [58]. The chemical composition and homogeneity of the as-cast alloys was evaluated by energy dispersive spectroscopy (EDX) using an Oxford EDX Detector in a Philips XL-30 FEG scanning electron microscope (SEM). The SEM-EDX analysis were conducted in the equipment available at the Laboratory of Structural Characterization (LCE) at Department of Materials Engineering (DEMa/UFSCar). For the XRD and EDX analysis, the as-cast ingot samples were crushed into powder inside argon filled MBRAUM glovebox ($H_2O$ and $O_2$ levels below 0.1 ppm) using an agate mortar and pestle.

Further, microstructure characterization of the samples was performed by SEM, using secondary electron (SE) and backscattered electron (BSE) signal

detectors that allow the evaluation of the morphology and chemical contrast of the different microstructural regions.

Oxygen determination by the inert gas fusion infrared detection method was applied in the samples as an additional chemical characterization analysis. The measurements were carried out in triplicate (0.1 g per analysis) in a LECO® equipment available in the Materials Characterization and Development Center (CCDM) at Department of Materials Engineering (DEMa/UFSCar). The test method applied for high precision oxygen and nitrogen determination in the alloys followed the ASTM 1409 standard [59].

### 4.2.3 Hydrogen storage properties

Hydrogen storage properties and performance were evaluated using structural and volumetric techniques. The storage properties evaluated in this work were: absorption kinetics, PCT diagrams, maximum hydrogen absorption capacity, desorption capacity, cyclability and reversibility for each of the evaluated alloys. The volumetric measurements were carried out in a Sieverts-type apparatus (Setaram PCT Pro version E&E) at the Laboratory of Hydrogen in Metals ($LH_2M$) at DEMa/UFSCar and Department of Heterogenous Catalysis at Max-Planck-Institut für kohlenforschung.

Initially, the absorption kinetics was evaluated by measuring the hydrogen uptake versus time for each alloy at room temperature by applying hydrogen pressure up to the maximum pressure of 80 bar. Before measurements, the ingot samples were crushed inside argon filled MBRAUM glovebox ($H_2O$ and $O_2$ levels below 0.1 ppm) using an agate mortar and pestle. The samples resulting from these experiments were characterized via XRD, and from Rietveld refinements the crystalline structures of the phase and their respective lattice parameters were determined. In addition, the microstructure and chemical homogeneity of these samples were evaluated by SEM-EDX.

PCT diagrams were assessed by acquiring PCI curves during hydrogen absorption and desorption at three different temperatures between 30 °C and 130 °C. The absorption and desorption PCI curves were recorded by applying doses of hydrogen up to the maximum pressure of 100 bar. After each measurement,

the sample was exposed to a dynamic vacuum for a few minutes at the current temperature. The thermodynamic properties of the hydride formation reactions (entropy and enthalpy in the pressure plateau region) were obtained through the Van't Hoff plot as shown by Equation 3.13 and Figure 3.4. In addition to determining the equilibrium pressure, and consequent comparison with the proposed thermodynamic modeling, other hydrogen storage properties and characteristics were evaluated for the selected alloys during the PCI measuments, such as the maximum hydrogen absorption capacity up to a maximum pressure of 100 bar, and the behavior during desorption.

The cycling behavior of the alloys was evaluated through absorption cycles followed by desorption cycles. The experimental conditions of temperature and initial hydrogen pressure were defined according to the first hydrogenation tests for each of the samples (kinetics and PCI measurements). For cycling experiments, the absorption kinetics were carried out under initial hydrogen pressures of 20 - 50 bar (small volume reservoir 13 - 17 $cm^3$, approximately). The desorption kinetics were carried out by reducing the hydrogen pressure in the sample to values below 1 bar. Therefore, the sample was not exposed to a vacuum during the desorption kinetics measurements. The hydrogen gas was expanded into the apparatus's largest volume reservoir (~ 1000 $cm^3$) to reach pressures below 1 bar. The alloys were subjected to a maximum of 50 cycles of hydrogen absorption and desorption without air or vacuum exposure. Some alloys had their cycling behavior analyzed with vacuum and temperature exposure.

Structural characterizations by XRD and EDX were performed on samples subjected to the first and last absorption/desorption cycles. In this way, it will be possible to relate the cycling behavior with possible structural and compositional changes of the alloys throughout the cycles.

### 4.2.4 Activation methodology

Using the empirical trial and error method based on the activation of other alloys reported in the literature, some activation procedures were evaluated for

some of the alloys that were not activated after synthesis, namely $(Ti_{0.5}Zr_{0.5})_1Mn_2$, $(Ti_{0.5}Zr_{0.5})_1(Fe_{0.5}Mn_{0.5})_2$, $(Ti_{0.33}Zr_{0.33}Nb_{0.33})_1(Fe_{0.5}Mn_{0.5})_2$, $(Ti_{0.5}Nb_{0.5})_1(Fe_{0.5}Mn_{0.5})_2$.

Firstly, the alloys were loaded into a Sieverts apparatus and exposed to dynamic vacuum for one hour. Then, an absorption kinetics measurement was carried out to verify whether the alloy was capable of absorbing hydrogen without the need for any activation procedure.

In the case of alloys capable of absorbing hydrogen without requiring any activation procedure, volumetric experiments were carried to fully characterize the hydrogen storage properties. Otherwise, the alloys that were not capable of absorbing hydrogen, some physical and physicochemical procedures were applied. One of the procedures applied was to subject the sample to heat treatment at 390 °C under dynamic vacuum for 12 h and subsequently cool it to room temperature before measuring the absorption kinetics.

Another procedure applied was to subject the sample to a thermo-chemical treatment. This procedure consisted of exposing the sample to a hydrogen pressure at room temperature for 1 h, then raising the temperature to 390 °C for 1 h under hydrogen pressure. Subsequently, the sample was cooled to room temperature while still under hydrogen pressure and finally exposed to a dynamic vacuum before measuring the absorption kinetics.

A doping procedure was applied through Ce addition. The $(Ti_{0.5}Zr_{0.5})_1(Fe_{0.5}Mn_{0.5})_2$ was doped with 0.4 wt.% of Ce. Ce is a rare earth metal and oxidizes very readily at room temperature. Due to this characteristic, Ce doping was used aiming at a possible reduction of oxygen content in the alloy, which would facilitate/induce the absorption of hydrogen by the alloy. After the production of the Ce-doped alloy, following the experimental procedure described in Section 4.2.1, the alloy was systematically studied by analyzing the effect of Ce on the microstructure, activation, and hydrogen storage properties.

# 5 RESULTS

## 5.1 Design methods

### 5.1.1 Prediction of phase stability

The phase stability of the 854 equiatomic compositions, resulted from all permutations between the A elements: Ti, Zr, and Nb; and B elements: V, Cr, Mn, Fe, Co, Ni, Cu, and Zn into ten equiatomic systems: $(A_1)(B_1)_2$, $(A_1A_2)(B_1)_2$, $(A_1)(B_1B_2)_2$, $(A_1A_2)(B_1B_2)_2$, $(A_1A_2A_3)(B_1)_2$, $(A_1)(B_1B_2B_3)_2$, $(A_1A_2)(B_1B_2B_3)_2$, $(A_1A_2A_3)(B_1B_2)_2$, $(A_1A_2A_3)(B_1B_2B_3)_2$ and $(A_1A_2)(B_1B_2B_3B_4)_2$, were evaluated.

VEC, $r_A/r_B$, and δ parameters have been calculated. As mentioned in the section 4.1.1 from the materials and methods, the $r_A/r_B$ values vary in the range from 1.05 to 1.28 for the 854 compositions. These values satisfied the geometrical factor required (1.05 – 1.68) to obtain the C14-type Laves phase. Besides, the δ values for most of the alloys (except 10 compositions) also satisfied the geometrical factor required (> 5 %) for the formation of the C14 Laves phase. Thereby, since the geometric factors $r_A/r_B$ and δ were favorable for most of the alloys, the electronic factor VEC became significant.

In this way, all the compositions had the phase stability investigated by CALPHAD calculation to determine the range of VEC values of the compositions predicted to form the C14 Laves phase.

Figure 5.1 display the 854 alloys in a $r_A/r_B$ versus VEC chart indicating the alloy classification as C14 Laves phase, multi-phase or C15 Laves phase alloys. 86 compositions were predicted to form C14 Laves phase structure by CALPHAD calculation and are represented by dark blue circles. The compositions that were predicted to form multi-phase alloys are represented by red rectangles. Finally, the 41 compositions predicted to form C15 Laves phase are represented by green triangles.

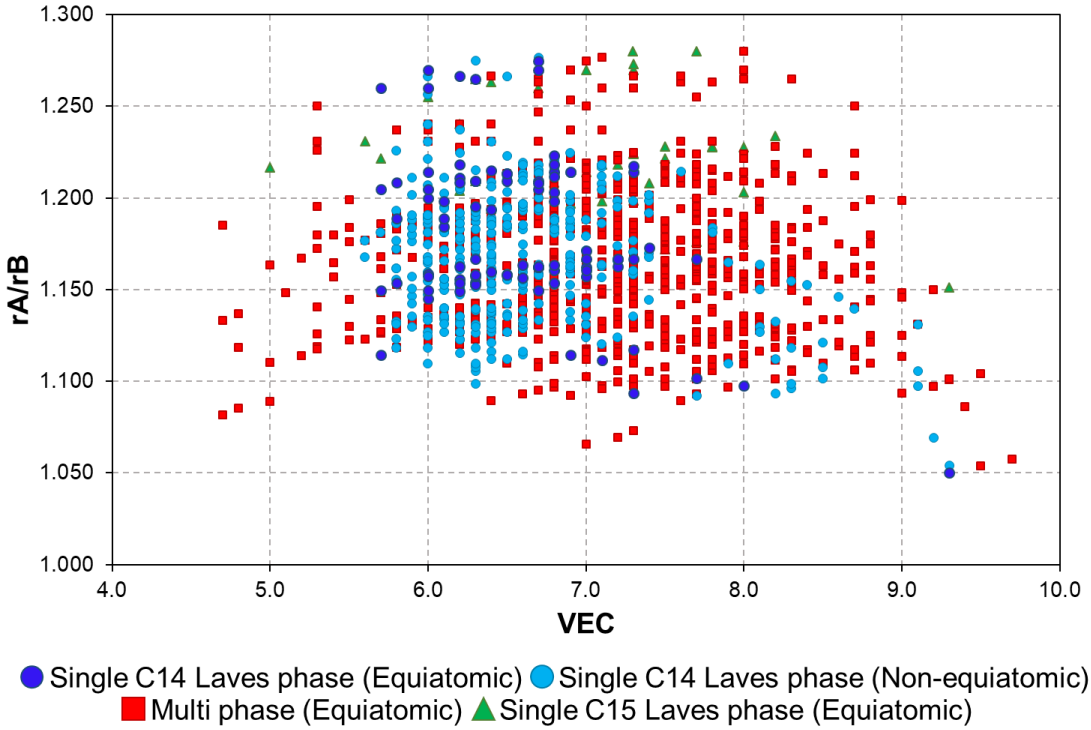


Figure 5. 1 - Results of the thermodynamic calculations by CALPHAD method from 854 equiatomic compositions and 354 non-equiatomic compositions displayed in a $r_A/r_B$ versus VEC chart.

As shown in Figure 5.1, the range of values with the highest incidence of C14 Laves phase alloys is 5.8 ≤ VEC ≤ 7.0 and 1.123 ≤ $r_A/r_B$ ≤ 1.223. Both ranges are in accordance with the reported values presented in the references (Section 3.2).

The highest incidence of compositions prone to solidify as C14 Laves phase could be related to the different lattices presented by the C14 and C15 Laves phase structures. The C14 Laves phase structure allows A-type elements to occupy one crystallographic position (A positions illustrated in Figure 3.6) and B-type elements to occupy two different crystallographic positions (B1 and B2 positions illustrated in Figure 3.6). The variable c/a lattice parameter ratio for the hexagonal structure of the C14 Laves phase is a consequence of such higher flexibility, which is not possible for the cubic C15-Laves phase. In C15 Laves phase structure both A and B atom sublattices are fixed and present only one crystallographic position for each of the atoms. Therefore, the accommodation of the different B-type elements is easier in the C14 structure compared to the C15

structure, which could be a reason for the greater number of compositions prone to solidify with the C14 Laves phase structure.

Among the equiatomic multi-phase compositions within the entire VEC range, 354 non-equiatomic compositions presented C14 Laves phase as one of the stable phases. These compositions were considered as new non-equiatomic alloys (represented by light blue circles) and their phase stability was evaluated by CALPHAD calculation. Therefore, in Figure 5.1, a total of 1208 compositions (854 equiatomic + 354 non-equiatomic) are displayed. According to the CALPHAD results the 354 non-equiatomic alloys were also classified as C14 Laves phase alloys. Therefore, through CALPHAD calculations we found 440 compositions predicted to form C14 Laves phase alloys (86 equiatomic + 354 non-equiatomic).

Table 5.1 shows the 86 equiatomic compositions with C14 Laves phase numbered from 1 to 86. The 354 non-equiatomic compositions with C14 Laves phase (numbered from 87 to 440) and the 41 equiatomic compositions with C15 Laves phase are shown in Table A1 and Table A2 in the Appendix A, respectively. The chemical composition in atomic fraction and the values of VEC, $r_A/r_B$, and δ are also given in Table 5.1, A1, and A2.

It is worth mentioning that among the 854 equiatomic compositions, 13 alloys solidified as BCC phase and these compositions are not presented in Figure 5.1, however, they are presented in Table A3 in the Appendix A.

Table 5. 1 - Equiatomic compositions predicted to form C14 Laves phase alloys by CALPHAD calculations. The alloys were numbered from 1 to 86. For each composition, the atomic fraction of the elements and their $r_A/r_B$, VEC, and δ parameter are presented.

| Alloy number | Concentration atomic fraction | | | | | | | | | | | $r_A/r_B$ | VEC | δ |
|---|---|---|---|---|---|---|---|---|---|---|---|---|---|---|
| | Ti | Zr | Nb | Fe | Mn | V | Cr | Ni | Co | Zn | Cu | | | |
| 1 | 0.3333 | | | 0.6667 | | | | | | | | 1.150 | 6.7 | 6.7 |
| 2 | 0.3333 | | | | 0.6667 | | | | | | | 1.159 | 6.0 | 7.1 |
| 3 | 0.3333 | | | | | | | | | 0.6667 | | 1.050 | 9.3 | 2.3 |
| 4 | | 0.3333 | | | 0.6667 | | | | | | | 1.270 | 6.0 | 11.7 |
| 5 | | | 0.3333 | 0.6667 | | | | | | | | 1.157 | 7.0 | 7.1 |
| 6 | | | 0.3333 | | 0.6667 | | | | | | | 1.167 | 6.3 | 7.4 |
| 7 | 0.1667 | 0.1667 | | 0.6667 | | | | | | | | 1.205 | 6.7 | 9.5 |
| 8 | 0.1667 | 0.1667 | | | 0.6667 | | | | | | | 1.214 | 6.0 | 9.9 |
| 9 | 0.1667 | | 0.1667 | 0.6667 | | | | | | | | 1.154 | 6.8 | 6.9 |
| 10 | 0.1667 | | 0.1667 | | 0.6667 | | | | | | | 1.163 | 6.2 | 7.3 |
| 11 | | 0.1667 | 0.1667 | | 0.6667 | | | | | | | 1.218 | 6.2 | 10.0 |
| 12 | 0.3333 | | | 0.3333 | 0.3333 | | | | | | | 1.154 | 6.3 | 6.9 |
| 13 | 0.3333 | | | 0.3333 | | 0.3333 | | | | | | 1.115 | 5.7 | 5.7 |
| 14 | 0.3333 | | | 0.3333 | | | 0.3333 | | | | | 1.145 | 6.0 | 6.5 |
| 15 | 0.3333 | | | 0.3333 | | | | | | 0.3333 | | 1.098 | 8.0 | 5.7 |

| | | | | | | | | | | | | |
|---|---|---|---|---|---|---|---|---|---|---|---|---|
| 16 | 0.3333 | | | | 0.3333 | 0.3333 | | | | 1.150 | 5.7 | 6.7 |
| 17 | 0.3333 | | | | 0.3333 | | | | 0.3333 | 1.102 | 7.7 | 6.0 |
| 18 | 0.3333 | | | | | 0.3333 | | | 0.3333 | 1.094 | 7.3 | 5.4 |
| 19 | | 0.3333 | | 0.3333 | 0.3333 | | | | | 1.265 | 6.3 | 11.5 |
| 20 | | 0.3333 | | | 0.3333 | 0.3333 | | | | 1.260 | 5.7 | 11.3 |
| 21 | | 0.3333 | | | 0.3333 | | | 0.3333 | | 1.275 | 6.7 | 11.9 |
| 22 | | | 0.3333 | 0.3333 | 0.3333 | | | | | 1.162 | 6.7 | 7.3 |
| 23 | | | 0.3333 | 0.3333 | | 0.3333 | | | | 1.153 | 6.3 | 6.9 |
| 24 | | | 0.3333 | 0.3333 | | | 0.3333 | | | 1.167 | 7.7 | 7.5 |
| 25 | | | 0.3333 | 0.3333 | | | | 0.3333 | | 1.167 | 7.3 | 7.5 |
| 26 | | | 0.3333 | | 0.3333 | 0.3333 | | | | 1.157 | 6.0 | 7.1 |
| 27 | | | 0.3333 | | 0.3333 | | | 0.3333 | | 1.171 | 7.0 | 7.6 |
| 28 | | | 0.3333 | | | 0.3333 | 0.3333 | | | 1.162 | 7.0 | 7.3 |
| 29 | | | 0.3333 | | | 0.3333 | | 0.3333 | | 1.162 | 6.7 | 7.3 |
| 30 | 0.1667 | 0.1667 | | 0.3333 | 0.3333 | | | | | 1.209 | 6.3 | 9.7 |
| 31 | 0.1667 | 0.1667 | | 0.3333 | | 0.3333 | | | | 1.200 | 6.0 | 9.3 |
| 32 | 0.1667 | 0.1667 | | 0.3333 | | | 0.3333 | | | 1.214 | 7.3 | 9.9 |
| 33 | 0.1667 | 0.1667 | | | 0.3333 | 0.3333 | | | | 1.205 | 5.7 | 9.5 |
| 34 | 0.1667 | 0.1667 | | | | 0.3333 | 0.3333 | | | 1.209 | 6.7 | 9.7 |
| 35 | 0.1667 | | 0.1667 | 0.3333 | 0.3333 | | | | | 1.158 | 6.5 | 7.1 |

| | | | | | | | | | | | | | |
|---|---|---|---|---|---|---|---|---|---|---|---|---|---|
| 36 | 0.1667 | | 0.1667 | 0.3333 | | 0.3333 | | | | 1.149 | 6.2 | 6.7 |
| 37 | 0.1667 | | 0.1667 | 0.3333 | | | 0.3333 | | | 1.163 | 7.2 | 7.3 |
| 38 | 0.1667 | | 0.1667 | | 0.3333 | 0.3333 | | | | 1.154 | 5.8 | 6.9 |
| 39 | 0.1667 | | 0.1667 | | | 0.3333 | 0.3333 | | | 1.158 | 6.5 | 7.1 |
| 40 | | 0.1667 | 0.1667 | 0.3333 | 0.3333 | | | | | 1.213 | 6.5 | 9.8 |
| 41 | | 0.1667 | 0.1667 | | 0.3333 | 0.3333 | | | | 1.209 | 5.8 | 9.6 |
| 42 | | 0.1667 | 0.1667 | | 0.3333 | | 0.3333 | | | 1.223 | 6.8 | 10.2 |
| 43 | 0.1111 | 0.1111 | 0.1111 | | 0.6667 | | | | | 1.198 | 6.1 | 9.2 |
| 44 | 0.3333 | | | 0.2222 | 0.2222 | 0.2222 | | | | 1.150 | 6.0 | 6.7 |
| 45 | 0.3333 | | | 0.2222 | 0.2222 | | | 0.2222 | | 1.117 | 7.3 | 6.4 |
| 46 | 0.3333 | | | 0.2222 | | 0.2222 | | 0.2222 | | 1.112 | 7.1 | 6.0 |
| 47 | 0.3333 | | | | 0.2222 | 0.2222 | 0.2222 | | | 1.156 | 6.2 | 7.0 |
| 48 | 0.3333 | | | | 0.2222 | 0.2222 | | 0.2222 | | 1.115 | 6.9 | 6.2 |
| 49 | | 0.3333 | | 0.2222 | 0.2222 | 0.2222 | | | | 1.260 | 6.0 | 11.3 |
| 50 | | 0.3333 | | 0.2222 | 0.2222 | | 0.2222 | | | 1.270 | 6.7 | 11.7 |
| 51 | | 0.3333 | | | 0.2222 | 0.2222 | 0.2222 | | | 1.266 | 6.2 | 11.6 |
| 52 | | | 0.3333 | 0.2222 | 0.2222 | 0.2222 | | | | 1.157 | 6.3 | 7.1 |
| 53 | | | 0.3333 | 0.2222 | 0.2222 | | 0.2222 | | | 1.167 | 7.2 | 7.5 |
| 54 | | | 0.3333 | 0.2222 | 0.2222 | | | 0.2222 | | 1.167 | 7.0 | 7.5 |
| 55 | | | 0.3333 | 0.2222 | | 0.2222 | 0.2222 | | | 1.161 | 7.0 | 7.2 |

| | | | | | | | | | | | |
|---|---|---|---|---|---|---|---|---|---|---|---|
| 56 | | | 0.3333 | 0.2222 | | 0.2222 | | 0.2222 | 1.161 | 6.8 | 7.2 |
| 57 | | | 0.3333 | | 0.2222 | 0.2222 | 0.2222 | | 1.164 | 6.8 | 7.4 |
| 58 | | | 0.3333 | | 0.2222 | 0.2222 | | 0.2222 | 1.164 | 6.6 | 7.4 |
| 59 | | | 0.3333 | | 0.2222 | | 0.2222 | 0.2222 | 1.173 | 7.4 | 7.7 |
| 60 | | | 0.3333 | | | 0.2222 | 0.2222 | 0.2222 | 1.167 | 7.2 | 7.5 |
| 61 | 0.1667 | 0.1667 | | 0.2222 | 0.2222 | 0.2222 | | | 1.205 | 6.0 | 9.5 |
| 62 | 0.1667 | 0.1667 | | 0.2222 | 0.2222 | | 0.2222 | | 1.214 | 6.9 | 9.9 |
| 63 | 0.1667 | 0.1667 | | 0.2222 | 0.2222 | | | 0.2222 | 1.214 | 6.8 | 9.9 |
| 64 | 0.1667 | 0.1667 | | 0.2222 | | 0.2222 | 0.2222 | | 1.208 | 6.7 | 9.7 |
| 65 | 0.1667 | 0.1667 | | 0.2222 | | | 0.2222 | 0.2222 | 1.218 | 7.3 | 10.0 |
| 66 | 0.1667 | 0.1667 | | | 0.2222 | 0.2222 | | 0.2222 | 1.211 | 6.2 | 9.8 |
| 67 | 0.1667 | 0.1667 | | | | 0.2222 | 0.2222 | 0.2222 | 1.214 | 6.9 | 9.9 |
| 68 | 0.1667 | | 0.1667 | 0.2222 | 0.2222 | 0.2222 | | | 1.154 | 6.2 | 6.9 |
| 69 | 0.1667 | | 0.1667 | 0.2222 | 0.2222 | | | 0.2222 | 1.163 | 6.7 | 7.3 |
| 70 | 0.1667 | | 0.1667 | 0.2222 | | 0.2222 | | 0.2222 | 1.157 | 6.6 | 7.1 |
| 71 | 0.1667 | | 0.1667 | | 0.2222 | 0.2222 | | 0.2222 | 1.160 | 6.4 | 7.2 |
| 72 | | 0.1667 | 0.1667 | 0.2222 | 0.2222 | 0.2222 | | | 1.209 | 6.2 | 9.6 |
| 73 | | 0.1667 | 0.1667 | 0.2222 | 0.2222 | | | 0.2222 | 1.218 | 6.8 | 10.0 |
| 74 | | 0.1667 | 0.1667 | | 0.2222 | 0.2222 | | 0.2222 | 1.215 | 6.4 | 9.9 |
| 75 | 0.1111 | 0.1111 | 0.1111 | 0.3333 | 0.3333 | | | | 1.194 | 6.4 | 9.0 |

| | | | | | | | | | | | |
|---|---|---|---|---|---|---|---|---|---|---|---|
| 76 | 0.1111 | 0.1111 | 0.1111 | 0.3333 | | 0.3333 | | | 1.184 | 6.1 | 8.6 |
| 77 | 0.1111 | 0.1111 | 0.1111 | | 0.3333 | 0.3333 | | | 1.189 | 5.8 | 8.8 |
| 78 | 0.1111 | 0.1111 | 0.1111 | | 0.3333 | | 0.3333 | | 1.203 | 6.8 | 9.4 |
| 79 | 0.1111 | 0.1111 | 0.1111 | 0.2222 | 0.2222 | 0.2222 | | | 1.189 | 6.1 | 8.8 |
| 80 | 0.1111 | 0.1111 | 0.1111 | 0.2222 | 0.2222 | | 0.2222 | | 1.198 | 6.8 | 9.2 |
| 81 | 0.1111 | 0.1111 | 0.1111 | | 0.2222 | 0.2222 | 0.2222 | | 1.195 | 6.3 | 9.1 |
| 82 | 0.1667 | 0.1667 | | 0.1667 | 0.1667 | 0.1667 | 0.1667 | | 1.209 | 6.5 | 9.7 |
| 83 | 0.1667 | 0.1667 | | 0.1667 | 0.1667 | 0.1667 | 0.1667 | | 1.209 | 6.3 | 9.7 |
| 84 | 0.1667 | 0.1667 | | 0.1667 | | 0.1667 | 0.1667 | 0.1667 | 1.212 | 6.8 | 9.8 |
| 85 | 0.1667 | 0.1667 | | 0.1667 | 0.1667 | 0.1667 | 0.1667 | | 1.158 | 6.3 | 9.7 |
| 86 | | 0.1667 | 0.1667 | 0.1667 | 0.1667 | 0.1667 | 0.1667 | | 1.213 | 6.5 | 9.8 |

Figure 5.2 shows diagrams of the amount of equilibrium phase as function of temperature calculated by CALPHAD for some evaluated compositions.

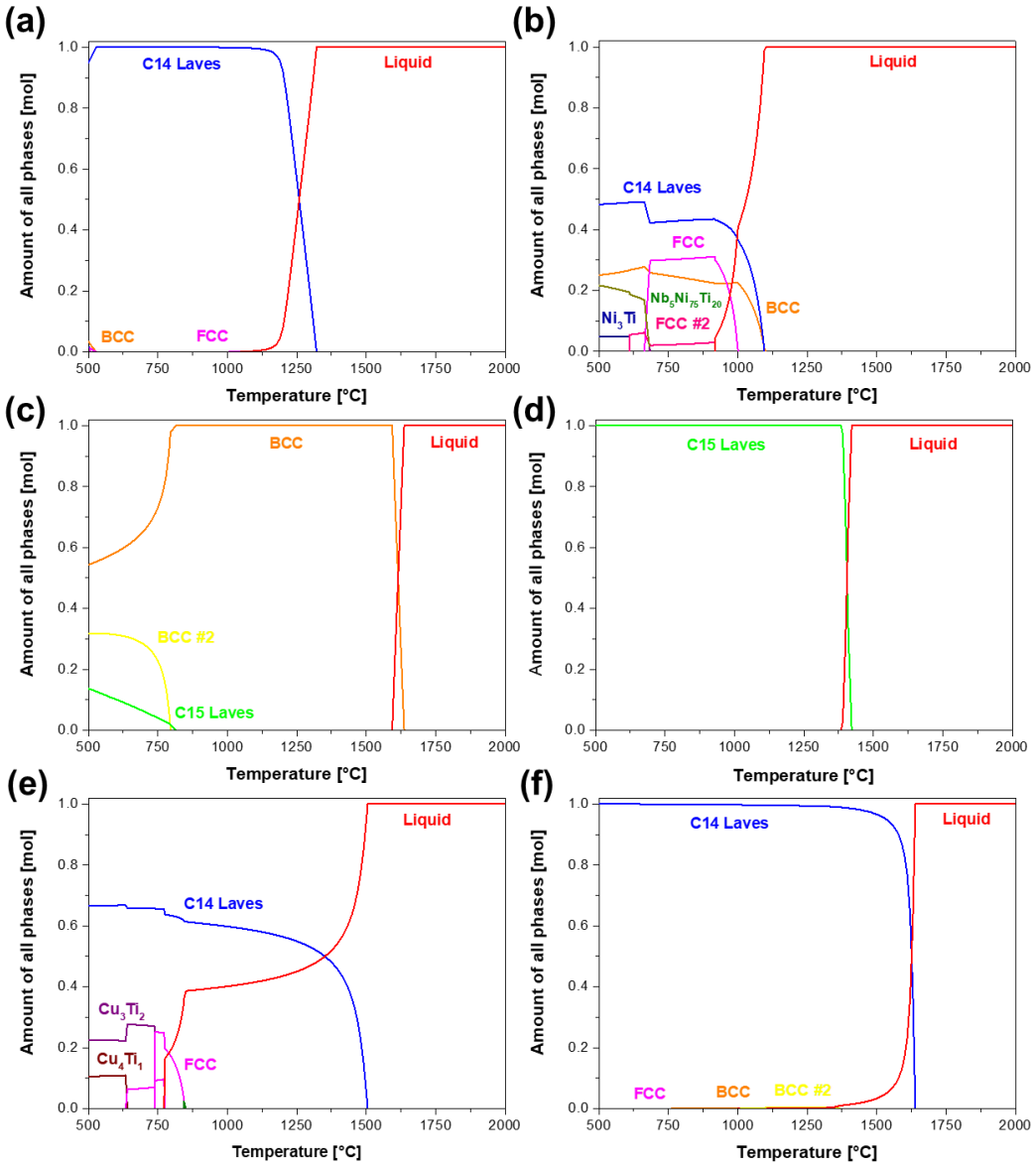


Figure 5. 2 - Amount of equilibrium phases as a function of temperature calculated for the $(Ti_{0.5}Zr_{0.5})_1(Fe_{0.33}Mn_{0.33}Co_{0.33})_2$, $(Ti_{0.5}Nb_{0.5})_1(Mn_{0.33}Ni_{0.33}Co_{0.33})_2$, $(Ti_{0.5}Nb_{0.5})_1(V_{0.5}Cr_{0.5})_2$, $(Ti_{0.5}Zr_{0.5})_1(Cr_{0.5}Co0.5)_2$, $(Ti_{0.5}Nb_{0.5})_1(Mn_{0.33}Cr_{0.33}Cu_{0.33})_2$, and $(Ti_{0.25}Nb_{0.75})_1(Mn_{0.49}Cr_{0.49}Cu_{0.02})_2$ compositions.

Figure 5.2 gives an example of each condition observed during the CALPHAD analyses, that is, calculations that resulted in a composition predicted

to solidify as: a C14 Laves phase composition - $(TiZr)_1(FeMnCo)_2$, a multiphase composition - $(Ti_{0.5}Nb_{0.5})_1(Mn_{0.33}Ni_{0.33}Co_{0.33})_2$, a BCC composition - $(TiNb)_1(VCr)_2$, a C15 Laves phase composition - $(Ti_{0.5}Zr_{0.5})_1(Cr_{0.5}Co_{0.5})_2$, a multiphase composition with a fraction of C14 Laves phase - $(Ti_{0.5}Nb_{0.5})_1(Mn_{0.33}Cr_{0.33}Cu_{0.33})_2$, and the non-equiatomic C14 Laves phase composition corresponding to this fraction - $(Ti_{0.25}Nb_{0.75})_1(Mn_{0.49}Cr_{0.49}Cu_{0.02})_2$.

The equiatomic $(Ti_{0.5}Zr_{0.5})_1(Fe_{0.33}Mn_{0.33}Co_{0.33})_2$ composition is indicated in Table 5.1 as alloy number 63. The thermodynamic calculation shows that the $(Ti_{0.5}Zr_{0.5})_1(Fe_{0.33}Mn_{0.33}Co_{0.33})_2$ alloy solidifies as single C14 Laves phase (Figure 5.2 (a)). In this case, the C14 Laves phase is stable below 1320 °C, and very small fraction (< 1%) of other phases are predicted to form upon cooling. The same behavior was reported by Edalati et al. in [10] for the $(TiZr)_1(CrMnFeNi)_2$ alloy, which indeed solidified with a major C14 Laves phase with a minor fraction of cubic phases when produced by arc melting.

Figure 5.2 (b) shows that the $(Ti_{0.5}Nb_{0.5})_1(Mn_{0.33}Ni_{0.33}Co_{0.33})_2$ solidifies as a multiphase alloy formed by C14 Laves phase, BCC phase and FCC phase. Upon cooling, the thermodynamic calculations predicted the formation of the $Ni_5Nb_{75}Ti_{20}$ (< 20%), and $Ni_3Ti$ (<5%) phases, in addition to the C14 Laves phase (< 50%) and BCC phase (< 25%).

Figure 5.2 (c) shows that the alloy $(Ti_{0.5}Nb_{0.5})_1(V_{0.5}Cr_{0.5})_2$ solidifies as single BCC phase. In this case, the BCC phase is stable below 1630 °C, and a fraction of other cubic phases (BCC and C15 Laves phase) are predicted to form upon cooling. Alloys of the Ti-Nb-V-Cr system have been widely studied for applications in hydrogen storage [60,61]. Some studies have reported that the alloys in this system have excellent hydrogen absorption capabilities and good reversibility at room temperature. Silva et al. [62] reported a similar CALPHAD diagram for the $Ti_{11}V_{30}Nb_{28}Cr_{31}$ alloy, and indeed the alloy solidify with the BCC phase structure. Strozi et al. [63] studied the $(TiVNb)_{100-x}Cr_x$ alloys and reported that when x =30, the alloy is single BCC phase, and when x = 35 and 40, the alloys are formed by BCC and C15 Laves phase.

The $(Ti_{0.5}Zr_{0.5})_1(Cr_{0.5}Co_{0.5})_2$ composition solidifies as single C15 Laves phase (Figure 5.2 (d)). The C15 Laves phase is stable below 1420 °C and no

other phase is predicted to form upon cooling. Figure 5.2 (e) shows that the $(Ti_{0.5}Nb_{0.5})_1(Mn_{0.33}Cr_{0.33}Cu_{0.33})_2$ composition solidifies as a multiphase alloy with a fraction of C14 Laves phase. The composition of this C14 Laves phase is non-equiatomic, i.e., it has an A and B sublattices with different atomic fractions. This non-equiatomic composition, $(Ti_{0.25}Nb_{0.75})_1(Mn_{0.49}Cr_{0.49}Cu_{0.02})_2$ is indicated in Table A1 in the Appendix A, as alloy number 211. The thermodynamic calculation shows that the $(Ti_{0.25}Nb_{0.75})_1(Mn_{0.49}Cr_{0.49}Cu_{0.02})_2$ alloy solidifies as single C14 Laves phase (Figure 5.2 (f)). In this case, the C14 Laves phase is stable below 1630 °C, and very small fraction (<1%) of other cubic phases are predicted to form upon cooling.

An alloy with a C14 Laves phase structure already reported in the literature by Edalati et al. [10] was taken as an example to validate the phase prediction experimentally. This composition $(Ti_{0.5}Zr_{0.5})_1(Cr_{0.25}Mn_{0.25}Fe_{0.25}Ni_{0.25})_2$ was reproduced in this work and the experimental characterization is presented below.

Firstly, the $(Ti_{0.5}Zr_{0.5})_1(Cr_{0.25}Mn_{0.25}Fe_{0.25}Ni_{0.25})_2$ composition presented the VEC, $r_A/r_B$, and δ values within the values range determined as ideal for the formation of the C14 Laves phase: VEC = 6.5, $r_A/r_B$ = 1.209, and δ = 9.7. Further, Figure 5.3 shows the diagram of the amount of equilibrium phase as function of temperature calculated by CALPHAD for the composition $(Ti_{0.5}Zr_{0.5})_1(Cr_{0.25}Mn_{0.25}Fe_{0.25}Ni_{0.25})_2$. One can see, the diagram shows that under equilibrium conditions, the alloy solidifies as a primary C14 Laves phase. Moreover, it is predicted that a minor fraction of BCC phase (<1%) forms in the final stage of the solidification at approximately 1190 °C. Other cubic phases are predicted to form upon cooling. Nonetheless, the formation of the cubic phases might be suppressed due to the high cooling rate imposed in the alloy synthesis process (arc-melting on a water-cooled copper base under an inert argon atmosphere).

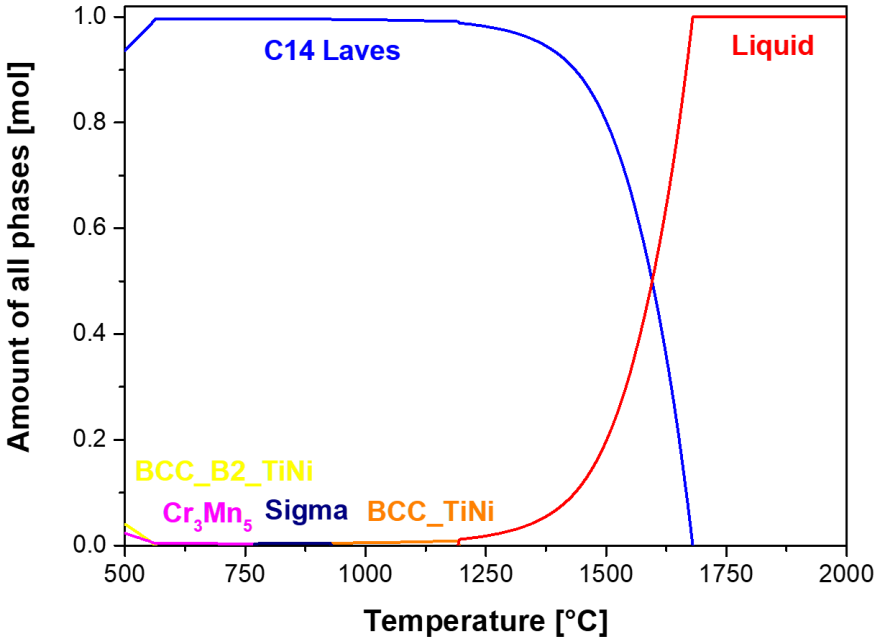


Figure 5. 3 - Amount of equilibrium phases as a function of temperature calculated for the $(Ti_{0.5}Zr_{0.5})_1(Cr_{0.25}Mn_{0.25}Fe_{0.25}Ni_{0.25})_2$ alloy.

Figure 5.4 presents the XRD pattern with the results of its Rietveld refinement for the as-cast $(Ti_{0.5}Zr_{0.5})_1(Cr_{0.25}Mn_{0.25}Fe_{0.25}Ni_{0.25})_2$ alloy confirming that the alloy has C14 Laves phase structure and a diminute fraction of a TiNi phase. According to CALPHAD, the TiNi phase can present a BCC structure (Im-3m) or an ordered B2 structure (Pm-3m). The lattice parameters obtained by the Rietveld refinement for the C14 Laves phase are a = 0.493 nm and c = 0.804 nm, and for the TiNi phase is a = 0.301 nm. These lattice parameters values are in accordance with the reported ones for this composition: C14 Laves phase a = 0.493 nm and c = 0.809 nm, and TiNi phase a = 0.305 nm [10]. Therefore, the proposed design method for phase stability prediction have been experimentally validate using the $(Ti_{0.5}Zr_{0.5})_1(Cr_{0.25}Mn_{0.25}Fe_{0.25}Ni_{0.25})_2$ composition.

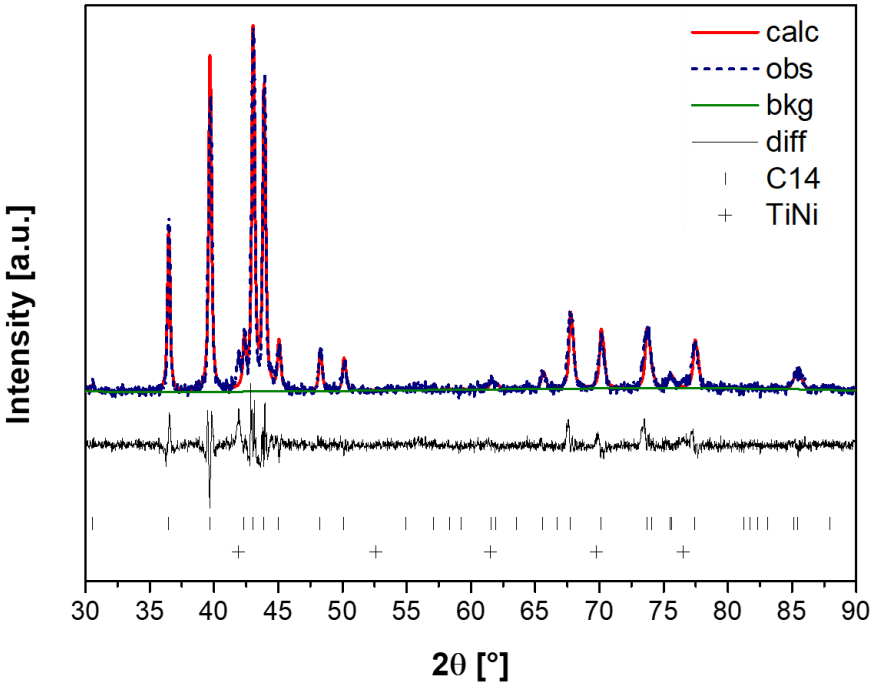


Figure 5. 4 - Rietveld refinement of the XRD pattern of the as-cast $(Ti_{0.5}Zr_{0.5})_1(Cr_{0.25}Mn_{0.25}Fe_{0.25}Ni_{0.25})_2$ alloy indicating that the sample formed C14 Laves phase structure and a very small amount of TiNi phase. (Measured with KαCu radiation).

Furthermore, the alloy's microstructure was investigated by SEM equipped with EDX. The result is shown in Figure 5.5. The as-cast sample presented a dendritic microstructure, as seen in the SEM-SE and SEM-BSE images. In these images it is also possible to see the small fraction of the cubic phase (darker region in the SE and BSE images).

Table 5.2 shows the chemical composition of the $(Ti_{0.5}Zr_{0.5})_1(Cr_{0.25}Mn_{0.25}Fe_{0.25}Ni_{0.25})_2$ alloy determined by SEM-EDX. EDX analyses were carried out in two ways: at all selected area (map measurement) and in the regions having only C14 Laves phase and only TiNi phase (point measurement). The results of the overall chemical composition and the chemical composition in the different phases regions are presented in Table 5.2.

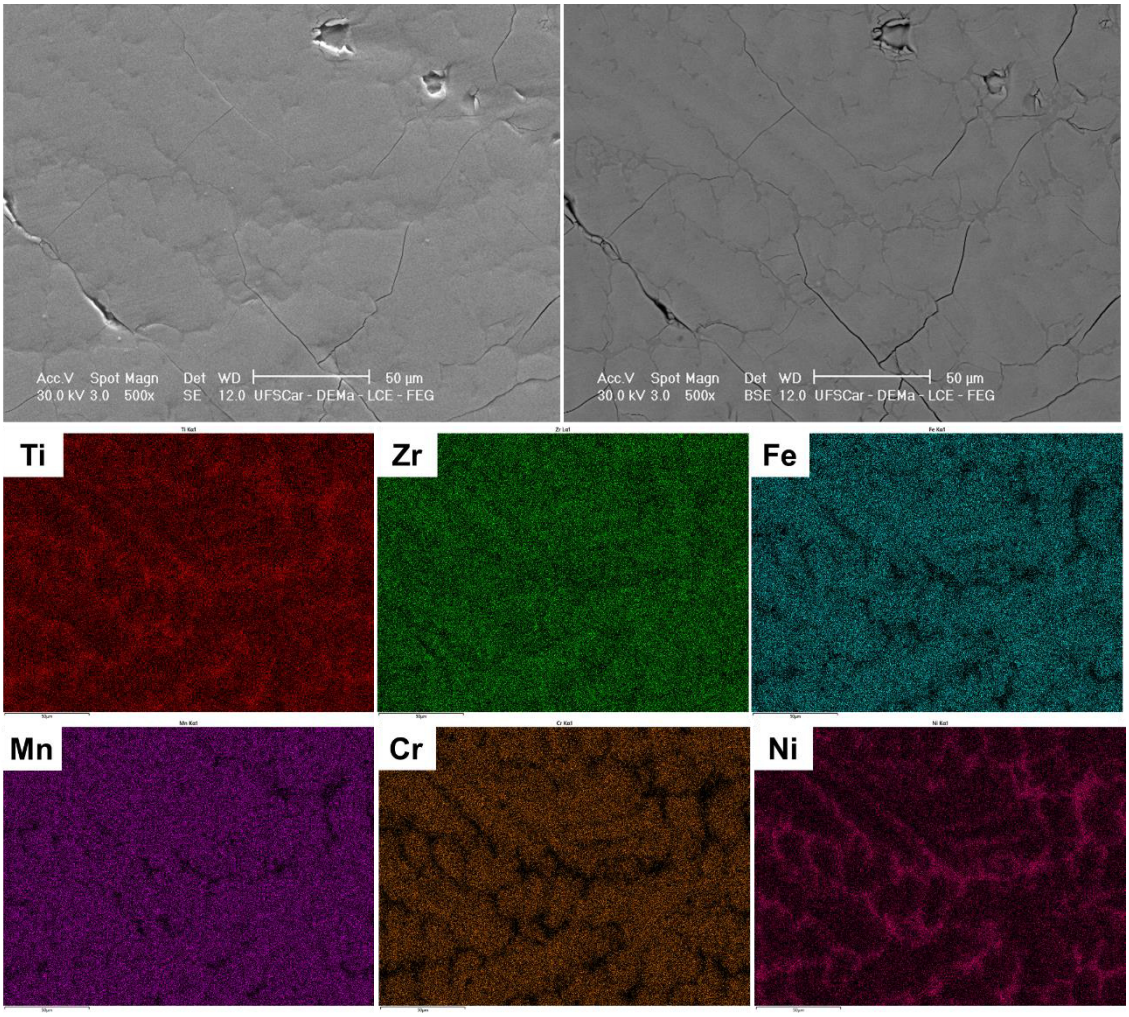


Figure 5. 5 - SEM (SE and BSE) images and corresponding EDX elemental maps of the as-cast $(Ti_{0.5}Zr_{0.5})_1(Cr_{0.25}Mn_{0.25}Fe_{0.25}Ni_{0.25})_2$ alloy.

Table 5. 2 - The chemical composition of the $(Ti_{0.5}Zr_{0.5})_1(Cr_{0.25}Mn_{0.25}Fe_{0.25}Ni_{0.25})_2$ alloy determined by SEM-EDX.

| | **Chemical composition in at% of the as-cast alloy** | | | | | |
|---|---|---|---|---|---|---|
| | **Ti** | **Zr** | **Fe** | **Mn** | **Cr** | **Ni** |
| **Nominal** | 16.67 | 16.67 | 16.67 | 16.67 | 16.67 | 16.67 |
| **Overall** | 17.85 | 17.05 | 16.75 | 16.95 | 14.75 | 16.65 |
| **C14** | 15.50 | 18.28 | 19.08 | 17.46 | 17.20 | 12.44 |
| **TiNi** | 29.44 | 12.69 | 7.14 | 9.79 | 4.04 | 36.84 |

As can be seen, the overall composition of the alloy is very close to the nominal one. In the C14 Laves phase region all the elements appear uniformly distributed; however, chemical composition of the phase is slightly poorer in Ti and Ni. In contrast, the TiNi phase region is richer in Ti and Ni.

### 5.1.2 Thermodynamic model for PCT diagrams calculation

As described in the materials and methods section (Section 4.1.2), the thermodynamic model to calculate PCT diagrams of multicomponent C14-type Laves phase alloys proposed in this project was based on the model reported by Zepon et al. [18], who proposed a thermodynamic model for BCC multicomponent alloy systems under PE conditions. Therefore, to develop the model to calculate the PCT diagrams of C14 Laves phase alloys the necessary considerations regarding the C14 Laves phase structure was applied.

As an initial consideration, it was assumed that the A-type elements (Ti, Zr, and Nb) occupy the A positions and that the B-type elements (V, Cr, Mn, Fe, Co, Ni, Cu, and Zn) occupy the B positions in the unit cell. In other words, there will be solid solution formation of the A-type elements at the A sites and B-type elements at the B sites. It is important to mention that especially for the non-equiatomic alloys A-type elements can partially occupy B sites and vice-versa, and this condition is considered in the model after CALPHAD calculation.

Further, it was considered that the C14 Laves phase absorbed hydrogen only by solid solution, meaning that no equilibrium between two solid phases was considered. This condition resulted in an important characteristic of the PCT diagram, which is the absence of a well-defined plateau. Furthermore, this thermodynamic model considered that hydrogen atoms formed an interstitial solid solution only in 12 $A_2B_2$ interstitial sites, resulting in H/M = 1. As discussed in Section 3.3, the $A_2B_2$ sites are preferentially occupied since their absolute value of the binding energy is substantially larger and consequently more energetically stable than $AB_3$ and $B_4$ sites. Moreover, their occupancy preference is related to the trend for hydrogen to fill the tetrahedron constituted by two A atoms with a high hydrogen affinity [16,36].

Regarding the thermodynamic equations for metal-hydrogen interaction, the equations for a general metal-hydrogen system (Section 3.1) become specific to C14 Laves phase as presented hereafter.

The entropy of a phase can be expressed as the sum of the configurational ($S_c$) and non-configurational ($S_{nc}$) terms. However, in this work it is assumed that the difference between the non-configurational terms of $MH_{C_H}$ and $M$ is negligible. Therefore, the entropy of hydrogen mixing given by Equation 3.4 becomes Equation 5.1 for the C14 Laves phase.

$$\Delta S_m(C_H) = S_c\left(MH_{c_H}^{C14}\right) - S_c(M^{C14}) - \frac{c_H}{2}S^0(H_2) \quad (5.1)$$

where $S_c\left(MH_{c_H}^{C14}\right)$ is the configurational entropy of the C14 Laves phase with hydrogen content equal to $c_H$ . $S_c(M^{C14})$ is the configurational entropy of the alloy in its reference state, which in this work is considered as being the alloy with C14 structure without hydrogen, i.e. $c_H = 0$. $S_c(M^{C14})$ can be calculated as the sum of the contribution of the ideal configurational entropy of the sublattice A and sublattice B weighted by their atomic fractions as given by Equation 5.2.

$$S_c(M^{C14}) = -R\left(\frac{1}{3}\sum_i c_i^A lnc_i^A + \frac{2}{3}\sum_i c_i^B lnc_i^B\right) \quad (5.2)$$

where R is the ideal gas constant, $c_i^A$ is the atomic fraction of element $i$ in the sublattice A, and $c_i^B$ is the atomic fraction of element $i$ in the sublattice B (therefore, $\sum c_i^A = \sum c_i^B = 1$).

$S_c\left(MH_{c_H}^{C14}\right)$ is described as the sum of the configurational entropy of the substitutional solid solution of the metal lattice and the configurational entropy of the interstitial solid solution of hydrogen in the interstitial sites as given in Equation 5.3. Is worth noting that the configurational entropy expression considers the SBE, as proposed by J. Garcés [46]. The occupation of an interstitial site is blocked by the previous occupation of a neighboring site when considering SBE.

$$S_c\left(MH_{c_H}^{C14}\right) = -R\left[\frac{1}{3}\sum_i c_i^A lnc_i^A + \frac{2}{3}\sum_i c_i^B lnc_i^B + c_H ln\left(\frac{c_H}{\theta - [(r-1)c_H]}\right)\right.$$
$$\left. + (\theta - rc_H) ln\left(\frac{\theta - rc_H}{\theta - [(r-1)c_H]}\right)\right] \quad (5.3)$$

where $\theta$ is the number of interstitial sites per atom of metal and $r$ is associated with the number of interstitial sites that are blocked and do not participate in the mixing process. Since we are considering that 12 interstitial sites $A_2B_2$ will be occupied by hydrogen atoms, and there are 12 atoms of metal per unit cell of C14 Laves phase, $\theta$ = 1. In this work, no site blocking effect (SBE) will be considered to occur for the C14 Laves phase, therefore, $r$ = 1. Thereby, by replacing Equations 3.6, 5.2 and 5.3, $\theta$ = 1, and $r$ = 1 into Equation 5.1, $\Delta S_m(C_H)$ becomes Equation 5.4.

$$\Delta S_m(C_H) = -R[c_H ln c_H + (1 - c_H) ln(1 - c_H)] - \frac{c_H}{2} S^{\circ}_{H_2} \quad (5.4)$$

A second approximation of this model is that the enthalpy of hydrogen mixing $\Delta H_m(c_H)$ in the C14 Laves phase varies linearly with the hydrogen concentration. Therefore, the enthalpy of hydrogen mixing given by Equation 3.5 becomes Equation 5.5 for the C14 Laves phase.

$$\Delta H_m(c_H) = H_{C14} + h_{C14} c_H \quad (5.5)$$

where $H_{C14}$ is a constant and $h_{C14}$ is the hydrogen partial molar enthalpy of the phase. Since the chosen reference state was the C14 Laves phase alloy without hydrogen, $c_H = 0$, then $H_{C14}$ = 0. For the C14 Laves phase, $h_{C14}$ will be described as a sum of the contribution of the hydrogen partial molar enthalpy of the pure elements in the sublattice A and sublattice B in the $A_2B_2$ tetrahedron occupied by the hydrogen, as given by Equation 5.6.

$$h_{C14} = \frac{1}{2}\sum_i c_i^A \Delta H_i^{\infty} + \frac{1}{2}\sum_i c_i^B \Delta H_i^{\infty} \quad (5.6)$$

In this work, we approximate the contribution of the hydrogen partial molar of an element $i$ by its enthalpy of hydrogen solution at infinite dilution $\Delta H_i^{\infty}$. Experimental values of $\Delta H_i^{\infty}$ are available in the literature [64]. Table 5.3 presents the values of $\Delta H_i^{\infty}$ for the A and B elements considered in this work.

Table 5. 3 - Hydrogen heat of hydrogen solution at infinite dilution of the A and B elements.

| Elements | | $\Delta H_i^{\infty}$ **[kJ/mol H]** [64] |
|---|---|---|
| **A** | **Ti** | -52 |
| | **Zr** | -52 |
| | **Nb** | -35 |
| **B** | **Fe** | 29 |
| | **Mn** | 1 |
| | **V** | -26 |
| | **Cr** | 28 |
| | **Ni** | 10 |
| | **Co** | 21 |
| | **Zn** | 15 |
| | **Cu** | 46 |

More details regarding the deduction of the Equation 4.6 can be obtained through the total bond energy between elements A and B with the hydrogen atom at the interstitial site $A_2B_2$, as shown in Figure 5.6. This model assumes that the binding energy of element $i$ with hydrogen is approximated by $\varepsilon_{i-H} = \frac{\Delta H_i^{\infty}}{4}$ (considering that in a tetrahedron site four metal-hydrogen bonds are formed). Therefore, $h_{C14} = 2\varepsilon_{A-H} + 2\varepsilon_{B-H}$, where $\varepsilon_{A-H} = \sum c_i^A \frac{\Delta H_i^{\infty}}{4}$ and $\varepsilon_{B-H} = \sum c_i^B \frac{\Delta H_i^{\infty}}{4}$, which yields Equation 5.6.

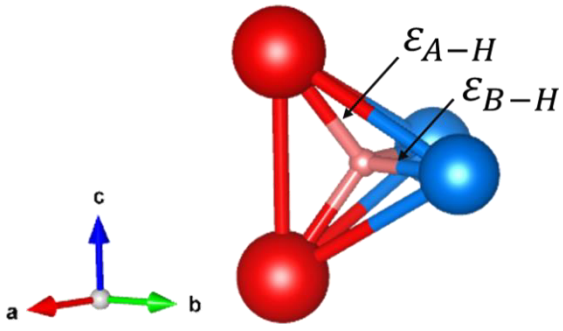


Figure 5. 6 - $A_2B_2$ sites formed by a tetrahedron having 2 bonds with energy $\varepsilon_{A-H}$ and 2 bonds with energy $\varepsilon_{B-H}$.

In possession of $\Delta S_m(c_H)$ and $\Delta H_m(c_H)$, the Gibbs free energy of hydrogen mixing in the C14 Laves phase can be easily assessed as given by Equation 3.3. It is important to emphasize that the Gibbs free energy of the C14 Laves phase depends only on $c_H$ because we are considering PE condition, therefore, the chemical composition of the C14 Laves phase in terms of metal atoms is maintained constant during hydrogenation.

The thermodynamic equilibrium of the M-H system depends on the hydrogen chemical potential of the possible phases in the system. Since we are considering that the C14 Laves phase will absorb hydrogen only by solid solution, there are just one solid phase in the system. Besides, the phase is in equilibrium when their chemical potential of hydrogen and chemical potential of the metal atoms are the same. Therefore, to determine the hydrogen concentration in solid solution in a C14 Laves phase for a given hydrogen pressure ($P_{H_2}$) and a given temperature, both hydrogen chemical potential of the C14 Laves (Equation 3.8) and the hydrogen chemical potential of $H_2$ gas (Equation 3.7) must be the same, i.e., $\mu_H^{C14} = \mu_H^{H_2}$. From Equations 3.3, 5.4, 5.5 and 5.6, $\mu_H^{C14}(c_H)$ can be determined analytically. Therefore, Equation 3.8 becomes Equation 5.7.

$$\mu_H^{C14}(c_H) = h_{C14} - T\left[-Rln\left(\frac{c_H}{1-c_H}\right) - \frac{S^{\circ}_{H_2}}{2}\right] \quad (5.7)$$

Thereby, having $\mu_H^{C14}(c_H)$ and $\mu_H^{H_2}$, PCI curves can be calculated using Equation 5.8, as show in Figure 5.7.

$$ln\left(\frac{P_{H_2}}{p^0}\right) = \frac{2}{RT}\left(h_{C14} - T\left[-Rln\left(\frac{c_H}{1-c_H}\right) - \frac{S^{\circ}_{H_2}}{2}\right]\right) \quad (5.8)$$

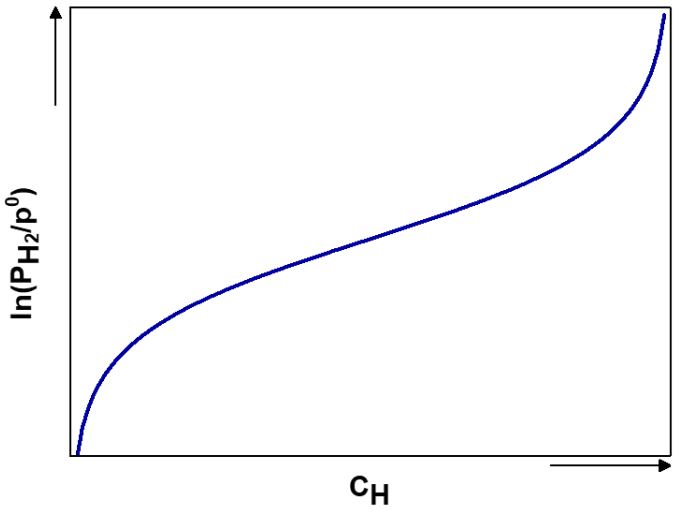


Figure 5. 7 - Hydrogen equilibrium pressure as a function of the hydrogen content in the C14 Laves phase for a hypothetical system at a constant temperature.

Once the equation to calculate the PCI curves was determined we could calculate the PCI curves at room temperature for all the alloys predicted to form C14 Laves phase structures. For the calculation of the PCI curves (or PCT diagrams), it is necessary first to calculate $h_{C14}$ for all the alloys. The $c_i^A$ and $c_i^B$ values for each one of the 440 alloys are shown in Table 5.4 for the equiatomic alloys and in Table A4 for the non-equiatomic alloys in the Appendix A. Tables 5.4 and A4 also presents the resultant $h_{C14}$ and equilibrium pressure at $c_H$ = 0.5 for each alloy.

Table 5. 4 - Atomic fraction of element $i$ in the sublattice A and sublattice B for each one of the 86 equiatomic alloys with tendency to form C14 Laves phase. For each composition are also presented the $h_{C14}$, molar weight (M), maximum theoretical hydrogen content (considering H/M=1), and equilibrium pressure at $c_H$ = 0.5.

| Alloy number | Site fraction sublattice A | | | Site fraction sublattice B | | | | | | | hC14 | M alloy [g/mol] | $c_{H_{MAX}}$ [wt.%] | $P_{H_2}$ [bar] |
|---|---|---|---|---|---|---|---|---|---|---|---|---|---|---|
| | Ti | Zr | Nb | Fe | Mn | V | Cr | Ni | Co | Zn | Cu | | | | |
| 1 | 1 | | | 1 | | | | | | | | -11.50 | 53.19 | 1.86 | $6.2x10^{5}$ |
| 2 | 1 | | | | 1 | | | | | | | -25.50 | 52.59 | 1.88 | $7.7x10^{-3}$ |
| 3 | 1 | | | | | | | | | 1 | | -18.50 | 59.55 | 1.67 | $2.2x10^{0}$ |
| 4 | | 1 | | | 1 | | | | | | | -25.50 | 67.03 | 1.48 | $7.7x10^{-3}$ |
| 5 | | | 1 | 1 | | | | | | | | -3.00 | 68.20 | 1.46 | $5.9x10^{5}$ |
| 6 | | | 1 | | 1 | | | | | | | -17.00 | 67.59 | 1.47 | $7.3x10^{0}$ |
| 7 | 0.5 | 0.5 | | 1 | | | | | | | | -11.50 | 60.41 | 1.64 | $6.2x10^{2}$ |
| 8 | 0.5 | 0.5 | | | 1 | | | | | | | -25.50 | 59.81 | 1.66 | $7.7x10^{-3}$ |
| 9 | 0.5 | | 0.5 | 1 | | | | | | | | -7.25 | 60.70 | 1.64 | $1.9x10^{4}$ |
| 10 | 0.5 | | 0.5 | | 1 | | | | | | | -21.25 | 60.09 | 1.65 | $2.4x10^{-1}$ |
| 11 | | 0.5 | 0.5 | | 1 | | | | | | | -21.25 | 67.31 | 1.48 | $2.4x10^{-1}$ |
| 12 | 1 | | | 0.5 | 0.5 | | | | | | | -18.50 | 52.89 | 1.87 | $2.2x10^{0}$ |
| 13 | 1 | | | 0.5 | | 0.5 | | | | | | -25.25 | 51.56 | 1.92 | $9.4x10^{-3}$ |
| 14 | 1 | | | 0.5 | | | 0.5 | | | | | -11.75 | 51.91 | 1.91 | $5.1x10^{2}$ |

| | | | | | | | | | | | | | | |
|---|---|---|---|---|---|---|---|---|---|---|---|---|---|---|
| 15 | 1 | | | 0.5 | | | | | 0.5 | -15.00 | 56.37 | 1.76 | $3.7x10^{1}$ |
| 16 | 1 | | | | 0.5 | 0.5 | | | | -18.75 | 51.60 | 1.92 | $1.8x10^{0}$ |
| 17 | 1 | | | | 0.5 | | | | 0.5 | -22.00 | 56.07 | 1.77 | $1.3x10^{-1}$ |
| 18 | 1 | | | | | 0.5 | | | 0.5 | -15.25 | 55.09 | 1.80 | $3.0x10^{1}$ |
| 19 | | 1 | | 0.5 | 0.5 | | | | | -18.50 | 67.34 | 1.48 | $2.2x10^{0}$ |
| 20 | | 1 | | | 0.5 | 0.5 | | | | -18.75 | 66.05 | 1.51 | $1.8x10^{0}$ |
| 21 | | 1 | | | 0.5 | | | 0.5 | | -20.50 | 68.36 | 1.46 | $4.4x10^{-1}$ |
| 22 | | | 1 | 0.5 | 0.5 | | | | | -10.00 | 67.90 | 1.47 | $2.1x10^{3}$ |
| 23 | | | 1 | 0.5 | | 0.5 | | | | -3.25 | 66.92 | 1.49 | $4.9x10^{5}$ |
| 24 | | | 1 | 0.5 | | | 0.5 | | | -7.75 | 69.15 | 1.44 | $1.3x10^{4}$ |
| 25 | | | 1 | 0.5 | | | | 0.5 | | -5.00 | 69.23 | 1.44 | $1.2x10^{5}$ |
| 26 | | | 1 | | 0.5 | 0.5 | | | | -10.25 | 66.61 | 1.49 | $1.7x10^{3}$ |
| 27 | | | 1 | | 0.5 | | | 0.5 | | -12.00 | 68.93 | 1.44 | $4.2x10^{2}$ |
| 28 | | | 1 | | | 0.5 | 0.5 | | | -8.00 | 67.86 | 1.47 | $1.0x10^{4}$ |
| 29 | | | 1 | | | 0.5 | | 0.5 | | -5.25 | 67.95 | 1.46 | $9.7x10^{4}$ |
| 30 | 0.5 | 0.5 | | 0.5 | 0.5 | | | | | -18.50 | 60.11 | 1.65 | $2.2x10^{0}$ |
| 31 | 0.5 | 0.5 | | 0.5 | | 0.5 | | | | -11.75 | 59.13 | 1.68 | $5.1x10^{2}$ |
| 32 | 0.5 | 0.5 | | 0.5 | | | 0.5 | | | -16.25 | 61.36 | 1.62 | $1.3x10^{1}$ |
| 33 | 0.5 | 0.5 | | | 0.5 | 0.5 | | | | -18.75 | 58.83 | 1.69 | $1.8x10^{0}$ |
| 34 | 0.5 | 0.5 | | | | 0.5 | 0.5 | | | -16.50 | 60.08 | 1.65 | $1.1x10^{1}$ |

| | | | | | | | | | | | | |
|---|---|---|---|---|---|---|---|---|---|---|---|---|
| 35 | 0.5 | | 0.5 | 0.5 | 0.5 | | | | -14.25 | 60.39 | 1.64 | $6.8x10^{1}$ |
| 36 | 0.5 | | 0.5 | 0.5 | | 0.5 | | | -7.50 | 59.41 | 1.67 | $1.6x10^{4}$ |
| 37 | 0.5 | | 0.5 | 0.5 | | | 0.5 | | -9.25 | 61.72 | 1.61 | $3.8x10^{3}$ |
| 38 | 0.5 | | 0.5 | | 0.5 | 0.5 | | | -14.50 | 59.11 | 1.68 | $5.5x10^{1}$ |
| 39 | 0.5 | | 0.5 | | | 0.5 | 0.5 | | -9.50 | 60.44 | 1.64 | $3.1x10^{3}$ |
| 40 | | 0.5 | 0.5 | 0.5 | 0.5 | | | | -14.25 | 67.62 | 1.47 | $6.8x10^{1}$ |
| 41 | | 0.5 | 0.5 | | 0.5 | 0.5 | | | -14.50 | 66.33 | 1.50 | $5.5x10^{1}$ |
| 42 | | 0.5 | 0.5 | | 0.5 | | 0.5 | | -16.25 | 68.64 | 1.45 | $1.3x10^{1}$ |
| 43 | 0.3333 | 0.3333 | 0.3333 | | 1 | | | | -22.67 | 62.40 | 1.59 | $7.6x10^{-2}$ |
| 44 | 1 | | | 0.3333 | 0.3333 | 0.3333 | | | -16.33 | 52.13 | 1.90 | $1.3x10^{1}$ |
| 45 | 1 | | | 0.3333 | 0.3333 | | | 0.3333 | -18.50 | 55.11 | 1.80 | $2.2x10^{0}$ |
| 46 | 1 | | | 0.3333 | | 0.3333 | | 0.3333 | -14.00 | 54.45 | 1.82 | $8.3x10^{1}$ |
| 47 | 1 | | | | 0.3333 | 0.3333 | 0.3333 | | -17.67 | 52.82 | 1.88 | $4.3x10^{0}$ |
| 48 | 1 | | | | 0.3333 | 0.3333 | | 0.3333 | -18.67 | 54.25 | 1.83 | $1.9x10^{0}$ |
| 49 | | 1 | | 0.3333 | 0.3333 | 0.3333 | | | -16.33 | 66.58 | 1.49 | $1.3x10^{1}$ |
| 50 | | 1 | | 0.3333 | 0.3333 | | 0.3333 | | -17.50 | 68.12 | 1.46 | $4.9x10^{0}$ |
| 51 | | 1 | | | 0.3333 | 0.3333 | 0.3333 | | -17.67 | 67.27 | 1.48 | $4.3x10^{0}$ |
| 52 | | | 1 | 0.3333 | 0.3333 | 0.3333 | | | -7.83 | 67.14 | 1.48 | $1.2x10^{4}$ |
| 53 | | | 1 | 0.3333 | 0.3333 | | 0.3333 | | -10.83 | 68.63 | 1.45 | $1.1x10^{3}$ |
| 54 | | | 1 | 0.3333 | 0.3333 | | 0.3333 | | -9.00 | 68.68 | 1.45 | $4.7x10^{3}$ |

| | | | | | | | | | | | | |
|---|---|---|---|---|---|---|---|---|---|---|---|---|
| 55 | | | 1 | 0.3333 | | 0.3333 | 0.3333 | | -6.33 | 67.98 | 1.46 | $4.0x10^{4}$ |
| 56 | | | 1 | 0.3333 | | 0.3333 | | 0.3333 | -4.50 | 68.03 | 1.46 | $1.8x10^{5}$ |
| 57 | | | 1 | | 0.3333 | 0.3333 | 0.3333 | | -11.00 | 67.77 | 1.47 | $9.3x10^{2}$ |
| 58 | | | 1 | | 0.3333 | 0.3333 | | 0.3333 | -9.17 | 67.83 | 1.47 | $4.1x10^{3}$ |
| 59 | | | 1 | | 0.3333 | | 0.3333 | 0.3333 | -12.17 | 69.32 | 1.44 | $3.6x10^{2}$ |
| 60 | | | 1 | | | 0.3333 | 0.3333 | 0.3333 | -7.67 | 68.66 | 1.45 | $1.4x10^{4}$ |
| 61 | 0.5 | 0.5 | | 0.3333 | 0.3333 | 0.3333 | | | -16.33 | 59.36 | 1.67 | $1.3x10^{1}$ |
| 62 | 0.5 | 0.5 | | 0.3333 | 0.3333 | | 0.3333 | | -19.33 | 60.84 | 1.63 | $1.1x10^{0}$ |
| 63 | 0.5 | 0.5 | | 0.3333 | 0.3333 | | | 0.3333 | -17.50 | 60.90 | 1.63 | $4.9x10^{0}$ |
| 64 | 0.5 | 0.5 | | 0.3333 | | 0.3333 | 0.3333 | | -14.83 | 60.19 | 1.65 | $4.2x10^{1}$ |
| 65 | 0.5 | 0.5 | | | 0.3333 | 0.3333 | | 0.3333 | -17.67 | 61.73 | 1.61 | $4.3x10^{0}$ |
| 66 | 0.5 | 0.5 | | 0.3333 | | | 0.3333 | 0.3333 | -16.00 | 60.04 | 1.65 | $1.6x10^{1}$ |
| 67 | 0.5 | 0.5 | | | | 0.3333 | 0.3333 | 0.3333 | -16.17 | 60.88 | 1.63 | $1.4x10^{1}$ |
| 68 | 0.5 | | 0.5 | 0.3333 | 0.3333 | 0.3333 | | | -12.08 | 59.64 | 1.67 | $3.9x10^{2}$ |
| 69 | 0.5 | | 0.5 | 0.3333 | 0.3333 | | | 0.3333 | -13.25 | 61.18 | 1.62 | $1.5x10^{2}$ |
| 70 | 0.5 | | 0.5 | 0.3333 | | 0.3333 | | 0.3333 | -8.75 | 60.53 | 1.64 | $5.7x10^{3}$ |
| 71 | 0.5 | | 0.5 | | 0.3333 | 0.3333 | 0.3333 | | -15.25 | 60.32 | 1.65 | $3.0x10^{1}$ |
| 72 | | 0.5 | 0.5 | 0.3333 | 0.3333 | 0.3333 | | | -12.08 | 66.86 | 1.49 | $3.9x10^{2}$ |
| 73 | | 0.5 | 0.5 | 0.3333 | 0.3333 | | | 0.3333 | -13.25 | 68.40 | 1.46 | $1.5x10^{2}$ |
| 74 | | 0.5 | 0.5 | | 0.3333 | 0.3333 | | 0.3333 | -13.42 | 67.55 | 1.47 | $1.3x10^{2}$ |

| | | | | | | | | | | | | |
|---|---|---|---|---|---|---|---|---|---|---|---|---|
| 75 | 0.3333 | 0.3333 | 0.3333 | 0.5 | 0.5 | | | | -15.67 | 62.71 | 1.59 | $2.2x10^1$ |
| 76 | 0.3333 | 0.3333 | 0.3333 | 0.5 | | 0.5 | | | -8.92 | 61.73 | 1.61 | $5.0x10^3$ |
| 77 | 0.3333 | 0.3333 | 0.3333 | | 0.5 | 0.5 | | | -15.92 | 61.42 | 1.62 | $1.8x10^1$ |
| 78 | 0.3333 | 0.3333 | 0.3333 | | 0.5 | | | 0.5 | -17.67 | 63.74 | 1.56 | $4.3x10^0$ |
| 79 | 0.3333 | 0.3333 | 0.3333 | 0.3333 | 0.3333 | 0.3333 | | | -13.50 | 61.95 | 1.60 | $1.2x10^2$ |
| 80 | 0.3333 | 0.3333 | 0.3333 | 0.3333 | 0.3333 | | | 0.3333 | -14.67 | 63.49 | 1.57 | $4.8x10^1$ |
| 81 | 0.3333 | 0.3333 | 0.3333 | | 0.3333 | 0.3333 | | 0.3333 | -14.83 | 62.64 | 1.59 | $4.2x10^1$ |
| 82 | 0.5 | 0.5 | | 0.25 | 0.25 | 0.25 | 0.25 | | -17.50 | 60.10 | 1.65 | $4.9x10^0$ |
| 83 | 0.5 | 0.5 | | 0.25 | 0.25 | 0.25 | | 0.25 | -16.13 | 60.14 | 1.65 | $1.5x10^1$ |
| 84 | 0.5 | 0.5 | | 0.25 | | 0.25 | 0.25 | 0.25 | -15.00 | 60.76 | 1.64 | $3.7x10^1$ |
| 85 | 0.5 | | 0.5 | 0.25 | 0.25 | 0.25 | | 0.25 | -11.88 | 60.14 | 1.65 | $4.6x10^2$ |
| 86 | | 0.5 | 0.5 | 0.25 | 0.25 | 0.25 | | 0.25 | -11.88 | 67.64 | 1.47 | $4.6x10^2$ |

As mentioned in the Section 3.3, the thermodynamic model considered that the C14 Laves phase absorbs hydrogen only by solid solution, which means that no equilibrium between two solid phases (a diluted hydrogen solid solution and a high concentration hydride) is considered. This condition results in an important characteristic of the PCI curve, which is the absence of a well-defined plateau pressure. Therefore, the equilibrium pressure is always considered at $c_H$ = 0.5 (in the middle of the calculated PCI curve).

Figure 5.8 shows the calculated PCI diagrams at room temperature for 86 equiatomic compositions predicted to solidify as C14 Laves phase (Table 5.1 shows all the information of the alloys identified by the alloy numbers). As can be seen, a wide range of hydrogen equilibrium pressure at room temperature was found (for the sake of clarity, we will always refer to the equilibrium pressure at $c_H$ = 0.5). The minimum hydrogen equilibrium pressure of $7.6 \times 10^{-3}$ bar was found for the $TiMn_2$, $ZrMn_2$, and $(Ti_{0.5}Zr_{0.5})_1Mn_2$ compositions (alloys 2, 4, and 8, respectively). The maximum hydrogen equilibrium pressure of $5.9 \times 10^{5}$ atm was observed for the $NbFe_2$ composition (alloy number 5).

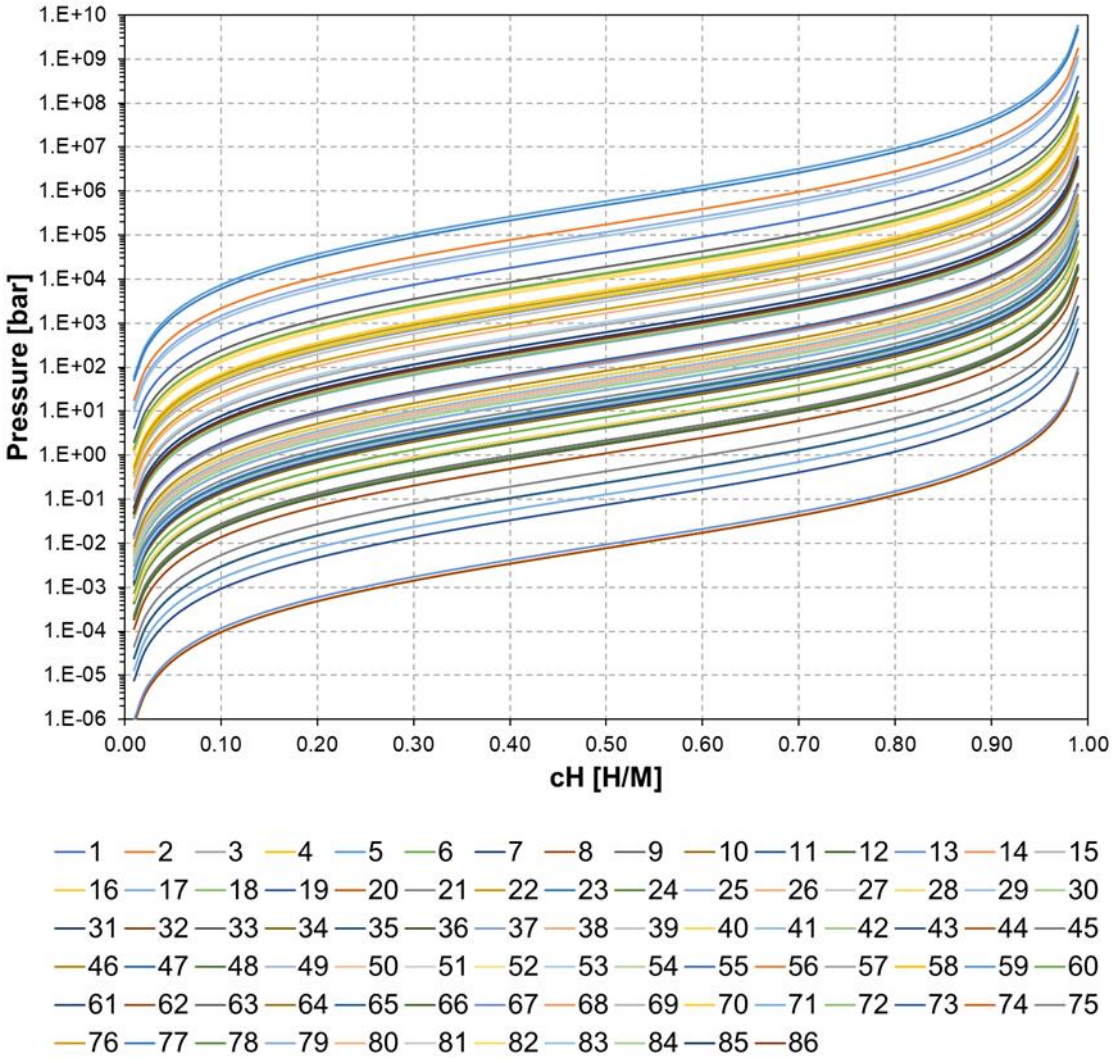


Figure 5. 8 - Calculated PCI diagrams at room temperature for 86 equiatomic C14 Laves phase alloys.

Figure 5.9 (alloy number 87 to 263) and Figure 5.10 (alloy number 264 to 440) shows the calculated PCIs curves at room temperature for the 354 non-equiatomic compositions predicted to form C14 Laves phase alloys. The complete information of the alloys identified by alloy numbers is also shown in Table A1. For the non-equiatomic alloys, the minimum hydrogen equilibrium pressure is equal to $6.1 \times 10^{-4}$ bar and the maximum is equal to $4.9 \times 10^{5}$ bar, alloys number 98 and 230, respectively. Again, a wide range of operation pressure-temperature can be found for the non-equiatomic alloys.

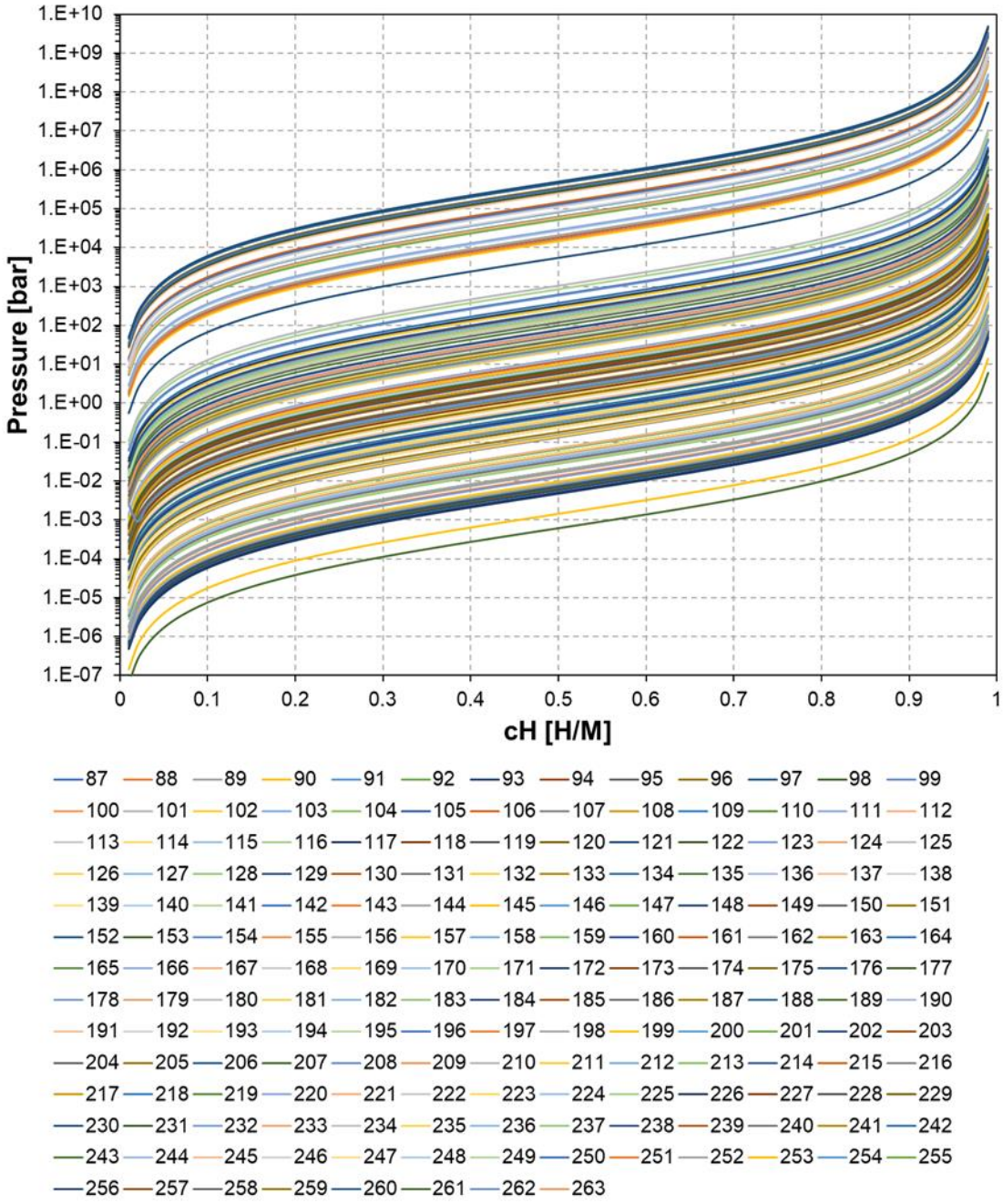


Figure 5. 9 - Calculated PCI diagrams at room temperature for the non-equiatomic C14 Laves phase alloys (alloys number 87 to 263).

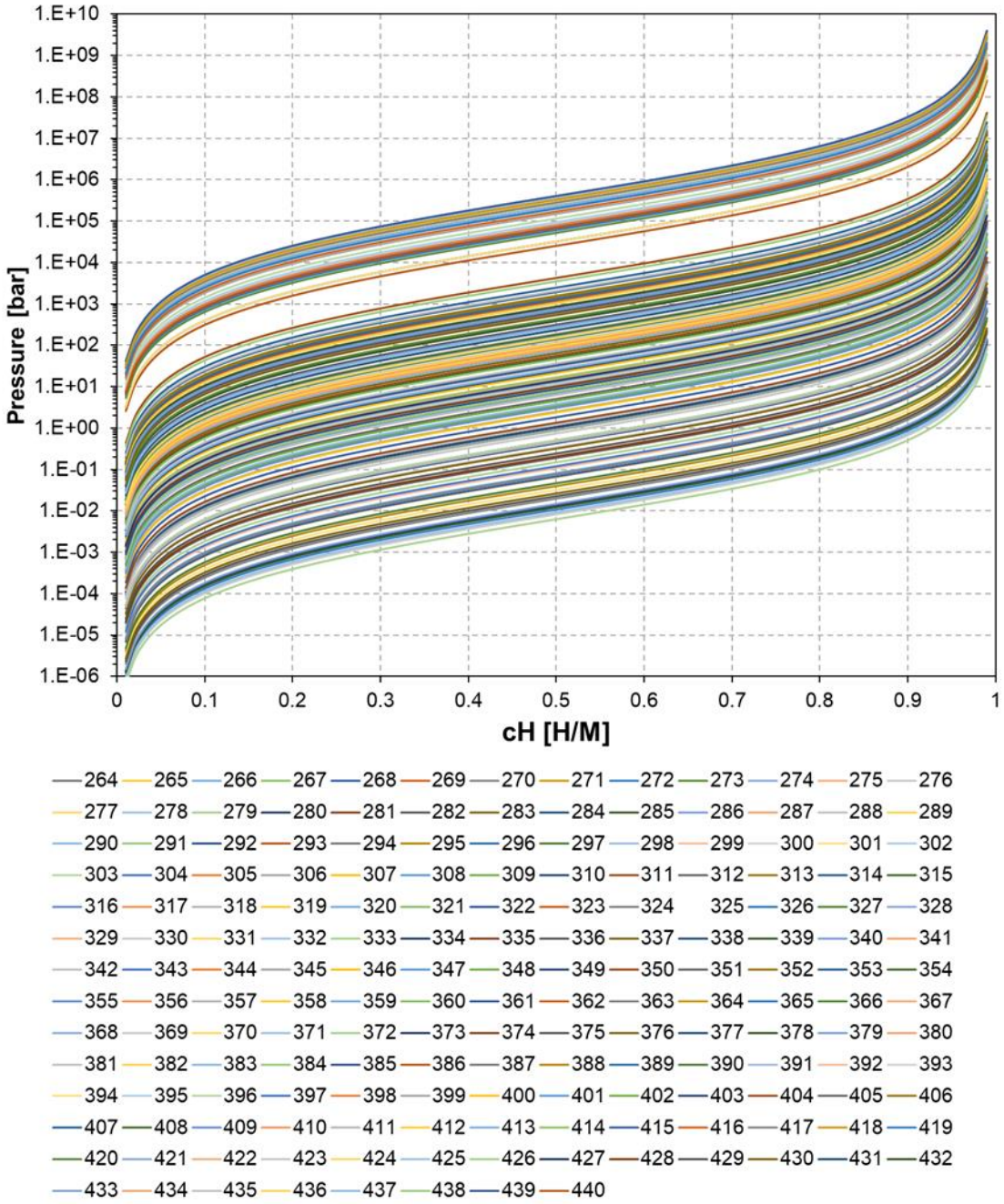


Figure 5. 10 - Calculated PCI diagrams at room temperature for the non-equiatomic C14 Laves phase alloys (alloys number 264 to 440).

Figure 5.11 shows a chart of the calculated equilibrium pressure (at $c_H$ = 0.5) versus the gravimetric hydrogen storage capacity considering $c_{H,max}$= 1, which is typically found for C14 Laves phase [7,10,12,13,52,65]. These values are also shown in Table 5.4 and Table A4 for equiatomic and non-equiatomic compositions, respectively. This chart provides a comprehensive overview of the

thermodynamic properties of hydrogen storage at room temperature for 440 C14 Laves phase alloys. It illustrates the diverse range of hydrogen storage characteristics within this alloy class, offering a strategic approach to selecting compositions tailored to specific hydrogen storage applications.

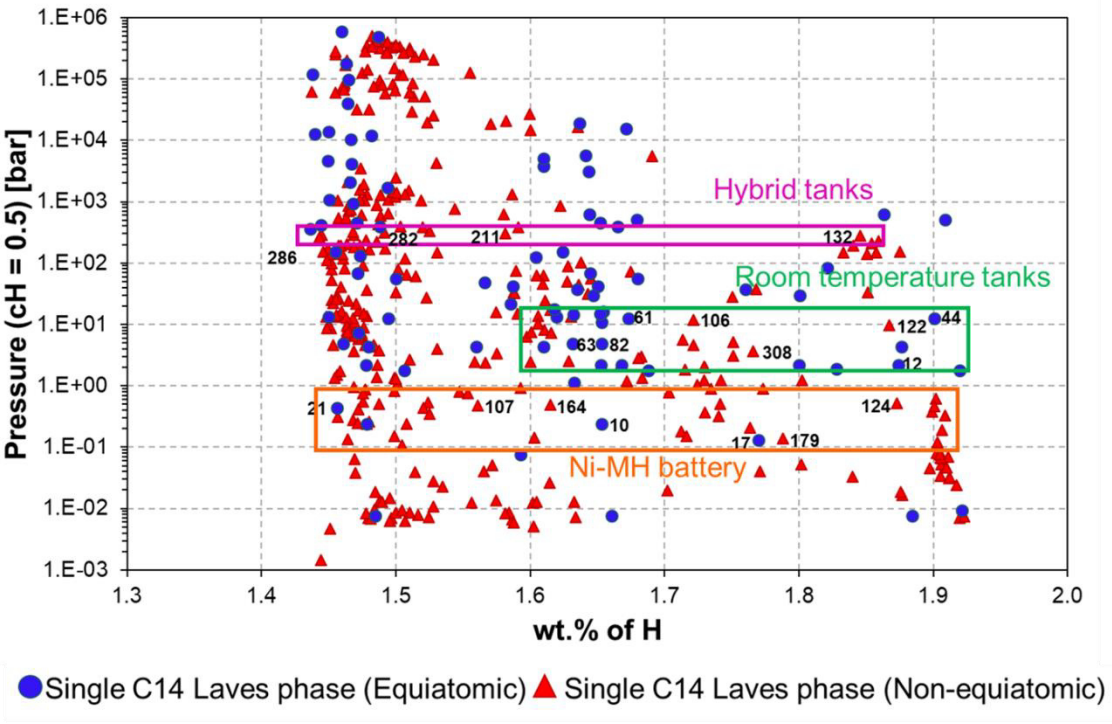


Figure 5. 11 - Chart of the hydrogen equilibrium pressure values (alloys having $c_H$ = 0.5) versus the maximum theoretical hydrogen content in weight percent of H considering $c_{H,max}$= 1. Some compositions (alloy number shown in Table 5.1 and A1) are indicated inside the three regions of potential applications.

For instance, in the context of room temperature hydrogen storage tanks, alloys exhibiting high hydrogen storage capacity and equilibrium pressures ranging from 2 to 20 bar are ideal. This enables effective hydrogen absorption at moderate pressures, with subsequent desorption at room temperature under atmospheric pressure. The alloys highlighted within the green rectangles in Figure 5.11 are promising candidates for this application. Another prospective application involves hybrid tanks that combine high-pressure $H_2$ (up to 700 bar) with high-pressure MHs [61,62]. In this scenario, alloys with equilibrium pressures around 200 to 400 bar at room temperature are required, and a high gravimetric

capacity becomes crucial for minimizing system weight. Alloys within the pink rectangle in Figure 5.11 might be promising candidates for this hybrid tank application.

Consider Ni-MH batteries as a final example, a high hydride gravimetric capacity is essential to enhance charging capacity. However, equilibrium pressure must be maintained between 0.1 and 1 bar to minimize self-discharge and prevent pressure levels exceeding atmospheric pressure inside the battery [63]. The widely used $AB_5$-type alloys currently available have a maximum hydrogen storage capacity of approximately 1.4 wt.%, making alloys within the orange rectangle in Figure 5.11 potential candidates for Ni-MH battery applications. Evaluations of additional properties, such as cycling stability in alkaline solutions, are necessary for comprehensive assessment.

To validate the thermodynamic model proposed, a comparison between the calculated and experimental PCI curves for different C14 Laves phase alloys was carried out. The PCI measurements for the $(Ti_{0.5}Zr_{0.5})_1(Cr_{0.25}Mn_{0.25}Fe_{0.25}Ni_{0.25})_2$ [10], $(Ti_{0.4}Zr_{0.6})_1(Nb_{0.1}Fe_{0.6}Ni_{0.2}Ti_{0.1})_2$ [11], $(Ti_{0.5}Zr_{0.5})_1(V_{0.25}Ni_{0.55}Mn_{0.1}Fe_{0.1})_2$ [12], and $(Ti)_1(Cr_{0.75}Mn_{0.25})_2$ [13] were taken from the literature.

Figure 5.12 shows the comparison between the calculated PCIs using the thermodynamic model and the experimental PCIs for these four alloys. Table 5.5 presents the calculated values of $h_{C14}$ for the four alloys. The atomic fractions of A and B sites ($c_i^A$ and $c_i^B$) for these alloys are presented in Table 5.6 (it is worth mentioning that the atomic fractions for the $(Ti_{0.4}Zr_{0.6})_1(Nb_{0.1}Fe_{0.6}Ni_{0.2}Ti_{0.1})_2$ alloy were calculated by CALPHAD and, in this case, some fraction of Ti and Nb occupy the B-type sites together with Fe and Ni whereas only Ti and Zr occupy the A-type site).

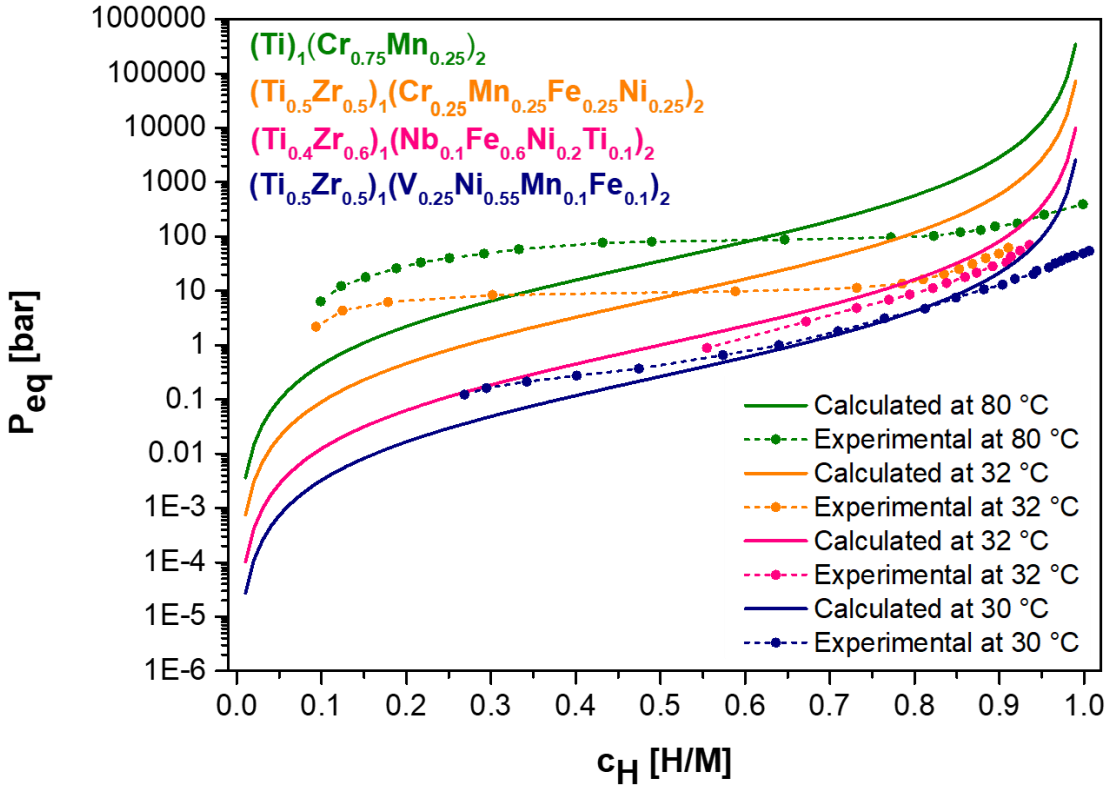


Figure 5. 12 - Experimental absorption PCIs of the $(Ti_{0.5}Zr_{0.5})_1(Cr_{0.25}Mn_{0.25}Fe_{0.25}Ni_{0.25})_2$ (experimental data taken from [10]), $(Ti_{0.4}Zr_{0.6})_1(Nb_{0.1}Fe_{0.6}Ni_{0.2}Ti_{0.1})_2$ (experimental data taken from [11]), $(Ti_{0.5}Zr_{0.5})_1(V_{0.25}Ni_{0.55}Mn_{0.1}Fe_{0.1})_2$ (experimental data taken from [12]), $(Ti)_1(Cr_{0.75}Mn_{0.25})_2$ (experimental data taken from [13]) alloys compared with the calculated PCIs using the thermodynamic model proposed in this study.

Table 5. 5 - Calculated $h_{C14}$ in kJ/mol of H calculated for the tested alloys.

| Alloy | $h_{C14}$ |
|---|---|
| $(Ti)_1(Cr_{0.75}Mn_{0.25})_2$ | -15.4 |
| $(Ti_{0.5}Zr_{0.5})_1(Cr_{0.25}Mn_{0.25}Fe_{0.25}Ni_{0.25})_2$ | -17.5 |
| $(Ti_{0.4}Zr_{0.6})_1(Nb_{0.1}Fe_{0.6}Ni_{0.2}Ti_{0.1})_2$ | -20.0 |
| $(Ti_{0.5}Zr_{0.5})_1(V_{0.25}Ni_{0.55}Mn_{0.1}Fe_{0.1})_2$ | -25.8 |

Table 5. 6 - Atomic fraction of element $i$ in the sublattice A and sublattice B for the $(Ti_{0.5}Zr_{0.5})_1(Cr_{0.25}Mn_{0.25}Fe_{0.25}Ni_{0.25})_2$, $(Ti_{13}Zr_{20})_1(Nb_{2.5}Fe_{20}Ni_{7.5}Ti_{3.5})_2$, $(Ti_{0.5}Zr_{0.5})_1(V_{0.25}Ni_{0.55}Mn_{0.1}Fe_{0.1})_2$, and $Ti_1(Cr_{0.75}Mn_{0.25})_2$ alloys.

| **Alloy** | **Site fraction sublattice A** | | **Site fraction sublattice B** | | | | | | |
|---|---|---|---|---|---|---|---|---|---|
| | **Ti** | **Zr** | **Ti** | **Nb** | **Fe** | **Mn** | **Cr** | **Ni** | **V** |
| $Ti_1(Cr_{0.75}Mn_{0.25})_2$ | 1 | | | | | 0.25 | 0.75 | | |
| $(Ti_{0.5}Zr_{0.5})_1(Cr_{0.25}Mn_{0.25}Fe_{0.25}Ni_{0.25})_2$ | 0.5 | 0.5 | | | 0.25 | 0.25 | 0.25 | 0.25 | |
| $(Ti_{0.4}Zr_{0.6})_1(Nb_{0.1}Fe_{0.6}Ni_{0.2}Ti_{0.1})_2$ | 0.39 | 0.61 | 0.1 | 0.08 | 0.6 | | | 0.22 | |
| $(Ti_{0.5}Zr_{0.5})_1(V_{0.25}Ni_{0.55}Mn_{0.1}Fe_{0.1})_2$ | 0.5 | 0.5 | | | 0.1 | 0.1 | | 0.55 | 0.25 |

One can see that the $(Ti_{0.5}Zr_{0.5})_1(V_{0.25}Ni_{0.55}Mn_{0.1}Fe_{0.1})_2$ alloy present the most negative value of $h_{C14}$ (-25.8 kJ/mol of H) amongst the tested alloys. There is a good agreement between the calculated and experimental PCI curves at 32 °C for the $(Ti_{0.5}Zr_{0.5})_1(V_{0.25}Ni_{0.55}Mn_{0.1}Fe_{0.1})_2$ alloy as can be seen in Figure 5.12. Moreover, the absence of a well-defined plateau pressure indicates that the hydrogen absorption in this alloy occurred only by interstitial solid solution as considered in the development of this model.

The second lower value of $h_{C14}$ was presented by the $(Ti_{0.4}Zr_{0.6})_1(Nb_{0.1}Fe_{0.6}Ni_{0.2}Ti_{0.1})_2$ alloy (-20.0 kJ/mol of H) and again a good agreement between the calculated and experimental PCI curves at 32 °C was observed. In this case, the calculated equilibrium pressures were only slightly higher than the experimental ones.

The $(Ti)_1(Cr_{0.75}Mn_{0.25})_2$ and $(Ti_{0.5}Zr_{0.5})_1(Cr_{0.25}Mn_{0.25}Fe_{0.25}Ni_{0.25})_2$ alloys presented intermediate values of $h_{C14}$, -15.4 and -17.5 kJ/mol of H, respectively. It is worth noting that the experimental PCIs at 80 °C and 32 °C, respectively, for these alloys presented a flat plateau, suggesting that a phase equilibrium between a low hydrogen content solid solution and high hydrogen content hydride occurs for these alloys. This phase equilibrium might be understood as a hydrogen miscibility gap in C14 Laves phase alloy. A miscibility gap typically results from two minimums in the $\Delta G_m(c_H)$ curve, which in its turn could result from a non-linear behavior of $\Delta H_m(c_H)$ or from hydrogen occupancy of preferential interstitial sites associated with SBE. The occupation of other interstitial sites than those considered in this model, for instance $AB_3$-type sites, could also affect the description of $\Delta G_m(c_H)$, therefore, affecting the PCI curves. These aspects were not considered in the model presented here, since it would require a more in-depth study of the hydrogen occupation in different interstitial sites for each specific alloy. The discussion of these effects is out of the scope of this work and deserves to be carefully investigated in the future with the aid of *ab initio* calculations, neutron diffraction analyses, and *in situ* XRD analyses. This model was proposed to allow the screening of a large number of alloy compositions without the need of a previous investigation of any specific alloy. Although the model presented here is not able to predict the formation of flat

plateaus, which inevitably will lead to a poor description of the PCI curves for alloys having this characteristic, it may give us information regarding the order of magnitude of the hydrogen absorption/desorption pressure for these alloys. This was indeed the case for the $Ti_1(Cr_{0.75}Mn_{0.25})_2$ and $(Ti_{0.5}Zr_{0.5})_1(Cr_{0.25}Mn_{0.25}Fe_{0.25}Ni_{0.25})_2$ alloys.

Despite the fact that the shapes of the calculated PCI curves for these alloys differ from the experimental ones, the experimental plateau pressures intersected the calculated PCIs curves at approximately $c_H$ = 0.5, meaning that the absorption/desorption pressure were somehow well determined. We attribute this result to a reasonable prediction of the $h_{C14}$ value for these alloys. As predicted by the model, the equilibrium pressures of the $(Ti)_1(Cr_{0.75}Mn_{0.25})_2$ were approximately one order of magnitude higher than the $(Ti_{0.5}Zr_{0.5})_1(Cr_{0.25}Mn_{0.25}Fe_{0.25}Ni_{0.25})_2$ alloy.

In addition to this comparison carried out with the experimental data taken from the literature, one of these compositions was selected, produced, and had its hydrogen storage properties determined experimentally for an additional comparison. The selected composition, $(Ti_{0.5}Zr_{0.5})_1(Cr_{0.25}Mn_{0.25}Fe_{0.25}Ni_{0.25})_2$, was reported by Edalati et al. [10]. The microstructural characterization of the synthesized sample was presented in section 5.1.1.

Figure 5.13 shows the experimental absorption and desorption PCI at 30 °C of the synthesized $(Ti_{0.5}Zr_{0.5})_1(Cr_{0.25}Mn_{0.25}Fe_{0.25}Ni_{0.25})_2$ alloy compared with the calculated PCI using the thermodynamic model proposed. The reproduced alloy followed the same behavior as reported by Edalati et al. [10]. The sample absorbed 0.92 H/M (1.52 wt.%) of hydrogen during the absorption PCI at 30 °C without any activation process. Moreover, the hydrogen equilibrium pressure was approximately 13 bar at $c_H$ = 0.5. Both values are very close to the reported ones, i.e., the reported hydrogen capacity and the hydrogen equilibrium pressure was 1.6 wt.% and 10 bar, respectively. Furthermore, the material desorbed hydrogen completely with almost no hysteresis in the isotherm. Concerning to the thermodynamic model, a good agreement was observed between the experimental and the calculated hydrogen equilibrium pressure, despite the fact that the shapes of the calculated curve for this alloy differ from the experimental

one, as discussed above. Therefore, with these results it was possible to validate experimentally the model for predicting the order of magnitude of the hydrogen equilibrium pressure for an alloy with the C14 Laves phase, in addition to the method for predicting and producing the alloy with the C14 Laves phase as shown in Section 5.1.1.

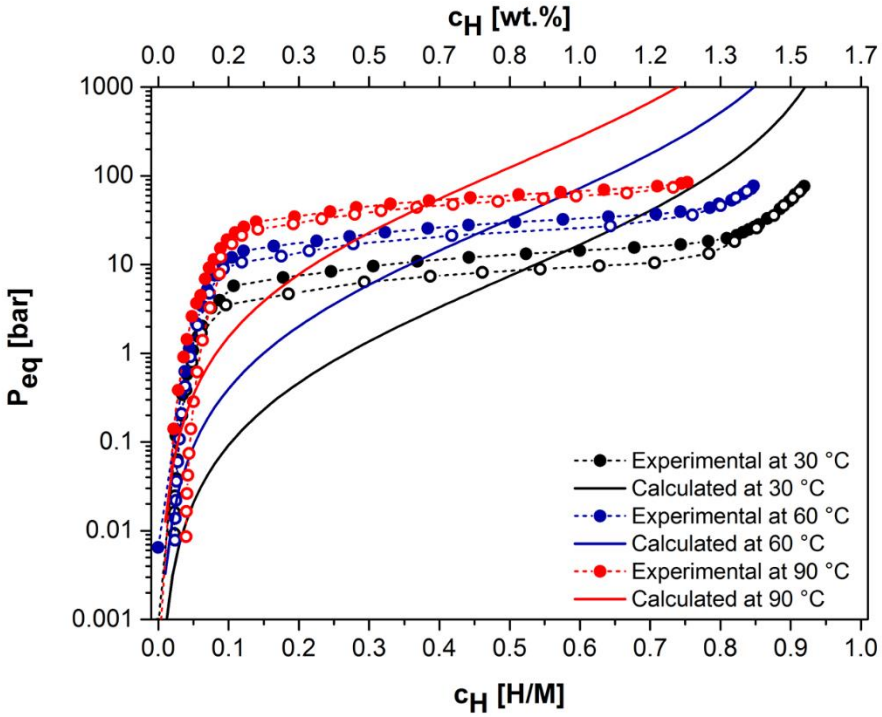


Figure 5. 13 - Experimental absorption and desorption PCT at 30 °C, 60 °C and 90 °C of the $(Ti_{0.5}Zr_{0.5})_1(Cr_{0.25}Mn_{0.25}Fe_{0.25}Ni_{0.25})_2$ alloy compared with the calculated PCI using the thermodynamic model proposed.

The PCI measurements at 60 °C and 90 °C were also carried out to further evaluate hydrogen absorption and desorption performance of the alloy and compare with the thermodynamic model, as shown in Figure 5.13. From these measurements it was possible to observe the influence of temperature on the model. The measurements were performed up to a maximum hydrogen pressure of 80 bar. It is worth mentioning that the same sample was used for the measurements at three different temperatures. After each PCI measurement, the sample was exposed to dynamic vacuum for a few minutes at the current temperature. Fig. 6 shows that the maximum hydrogen uptake at 80 bar

decreases as the temperature increases: H/M = 0.92 (1.52 wt.%), H/M = 0.85 (1.40 wt.%), and H/M = 0.75 (1.25 wt.%) for 30 °C, 60 °C, and 90 °C, respectively. For these temperatures, the observed hydrogen equilibrium pressures for the alloy having $c_H$ = 0.5 were approximately 13, 30, and 61 bar, respectively. Whereas the calculated hydrogen equilibrium pressures for the alloy having $c_H$ = 0.5 were approximately 8, 32, and 124 bar respectively. This result indicates excellent agreement between the model and experimental measurements. especially for 30 °C and 60 °C.

The value $c_H$ = 0.5 was adopted as a standard for determining the hydrogen equilibrium pressure and consequently for calculating thermodynamic properties using the van't Hoff equation. The $c_H$ = 0.5 was used both for alloys that present a pressure plateau, as the $(Ti_{0.5}Zr_{0.5})_1(Cr_{0.25}Mn_{0.25}Fe_{0.25}Ni_{0.25})_2$ alloy and for alloys that present a pressure slope in the PCI diagrams, as will be presented later. The van't Hoff plot for the $(Ti_{0.5}Zr_{0.5})_1(Cr_{0.25}Mn_{0.25}Fe_{0.25}Ni_{0.25})_2$ alloy is shown in Figure 5.14. For the absorption reaction, the enthalpy (ΔH) value was -11.71 kJ/mol H, and the entropy (ΔS) value was -49.35 J/K.mol H. For the desorption reaction, the ΔH was +13.41 kJ/mol H, and the ΔS was +53.45 J/K.mol H.

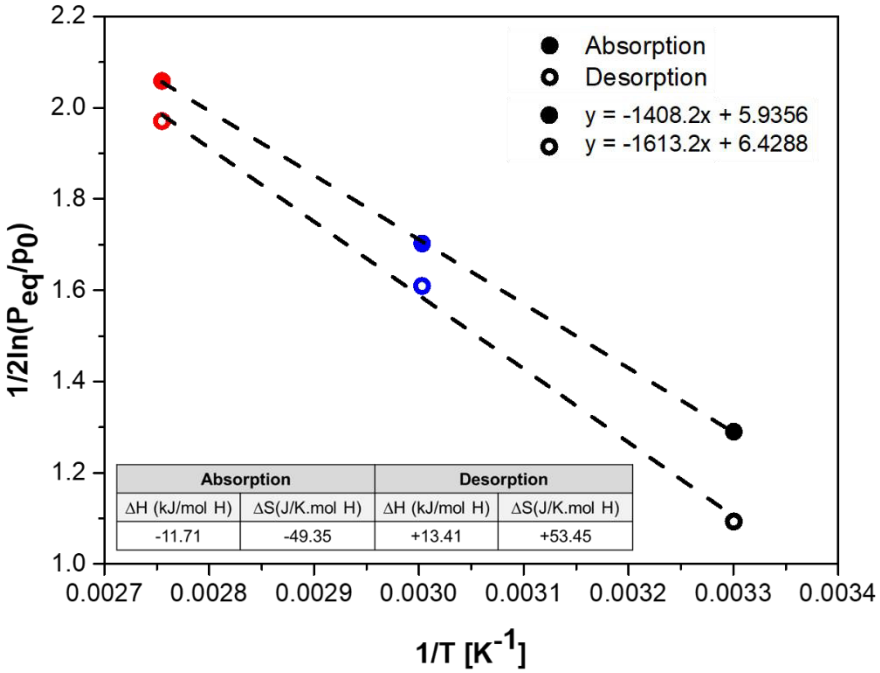


Figure 5. 14 - Van´t Hoff plot for the absorption and desorption pressures at $c_H$ = H/M = 0.5 for the $(Ti_{0.5}Zr_{0.5})_1(Cr_{0.25}Mn_{0.25}Fe_{0.25}Ni_{0.25})_2$ alloy.

These values are in the same range than values reported in the literature for hydrides of intermetallic compounds such as $LaNi_5$, $ZrMn_2$, and TiFe [22]. The ΔH measured in absorption for these compounds is approximately -15 kJ/mol H, -15 kJ/mol H, and -17 kJ/mol H, respectively. Whereas the ΔS are approximately -46 J/K.mol H and -51 J/K.mol H for the $ZrMn_2$ and TiFe, respectively.

Li et al. [66] reported the thermodynamic values for the $Ti_{0.8}Zr_{0.2}Mn_{0.9}Cr_{0.6}V_{0.3}M_{0.2}$ (M = Fe, Ni, Co) alloys. These alloys have single C14 Laves phase and present reversibility at room temperature. The authors reported a ΔH varying between -11.9 and -13.1 kJ/mol H, and a ΔS varying from -45.2 to -48.3 J/K.mol H for these three compositions. The values are also in the same range obtained for the $(Ti_{0.5}Zr_{0.5})_1(Cr_{0.25}Mn_{0.25}Fe_{0.25}Ni_{0.25})_2$ alloy in this work.

Therefore, once the predictability of the thermodynamic model to calculate the PCI curves was assessed, it was possible to move forward through the selection of alloys with the Laves C14 phase for different hydrogen storage applications, i.e., over a range of hydrogen equilibrium pressures.

## 5.2 Alloy design for different hydrogen storage applications

### 5.2.1 Selection of the compositions

Aiming to study C14 Laves phase alloys in a wide range of equilibrium pressures for different hydrogen storage applications, seven compositions were selected among the 86 equiatomic compositions with C14 Laves phase shown in Table 5.1 and Figure 5.8. Table 5.7 shows the VEC, $r_A/r_B$, and δ values of the selected alloys.

Table 5. 7 - VEC, $r_A/r_B$, and δ values of the selected alloys.

| Alloy | $r_A/r_B$ | VEC | δ |
|---|---|---|---|
| $(Ti_{0.5}Zr_{0.5})_1Mn_2$ | 1.214 | 6.0 | 9.9 |
| $(Ti_{0.5}Zr_{0.5})_1(Mn_{0.5}Cr_{0.5})_2$ | 1.205 | 5.7 | 9.5 |
| $(Ti_{0.5}Zr_{0.5})_1(Fe_{0.5}Mn_{0.5})_2$ | 1.209 | 6.3 | 9.7 |
| $(Ti_{0.5}Zr_{0.5})_1(Fe_{0.33}Mn_{0.33}Cr_{0.33})_2$ | 1.205 | 6.0 | 9.5 |
| $(Ti_{0.33}Zr_{0.33}Nb_{0.33})_1(Mn_{0.5}Cr_{0.5})_2$ | 1.189 | 5.8 | 8.8 |
| $(Ti_{0.33}Zr_{0.33}Nb_{0.33})_1(Fe_{0.5}Mn_{0.5})_2$ | 1.194 | 6.4 | 9.0 |
| $(Ti_{0.5}Nb_{0.5})_1(Fe_{0.5}Mn_{0.5})_2$ | 1.158 | 6.5 | 7.1 |

The mole fraction of equilibrium phases as a function of temperature calculated by CALPHAD for these seven compositions are shown in Figures 5.16 to 5.22. The thermodynamic calculation indicates that under equilibrium conditions, all the seven alloys solidify as a primary C14 Laves phase.

Figure 5.15 shows the diagram of the amount of equilibrium phase as function of temperature for the $(Ti_{0.5}Zr_{0.5})_1Mn_2$ composition. The diagram shows that under equilibrium conditions, the alloy solidifies as a single C14 Laves phase. The C14 Laves phase is stable below 1420 °C and no other phase is predicted to form upon cooling.

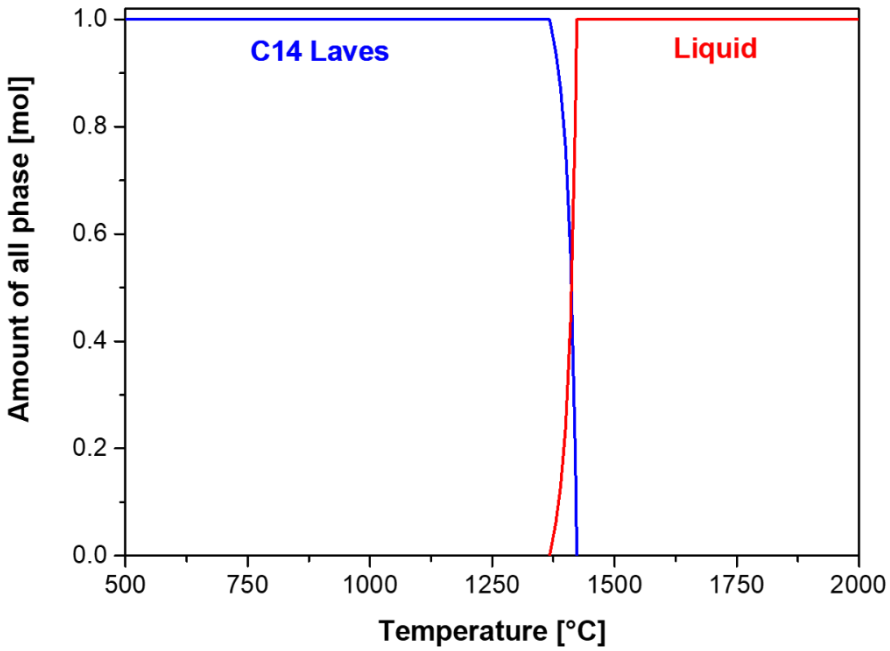


Figure 5. 15 - Amount of equilibrium phases as a function of temperature calculated for the $(Ti_{0.5}Zr_{0.5})_1Mn_2$ composition.

Figure 5.16 shows the mole fraction of equilibrium phases as a function of temperature calculated for the $(Ti_{0.5}Zr_{0.5})_1(Mn_{0.5}Cr_{0.5})_2$ composition. The calculation indicates that under equilibrium conditions, the alloy solidifies as a primary C14 Laves phase. Moreover, it is predicted that a minor fraction of BCC phase (<1%) forms in the final stage of the solidification at approximately 1390 °C. Other phases, C15 Laves and $Cr_3Mn_5$ phases, are also predicted to form upon cooling.

The same behavior was observed for the $(Ti_{0.5}Zr_{0.5})_1(Fe_{0.33}Mn_{0.33}Cr_{0.33})_2$ and $(Ti_{0.33}Zr_{0.33}Nb_{0.33})_1(Mn_{0.5}Cr_{0.5})_2$ compositions, as shown in Figure 5.18 and Figure 5.19, respectively. For these compositions, the minor fraction of BCC phase forms at approximately 1330 °C and 1400 °C, in the final stage of the solidification, respectively. The C15 Laves and $Cr_3Mn_5$ phases, are also predicted to form upon cooling for these two compositions. Nonetheless, the formation of these phases might be suppressed due to the high cooling rate imposed in the alloy synthesis process used in this work (arc-melting on a water-cooled copper base under an inert argon atmosphere).

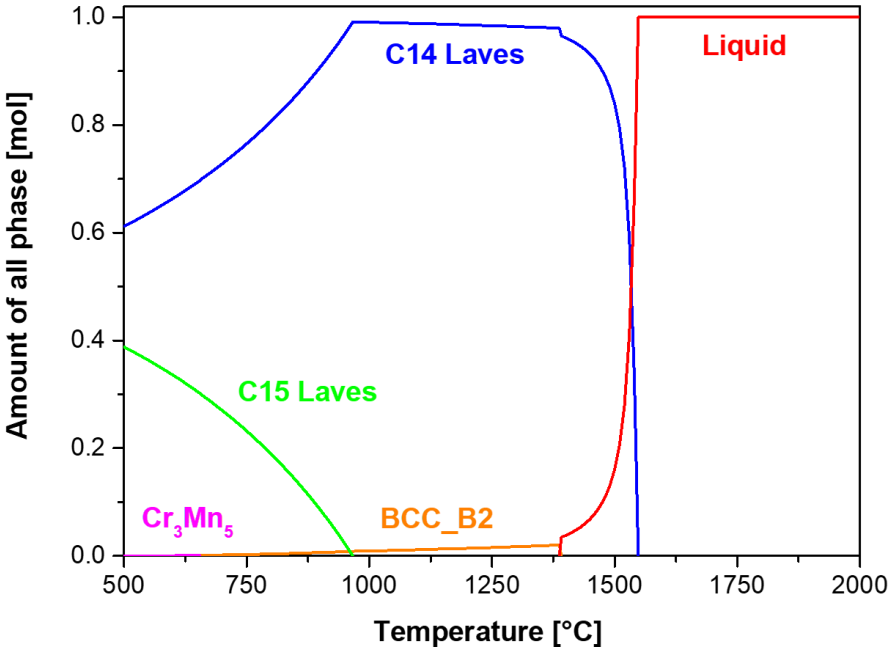


Figure 5. 16 - Amount of equilibrium phases as a function of temperature calculated for the $(Ti_{0.5}Zr_{0.5})_1(Mn_{0.5}Cr_{0.5})_2$ composition.

Figure 5.17 and Figure 5.21 shows the mole fraction of equilibrium phases as a function of temperature calculated for the $(Ti_{0.5}Zr_{0.5})_1(Fe_{0.5}Mn_{0.5})_2$ and $(Ti_{0.33}Nb_{0.5})_1(Fe_{0.5}Mn_{0.5})_2$ compositions, respectively. The thermodynamic calculation for both alloys shows that the alloys solidify as single C14 Laves phase. However, in these cases, the C14 Laves phase is stable below 1460 °C and 1500 °C, respectively, and very small fraction of other phases are predicted to form upon cooling.

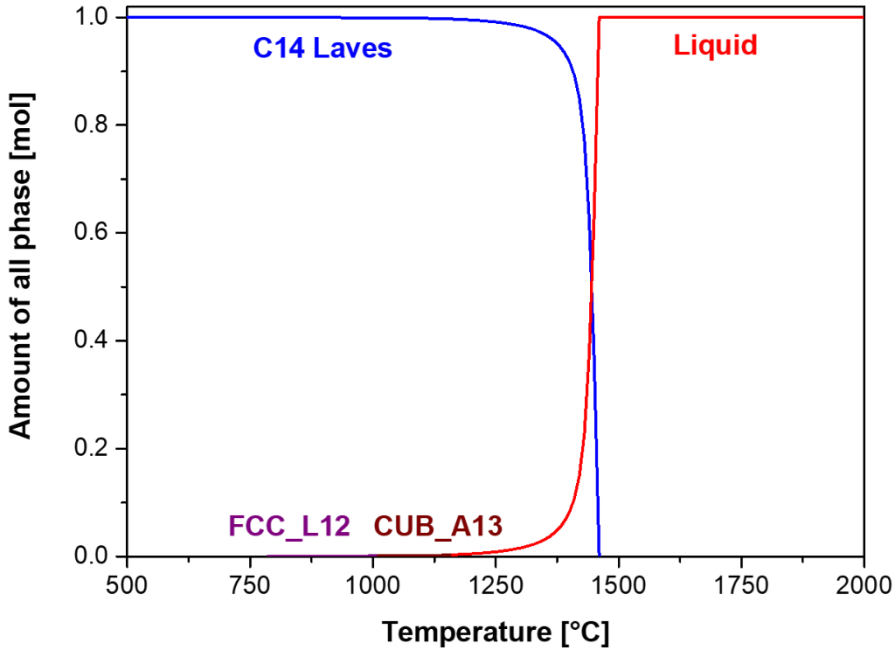


Figure 5. 17 - Amount of equilibrium phases as a function of temperature calculated for the $(Ti_{0.5}Zr_{0.5})_1(Fe_{0.5}Mn_{0.5})_2$ composition.

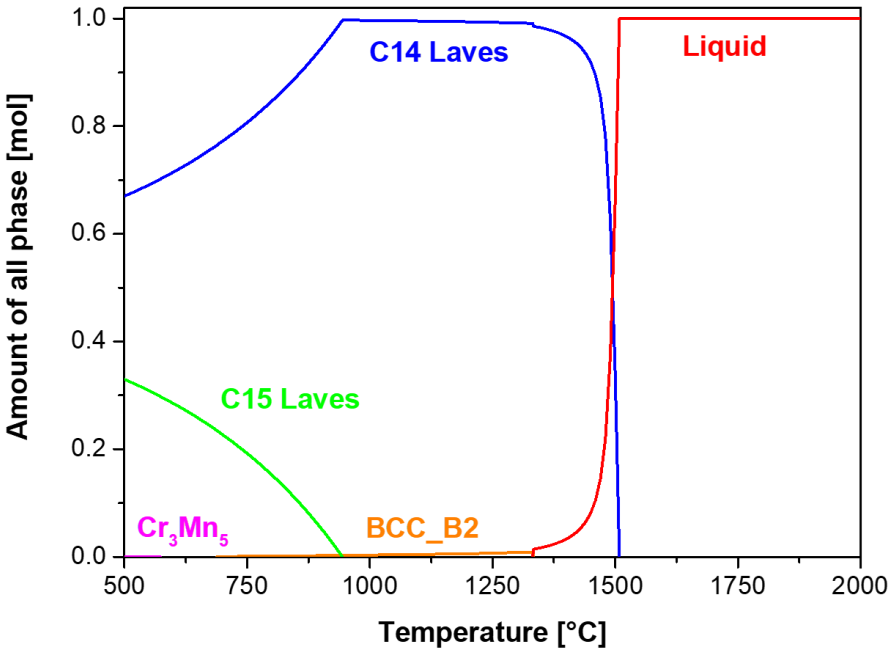


Figure 5. 18 - Amount of equilibrium phases as a function of temperature calculated for the $(Ti_{0.5}Zr_{0.5})_1(Fe_{0.33}Mn_{0.33}Cr_{0.33})_2$ composition.

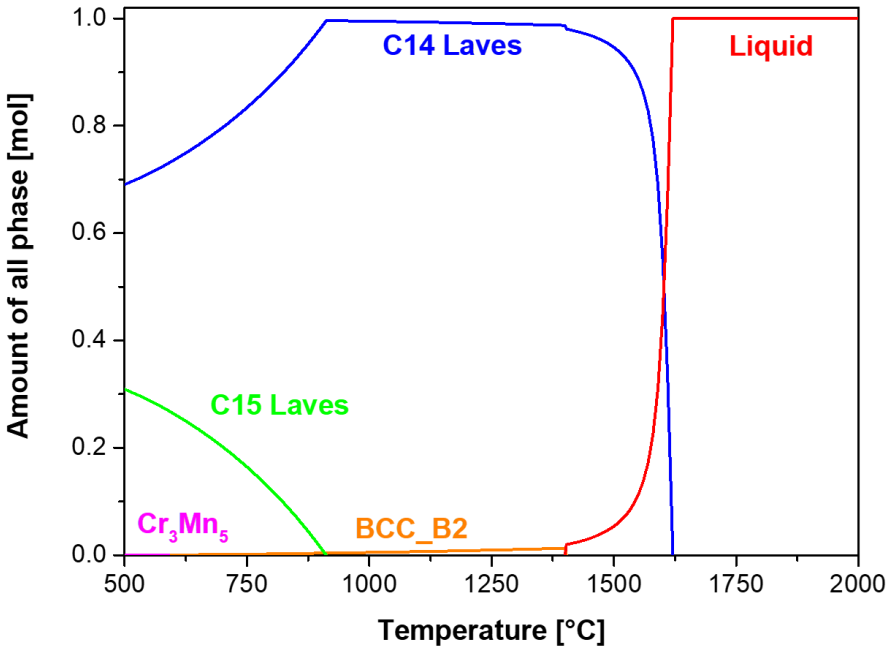


Figure 5. 19 - Amount of equilibrium phases as a function of temperature calculated for the $(Ti_{0.33}Zr_{0.33}Nb_{0.33})_1(Mn_{0.5}Cr_{0.5})_2$ composition.

Figure 5.20 shows the mole fraction of equilibrium phases as a function of temperature calculated for the $(Ti_{0.33}Zr_{0.33}Nb_{0.33})_1(Fe_{0.5}Mn_{0.5})_2$ composition. For this composition the thermodynamic calculation indicates that under equilibrium conditions the alloy solidifies a primary C14 Laves phase, nonetheless, it is predicted that a second C14 Laves phase forms upon cooling. This second C14 Laves phase appears in the calculations as a phase richer in Zr and poorer in Nb. Beyond that, small fraction of other cubic phases is also predicted to form upon cooling.

However, as discussed above, the high cooling rate imposed by the arc-melting on a water-cooled copper base in the alloy synthesis process might suppress the formation of the cubic phases and the second C14 Laves phase, resulting in a single C14 Laves phase alloy.

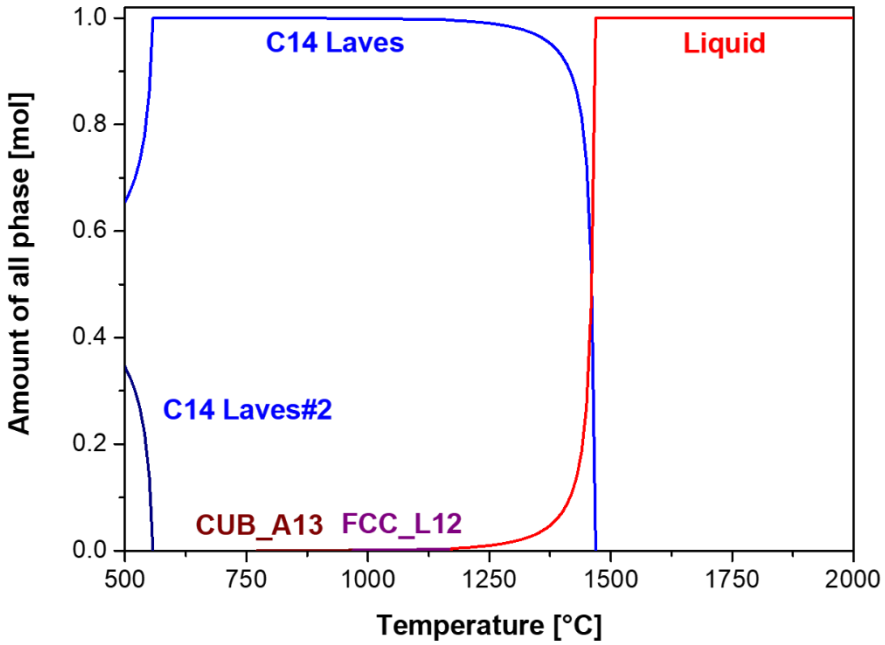


Figure 5. 20 - Amount of equilibrium phases as a function of temperature calculated for the $(Ti_{0.33}Zr_{0.33}Nb_{0.33})_1(Fe_{0.5}Mn_{0.5})_2$ composition.

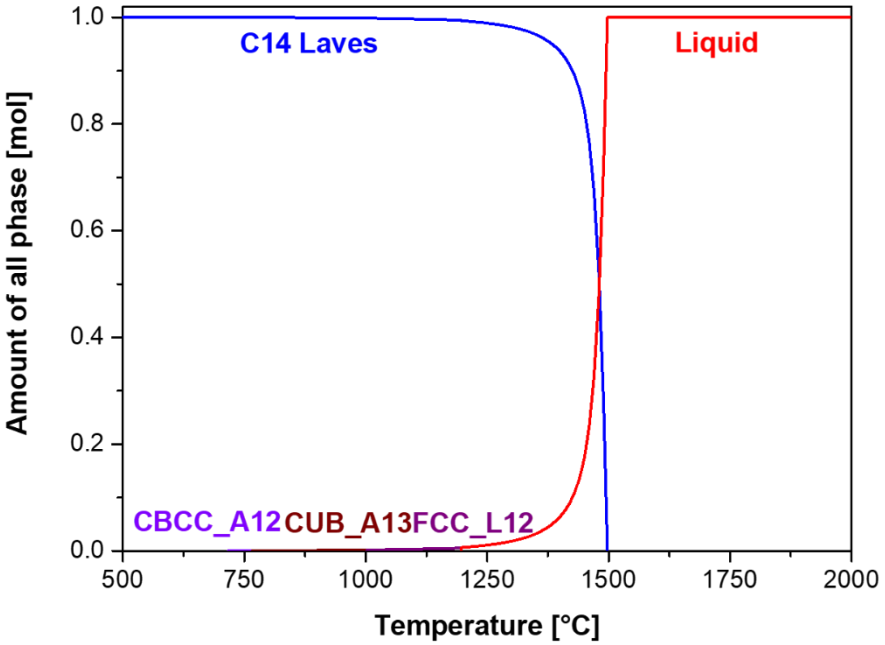


Figure 5. 21 - Amount of equilibrium phases as a function of temperature calculated for the $(Ti_{0.5}Nb_{0.5})_1(Fe_{0.5}Mn_{0.5})_2$ composition.

After the first two steps of the alloy design method, which were the analysis of the electronic and geometric factors (VEC, $r_a/r_b$, and δ), and the CALPHAD calculations to obtain the mole fraction of equilibrium phases as a function of temperature, the next step was the calculation of the equilibrium pressure of hydrogen using the proposed thermodynamic modeling to calculate PCT diagrams of multicomponent C14-type Laves phase alloys.

Figure 5.22 illustrates the calculated PCI curves at 25 °C for the seven selected compositions. One can see, the selected alloys are within a wide range of hydrogen equilibrium pressures. The $(Ti_{0.5}Zr_{0.5})_1Mn_2$ composition presents the lower hydrogen partial molar enthalpy ($h_{C14}$ = -25.50 kJ mol$^{-1}$ H), which implies in the lower hydrogen equilibrium pressure ($P_{H_2}$= 0.01 bar), while the $(Ti_{0.33}Nb_{0.5})_1(Fe_{0.5}Mn_{0.5})_2$ composition presents the higher $h_{C14}$ = -14.25 kJ mol$^{-1}$ H, which implies in the higher $P_{H_2}$= 68.45 bar.

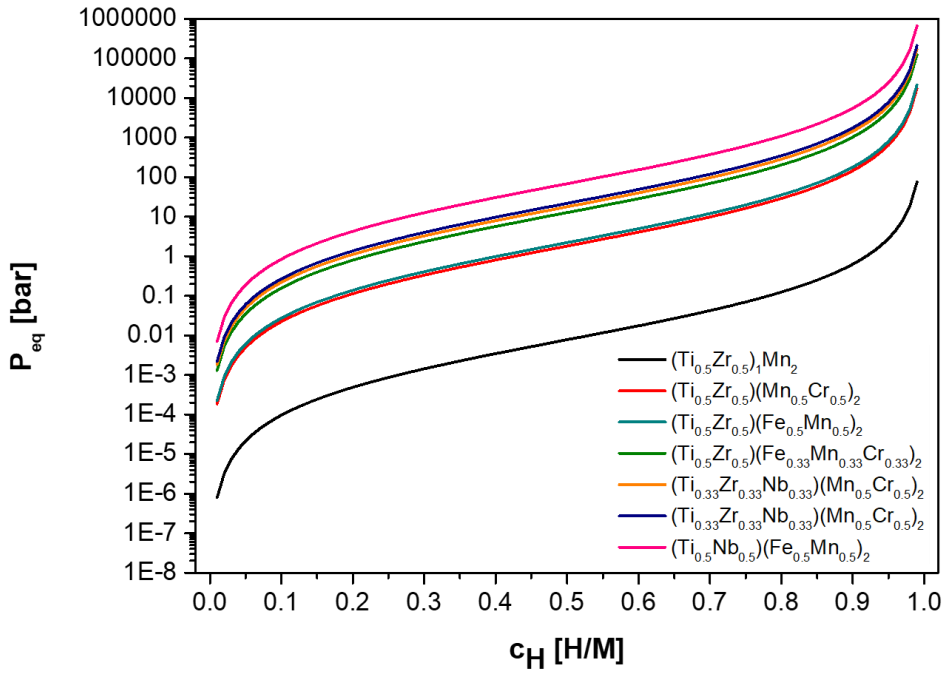


Figure 5. 22 - Calculated PCI curves for the selected alloys at 25 °C.

The other five compositions present $h_{C14}$ and $P_{H_2}$ values between these two extremes. The $h_{C14}$ and $P_{H_2}$ values for all the seven compositions are shown

in Table 5.8. It is worth noting that the hydrogen equilibrium pressures shown in Table 5.8 are correspond to $c_H$= 0.5 H/M.

Table 5. 8 - Calculated hydrogen partial molar enthalpy of the phase ($h_{C14}$) and hydrogen equilibrium pressure ($P_{H_2}$) at $c_H$= 0.5 of the selected alloys.

| Alloy | $h_{C14}$ [kJ mol$^{-1}$ H] | $P_{H_2}$ [bar] |
|---|---|---|
| $(Ti_{0.5}Zr_{0.5})_1Mn_2$ | -25.5 | 1.0x10$^{-2}$ |
| $(Ti_{0.5}Zr_{0.5})_1(Mn_{0.5}Cr_{0.5})_2$ | -18.75 | 1.8x10$^{0}$ |
| $(Ti_{0.5}Zr_{0.5})_1(Fe_{0.5}Mn_{0.5})_2$ | -18.50 | 2.2x10$^{0}$ |
| $(Ti_{0.5}Zr_{0.5})_1(Fe_{0.33}Mn_{0.33}Cr_{0.33})_2$ | -16.33 | 1.3x10$^{1}$ |
| $(Ti_{0.33}Zr_{0.33}Nb_{0.33})_1(Mn_{0.5}Cr_{0.5})_2$ | -15.92 | 1.8x10$^{1}$ |
| $(Ti_{0.33}Zr_{0.33}Nb_{0.33})_1(Fe_{0.5}Mn_{0.5})_2$ | -15.67 | 2.2x10$^{1}$ |
| $(Ti_{0.5}Nb_{0.5})_1(Fe_{0.5}Mn_{0.5})_2$ | -14.25 | 6.9x10$^{1}$ |

### 5.2.2 Structure characterization

The selected compositions presented above were synthesized by arc-melting under an inert argon atmosphere in electric arc furnaces and initially structurally characterized by XRD and SEM-EDX analyses. These analyses aimed to confirm the formation of single C14 Laves phase in the selected alloys.

Figures 5.23 to 5.29 present the XRD patterns of the as-cast $(Ti_{0.5}Zr_{0.5})_1Mn_2$, $(Ti_{0.5}Zr_{0.5})_1(Mn_{0.5}Cr_{0.5})_2$, $(Ti_{0.5}Zr_{0.5})_1(Fe_{0.5}Mn_{0.5})_2$, $(Ti_{0.5}Zr_{0.5})_1(Fe_{0.33}Mn_{0.33}Cr_{0.33})_2$, $(Ti_{0.33}Zr_{0.33}Nb_{0.33})_1(Mn_{0.5}Cr_{0.5})_2$, $(Ti_{0.33}Zr_{0.33}Nb_{0.33})_1(Fe_{0.5}Mn_{0.5})_2$, and $(Ti_{0.33}Nb_{0.5})_1(Fe_{0.5}Mn_{0.5})_2$ alloys confirming that all of them have C14 Laves phase structure. No reflections from a secondary phase can be observed.

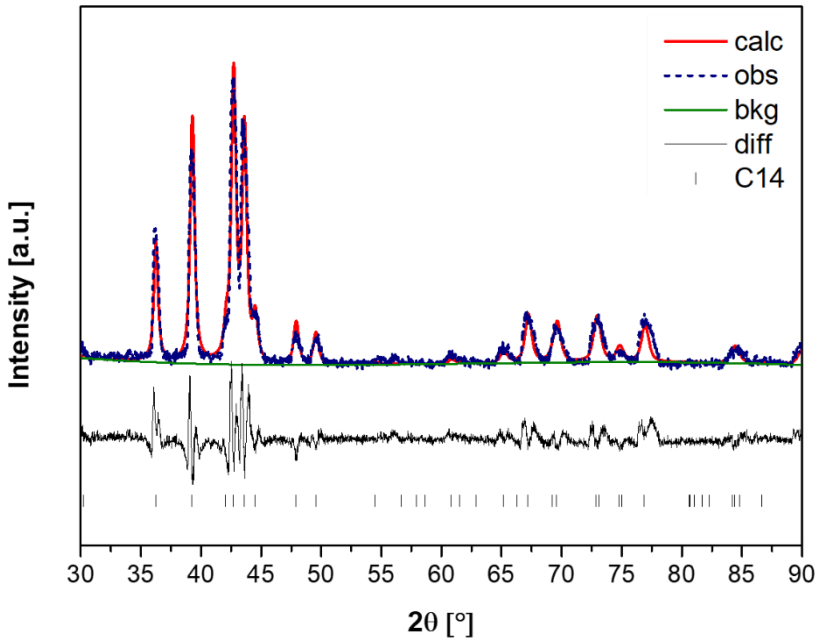


Figure 5. 23 - Rietveld refinement of the XRD pattern of the as-cast $(Ti_{0.5}Zr_{0.5})_1Mn_2$ alloy indicating that the sample formed C14 Laves phase structure (measured with KαCu radiation).

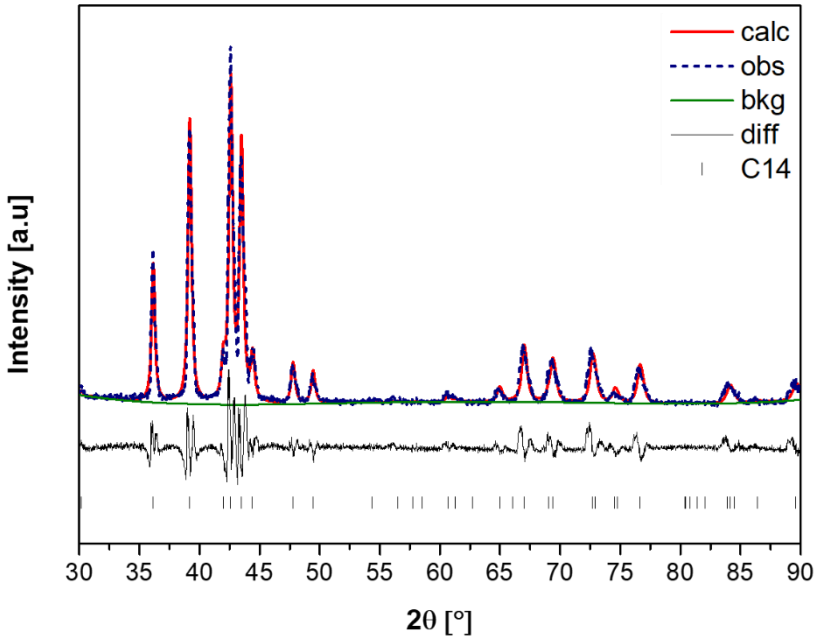


Figure 5. 24 - Rietveld refinement of the XRD pattern of the as-cast $(Ti_{0.5}Zr_{0.5})_1(Mn_{0.5}Cr_{0.5})_2$ alloy indicating that the sample formed C14 Laves phase structure (measured with KαCu radiation).

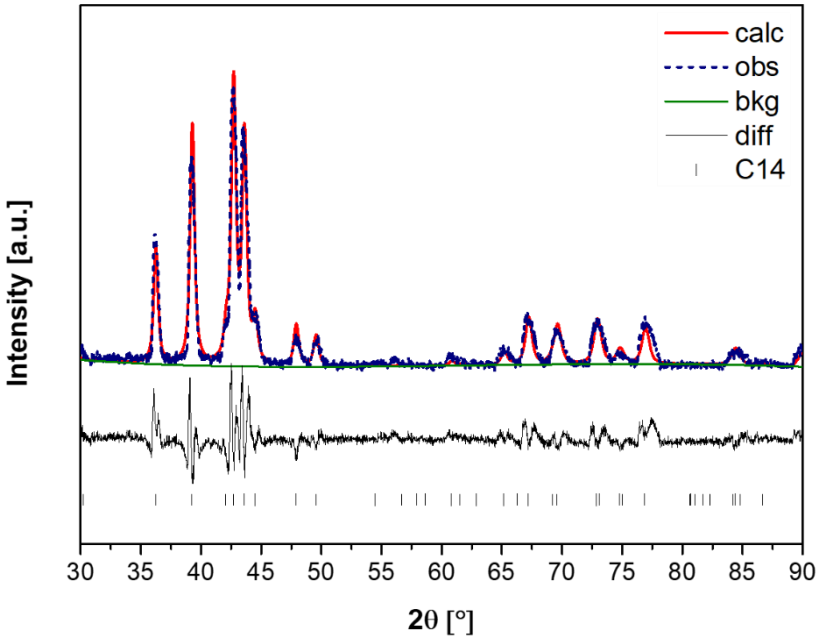


Figure 5. 25 - Rietveld refinement of the XRD pattern of the as-cast $(Ti_{0.5}Zr_{0.5})_1(Fe_{0.5}Mn_{0.5})_2$ alloy indicating that the sample formed C14 Laves phase structure (measured with KαCu radiation).

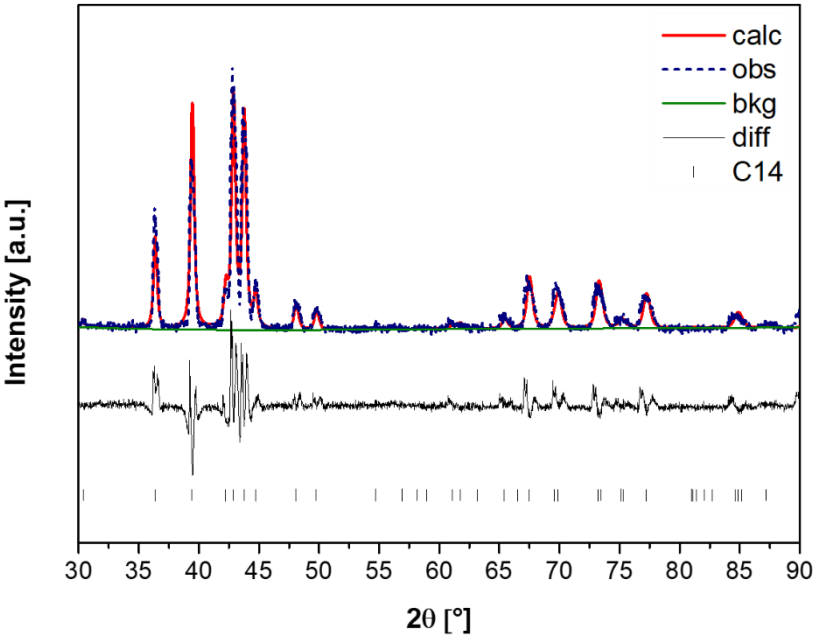


Figure 5. 26 - Rietveld refinement of the XRD pattern of the as-cast $(Ti_{0.5}Zr_{0.5})_1(Fe_{0.33}Mn_{0.33}Cr_{0.33})_2$ alloy indicating that the sample formed C14 Laves phase structure (measured with KαCu radiation).

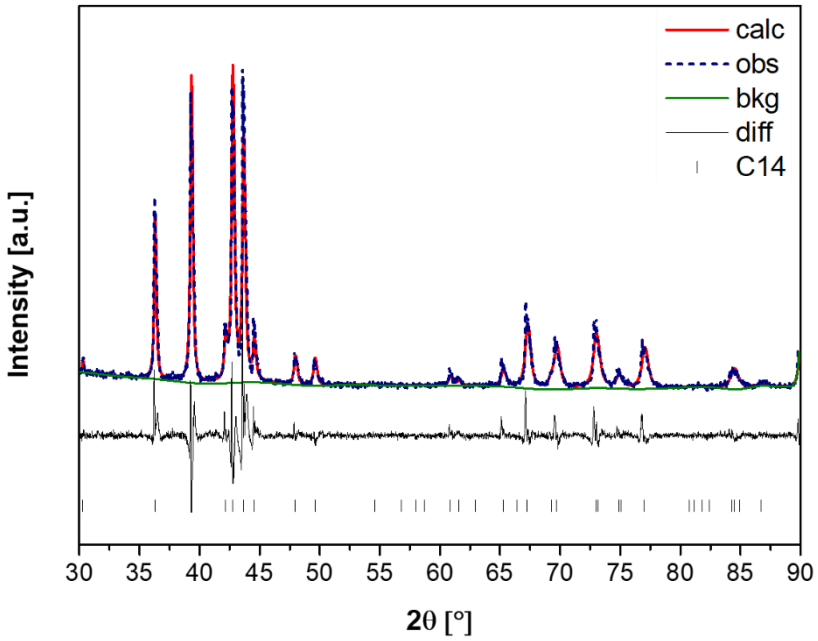


Figure 5. 27 - Rietveld refinement of the XRD pattern of the as-cast $(Ti_{0.33}Zr_{0.33}Nb_{0.33})_1(Mn_{0.5}Cr_{0.5})_2$ alloy indicating that the sample formed C14 Laves phase structure (measured with KαCu radiation).

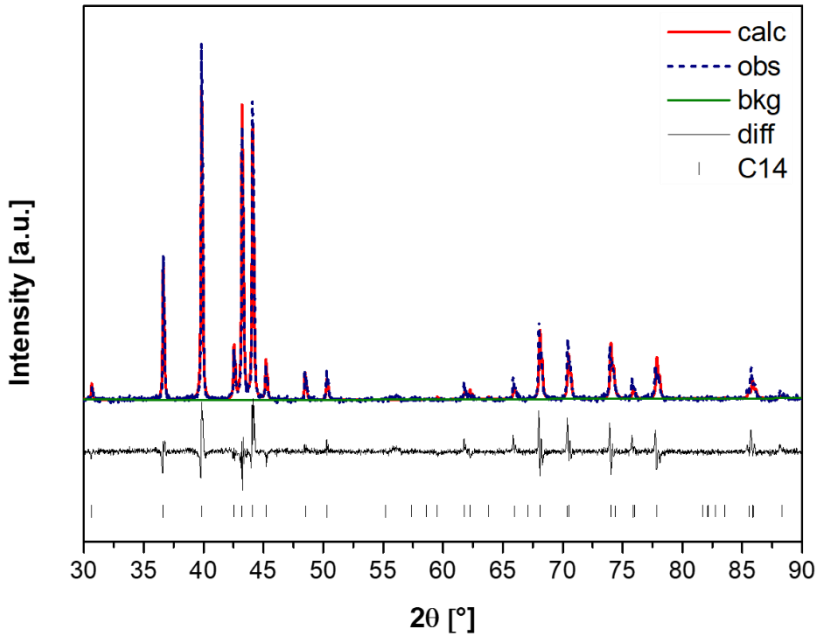


Figure 5. 28 - Rietveld refinement of the XRD pattern of the as-cast $(Ti_{0.33}Zr_{0.33}Nb_{0.33})_1(Fe_{0.5}Mn_{0.5})_2$ alloy indicating that the sample formed C14 Laves phase structure (measured with KαCu radiation).

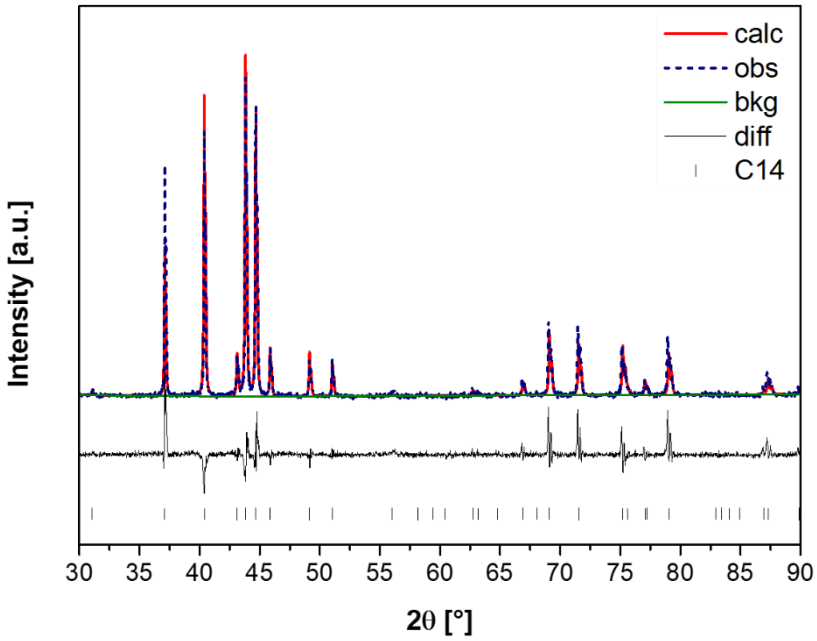


Figure 5. 29 - Rietveld refinement of the XRD pattern of the as-cast $(Ti_{0.5}Nb_{0.5})_1(Fe_{0.5}Mn_{0.5})_2$ alloy indicating that the sample formed C14 Laves phase structure (measured with KαCu radiation).

The lattice parameters obtained by the Rietveld refinement for the C14 Laves phase for the different alloys are presented in Table 5.9.

Table 5. 9 – Lattice parameters a and c obtained by the Rietveld refinement.

| Alloy | a [nm] | c [nm] |
|---|---|---|
| $(Ti_{0.5}Zr_{0.5})_1Mn_2$ | 0.495 | 0.814 |
| $(Ti_{0.5}Zr_{0.5})_1(Mn_{0.5}Cr_{0.5})_2$ | 0.497 | 0.816 |
| $(Ti_{0.5}Zr_{0.5})_1(Fe_{0.5}Mn_{0.5})_2$ | 0.492 | 0.805 |
| $(Ti_{0.5}Zr_{0.5})_1(Fe_{0.33}Mn_{0.33}Cr_{0.33})_2$ | 0.496 | 0.814 |
| $(Ti_{0.33}Zr_{0.33}Nb_{0.33})_1(Mn_{0.5}Cr_{0.5})_2$ | 0.494 | 0.812 |
| $(Ti_{0.33}Zr_{0.33}Nb_{0.33})_1(Fe_{0.5}Mn_{0.5})_2$ | 0.490 | 0.802 |
| $(Ti_{0.5}Nb_{0.5})_1(Fe_{0.5}Mn_{0.5})_2$ | 0.484 | 0.790 |

According to these XRD results, all the alloys are formed by a C14 Laves phase structure, and no other phase can be observed. However, some alloys presented a broadening of the C14 Laves phase reflections, such as the $(Ti_{0.5}Zr_{0.5})_1Mn_2$, $(Ti_{0.5}Zr_{0.5})_1(Mn_{0.5}Cr_{0.5})_2$, $(Ti_{0.5}Zr_{0.5})_1(Fe_{0.5}Mn_{0.5})_2$, $(Ti_{0.5}Zr_{0.5})_1(Fe_{0.33}Mn_{0.33}Cr_{0.33})_2$ alloys. It is possible to relate the slight broadening of the C14 Laves phase reflections to a minor deviation in the chemical composition due to segregation during solidification. A gradient in the chemical composition caused by segregation can also lead to a small gradient in the lattice parameters of the C14 Laves phase, resulting in the peak broadening.

The deviation in the composition throughout the bulk of the C14 Laves phase alloys synthesized arc-melting is commonly observed due to the dendritic microstructure resulting from this casting process [10,61,62].

In this way the alloys microstructure was further investigated by SEM equipped with EDX, and the results are shown in Figures 5.30 to 5.36.

Figure 5.30 shows the SEM-BSE image of the as-cast $(Ti_{0.5}Zr_{0.5})_1Mn_2$ alloy. As can be seen, the as-cast sample presented a dendritic microstructure. Further, the SEM-BSE image, which is sensitivity to differences in atomic number, reveals that there is a difference in composition between the dendritic and interdendritic regions. Figure 5.30 also shows the corresponding EDX elemental maps of the selected region. EDX analyses were carried out in map mode in all the selected region, and as point mode in the two areas: at the interdendritic regions and in the middle of dendrites. The results of the overall chemical composition and the chemical composition in the dendritic and interdendritic regions are presented in Table 5.10. One can see that the overall composition of the alloy is very close to the nominal one. Ti and Zr are not homogeneously distributed between the dendritic and interdendritic regions as a result of segregation during solidification. On the other hand, Mn appears to be uniformly distributed in both regions. The chemical composition measured in the interdendritic region is slightly richer in Ti and poorer in Zr. In contrast, the chemical composition measured in the middle of the dendrites is slightly richer in Zr and poorer in Ti.

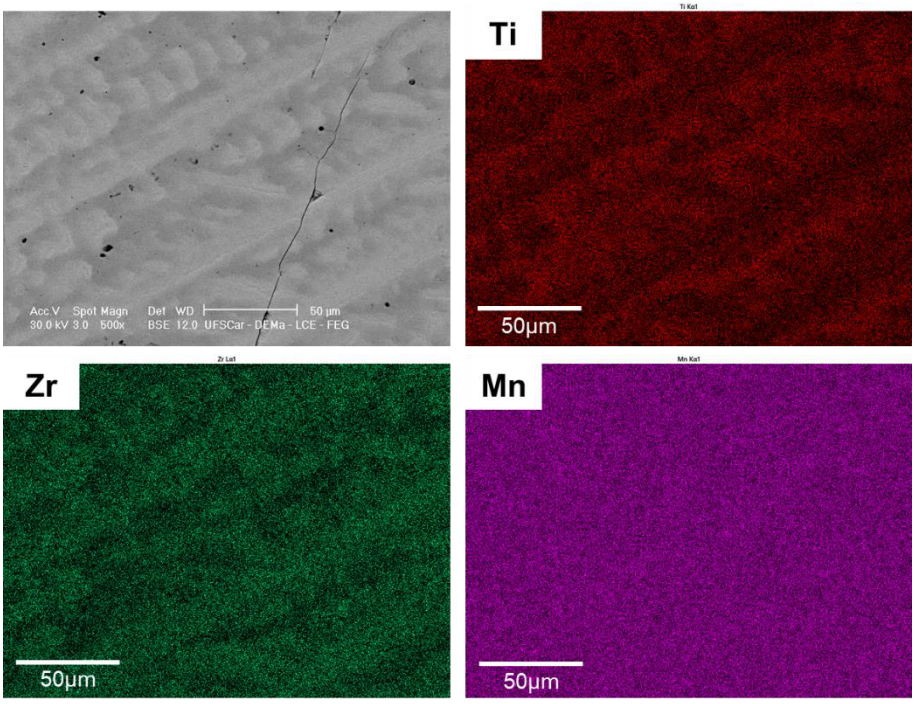


Figure 5. 30 - SEM-BSE image and corresponding EDX elemental maps of the as-cast $(Ti_{0.5}Zr_{0.5})_1Mn_2$ alloy.

Table 5. 10 - The chemical composition of the $(Ti_{0.5}Zr_{0.5})_1Mn_2$ alloy determined by SEM-EDX.

| | **Chemical composition in at% of the as-cast alloy** | | |
|---|---|---|---|
| | **Ti** | **Zr** | **Mn** |
| **Nominal** | 16.7 | 16.7 | 66.7 |
| **Overall** | 18.1 | 16.7 | 65.2 |
| **Dendritic** | 14.1 | 20.4 | 65.5 |
| **Interdendritic** | 21.8 | 12.6 | 65.7 |

Despite the substitution behavior between Ti and Zr elements observed in these regions of the sample, no substantial influence on the alloy crystal structure was observed in the XRD analysis presented above. However, this minor deviations in the chemical composition of different alloy regions can be relate to the slight broadening of the C14 Laves phase reflections observed for the alloy.

Figure 5.31 shows the SEM-BSE image and corresponding EDX elemental maps of the as-cast $(Ti_{0.5}Zr_{0.5})_1(Mn_{0.5}Cr_{0.5})_2$ alloy. As observed for the

$(Ti_{0.5}Zr_{0.5})_1Mn_2$ alloy, the as-cast sample presented a dendritic microstructure and there is a difference in composition between the dendritic and interdendritic regions.

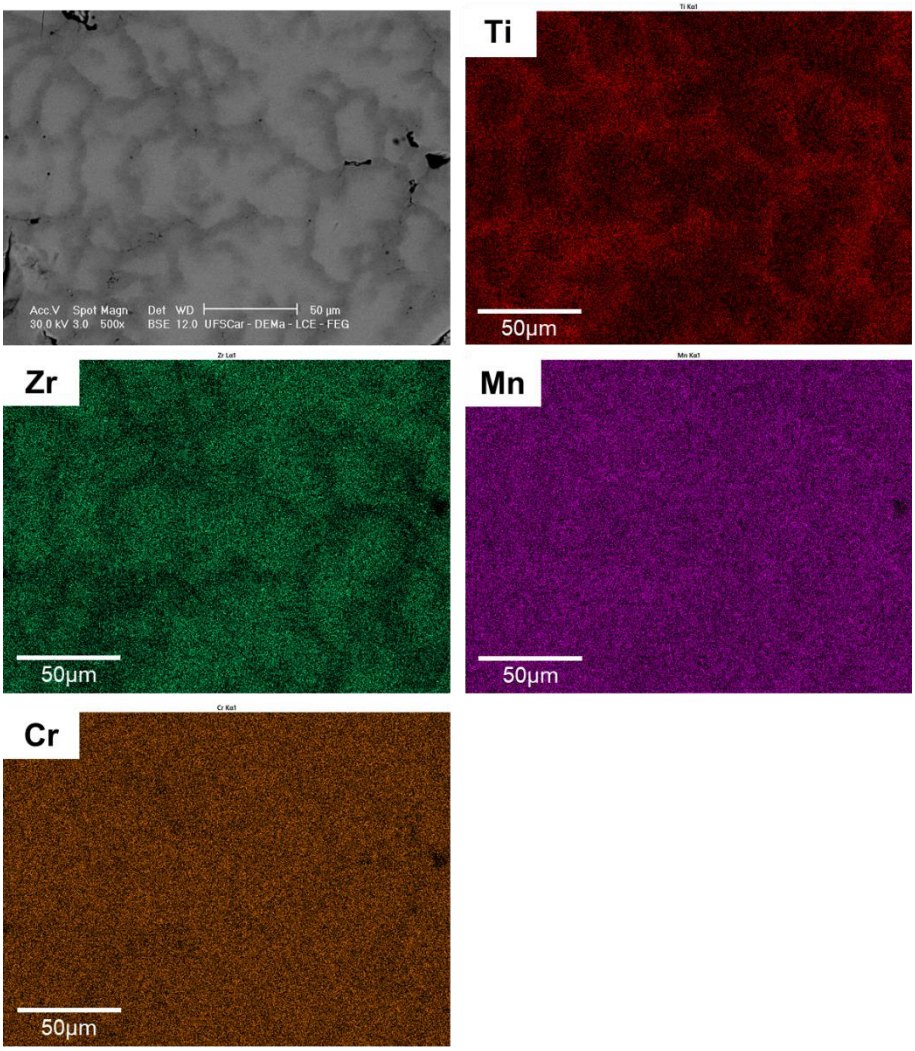


Figure 5. 31 - SEM-BSE image and corresponding EDX elemental maps of the as-cast $(Ti_{0.5}Zr_{0.5})_1(Mn_{0.5}Cr_{0.5})_2$ alloy.

The results of the overall chemical composition and the chemical composition in the dendritic and interdendritic regions are presented in Table 5.11. As observed, the overall composition of the alloy is very close to the nominal one. And again, Ti and Zr are not homogeneously distributed between the dendritic and interdendritic regions. Furthermore, in this alloy, although the Mn and Cr elements appear to be uniformly distributed in the EDX maps, the

point EDX analyzes showed that there is a small variation of these elements between the dendritic and interdendritic regions. The chemical composition measured in the interdendritic region is slightly richer in Ti and Mn, and poorer in Zr and Cr. In contrast, the chemical composition measured in the middle of the dendrites is slightly richer in Zr and Cr, and poorer in Ti and Mn.

Table 5. 11 - The chemical composition of the $(Ti_{0.5}Zr_{0.5})_1(Mn_{0.5}Cr_{0.5})_2$ alloy determined by SEM-EDX.

| | **Chemical composition in at% of the as-cast alloy** | | | |
|---|---|---|---|---|
| | **Ti** | **Zr** | **Mn** | **Cr** |
| **Nominal** | 16.7 | 16.7 | 33.3 | 33.3 |
| **Overall** | 18.2 | 17.3 | 31.3 | 33.2 |
| **Dendritic** | 13.1 | 21.6 | 29.7 | 35.6 |
| **Interdendritic** | 23.4 | 11.9 | 34.0 | 30.6 |

It is worth noting that in most of the alloys the Mn content is slightly lower than the nominal one. This behavior can be explained by its partial vaporization during the arc melting procedure due to its lower melting and boiling point and higher vapor pressure compared to the other alloying elements.

The SEM-BSE image and corresponding EDX elemental maps of the as-cast $(Ti_{0.5}Zr_{0.5})_1(Fe_{0.5}Mn_{0.5})_2$ alloy is shown in Figure 5.32. As expected, the dendritic microstructure is also observed in this alloy. The EDX elemental maps of the alloy show that there is also a difference in composition between the dendritic and interdendritic regions. Table 5.12 shows that the overall composition of the alloy is very close to the nominal one, and that the composition difference between the dendritic and interdendritic regions is not as pronounced as for the $(Ti_{0.5}Zr_{0.5})_1Mn_2$ and $(Ti_{0.5}Zr_{0.5})_1(Mn_{0.5}Cr_{0.5})_2$ alloys. Nonetheless, the chemical composition measured in the interdendritic region is slightly richer in Ti and Mn, and poorer in Zr and Fe. In contrast, the chemical composition measured in the middle of the dendrites is slightly richer in Zr and Fe, and poorer in Ti and Mn.

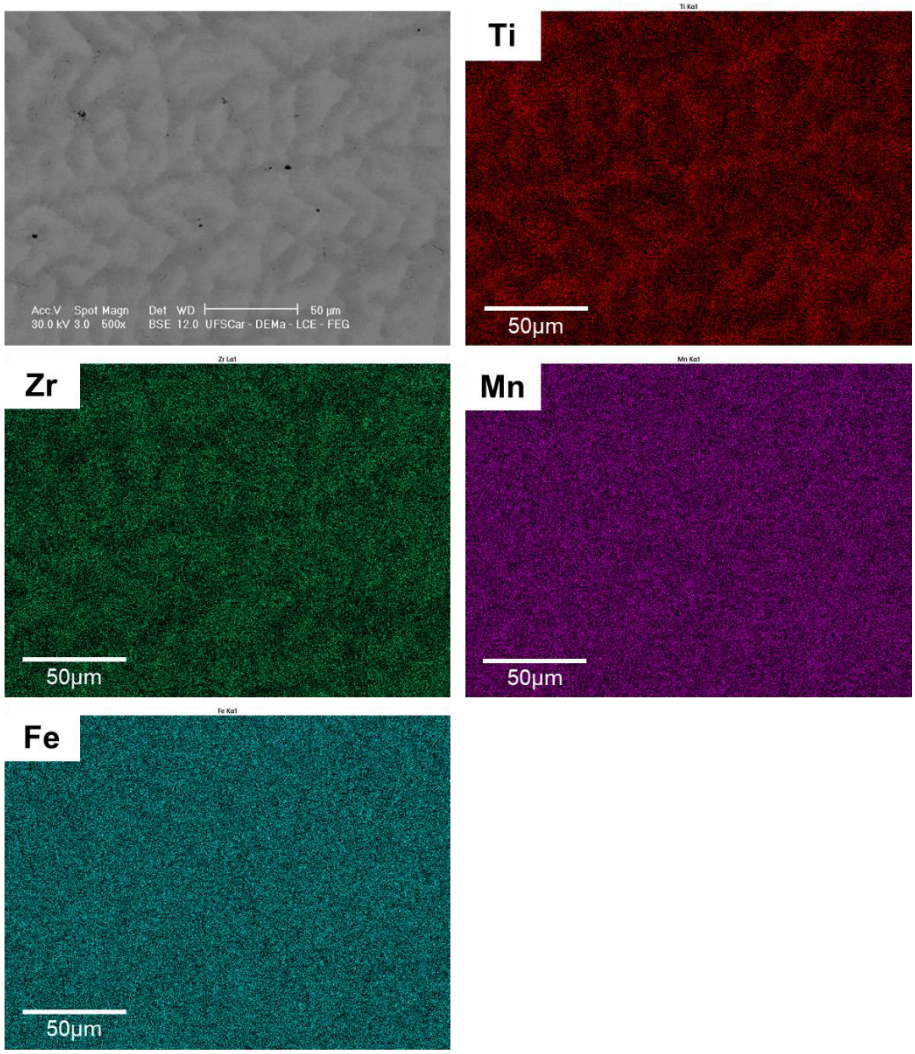


Figure 5. 32 - SEM-BSE image and corresponding EDX elemental maps of the as-cast $(Ti_{0.5}Zr_{0.5})_1(Fe_{0.5}Mn_{0.5})_2$ alloy.

Table 5. 12 - The chemical composition of the $(Ti_{0.5}Zr_{0.5})_1(Fe_{0.5}Mn_{0.5})_2$ alloy determined by SEM-EDX.

| | **Chemical composition in at% of the as-cast alloy** | | | |
|---|---|---|---|---|
| | **Ti** | **Zr** | **Fe** | **Mn** |
| **Nominal** | 16.7 | 16.7 | 33.3 | 33.3 |
| **Overall** | 18.5 | 16.7 | 33.2 | 31.7 |
| **Dendritic** | 16.0 | 18.2 | 34.5 | 31.3 |
| **Interdendritic** | 19.1 | 15.8 | 32.1 | 33.0 |

Figure 5.33 presents the SEM-BSE image and corresponding EDX elemental maps of the as-cast $(Ti_{0.5}Zr_{0.5})_1(Fe_{0.33}Mn_{0.33}Cr_{0.33})_2$ alloy. The dendritic microstructure and the difference in composition between the dendritic and interdendritic regions are also presented in this alloy.

The overall composition of the alloy is very close to the nominal one. However, differently of the alloys presented so far, this alloy presents the interdendritic region slightly richer in Zr and Cr, and poorer in Ti and Mn, while the dendrite region is slightly richer in Ti and Mn, and poorer in Zr and Cr. Fe appears to be uniformly distributed in both regions. The chemical composition is described in Table 5.13.

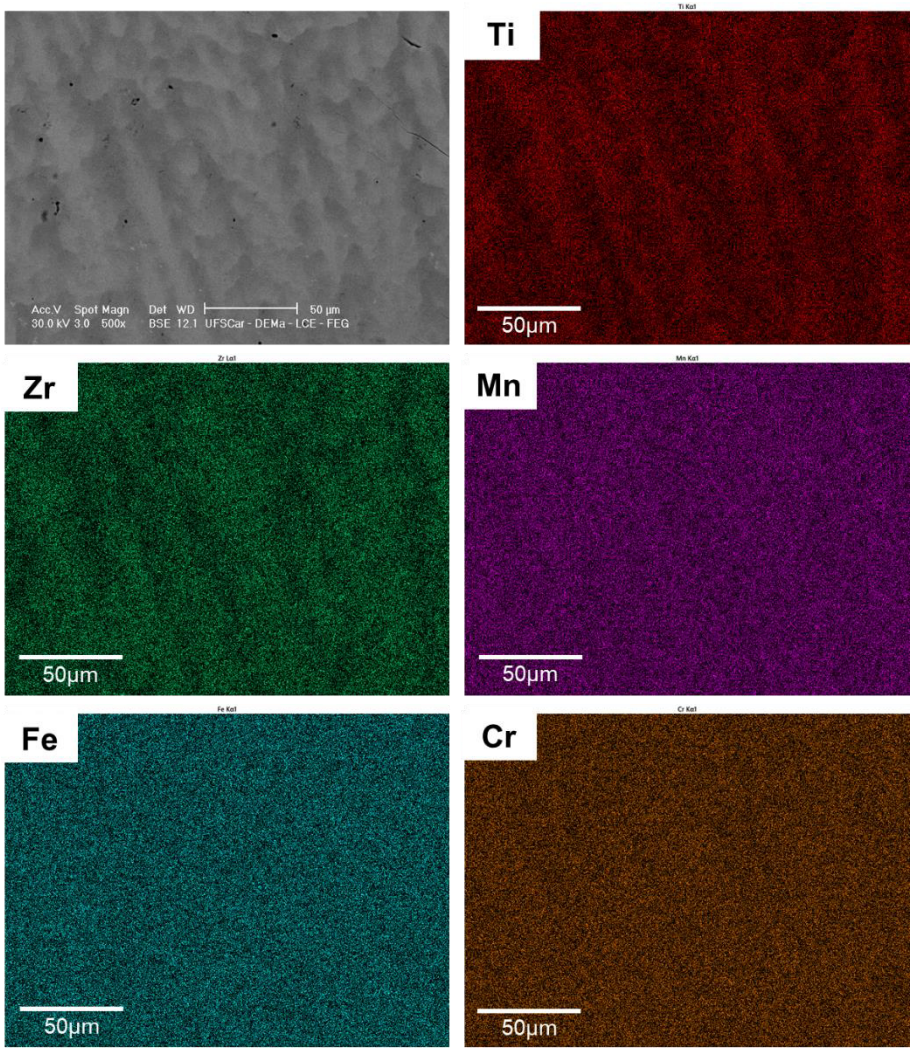


Figure 5. 33 - SEM-BSE image and corresponding EDX elemental maps of the as-cast $(Ti_{0.5}Zr_{0.5})_1(Fe_{0.33}Mn_{0.33}Cr_{0.33})_2$ alloy.

Table 5. 13 - The chemical composition of the $(Ti_{0.5}Zr_{0.5})_1(Fe_{0.33}Mn_{0.33}Cr_{0.33})_2$ alloy determined by SEM-EDX.

| | **Chemical composition in at% of the as-cast alloy** | | | | |
|---|---|---|---|---|---|
| | **Ti** | **Zr** | **Fe** | **Mn** | **Cr** |
| **Nominal** | 16.7 | 16.7 | 22.2 | 22.2 | 22.2 |
| **Overall** | 18.0 | 16.6 | 21.9 | 20.7 | 22.7 |
| **Dendritic** | 21.3 | 13.3 | 21.7 | 22.1 | 21.9 |
| **Interdendritic** | 15.1 | 19.5 | 22.5 | 19.6 | 23.4 |

Figure 5.34 shows the SEM-BSE image and corresponding EDX elemental maps of the as-cast $(Ti_{0.33}Zr_{0.33}Nb_{0.33})_1(Mn_{0.5}Cr_{0.5})_2$ alloy. This alloy follows the same behavior observed in the alloys showed so far regarding the microstructure and elements distribution. However, due to a melting issue during the synthesis of the alloy, the resulting overall composition differs significantly from the nominal one in relation to Nb, as seen in Table 5.14. This problem might be related to a poor homogenization of the elements during the synthesis, which is directly related to the melting point of the elements. Nb has a melting point equal to 2477 °C, higher than the other alloy elements (Ti = 1668 °C, Zr =1855 °C, Mn = 1246 °C, and Cr =1907 °C), requiring more attention during processing.

Beyond that, the chemical composition measured in the interdendritic region is richer in Ti, and poorer in Zr and Nb. In contrast, the chemical composition measured in the middle of the dendrites is richer in Zr and Nb, and poorer in Ti and Mn.

The compositional difference in comparison with the nominal one had no substantial influence on the alloy crystal structure as shown in the XRD pattern in Figure 5.27.

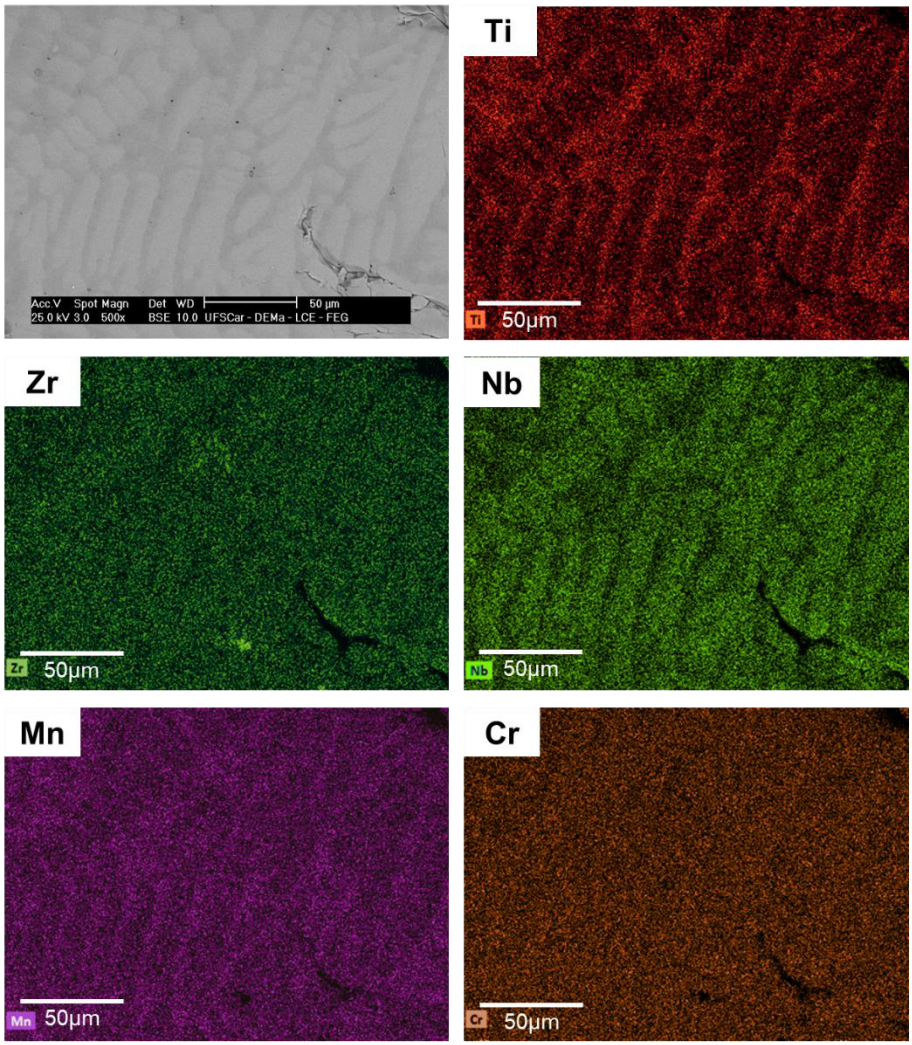


Figure 5. 34 - SEM-BSE image and corresponding EDX elemental maps of the as-cast $(Ti_{0.33}Zr_{0.33}Nb_{0.33})_1(Mn_{0.5}Cr_{0.5})_2$ alloy.

Table 5. 14 - The chemical composition of the $(Ti_{0.33}Zr_{0.33}Nb_{0.33})_1(Mn_{0.5}Cr_{0.5})_2$ alloy determined by SEM-EDX.

| | **Chemical composition in at% of the as-cast alloy** | | | | |
|---|---|---|---|---|---|
| | **Ti** | **Zr** | **Nb** | **Mn** | **Cr** |
| **Nominal** | 11.1 | 11.1 | 11.1 | 33.3 | 33.3 |
| **Overall** | 14.6 | 12.3 | 7.9 | 30.3 | 33.8 |
| **Dendritic** | 10.0 | 14.1 | 12.2 | 25.8 | 38.0 |
| **Interdendritic** | 16.3 | 11.9 | 6.6 | 31.6 | 32.6 |

The last two compositions $(Ti_{0.33}Zr_{0.33}Nb_{0.33})_1(Fe_{0.5}Mn_{0.5})_2$ and $(Ti_{0.33}Nb_{0.5})_1(Fe_{0.5}Mn_{0.5})_2$ also present the same characteristics. The $(Ti_{0.33}Zr_{0.33}Nb_{0.33})_1(Fe_{0.5}Mn_{0.5})_2$ alloy, showed in Figure 5.35 and Table 5.15, has an overall composition very close to the nominal one. Besides, Ti, Zr, and Nb are not homogeneously distributed between the dendritic and interdendritic regions. The chemical composition measured in the interdendritic region is richer in Ti and Mn, and poorer in Zr and Nb. In contrast, the chemical composition measured in the middle of the dendrites is richer in Zr, Nb, and Fe, and poorer in Ti and Mn.

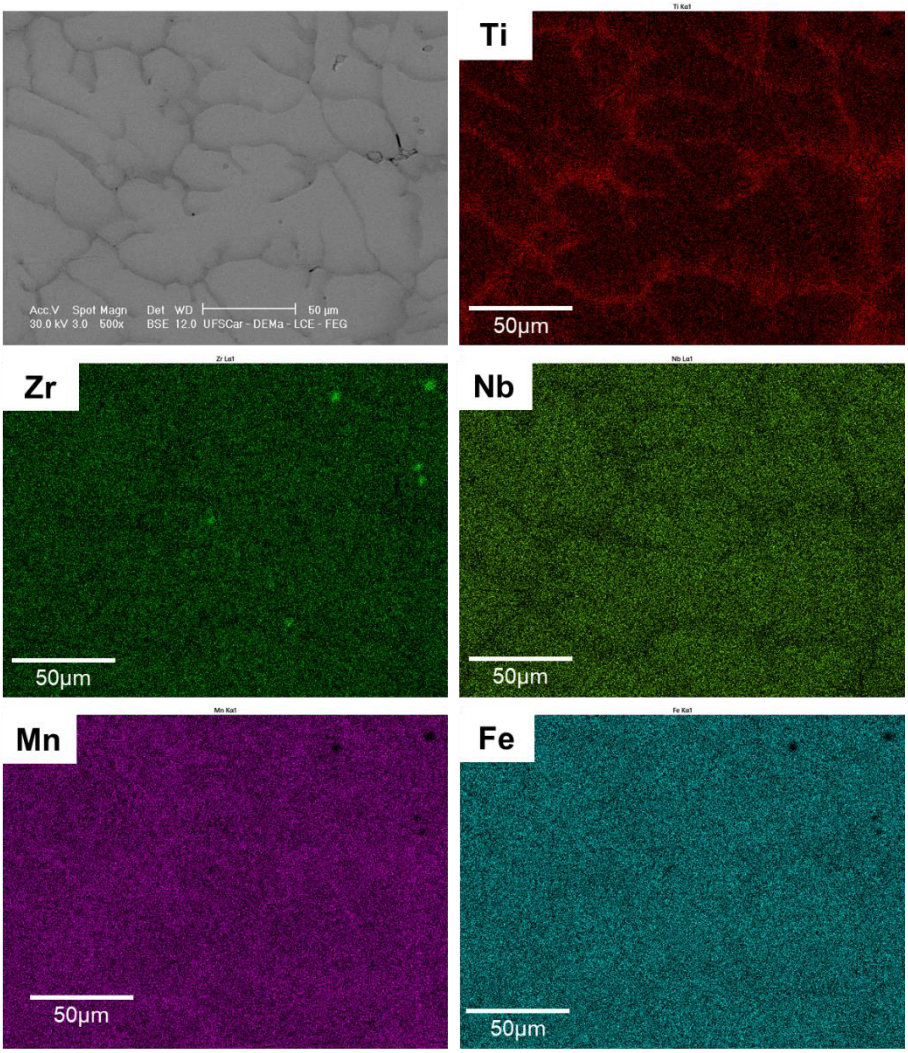


Figure 5. 35 - SEM-BSE image and corresponding EDX elemental maps of the as-cast $(Ti_{0.33}Zr_{0.33}Nb_{0.33})_1(Fe_{0.5}Mn_{0.5})_2$ alloy.

Table 5. 15 - The chemical composition of the $(Ti_{0.33}Zr_{0.33}Nb_{0.33})_1(Fe_{0.5}Mn_{0.5})_2$ alloy determined by SEM-EDX.

| | **Chemical composition in at% of the as-cast alloy** | | | | |
|---|---|---|---|---|---|
| | **Ti** | **Zr** | **Nb** | **Fe** | **Mn** |
| **Nominal** | 11.1 | 11.1 | 11.1 | 33.3 | 33.3 |
| **Overall** | 11.9 | 11.9 | 11.9 | 34.4 | 30.4 |
| **Dendritic** | 8.6 | 12.7 | 12.9 | 36.9 | 28.9 |
| **Interdendritic** | 18.5 | 9.8 | 8.5 | 30.5 | 32.8 |

The $(Ti_{0.5}Nb_{0.5})_1(Fe_{0.5}Mn_{0.5})_2$ alloy, showed in Figure 5.36 and Table 5.16, also has an overall composition very close to the nominal one. Regarding the elemental distribution between the dendritic and interdendritic regions, it is possible to see that the interdendritic region is richer in Ti and Mn, and poorer in Nb and Fe. In contrast, the chemical composition measured in the middle of the dendrites shows that the region is richer in Nb and Fe, and poorer in Ti and Mn.

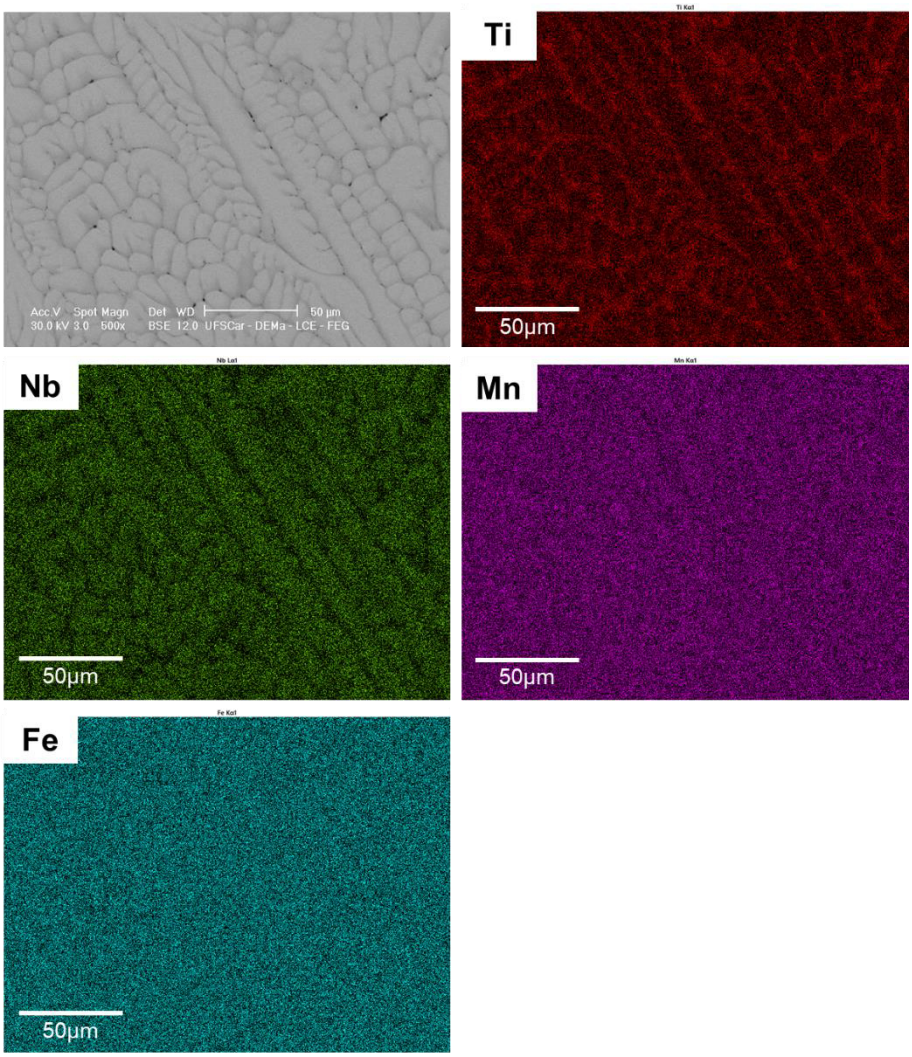


Figure 5. 36 - SEM-BSE image and corresponding EDX elemental maps of the as-cast $(Ti_{0.5}Nb_{0.5})_1(Fe_{0.5}Mn_{0.5})_2$ alloy.

Table 5. 16 - The chemical composition of the $(Ti_{0.5}Nb_{0.5})_1(Fe_{0.5}Mn_{0.5})_2$ alloy determined by SEM-EDX.

| | **Chemical composition in at% of the as-cast alloy** | | | |
|---|---|---|---|---|
| | **Ti** | **Nb** | **Fe** | **Mn** |
| **Nominal** | 16.7 | 16.7 | 33.3 | 33.3 |
| **Overall** | 18.3 | 16.2 | 33.5 | 31.9 |
| **Dendritic** | 13.9 | 19.7 | 35.7 | 30.7 |
| **Interdendritic** | 24.8 | 10.0 | 31.1 | 34.1 |

### 5.2.3 Hydrogen storage properties

#### 5.2.3.1 Kinetics measurements

The hydrogen storage performance of the selected alloys was first investigated by absorption kinetic measurement at room temperature. Initially, the alloys were not subjected to activation procedures, such as temperature or dynamic vacuum. Thus, only the alloy that does not require any activation treatment to absorb hydrogen will be shown in this section.

Among the seven alloys studied, four of them (namely, $(Ti_{0.5}Zr_{0.5})_1Mn_2$, $(Ti_{0.5}Zr_{0.5})_1(Fe_{0.5}Mn_{0.5})_2$, $(Ti_{0.33}Zr_{0.33}Nb_{0.33})_1(Fe_{0.5}Mn_{0.5})_2$, $(Ti_{0.5}Nb_{0.5})_1(Fe_{0.5}Mn_{0.5})_2$) did not absorb hydrogen without activation procedure and required additional activation procedures to be capable of absorbing hydrogen. These procedures will be presented and discussed in Section 5.3.

Figure 5.37 shows the first and second measurements of hydrogen absorption kinetics at 25 °C in H/M of the $(Ti_{0.5}Zr_{0.5})_1(Mn_{0.5}Cr_{0.5})_2$ alloy.

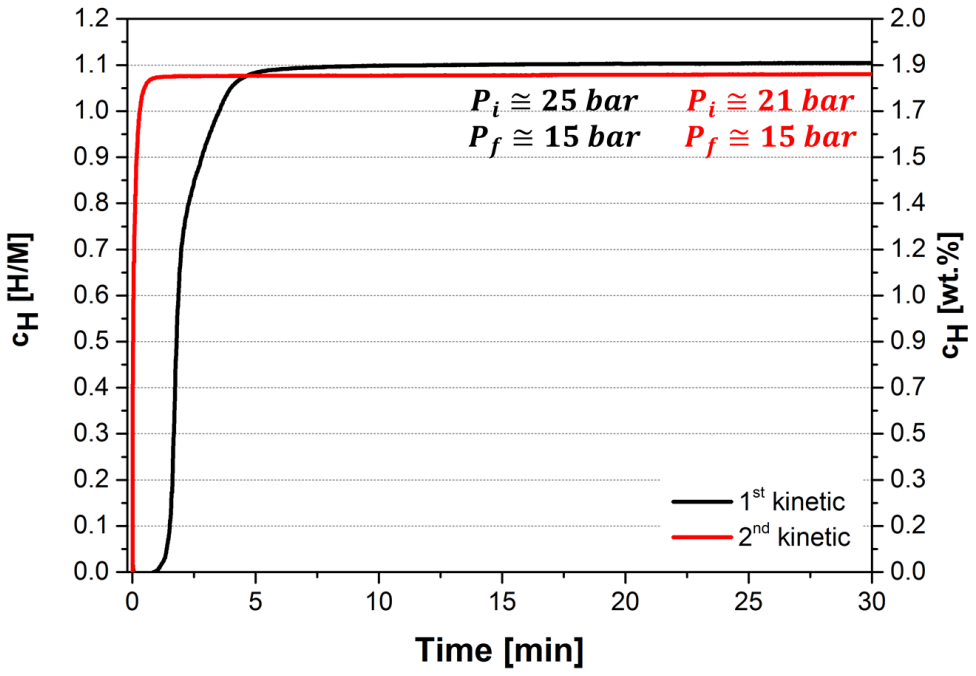


Figure 5. 37 - Measurement of hydrogen absorption kinetics at 25 °C in H/M of the $(Ti_{0.5}Zr_{0.5})_1(Mn_{0.5}Cr_{0.5})_2$ alloy under an initial hydrogen pressure $P_i$ = 25 bar (1st kinetic – black curve) and $P_i$ = 21 bar (2nd kinetic – red curve).

The first kinetic measurement (black curve) was carried out under an initial hydrogen pressure $P_i$ = 25 bar and 30 ºC. One can see that the alloy presented a short incubation time (approximately 1 min) before starting to absorb hydrogen. In addition, it took approximately 5 minutes to absorb the total capacity of H/M ≅ 1.13 (1.90 wt.%). Whereas, in the second kinetic measurement (red curve), carried out under an initial hydrogen pressure $P_i$ = 21 bar, the alloy did not present an incubation time, and started to absorb hydrogen as soon as it came into contact with the gas. Moreover, it took some seconds to reach the total hydrogen absorption capacity of H/M ≅ 1.08 (1.82 wt.%).

Another composition that did not require activation treatment to absorb hydrogen was the $(Ti_{0.5}Zr_{0.5})_1(Fe_{0.33}Mn_{0.33}Cr_{0.33})_2$ alloy, as show in Figure 5.38.

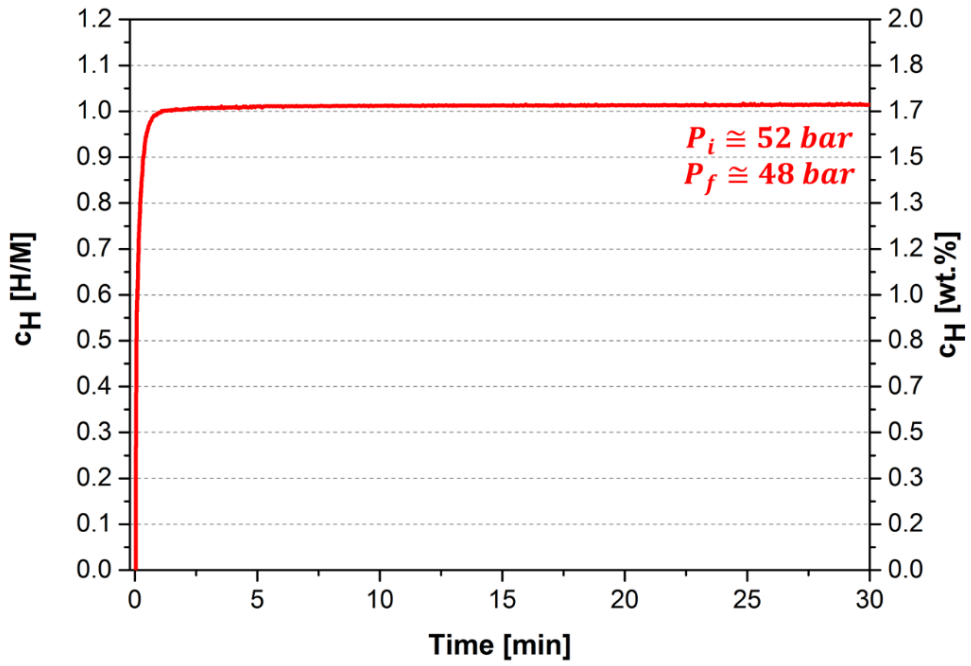


Figure 5. 38 - Measurement of hydrogen absorption kinetics at 30 °C in H/M of the $(Ti_{0.5}Zr_{0.5})_1(Fe_{0.33}Mn_{0.33}Cr_{0.33})_2$ alloy under an initial hydrogen pressure $P_i$ = 52 bar.

The alloy absorbs approximately H/M ≅ 1.02 (1.71 wt.%) of hydrogen, during the first absorption cycle under an initial hydrogen pressure of 52 bar and 30 ºC. It is possible to see that the material absorbs hydrogen extremely fast,

reaching 99% of the total hydrogen capacity in less than one minute. It is important to mention that the alloy does not require any activation treatment to absorb hydrogen. The alloy was observed to absorb hydrogen during the necessary high-pressure hydrogen leak tests conducted prior to the start of the experiments (this alloy was experimentally tested at Department of Heterogenous Catalysis at Max-Planck-Institut für kohlenforschung). However, before the first absorption kinetics measurement, a heat treatment at 390 °C under a dynamic vacuum for 12 h was employed to ensure the sample was completely hydrogen-free.

Figure 5.39 shows the first and second measurements of hydrogen absorption kinetics at 25 °C in H/M of the $(Ti_{0.33}Zr_{0.33}Nb_{0.33})_1(Mn_{0.5}Cr_{0.5})_2$ alloy.

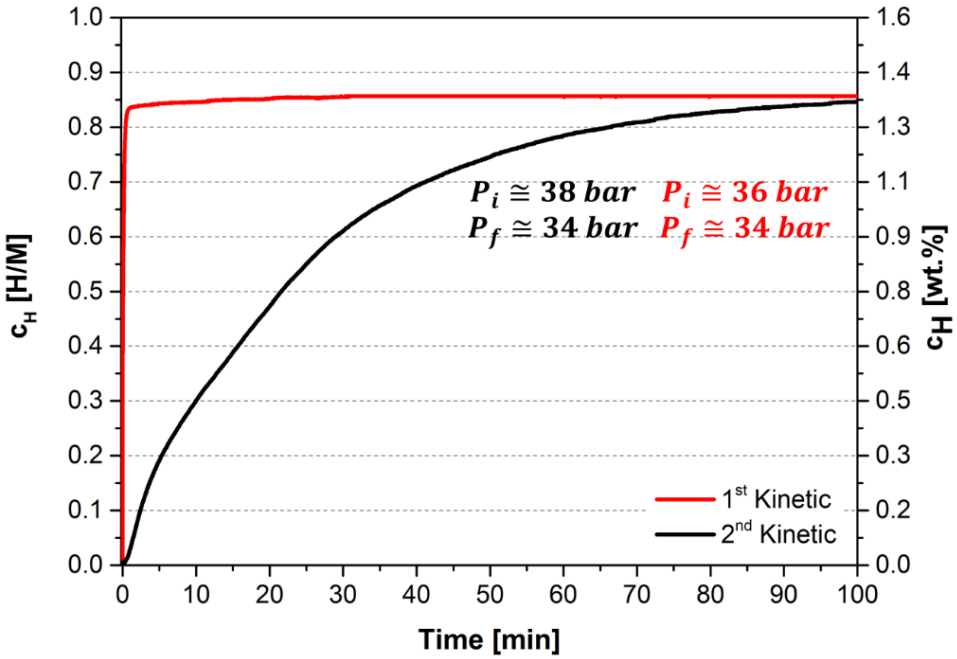


Figure 5. 39 - Measurement of hydrogen absorption kinetics at 25 °C in H/M of the $(Ti_{0.33}Zr_{0.33}Nb_{0.33})_1(Mn_{0.5}Cr_{0.5})_2$ alloy under an initial hydrogen pressure $P_i$ = 38 bar (1st kinetic – black curve) and $P_i$ = 36 bar (2nd kinetic – red curve).

The first kinetic measurement (black curve) was carried out under an initial hydrogen pressure $P_i$ = 38 bar. As can be seen, the alloy started to absorb hydrogen as soon in contact with the gas, however, it presented a slow kinetics. It took approximately 100 minutes to absorb the total capacity of H/M ≅ 0.86 (1.38

wt.%). Whereas, in the second kinetic measurement (red curve), carried out under an initial hydrogen pressure $P_i$ = 36 bar, the alloy absorb hydrogen as soon as in contact with the gas. Moreover, it took some seconds to reach the total hydrogen absorption capacity of H/M ≅ 0.86 (1.38 wt.%).

It is worth mentioning that between the first and second kinetics measurements of the $(Ti_{0.5}Zr_{0.5})_1(Mn_{0.5}Cr_{0.5})_2$, and $(Ti_{0.33}Zr_{0.33}Nb_{0.33})_1(Mn_{0.5}Cr_{0.5})_2$ alloys, dynamic vacuum was applied for one hour. For the $(Ti_{0.5}Zr_{0.5})_1(Mn_{0.5}Cr_{0.5})_2$ it was carried out at room temperature, and for the $(Ti_{0.33}Zr_{0.33}Nb_{0.33})_1(Mn_{0.5}Cr_{0.5})_2$ at 350 °C.

Similar kinetics behavior was observed for some reported alloys, such as $(TiZr)_1(CrMnFeNi)_2$ [10], $Ti_{0.8}Zr_{0.2}Cr_{0.75}M_{1.25}Ce_{0.02}$ [45], $Ti_{0.8}Zr_{0.2}Mn_{0.9}Cr_{0.6}V_{0.3}M_{0.2}$ (M = Fe, Ni, Co) [66], and $(Ti_{0.8}Zr_{0.2})_{1.1}Mn_{1.2}Cr_{0.55}Ni_{0.2}V_{0.05}$ [44]. Most of the reported alloys require a few minutes to reach the maximum absorption capacity. The study reported by Tu et al. [44] for the $(Ti_{0.8}Zr_{0.2})_{1.1}Mn_{1.2}Cr_{0.55}Ni_{0.2}V_{0.05}$ alloy clearly shows the decrease in the time for hydrogen absorption throughout the kinetics measurements. In other words, only in the fourth measurement the alloy presented a fast absorption kinetics, requiring only a few seconds to reach the full hydrogen absorption capacity.

#### 5.2.3.2 PCT measurements and cycling tests.

The hydrogen absorption and desorption performance of the $(Ti_{0.5}Zr_{0.5})_1(Mn_{0.5}Cr_{0.5})_2$, $(Ti_{0.5}Zr_{0.5})_1(Fe_{0.33}Mn_{0.33}Cr_{0.33})_2$, and $(Ti_{0.33}Zr_{0.33}Nb_{0.33})_1(Mn_{0.5}Cr_{0.5})_2$ alloys were further evaluated by PCI measurements at different temperatures and cycling tests at different conditions. It is worth mentioning that the same sample was used for the measurements at the different temperatures, and after each PCI measurement, the sample was exposed to dynamic vacuum for a few minutes at the current temperature. A different cycling strategy was applied for each alloy based on its PCT diagram.

#### 5.2.3.2.1 PCT measurements and comparison

The PCT diagram for the $(Ti_{0.5}Zr_{0.5})_1(Mn_{0.5}Cr_{0.5})_2$, $(Ti_{0.5}Zr_{0.5})_1(Fe_{0.33}Mn_{0.33}Cr_{0.33})_2$, and $(Ti_{0.33}Zr_{0.33}Nb_{0.33})_1(Mn_{0.5}Cr_{0.5})_2$ alloys is shown in Figure 5.40, 5.41, and 5.42, respectively.

Figure 5.40 shows the PCI measurements for the $(Ti_{0.5}Zr_{0.5})_1(Mn_{0.5}Cr_{0.5})_2$ alloy at 30 °C, 60 °C, and 90 °C up to the maximum hydrogen pressure of 80 bar. One can see, the maximum hydrogen uptake at 80 bar decreases as the temperature increases: H/M = 1.14 (1.92 wt.%), H/M = 1.07 (1.81 wt.%), and H/M = 1.01 (1.70 wt.%) for 30 °C, 60 °C, and 90 °C, respectively. For these temperatures, the observed hydrogen equilibrium pressures for the alloy having H/M = 0.5 were approximately 0.4, 1.3, and 3.5 bar, respectively.

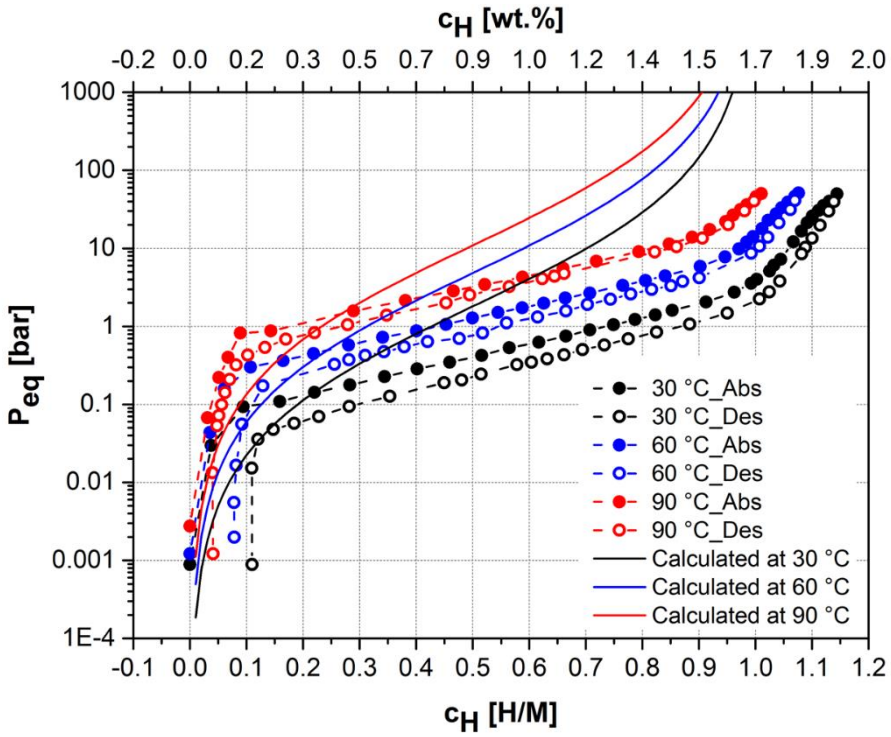


Figure 5. 40 - Comparison between calculated and experimental PCIs of the $(Ti_{0.5}Zr_{0.5})_1(Mn_{0.5}Cr_{0.5})_2$ alloy with $c_H$ = H/M = 0.5 at 30 °C, 60 °C, and 90 °C.

The hydrogen storage capacity observed for the $(Ti_{0.5}Zr_{0.5})_1(Mn_{0.5}Cr_{0.5})_2$ alloy in the kinetics and PCI measurements are close to the theoretical value of 1.70 wt.% calculated considering the formation of an $AB_2H_3$ system. Moreover,

the PCI curves at the three measured temperatures presented minimal hysteresis.

Figure 5.41 shows the PCI measurements for the $(Ti_{0.5}Zr_{0.5})_1(Fe_{0.33}Mn_{0.33}Cr_{0.33})_2$ alloy at 30 °C, 60 °C, 90 °C, and 130 °C up to the maximum hydrogen pressure of 100 bar. The maximum hydrogen uptake at 100 bar decreases as the temperature increases: H/M = 1.04 (1.75 wt.%), H/M = 0.99 (1.66 wt.%), H/M = 0.93 (1.56 wt.%), and H/M = 0.81 (1.35 wt.%), for 30 °C, 60 °C, 90°C, and 130 °C, respectively. For these temperatures, the observed hydrogen equilibrium pressures for the alloy having $c_H$ = 0.5 were approximately 6.7, 12.7, 26.2, and 53.7 bar, respectively.

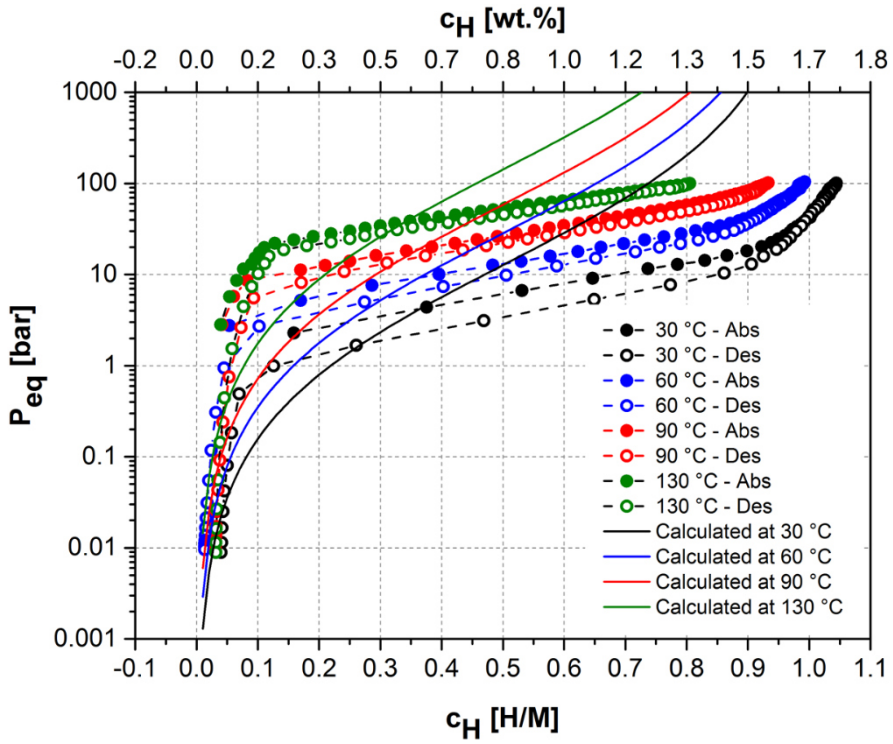


Figure 5. 41 - Comparison between calculated and experimental PCIs of the $(Ti_{0.5}Zr_{0.5})_1(Fe_{0.33}Mn_{0.33}Cr_{0.33})_2$ alloy with $c_H$ = H/M = 0.5 at 30 °C, 60 °C, 90 °C and 130 °C.

It is important to note that the hydrogen absorption capacity decreases as temperature increases, primarily due to the constraints of the experimental pressure limit. Nonetheless, it is possible that the hydrogen uptake would

increase at higher temperatures if pressure above 100 bar was applied to the sample.

The hydrogen storage capacity observed for the $(Ti_{0.5}Zr_{0.5})_1(Fe_{0.33}Mn_{0.33}Cr_{0.33})_2$ alloy in the kinetics and PCI measurements are close to the theoretical value of 1.67 wt.% calculated considering the formation of an $AB_2H_3$ system. In addition, as observed for the $(Ti_{0.5}Zr_{0.5})_1(Mn_{0.5}Cr_{0.5})_2$ alloy, the PCI curves at the different measured temperatures presented minimal hysteresis. Moreover, the absence of a well-defined plateau pressure was also observed in the PCI curves.

The third alloy evaluated by PCI measurements at different temperatures was the $(Ti_{0.5}Zr_{0.5}Nb0.33)_1(Mn_{0.5}Cr_{0.5})_2$ alloy, as illustrated in Figure 5.42. The PCI measurements were performed at 30 °C, 50 °C, and 70 °C up to the maximum hydrogen pressure of 80 bar. The maximum hydrogen uptake at 80 bar decreases as the temperature increases as expected: H/M = 0.92 (1.50 wt.%), H/M = 0.90 (1.46 wt.%), and H/M = 0.83 (1.35 wt.%), for 30 °C, 50 °C, and 70 °C, respectively. For these temperatures, the observed hydrogen equilibrium pressures for the alloy having H/M = 0.5 were approximately 9.6, 15.1, and 26.2 bar, respectively. The hydrogen storage capacity observed for the $(Ti_{0.5}Zr_{0.5}Nb_{0.33})_1(Mn_{0.5}Cr_{0.5})_2$ alloy in the kinetics and PCI measurements are slightly lower than the theoretical value of 1.62 wt.% calculated considering the formation of an $AB_2H_3$ system. This condition should be related primarily due to the constraints of the experimental pressure limit around 80 bar. It is possible that the hydrogen uptake would increase if pressure above 80 bar was applied to the sample, since this composition presents a higher hydrogen equilibrium pressure compared to the two compositions discussed previously. This pressure limit is also the cause of the decrease in the hydrogen absorption capacity as temperature increases. As observed for the two previously alloys, the PCI curves at the different measured temperatures presented minimal hysteresis. Moreover, even with less sloppy PCI curves, the absence of a well-defined plateau pressure was also observed in the PCI curves of the $(Ti_{0.5}Zr_{0.5}Nb_{0.33})_1(Mn_{0.5}Cr_{0.5})_2$ alloy.

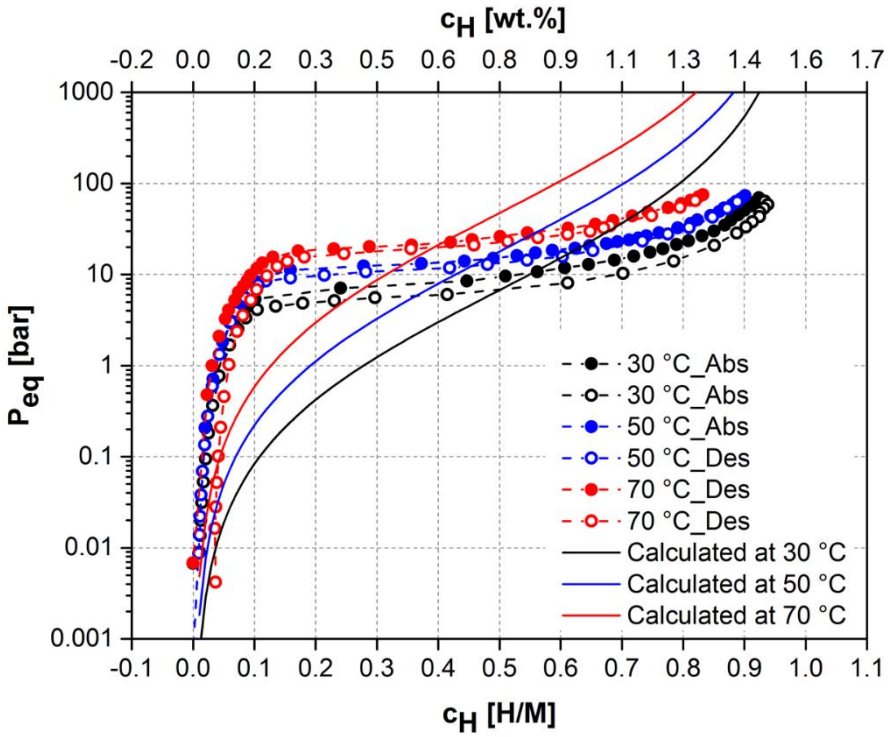


Figure 5. 42 - Comparison between calculated and experimental PCIs of the $(Ti_{0.33}Zr_{0.33}Nb_{0.33})_1(Mn_{0.5}Cr_{0.5})_2$ alloy with $c_H$ = H/M = 0.5 at 30 °C, 50 °C, and 70 °C. For the calculated PCIs curves the overall composition measured by EDS was used (Table 5.14).

Even with almost complete desorption of the samples by reducing the hydrogen pressure to approximately 1 bar, after each PCI measurement, the samples were exposed to a dynamic vacuum for a few minutes at the current temperature to ensure no remaining absorbed hydrogen was left.

Furthermore, the absence of a well-defined plateau pressure was observed in the PCI curves for the three alloys. As presented in Section 3.3, in the literature, experimental PCT diagrams of alloys solidifying in a major C14 Laves phase are found in two typical shapes: with a flat plateau region with well-defined pressure and without a well-defined plateau pressure. These shapes are related to the occurrence or not, respectively, of phase separation between a low hydrogen content solid solution and high hydrogen content hydride. PCT curves with a well-defined plateau pressure were reported for the Laves phase alloys $(TiZr)_1(CrMnFeNi)_2$ [10], $Ti_{1-y}Cr_{2-x}Mn_x$ [13], $Ti_{0.8}Zr_{0.2}Mn_{0.9}Cr_{0.6}V_{0.3}M_{0.2}$ (M = Fe, Ni, Co) [66] and $(Ti_{0.8}Zr_{0.2})_{1.1}Mn_{1.2}Cr_{0.55}Ni_{0.2}V_{0.05}$ [44].

In contrast, the absence of a well-defined plateau pressure suggests hydrogen absorption only by interstitial solid solution. This behavior was reported for $Ti_{20}Zr_{20}Nb_5Fe_{40}Ni_{15}$ [11], $Ti_{0.5}Zr_{0.5}V_{0.5}Ni_{1.1}Mn_{0.2}Fe_{0.2}$ [12], and $Cr_uFe_vMn_wTi_xV_yZr_z$ [14] alloys with the predominant presence of C14 Laves phase.

Although the experimental PCI curves do not show a well-defined plateau pressure, the van't Hoff plot was calculated for the pressure corresponding to $c_H$ = H/M = 0.5 for the three compositions. The van't Hoff plot and the thermodynamic data determined by it are shown in Figure 5.43 and Table 5.17.

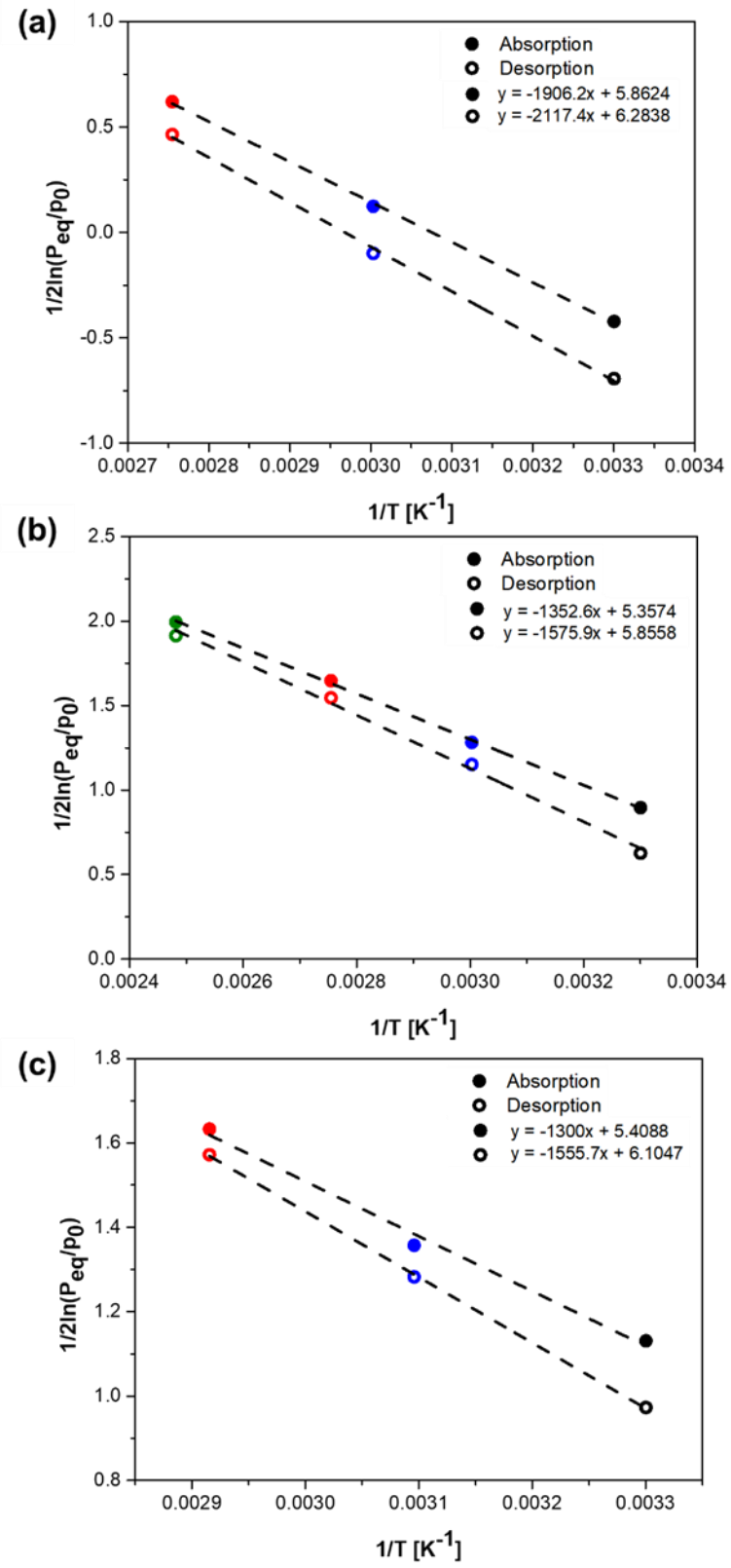


Figure 5. 43 - Van´t Hoff plot for the absorption and desorption pressure at $c_H$ = H/M = 0.5 for the (a) $(Ti_{0.5}Zr_{0.5})_1(Mn_{0.5}Cr_{0.5})_2$, (b) $(Ti_{0.5}Zr_{0.5})_1(Fe_{0.33}Mn_{0.33}Cr_{0.33})_2$, and (c) $(Ti_{0.33}Zr_{0.33}Nb_{0.33})_1(Mn_{0.5}Cr_{0.5})_2$ alloys.

Table 5. 17 - Thermodynamic data determined by van´t Hoff analyses in absorption and desorption from the experimental PCI curves. The values of enthalpy and entropy are given in kJ/mol of H and J/K.mol of H, respectively, and correspond to a hydrogen concentration equal to $c_H$ = H/M = 0.5.

| | **Absorption** | | **Desorption** | |
|---|---|---|---|---|
| | **ΔH** | **ΔS** | **ΔH** | **ΔS** |
| | **[kJ/mol H]** | **[J/K.mol H]** | **[J/K.mol H]** | **[J/K.mol H]** |
| **$(Ti_{0.5}Zr_{0.5})_1(Mn_{0.5}Cr_{0.5})_2$** | -15.84 | -48.74 | +17.06 | +52.24 |
| **$(Ti_{0.5}Zr_{0.5})_1(Fe_{0.33}Mn_{0.33}Cr_{0.33})_2$** | -11.25 | -44.54 | +13.10 | +48.68 |
| **$(Ti_{0.33}Zr_{0.33}Nb_{0.33})_1(Mn_{0.5}Cr_{0.5})_2$** | -10.81 | -44.97 | +12.93 | +50.75 |

These values are in the same range of values already reported in the literature for intermetallic compounds and for multicomponent alloys with C14 Laves phase that show reversibility in the absorption of hydrogen, and often at room temperature [22,44,45,66].

The calculated PCI curves for the $(Ti_{0.5}Zr_{0.5})_1(Mn_{0.5}Cr_{0.5})_2$ $(Ti_{0.5}Zr_{0.5})_1(Fe_{0.33}Mn_{0.33}Cr_{0.33})_2$, and $(Ti_{0.33}Zr_{0.33}Nb_{0.33})_1(Mn_{0.5}Cr_{0.5})_2$ alloys are also presented in Figures 5.40, 5.41, and 5.42. The curves presented some differences in terms of shape, equilibrium pressures and maximum hydrogen uptake at 80 or 100 bar for the different temperatures. The differences between the calculated and experimental PCI curves are expected because of some simplifications of the thermodynamic model employed, as discussed bellow.

The calculated PCIs exhibit S-shaped curves, where equilibrium pressure tends towards infinity as H/M approaches unity. This pattern arises because the model assumes only 12 $A_2B_2$-type interstitial sites per unit cell for hydrogen occupancy. As H/M approaches one, the model predicts nearly complete interstitial sites occupation, leading to excessively high equilibrium pressure, diverging from experimental PCIs.

To enhance the predictability of the model regarding PCI curve shapes, certain considerations should be incorporated into the thermodynamic description of $\Delta G_m(c_H)$. Currently, the model assumes a random occupation of $A_2B_2$-type interstitial sites by hydrogen atoms, considering all sites with the same average

binding energy. However, it overlooks the possibility that sites with lower binding energy may be more favorable for hydrogen occupation, resulting in a non-linear $\Delta H_m(c_H)$ curve and impacting the configuration entropy component of the C14 Laves phase, $\Delta S_m(c_H)$.

Additionally, by assuming that only 12 $A_2B_2$-type tetrahedral sites are available for hydrogen accommodation, the model does not consider the occupation of higher binding energy sites ($AB_3$- and $B_4$-type sites) especially at elevated temperatures, which is probable to occur in practice, resulting in a maximum hydrogen storage capacity higher than H/M = 1. Hence, there exists an opportunity for improvement of the model in this aspect.

Another simplification involves estimating the hydrogen partial enthalpy for the C14 Laves phase by considering the enthalpy of hydrogen solution at infinite dilution of pure elements in $A_2B_2$-type tetrahedral sites. This approach do not consider the interaction between atoms when estimating the enthalpy of hydrogen absorption in the C14 Laves phase.

These aspects, beyond of the scope of this study, should be addressed in future modeling. Considering these factors could enhance predictions of PCI curve shapes and, consequently, improve the accuracy of predicting hydrogen storage properties.

However, despite the differences between calculation and experiment, the proposed model allowed us to reasonably determine the equilibrium pressure of the $(Ti_{0.5}Zr_{0.5})_1(Mn_{0.5}Cr_{0.5})_2$, $(Ti_{0.5}Zr_{0.5})_1(Fe_{0.33}Mn_{0.33}Cr_{0.33})_2$, and $(Ti_{0.33}Zr_{0.33}Nb_{0.33})_1(Mn_{0.5}Cr_{0.5})_2$ alloys as shown in Figure 5.44. Each of the alloys is represented by a different geometric symbol, and the temperatures are differentiated by colors in Figure 5.44.

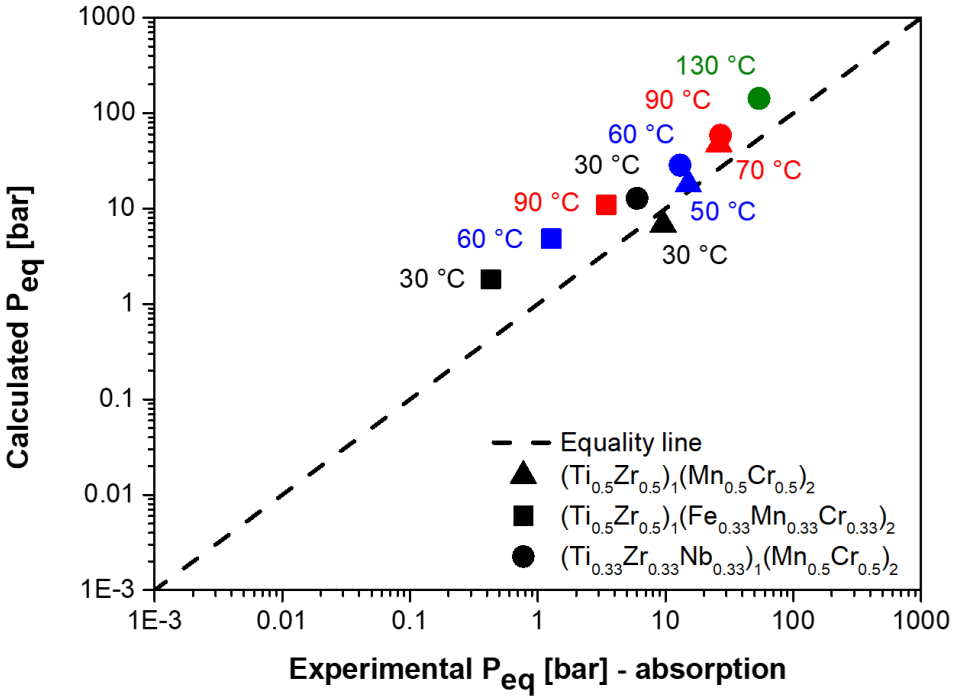


Figure 5. 44 - Comparison between calculated and experimental (measured in absorption) equilibrium pressure for the $(Ti_{0.5}Zr_{0.5})_1(Mn_{0.5}Cr_{0.5})_2$ (square), $(Ti_{0.5}Zr_{0.5})_1(Fe_{0.33}Mn_{0.33}Cr_{0.33})_2$ (circle), and $(Ti_{0.33}Zr_{0.33}Nb_{0.33})_1(Mn_{0.5}Cr_{0.5})_2$ (triangle) alloys with $c_H$ = H/M = 0.5. The temperatures are indicated by colors.

The calculated equilibrium pressures $(Ti_{0.5}Zr_{0.5})_1(Mn_{0.5}Cr_{0.5})_2$ and $(Ti_{0.5}Zr_{0.5})_1(Fe_{0.33}Mn_{0.33}Cr_{0.33})_2$ were slightly overestimated but remained within the same order of magnitude as the experimental values. Regarding the $(Ti_{0.33}Zr_{0.33}Nb_{0.33})_1(Mn_{0.5}Cr_{0.5})_2$ the calculated equilibrium pressures were even closer to those obtained experimentally. For this alloy the PCI curves, and consequently the equilibrium pressures, were calculated considering the composition calculated by EDS. The Nb concentration measured by EDS differs significantly from the nominal one due to melting issue as previously mentioned. For temperatures of 30 °C and 50 °C, the calculated pressures were very close to those observed experimentally (for 30 °C: calculated = 6.8 bar and experimental = 9.6 bar, for 50 °C: calculated = 17.9 bar and experimental = 15.1 bar). For 70 °C, the difference was a bit higher, with the calculated value being 47.5 bar and the observed value being 26.2 bar.

#### 5.2.3.2.2 Cycling tests

The hydrogen absorption/desorption cycling performance of the $(Ti_{0.5}Zr_{0.5})_1(Mn_{0.5}Cr_{0.5})_2$, $(Ti_{0.5}Zr_{0.5})_1(Fe_{0.33}Mn_{0.33}Cr_{0.33})_2$, and $(Ti_{0.33}Zr_{0.33}Nb_{0.33})_1(Mn_{0.5}Cr_{0.5})_2$ alloys were evaluated by measuring the hydrogen absorption capacity over different cycling strategies.

The hydrogen absorption/desorption performance of the $(Ti_{0.5}Zr_{0.5})_1(Mn_{0.5}Cr_{0.5})_2$ alloy was further evaluated by measuring the cycling hydrogen absorption capacity over 20 cycles at 30 ºC. The results of the cycling test are shown in Figure 5.45, where it is possible to see the hydrogen absorption and desorption curves for all de 20 cycles.

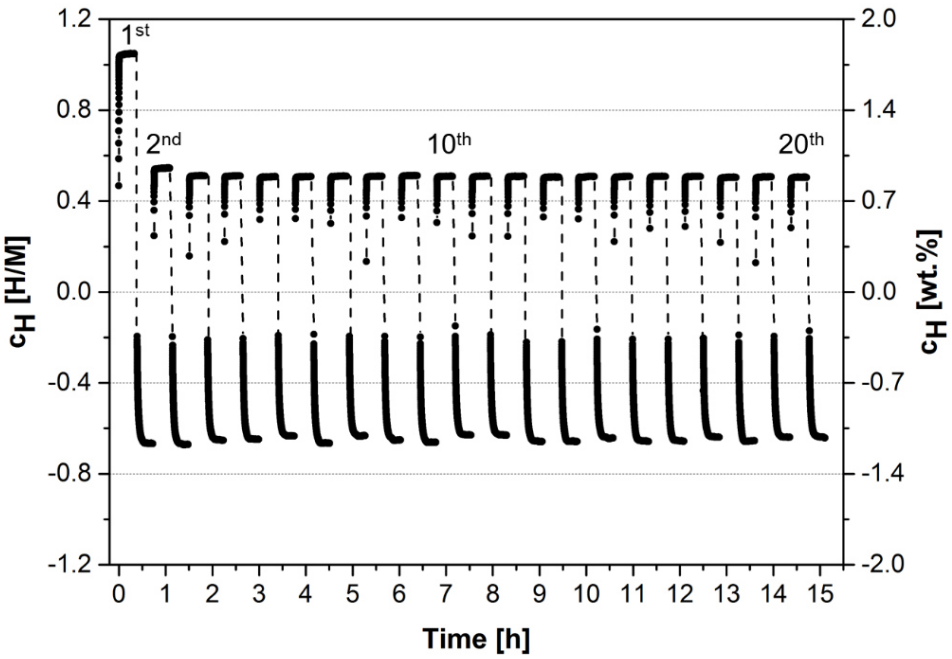


Figure 5. 45 - Hydrogen absorption capacity in H/M of the $(Ti_{0.5}Zr_{0.5})_1(Mn_{0.5}Cr_{0.5})_2$ alloy over the 20$^{th}$ cycles of absorption and desorption at 30 °C. During the absorption cycles, the initial hydrogen pressure was 21 bar, and the final pressure was 16 bar, approximately; the desorption was carried without vacuum exposure.

The hydrogen absorption behavior was performed at 30 °C under an initial pressure of 21 bar for 20 min, while the hydrogen desorption was carried out at the same temperature under an initial pressure of approximately 0.3 bar for 20 min (the sample was not subjected to dynamic vacuum). The hydrogen

absorption capacity in the first cycle was H/M = 1.05 (1.76 wt.%), decreased in the second cycle to H/M = 0.54 (0.93 wt.%). After the second cycle, a slight decrease in hydrogen absorption was observed during the subsequent cycles to a 0.50 H/M (0.86 wt.%), which indicates that the alloy can store the capacity after the second cycle.

It is important to emphasize that the sample was not exposed to a dynamic vacuum during the dehydrogenation kinetics measurements. Therefore, the decrease in the hydrogen absorption capacity should be related to the remaining hydrogen in the alloy under cycling measurements.

Therefore, two other cycling methodologies were performed to test the reversibility of the alloy, as follow.

Figure 5.46 (a) shows the cycling hydrogen absorption capacity over 20 cycles. During the absorption measurement the initial hydrogen pressure was 21 bar. Thus, to verify if the decrease in the hydrogen capacity was related with the remaining hydrogen in the sample holder, the desorption was carried out under dynamic vacuum. As can be seen, the hydrogen absorption capacity remained practically constant over the 20 cycles. The hydrogen absorption capacity in the first cycle was H/M = 1.05 (1.77 wt.%), and in the second cycle was H/M = 1.04 (1.75 wt.%). No decrease in hydrogen absorption was observed during the subsequent cycles, in the $20^{th}$ cycle the capacity was 1.03 H/M (1.74 wt.%), which indicates that the alloy can store 98% of the capacity over 20 cycles.

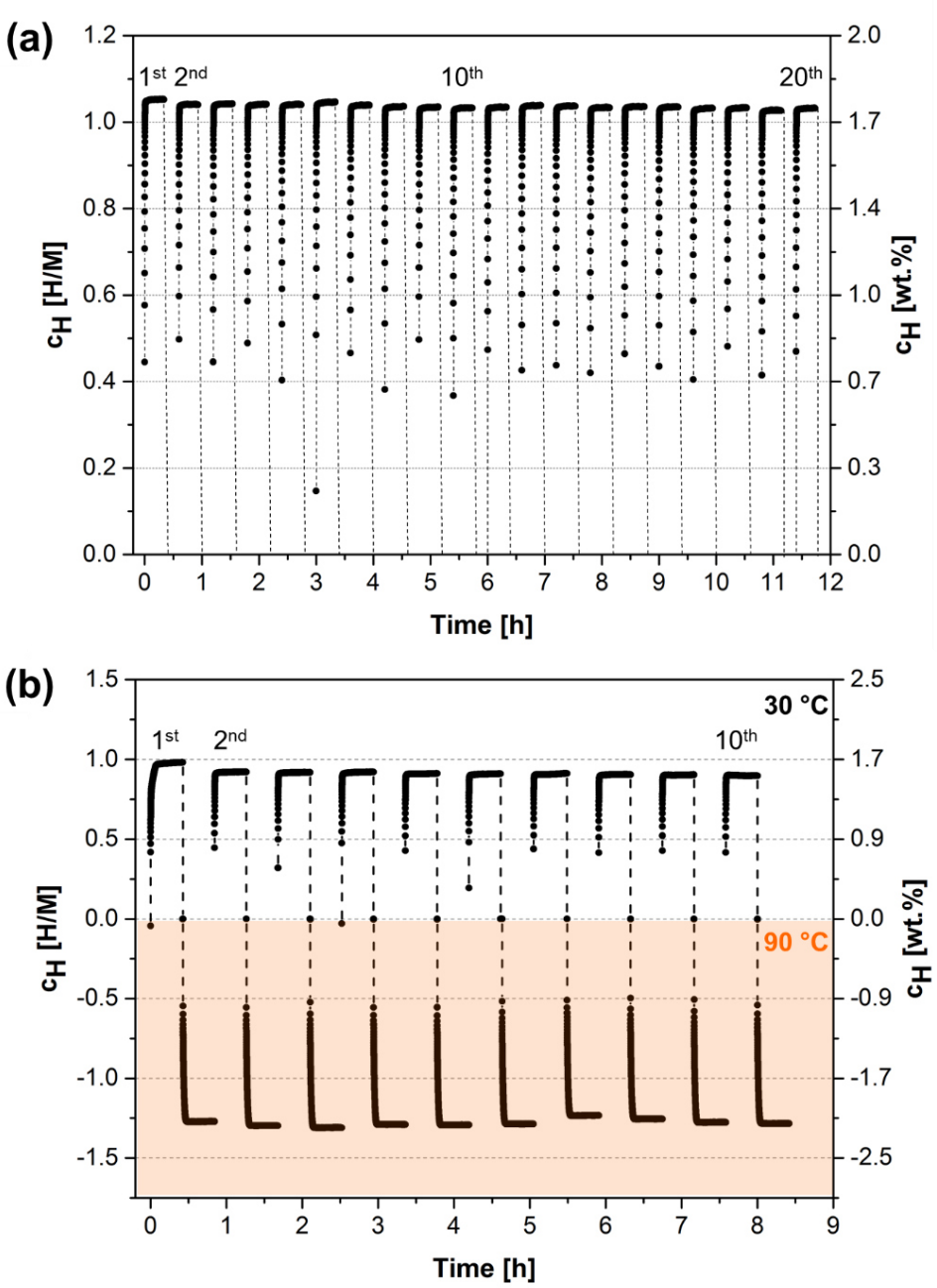


Figure 5. 46 - Hydrogen absorption capacity in H/M of the $(Ti_{0.5}Zr_{0.5})_1(Mn_{0.5}Cr_{0.5})_2$ alloy. (a) Over the 20$^{th}$ cycles of absorption at 30 °C. During the absorption cycles, the initial hydrogen pressure was 21 bar, and the final pressure was 16 bar; the desorption was carried out under dynamic vacuum. (b) Over 10$^{th}$ cycles of absorption and desorption. During the absorption cycles the temperature was at 30 °C and the initial hydrogen pressure was 21 bar, and the final pressure was 16 bar, approximately; the desorption was carried without vacuum exposure at 90 °C under an initial pressure of 0.2 bar.

Figure 5.46 (b) shows another cycling methodology that was carried out. The cycling performance of the alloy was evaluated over ten cycles. During the absorption cycles the temperature was at 30 °C and the initial hydrogen pressure was 21 bar for 20 min, and the desorption was carried without vacuum exposure (0.2 bar) at 90 °C. This temperature was chosen to overcome the barrier to complete desorption without the need for vacuum application. As observed in the PCT diagram (Figure 5.41), at 30 °C the equilibrium pressure was close to the atmospheric pressure (0.43 bar), which implies incomplete desorption when the hydrogen pressure is released (without applying a vacuum). However, the PCT diagram showed that the equilibrium pressure of the alloy is higher at 90 °C (3.5 bar), which would facilitate the desorption. Thus, even without exposing the sample to a dynamic vacuum, the alloy should desorb almost completely when the hydrogen pressure was released to around 1 bar.

The maximum hydrogen absorption capacity was H/M = 1.01 (1.70 wt.%) for the first cycle, then decreases to H/M = 0.92 (1.55 wt.%) at the second cycle, and to H/M = 0.90 (1.51 wt.%) during the eight subsequent cycles, which indicates that the alloy exhibits good reversible hydrogen storage properties and can store at least 89% of its initial capacity after ten cycles. The desorption behavior without dynamic vacuum application is a facilitating factor for the practical use of an alloy, therefore, this methodology was a good alternative.

For enhanced visualization of the cycling strategies, Figure 5.47 illustrates the pressure and capacity ranges observed during cycling tests. The red-colored rectangle highlights the cycling range showed in Figure 5.46. In this test, conducted at 30°C, the sample exhibited a capacity loss due to the relatively high hydrogen concentration (approximately 0.4 H/M) during desorption at that temperature. Subsequently, in the cycling test involving absorption at 30°C and desorption at 90°C (Figure 5.46 (b)), the cycling range expands and include both the red and green-colored regions.

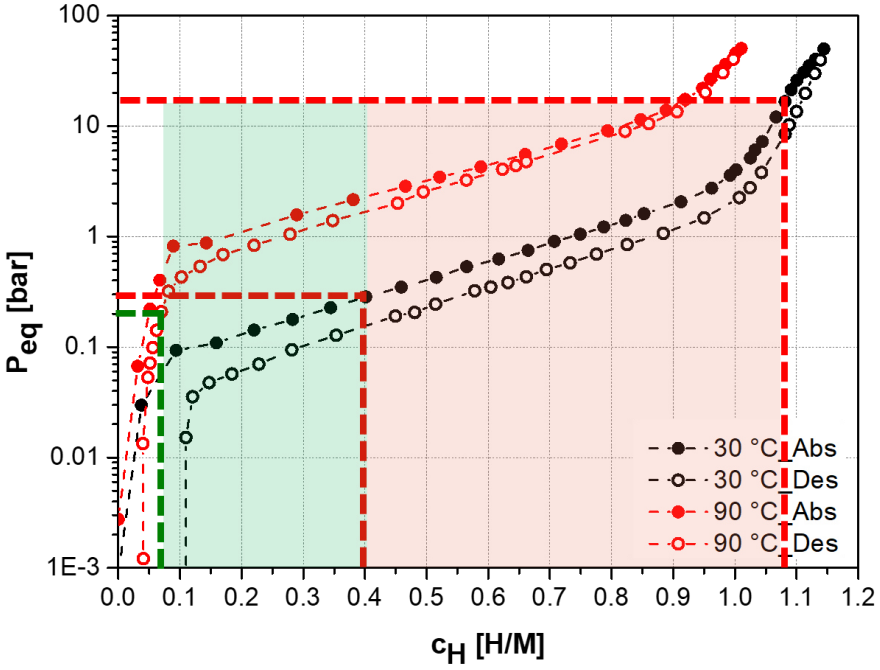


Figure 5. 47 - Pressure and capacity ranges observed during cycling tests of the $(Ti_{0.5}Zr_{0.5})_1(Mn_{0.5}Cr_{0.5})_2$ alloy. The red-colored rectangle highlights the cycling range showed in Figure 5.46 and the red- plus green-colored the cycling test showed in Figure 5.46 (b).

Moreover, it is worth noting that in Figures 5.45 and 5.46 (b), the desorption capacity exceeds that of absorption. During desorption the capacity is on average H/M = 1.27 and in absorption it is on average H /M = 0.92. This difference has no influence on the absorption capacity throughout the cycles, as discussed above. This difference is related to a set of factors that occur during cycling tests. Initially, there exists a difference in the volumes of the reservoirs used during absorption and desorption measurements. For absorption, the reservoir volume ranged between 13 and 17 $cm^3$, whereas during desorption, the gas was expanded into a reservoir with a volume of approximately 1000 $cm^3$. Furthermore, the calibration of the larger volume reservoir was not conducted prior to cycling tests. Additionally, a transition from the high-pressure sensor (associated with the smaller volume reservoir) to the low-pressure sensor (linked with the larger volume reservoir) occurs during desorption. Therefore, the higher capacity measured during desorption must be seen as an artifact of the

measurement and the real reversible capacity of the alloy must be considered those measured in absorption measurements.

The hydrogen absorption and desorption cycling performance of the $(Ti_{0.5}Zr_{0.5})_1(Fe_{0.33}Mn_{0.33}Cr_{0.33})_2$ alloy was assessed by measuring its hydrogen absorption capacity over 50 cycles. The results of the cycling test are show in Figure 5.48.

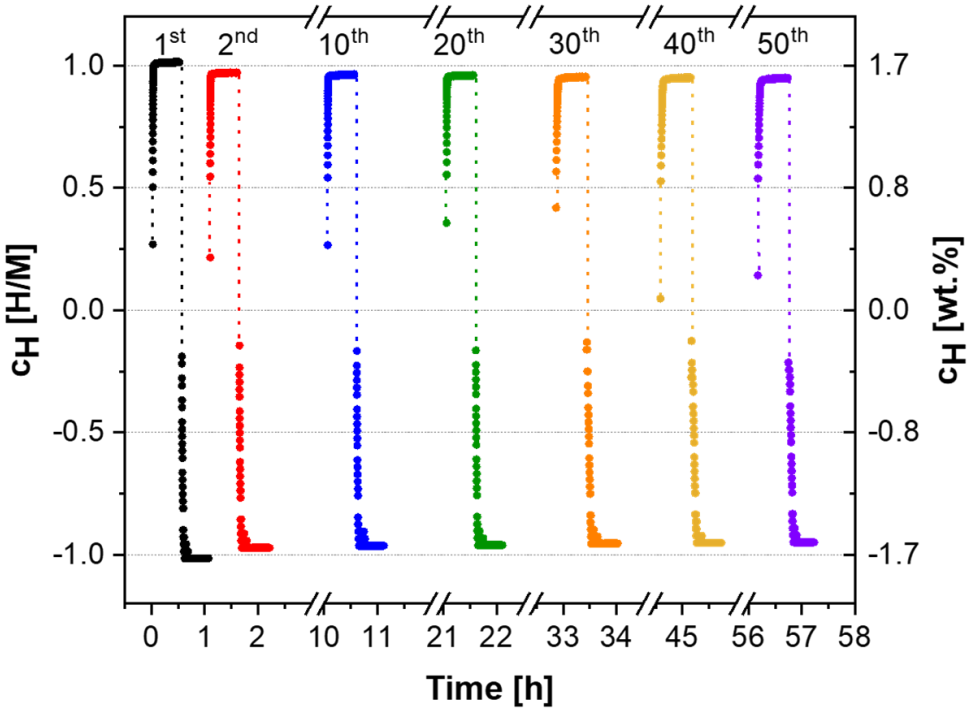


Figure 5. 48 - Hydrogen absorption capacity in H/M of the $(Ti_{0.5}Zr_{0.5})_1(Fe_{0.33}Mn_{0.33}Cr_{0.33})_2$ alloy over the 1st, 2nd, 10th, 20th, 30th, 40th, and 50th cycles of absorption and desorption at 30 °C. During the absorption cycles, the initial hydrogen pressure was 52 bar, and the final pressure was 48 bar, approximately; the desorption was carried without vacuum exposure.

The hydrogen absorption behavior was carried out at 30 °C under an initial pressure of 52 bar for 30 min, while the hydrogen desorption was carried out at the same temperature under an initial pressure of approximately 0.6 bar for 30 min. Figure 5.48 shows the hydrogen absorption and desorption curves for the 1st, 2nd, 10th, 20th, 30th, 40th, and 50th cycles. The hydrogen absorption capacity in the first cycle was H/M = 1.02 (1.71 wt.%), and decreased in the second cycle to

H/M = 0.97 (1.62 wt.%). After the second cycle, a slight decrease in hydrogen absorption from 0.97 wt.% to 0,94 (1.59 wt.%) was observed during the subsequent cycles. Figure 5.49 illustrates the pressure and capacity ranges observed during the cycling test.

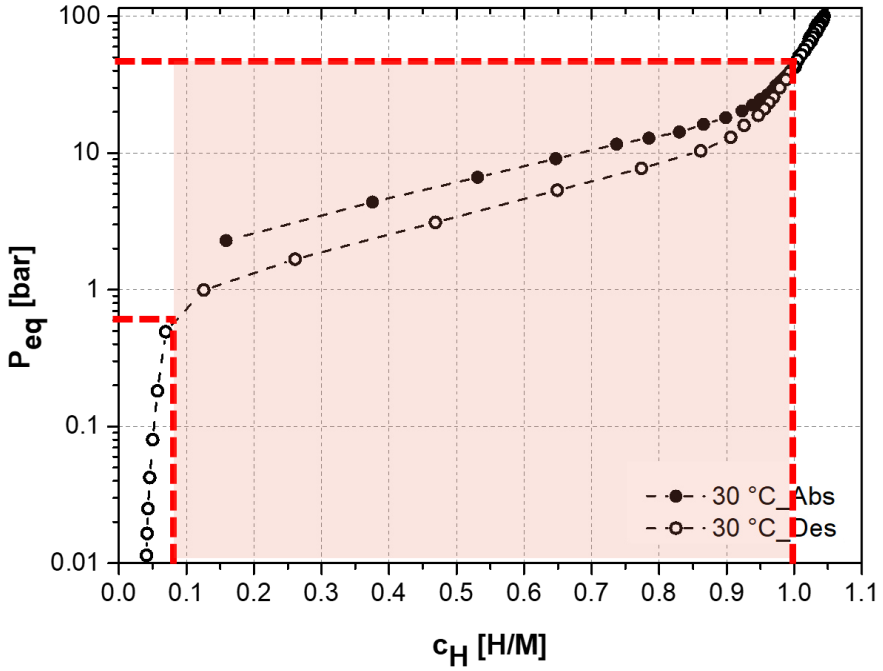


Figure 5. 49 - Pressure and capacity range observed during cycling test of the $(Ti_{0.5}Zr_{0.5})_1(Fe_{0.33}Mn_{0.33}Cr_{0.33})_2$ alloy. The red-colored rectangle highlights the cycling range showed in Figure 5.48.

This slight decrease in the hydrogen storage capacity can be attributed to the size refinement of the alloy particles, which takes place during the initial hydrogenation. This refinement could lead to an increase in crystalline defects, such as dislocations and grain boundaries, known to reduce the hydrogen storage capacity of metal hydrides [66]. Additionally, the sample was not exposed to a dynamic vacuum during the dehydrogenation kinetics measurements. Therefore, the decrease in the hydrogen absorption capacity could also be related to the remaining hydrogen in the crystal under cycling measurements. Nonetheless, the cycling results indicates that the alloy can store at least 93% of its initial capacity after 50 cycles, which indicates that the alloy exhibits excellent

reversible hydrogen storage properties. For this alloy, no temperature increasing or vacuum was required to performing cycling experiments, since the PCT diagram (Figure 5.41) showed that the sample could be desorbed almost entirely (H/M < 0.1) by reducing the hydrogen pressure to approximately 1 bar, even at 30 °C.

The hydrogen absorption and desorption cycling performance of the $(Ti_{0.5}Zr_{0.5}Nb_{0.33})_1(Mn_{0.5}Cr_{0.5})_2$ alloy was evaluated by measuring its hydrogen absorption capacity over 50 cycles. The results of the cycling test are show in Figure 5.50. The hydrogen absorption behavior was performed at 30 °C under an initial pressure of 35 bar for 20 min, while the hydrogen desorption was performed at the same temperature under an initial pressure of approximately 4 bar for 20 min.

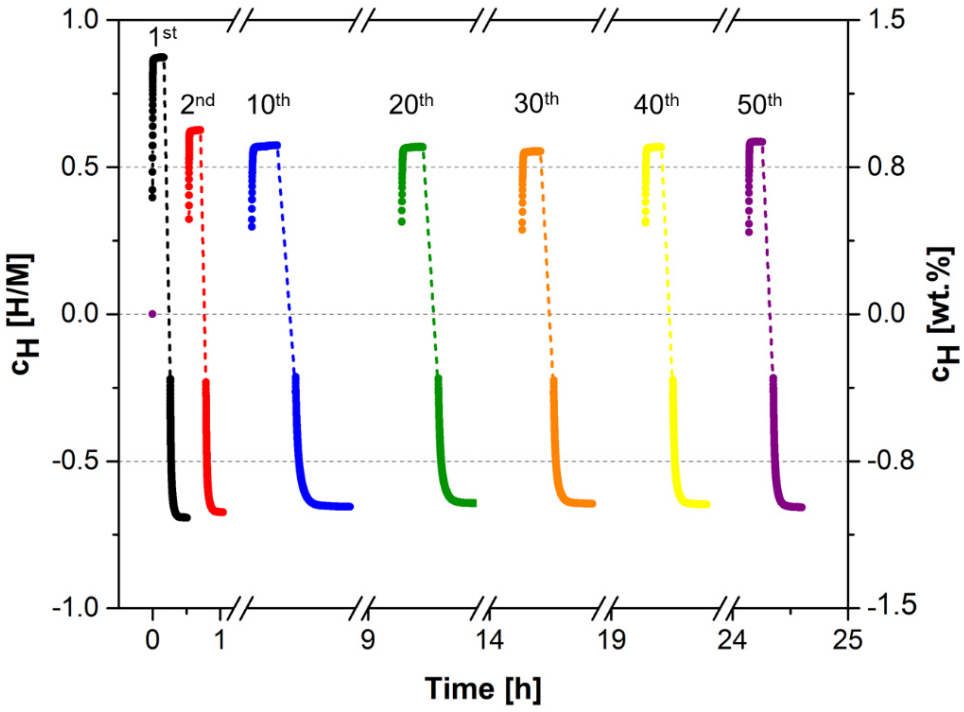


Figure 5. 50 - Hydrogen absorption capacity in H/M of the $(Ti_{0.33}Zr_{0.33}Nb_{0.33})_1(Mn_{0.5}Cr_{0.5})_2$ alloy over the (a) 1st, 2nd, 10th, 20th, 30th, 40th, and 50th cycles of absorption and desorption. During the absorption cycles, the initial hydrogen pressure was 35 bar, and the final pressure was 33 bar, approximately; the desorption was carried without vacuum exposure.

Figure 5.50 shows the hydrogen absorption and desorption curves for the 1st, 2nd, 10th, 20th, 30th, 40th, and 50th cycles. The hydrogen absorption capacity in the first cycle was H/M = 0.87 (1.41 wt.%), and decreased in the second cycle to H/M = 0.63 (1.02 wt.%). After all the fifty cycles, a slight decrease in hydrogen absorption from 0.63 to 0.59 (0.95 wt.%) was observed. Figure 5.51 illustrates the pressure and capacity ranges observed during this cycling test.

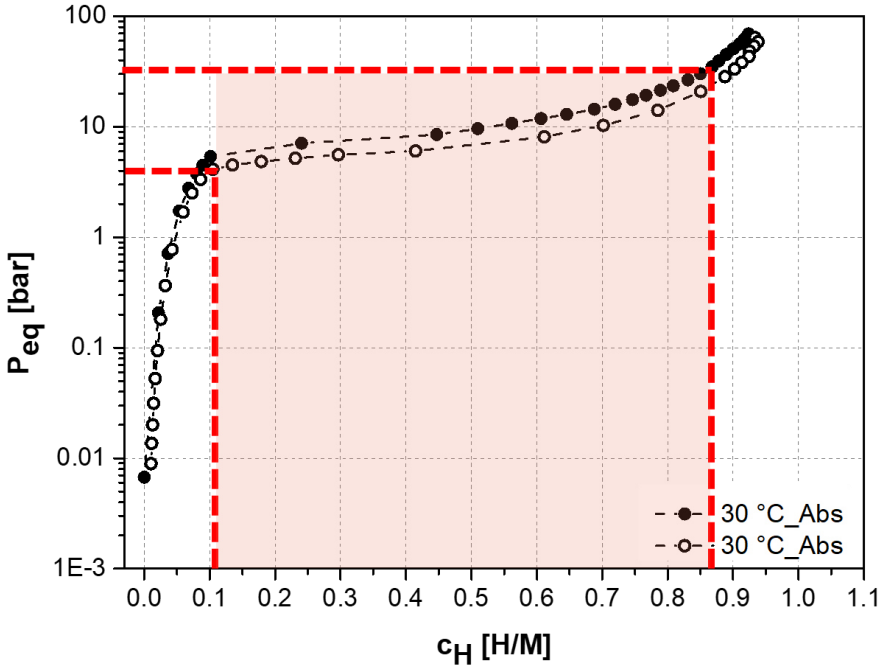


Figure 5. 51 - Pressure and capacity range observed during cycling test of the $(Ti_{0.33}Zr_{0.33}Nb_{0.33})_1(Mn_{0.5}Cr_{0.5})_2$ alloy. The red-colored rectangle highlights the cycling range showed in Figure 5.48.

This decrease in the hydrogen storage capacity from the first to the second cycle can be attributed to the relatively high hydrogen pressure (≅ 4 bar) remained in the sample holder during the desorption measurement. This pressure level did not allow the complete hydrogen desorption of the sample. As can be observed in the PCT diagram (Figure 5.42) and Figure 5.51, at 30 °C and approximately 4 bar, the hydrogen concentration in the sample still higher than 0.1 H/M. If the desorption measurements were carried out at pressures below 1 bar, probably no loss of capacity would have been observed. Furthermore, the

subsequent slight decrease can be attributed to the size refinement of the alloy particles, which occurs during the hydrogenations, as previously discussed.

To better understand the hydrogen storage behavior of the alloys, the samples after the first and the last cycle of absorption and desorption were characterized by XRD.

Figure 5.52 shows the XRD patterns of these samples and the XRD pattern of the as-cast $(Ti_{0.5}Zr_{0.5})_1(Mn_{0.5}Cr_{0.5})_2$ sample. The lattice parameters obtained by Rietveld refinement for the C14 Laves phase in these three samples are also shown in Figure 5.52.

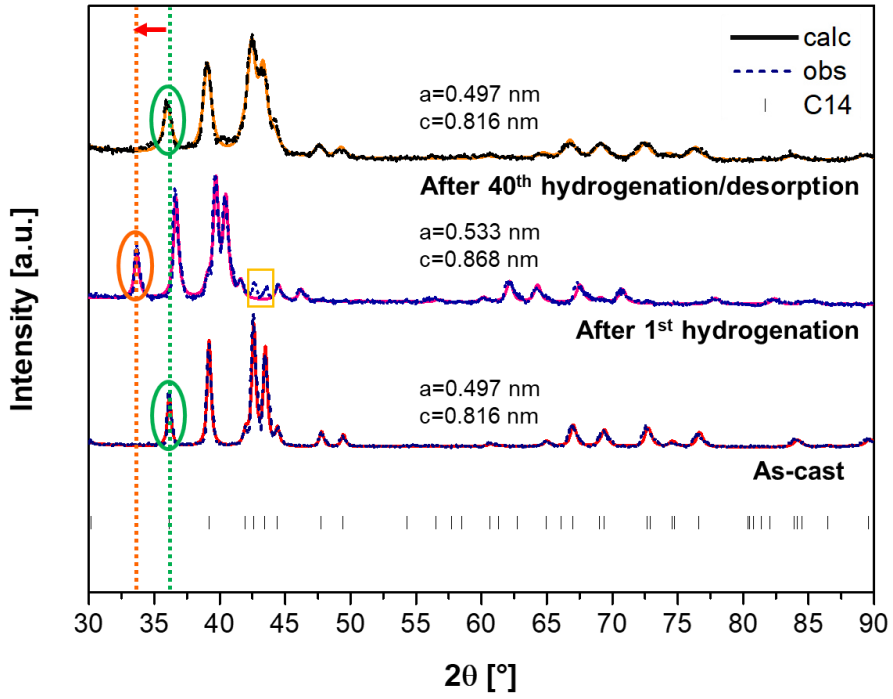


Figure 5. 52 - XRD patterns of the $(Ti_{0.5}Zr_{0.5})_1(Mn_{0.5}Cr_{0.5})_2$ alloy. (a) as-cast, (b) after one absorption cycle, and (c) after forty absorption/desorption cycles (measured with KαCu radiation).

One can see that after one and forty hydrogenation cycles, the samples still presented a single C14 Laves phase. However, changes in lattice parameters were observed. As presented in Figure 5.40, this composition has a hydrogen equilibrium pressure lower than 1 bar, then it is not able to desorb completely without exposure to vacuum. In order to characterize the hydride, the sample was

not desorbed after the first exposure to hydrogen and it was sent to XRD characterization as soon as the hydrogenation was finished. In this way, it was possible to observe a shift to the left of the C14 phase reflections (shift from the green dashed line to the orange one). This shift to the left is a consequence of the increase in the lattice parameters of the crystals, which increased from a = 0.497 nm and c = 0.816 nm to a = 0.533 nm and c = 0.868 nm. In terms of unit cell volume, it corresponds to an increase from 174.56 $Å^3$ to 213.39 $Å^3$. According to the well-known Peisl relationship [67], such volume expansion should correspond to a hydrogen uptake of 1.1 H/M, which agree well with the 2.9 $Å^3$ per hydrogen atom absorbed, as proposed by Peisl, and with the capacity observed in the kinetic measurement (Figure 3.38), that was the measurement carried out before the this XRD analysis. Additionally, two non-identified reflections were observed between 42° e 45° (yellow rectangle). Moreover, the diffraction pattern of the sample after 40 absorption/desorption cycles did not show such a significant change in lattice parameters, since it was subjected to a desorption measurement before XRD analysis. However, a peak broadening was observed in this sample. These broadening could be related to smaller or greater lattice parameters in different crystals or to an increase in crystalline defects, such as dislocations and grain boundaries that occurs over the hydrogenation cycles.

Figure 5.53 displays the XRD patterns for samples of the $(Ti_{0.5}Zr_{0.5})_1(Fe_{0.33}Mn_{0.33}Cr_{0.33})_2$ composition. The lattice parameters obtained through Rietveld refinement for the C14 Laves phase in these samples are also illustrated in Figure 5.53. Remarkably, even after multiple hydrogenation cycles, there were no changes in the constituent phases. After one and fifty hydrogenation cycles, the samples still presented a single C14 Laves phase, and no changes in lattice parameters were observed. These XRD results, along with the PCI curves showed in Figure 5.41 and the cycling test curves in Fig. 5.48, indicate that the $(Ti_{0.5}Zr_{0.5})_1(Fe_{0.33}Mn_{0.33}Cr_{0.33})_2$ alloy rapidly desorbs most of the hydrogen when the pressure is reduced to 1 bar. In addition, during the cycling test at room temperature and at an initial hydrogen pressure of 0.6 bar, the alloy was almost completely desorbed (H/M < 0.1). The same procedure was applied during the PCT tests, where nearly full desorption (H/M < 0.05) was achieved at

desorption temperatures of 30 °C, 60 °C, 90 °C, and 130 °C, with equilibrium pressure steps down to 0.01 bar. Moreover, any remaining hydrogen in the alloy structure was released during sample evacuation preceding further characterization. Consequently, the characterization of the hydrogenated phase by XRD was not possible after the hydrogenation test.

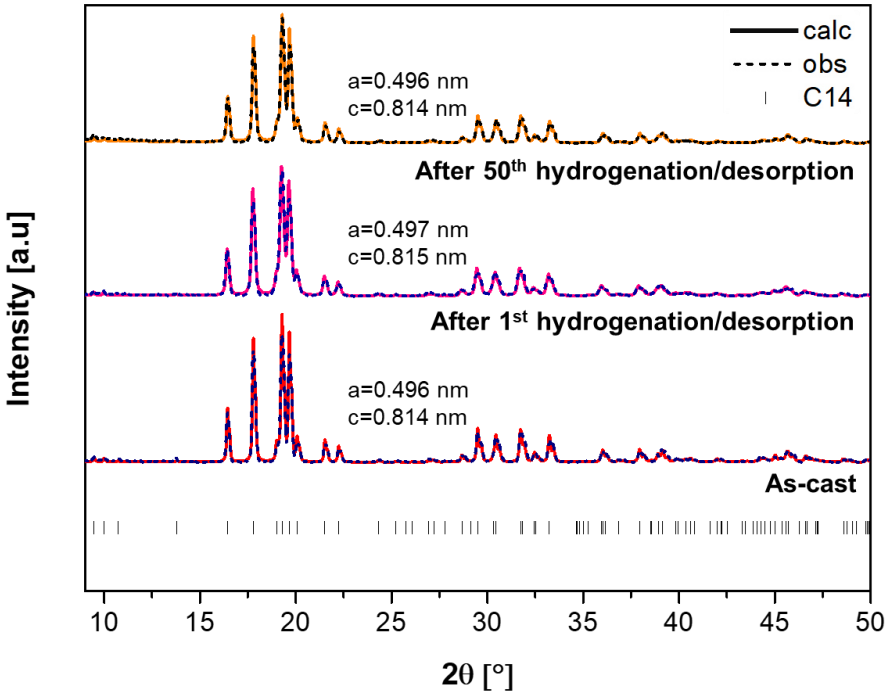


Figure 5. 53 - XRD patterns of the $(Ti_{0.5}Zr_{0.5})_1(Fe_{0.33}Mn_{0.33}Cr_{0.33})_2$ alloy. (a) as-cast, (b) after one absorption/desorption cycle, and (c) after fifty absorption/desorption cycles (measured with KαMo radiation).

Figure 5.54 shows the XRD patterns of these samples and the XRD pattern of the as-cast $(Ti_{0.33}Zr_{0.33}Nb_{0.33})_1(Mn_{0.5}Cr_{0.5})_2$ sample. The lattice parameters obtained by Rietveld refinement for the C14 Laves phase in these three samples are also shown in Figure 5.54. As observed for the $(Ti_{0.5}Zr_{0.5})_1(Fe_{0.33}Mn_{0.33}Cr_{0.33})_2$ alloy, even after several hydrogenation cycles, there were no changes in the constituent phases. After one and fifty hydrogenation/dehydrogenation cycles, the samples still presented a single C14 Laves phase, and no changes in lattice parameters were observed. These XRD findings, along with the PCI curves showed in Figure 5.42, indicate that the

$(Ti_{0.33}Zr_{0.33}Nb_{0.33})_1(Mn_{0.5}Cr_{0.5})_2$ alloy easily desorbs most of the hydrogen when the pressure is reduced to 1 bar. In addition, the hydrogen remaining in the alloy structure was released during the evacuation of the sample prior to the further characterization of the alloy. Thus, the characterization of the hydrogenated phase by XRD was not possible after the hydrogenation tests.

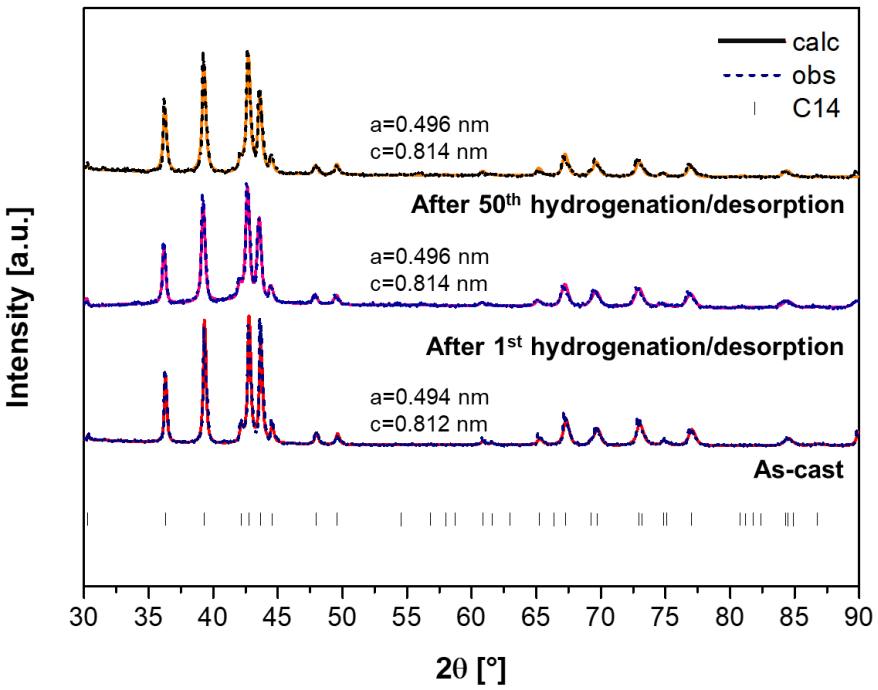


Figure 5. 54 - XRD patterns of the $(Ti_{0.33}Zr_{0.33}Nb_{0.33})_1(Mn_{0.5}Cr_{0.5})_2$ alloy. (a) as-cast, (b) after one absorption/desorption cycle, and (c) after fifty absorption/desorption cycles (measured with KαCu radiation).

Figures 5.55, 5.56, and 5.57 shows the microstructural characteristics of the $(Ti_{0.5}Zr_{0.5})_1(Mn_{0.5}Cr_{0.5})_2$, $(Ti_{0.5}Zr_{0.5})_1(Fe_{0.33}Mn_{0.33}Cr_{0.33})_2$, $(Ti_{0.33}Zr_{0.33}Nb_{0.33})_1(Mn_{0.5}Cr_{0.5})_2$ alloys in two conditions. Figures (a) and (c) show the as-cast sample after being crushed into powder (used to load into a Sieverts-type apparatus) in two different magnifications. The particle size of the alloy is in the range of about 200 μm. Figures (b) and (d) corresponding to the sample after 40 or 50 cycles of hydrogen absorption and desorption. The reduction in alloy particle size is clearly observable, accompanied by the development of surface cracks on the particles. Similar behavior was observed in previous studies and was related to the volume

expansion of the C14 Laves phase after hydrogen absorption. This expansion induces significant internal stress concentration in the host metal, leading to its embrittlement post-absorption, thus yielding a powder characterized by fine particle sizes ranging from 10 to 100 μm [5,19,66]. As mentioned before, this reduction in at least one order of magnitude in the size of the alloy particles increases crystalline defects, such as dislocations and grain boundaries, contributing to the slight reduction of capacity during cycling, as seen for $(Ti_{0.5}Zr_{0.5})_1(Fe_{0.33}Mn_{0.33}Cr_{0.33})_2$ and $(Ti_{0.33}Zr_{0.33}Nb_{0.33})_1$ $(Mn_{0.5}$ $Cr_{0.5})_2$ alloys. In addition, contributing to reflection broadening in the XRD patterns, as observed for $(Ti_{0.5}Zr_{0.5})_1(Mn_{0.5}Cr_{0.5})_2$ alloy.

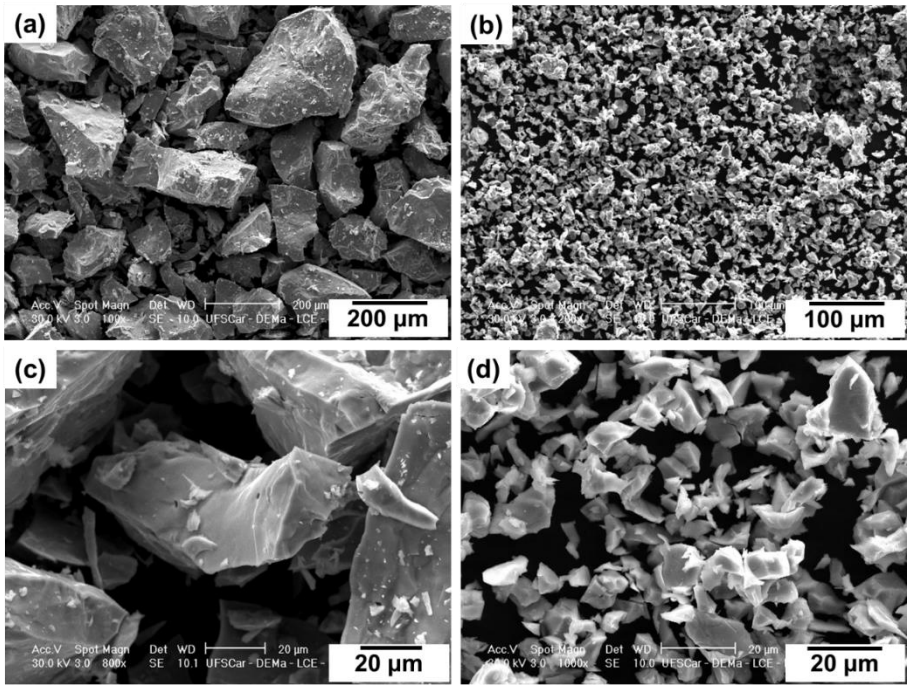


Figure 5. 55 - SEM images of the $(Ti_{0.5}Zr_{0.5})_1(Mn_{0.5}Cr_{0.5})_2$ alloy in as cast (a) and (c), and after 40th cycles of hydrogenation/dehydrogenation (b) and (d).

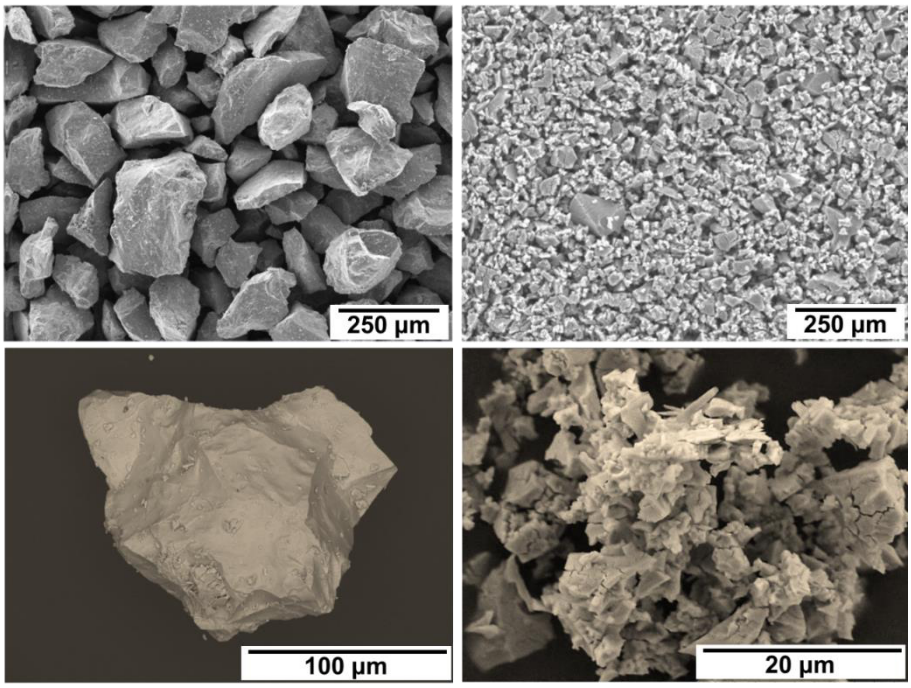


Figure 5. 56 - SEM images of the $(Ti_{0.5}Zr_{0.5})_1(Fe_{0.33}Mn_{0.33}Cr_{0.33})_2$ alloy in as cast (a) and (c), and after 50th cycles of hydrogenation/dehydrogenation (b) and (d).

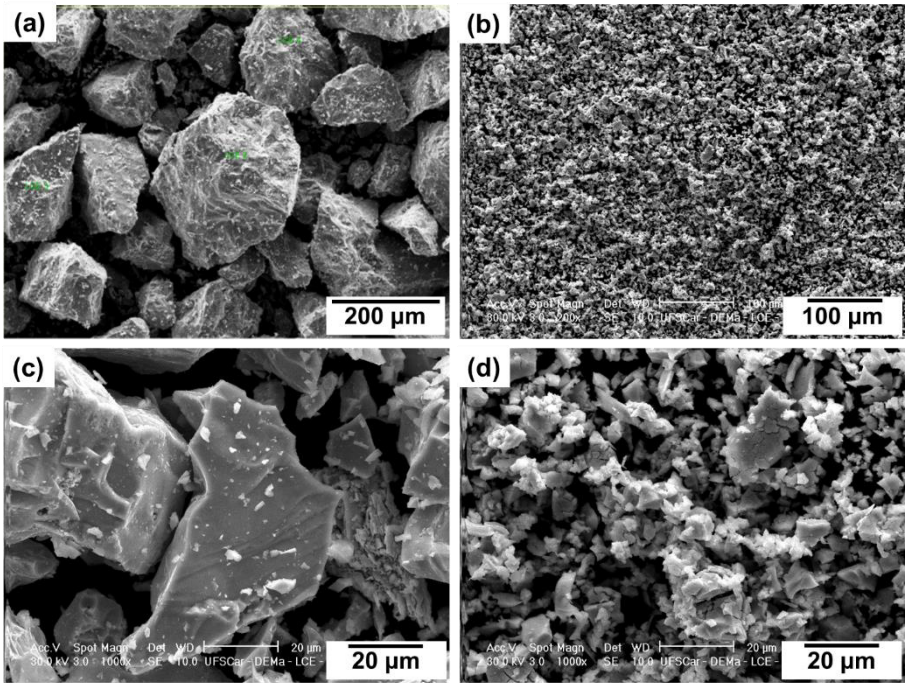


Figure 5. 57 - SEM images of the $(Ti_{0.33}Zr_{0.33}Nb_{0.33})_1(Mn_{0.5}Cr_{0.5})_2$ alloy in as cast (a) and (c), and after 50th cycles of hydrogenation/dehydrogenation (b) and (d).

## 5.3 Activation

### 5.3.1 Activation procedure

In Section 5.2.3.1 it was mentioned that the hydrogen storage performance of the seven selected alloys of this study was first investigated by absorption kinetic measurement at room temperature. In addition, the alloys were not subjected to activation procedures, such as temperature or dynamic vacuum. However, some alloys among the seven compositions studied in this project did not absorb hydrogen as soon as they were exposed to hydrogen and required activation procedures to try to make them capable of absorbing hydrogen. The alloys that did not require activation: $(Ti_{0.5}Zr_{0.5})_1(Mn_{0.5}Cr_{0.5})_2$, $(Ti_{0.5}Zr_{0.5})1(Fe_{0.33}Mn_{0.33}Cr_{0.33})_2$, $(Ti_{0.33}Zr_{0.33}Nb_{0.33})_1(Mn_{0.5}Cr_{0.5})_2$, were deeply studied, as previously presented in Section 5.2.3.1.

On the other hand, alloys that did not absorb when directly exposed to hydrogen, such as $(Ti_{0.5}Zr_{0.5})_1Mn_2$, $(Ti_{0.5}Zr_{0.5})_1(Fe_{0.5}Mn_{0.5})_2$, $(Ti_{0.33}Zr_{0.33}Nb_{0.33})_1$ $(Fe_{0.5}Mn_{0.5})_2$, and $(Ti_{0.5}Nb_{0.5})_1(Fe_{0.5}Mn_{0.5})_2$, were subjected to different activation procedures, as described below.

Firstly, the alloys were loaded into a Sieverts apparatus and exposed to dynamic vacuum for one hour, as schematic illustrated in Figure 5.58 (a). Then, an absorption kinetics measurement was carried out to verify whether the alloy was capable of absorbing hydrogen. After applying this procedure, none of the four samples described above was able to absorb hydrogen. Consequently, some of physical and physicochemical procedures were sequentially employed.

One of the procedures involved was to subject the sample to heat treatment at 390°C under dynamic vacuum for 12 hours, followed by cooling it to room temperature prior to measuring the absorption kinetics, as schematic illustrated in Figure 5.58 (b). This procedure yielded no success with any of the four alloys tested.

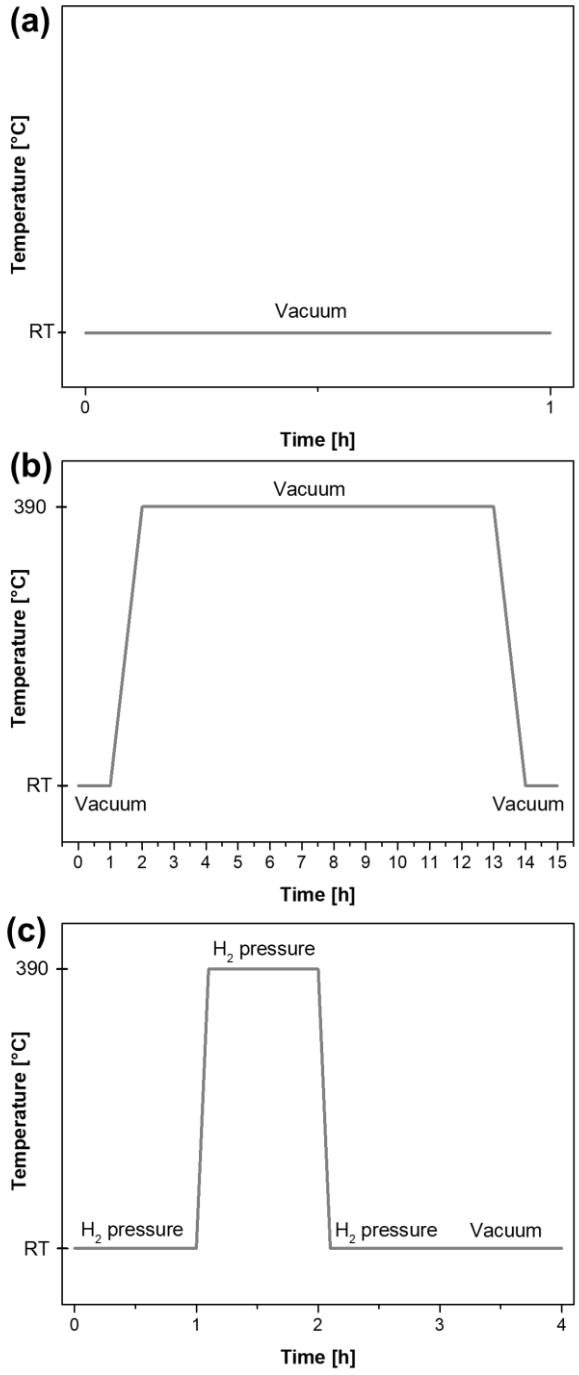


Figure 5. 58 - Schematic illustration of the activation procedures in terms of time, temperature and atmosphere. The procedures consisted of (a) exposing the sample to dynamic vacuum for one hour at RT, (b) heating the sample to 390 °C under dynamic vacuum for 12 h and subsequently cool it to RT, and (c) exposing the sample to a hydrogen pressure at RT for 1 h, then heat it to 390 °C for 1 h under hydrogen pressure, then cool it to RT while still under hydrogen pressure and finally exposed to a dynamic vacuum before absorption measurements.

Another procedure applied involved subjecting the sample to a thermochemical treatment. This process consisted of exposing the sample to hydrogen pressure at room temperature for 1 hour, followed by increasing the temperature to 390°C for 1 hour under hydrogen pressure. Subsequently, the sample was cooled to room temperature while still under hydrogen pressure, and then exposed to dynamic vacuum before measuring the absorption kinetics, as schematic illustrated in Figure 5.58 (c). Once more, none of the four alloys exhibited the capability to absorb hydrogen upon exposure to the gas.

Finally, a doping procedure was applied, consisting of Ce-addition. Ce is one of the so-called rare earth metals and oxidizes very readily at room temperature, as illustrated by the blue line in the Ellingham diagram (Figure 5.59).

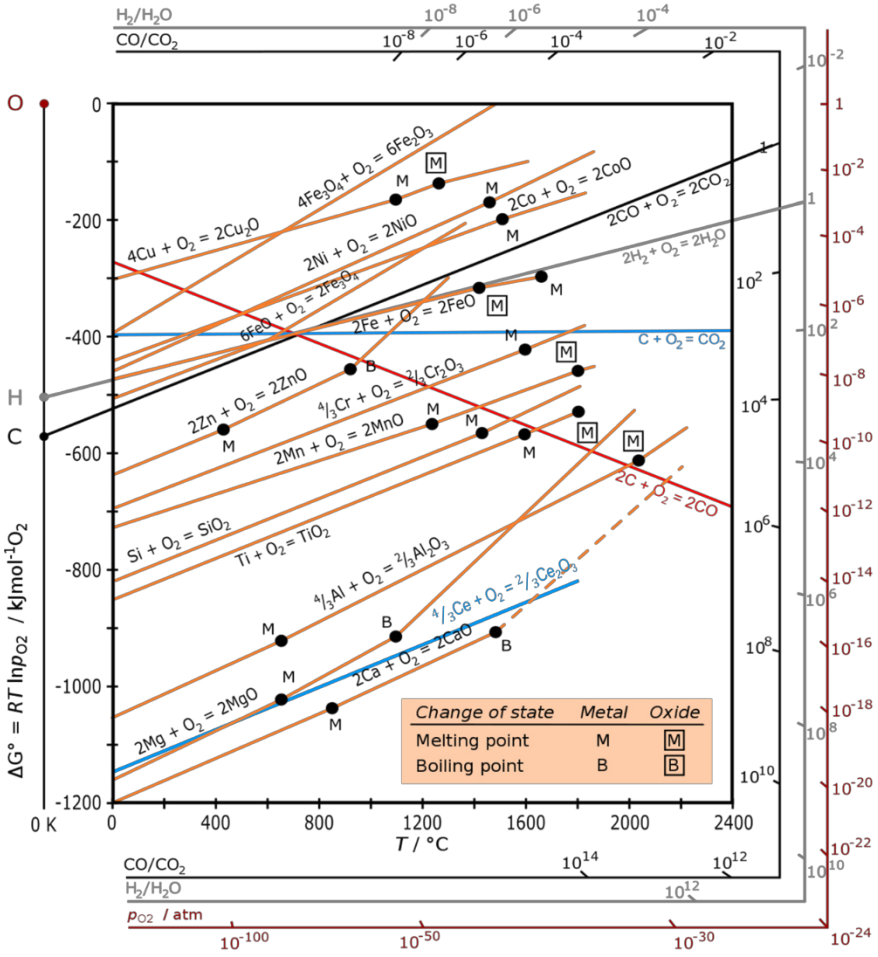


Figure 5. 59 - Ellingham diagram for several metals giving the free energy of formation of metal oxides. Ce is highlighted in blue color.

Due to this characteristic, Ce doping was used aiming at a possible reduction of oxygen in solution in the alloy, which would facilitate or induce the absorption of hydrogen by the alloy. Remarkably, the composition selected to receive the addition of 0.4 wt.% of Ce: $(Ti_{0.5}Zr_{0.5})_1(Fe_{0.5}Mn_{0.5})_2$, was successful in absorbing hydrogen, as can be seen in the hydrogen absorption kinetics of the $(Ti_{0.5}Zr_{0.5})_1(Fe_{0.5}Mn_{0.5})_2$+Ce alloy in Figure 5.60. Then, the alloy was systematically studied by analyzing the effect of Ce on the microstructure and hydrogen storage properties, as will be seen in Section 5.3.2.

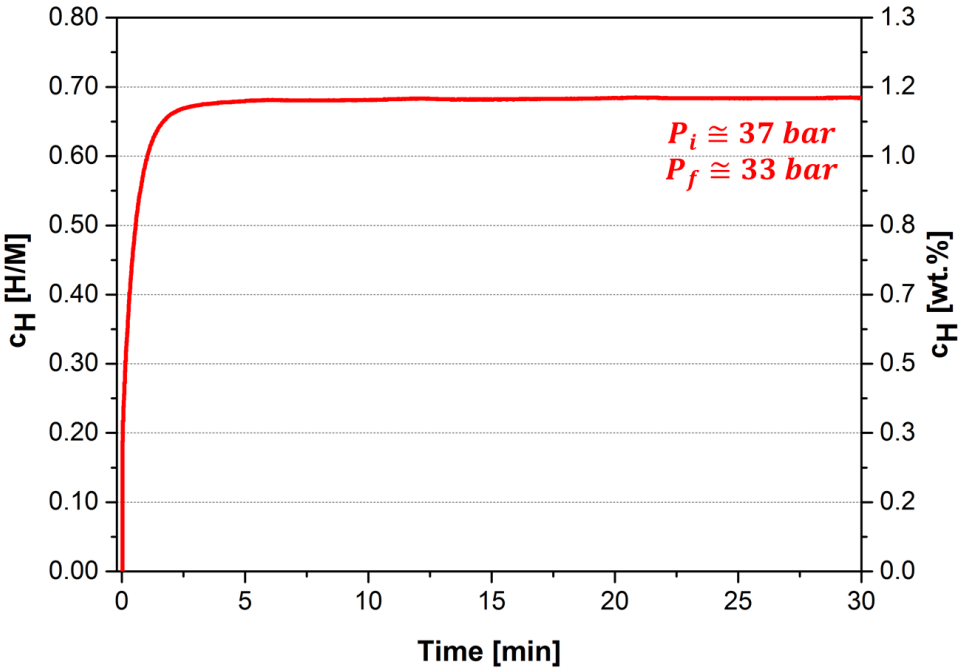


Figure 5. 60 - Measurement of hydrogen absorption kinetics at 25 °C in H/M of the $(Ti_{0.5}Zr_{0.5})_1(Fe_{0.5}Mn_{0.5})_2$+Ce alloy under an initial hydrogen pressure $P_i$ = 33 bar.

### 5.3.2 Ce addition

Figure 5.61 present the XRD pattern of the as-cast $(Ti_{0.5}Zr_{0.5})_1(Fe_{0.5}Mn_{0.5})_2$+Ce alloy confirming that the composition has C14 Laves phase structure. No reflections from a secondary phase can be observed.

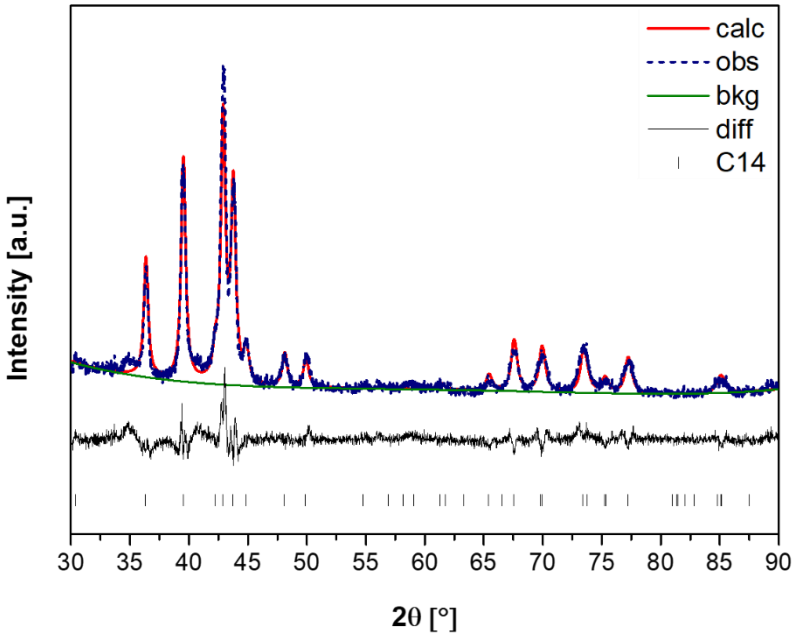


Figure 5. 61 - Rietveld refinement of the XRD pattern of the as-cast $(Ti_{0.5}Zr_{0.5})_1(Fe_{0.5}Mn_{0.5})_2$+Ce alloy indicating that the sample formed C14 Laves phase structure (measured with KαCu radiation).

The lattice parameters obtained by the Rietveld refinement for the C14 Laves phase in the alloys are a = 0.493 nm and c = 0.808 nm. These values closely approximate those obtained for the same composition but without Ce, which are: a = 0.492 nm and c = 0.805. The observed broadening of the C14 Laves phase reflections could be related the to a minor deviation in the chemical composition due segregation during solidification. The same composition, but without Ce, also presented the same characteristic (Figure 5.26). The deviation in the composition throughout the bulk of the C14 Laves phase alloy synthesized arc-melting is commonly observed due to the dendritic microstructure resulting from this casting process, as previously discussed.

In this way the alloys microstructure was further investigated by SEM equipped with EDX, and the results are shown in Figures 5.62. As can be seen, the as-cast sample presented a dendritic microstructure. Further, the SEM-BSE image, reveals that there is a difference in composition between the dendritic and interdendritic regions. Figure 5.62 also shows the corresponding EDX elemental maps of the selected region. EDX analyses were carried out in map mode in all

the selected region, and as point mode in the two areas: at the interdendritic regions and in the middle of dendrites.

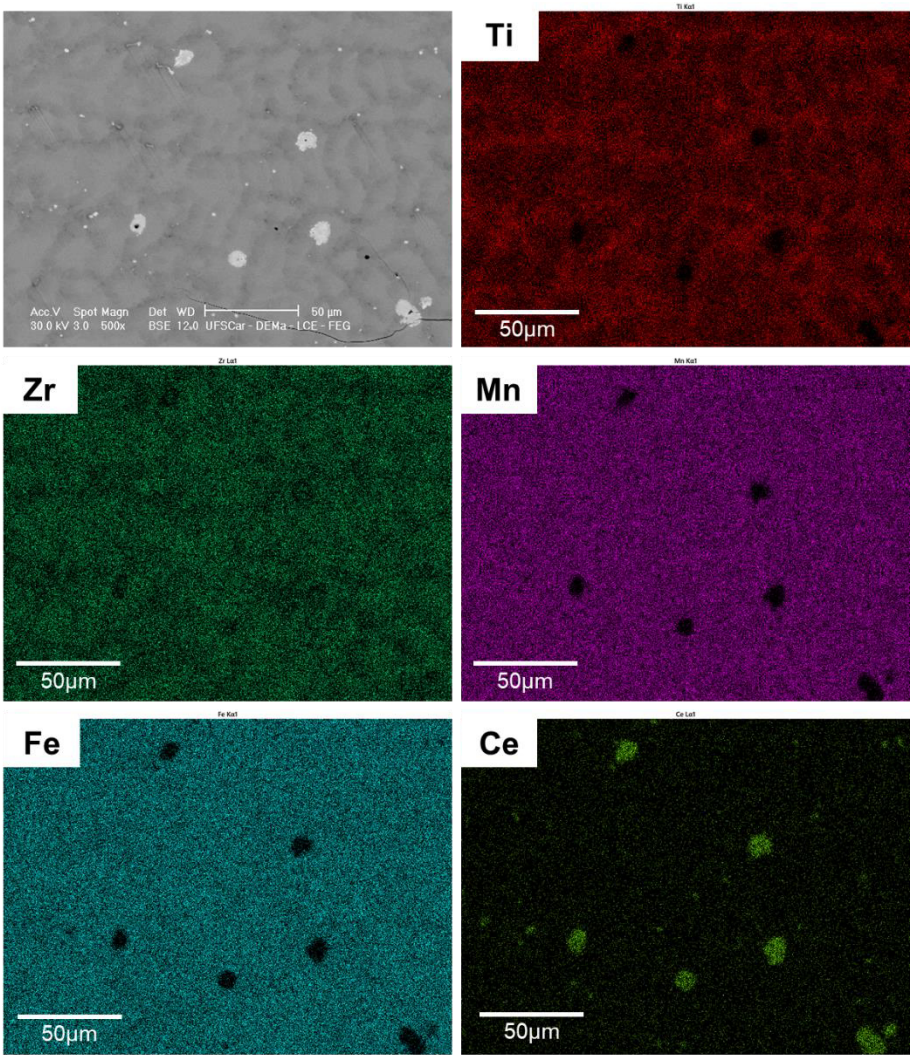


Figure 5. 62 - SEM-BSE image and corresponding EDX elemental maps of the as-cast $(Ti_{0.5}Zr_{0.5})_1(Fe_{0.5}Mn_{0.5})_2$+Ce alloy.

The results of the overall chemical composition and the chemical composition in the dendritic and interdendritic regions are presented in Table 5.18. As can be seen, the overall composition of the alloy is very close to the nominal one. Ti and Zr are not homogeneously distributed between the dendritic and interdendritic regions as a result of segregation during solidification. The chemical composition measured in the interdendritic region is slightly richer in Ti and Mn, and poorer in Zr and Fe. In contrast, the chemical composition measured

in the middle of the dendrites is slightly richer in Zr and Fe, and poorer in Ti and Mn. This minor deviations in the chemical composition of different alloy regions can be related to the slight broadening of the C14 Laves phase reflections observed in the XRD pattern of the alloy.

Table 5. 18 - The chemical composition of the $(Ti_{0.5}Zr_{0.5})_1(Fe_{0.5}Mn_{0.5})_2$+Ce alloy determined by SEM-EDX.

| | **Chemical composition in at% of the as-cast alloy** | | | | |
|---|---|---|---|---|---|
| | **Ti** | **Zr** | **Fe** | **Mn** | **Ce** |
| **Nominal** | 16.6 | 16.6 | 33.3 | 33.3 | 0.2 |
| **Overall** | 18.1 | 17.4 | 33.5 | 30.6 | 0.5 |
| **Dendritic** | 13.9 | 20.9 | 35.6 | 29.6 | 0.0 |
| **Interdendritic** | 19.1 | 15.8 | 32.0 | 33.0 | 0.0 |

Regarding the concentration and distribution of Ce, the results from the EDX analysis reveal that the observed Ce is higher than the nominal value. Additionally, the Ce particles, exhibiting a rounded geometry, are dispersed throughout the microstructure.

Figure 5.63 presents a comparison between the $(Ti_{0.5}Zr_{0.5})_1(Fe_{0.5}Mn_{0.5})_2$ and $(Ti_{0.5}Zr_{0.5})_1(Fe_{0.5}Mn_{0.5})_2$+Ce alloys. As observed, the microstructures are remarkable similar, except for the Ce particles dispersed in the alloy presented on the left side.

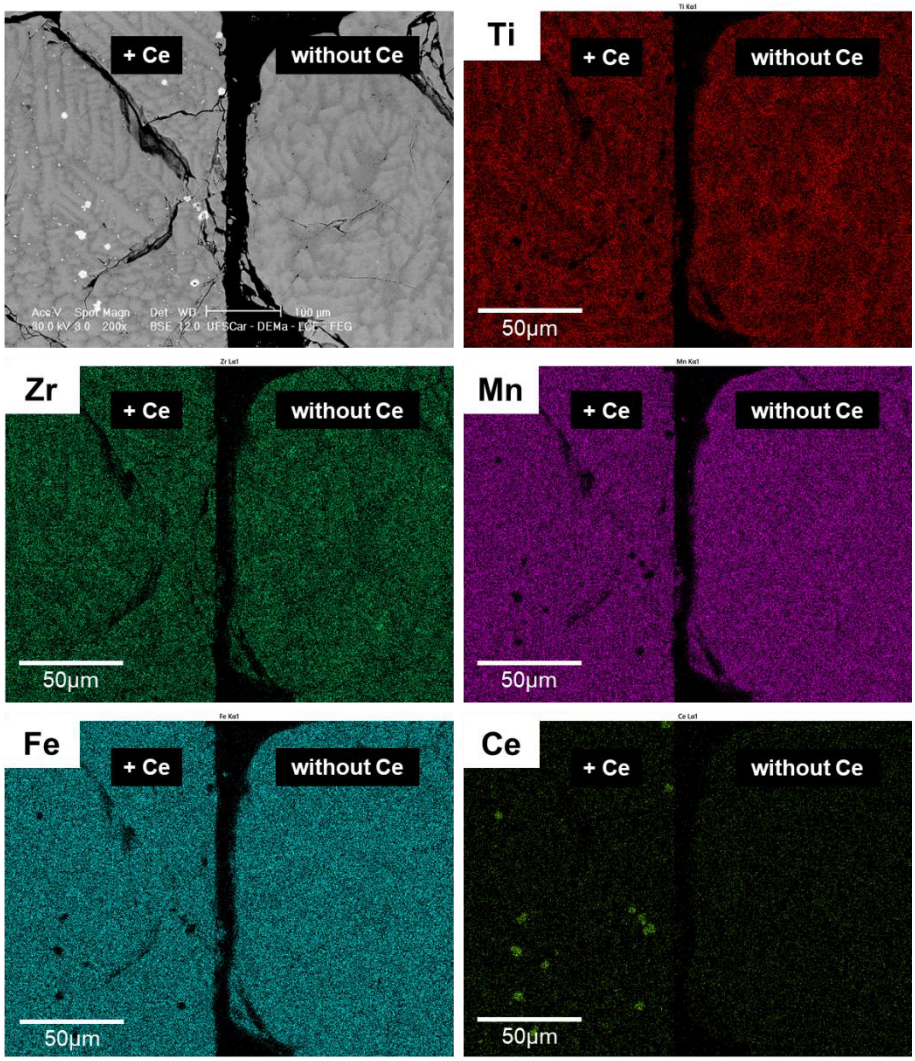


Figure 5. 63 - SEM-BSE image and corresponding EDX elemental maps of the as-cast $(Ti_{0.5}Zr_{0.5})_1(Fe_{0.5}Mn_{0.5})_2$ alloy (left side) compared with the $(Ti_{0.5}Zr_{0.5})_1(Fe_{0.5}Mn_{0.5})_2$+Ce alloy (right side).

Concerning the oxygen content an EDX analysis was performed in a SEM image with higher magnification, as illustrated in Figure 5.64. This analysis is only qualitative, and one can see that the rounded particles dispersed on the microstructure are formed only by Ce and O. Therefore, Ce act as a deoxidizing element, reacting with O and removing it from solid solution in the alloy. Zhou et al. [45] demonstrated that the Ce-doping in the TiZrMnCr alloy improved the activation of the alloy at room temperature and enhanced the cyclic performance during the hydrogenation and dehydrogenation. Moreover, the authors demonstrated that the Ce addition resulted in the formation of a $CeO_2$ phase, and

in a homogeneous elemental distribution due to the inhibition of the enrichment of the Ti phase by the Ce.

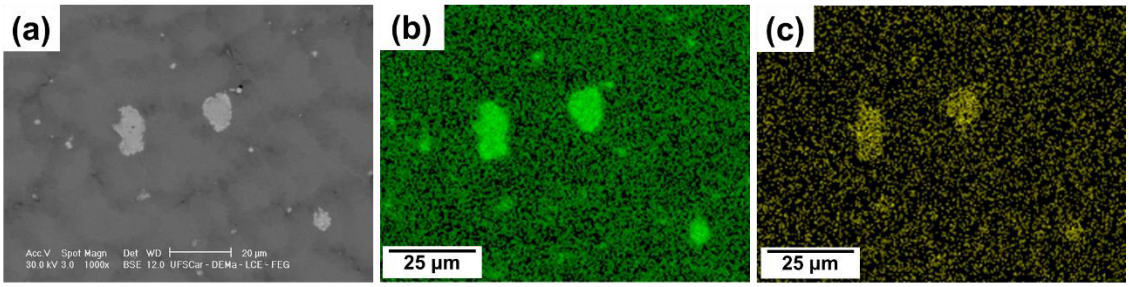


Figure 5. 64 - (a) SEM-BSE image and corresponding EDX elemental (b) Ce and (c) Oxygen maps of the as-cast $(Ti_{0.5}Zr_{0.5})_1(Fe_{0.5}Mn_{0.5})_2$+Ce alloy.

A line scan analysis was also carried out to identify the composition variation through the microstructure. These results are shown in Figure 5.62. Figure 5.65 (a) shows the SEM-BSE image used to perform the line scan. Figure 5.65 (b) shows the corresponding line, in Figure 5.65 (c) the line is illustrated in the horizontal position, and the variation of elements along the line is shown in Figure 5.65 (d). As observed, within the Ce-rich particles, it is possible to see a higher signal from Ce (green line) and O (orange line). In addition, the Zr content is practically constant through the line with a slight reduction in the Ce particle region, while the signal the other elements (Ti, Fe and Mn) presented a significant reduction on the Ce-rich particle.

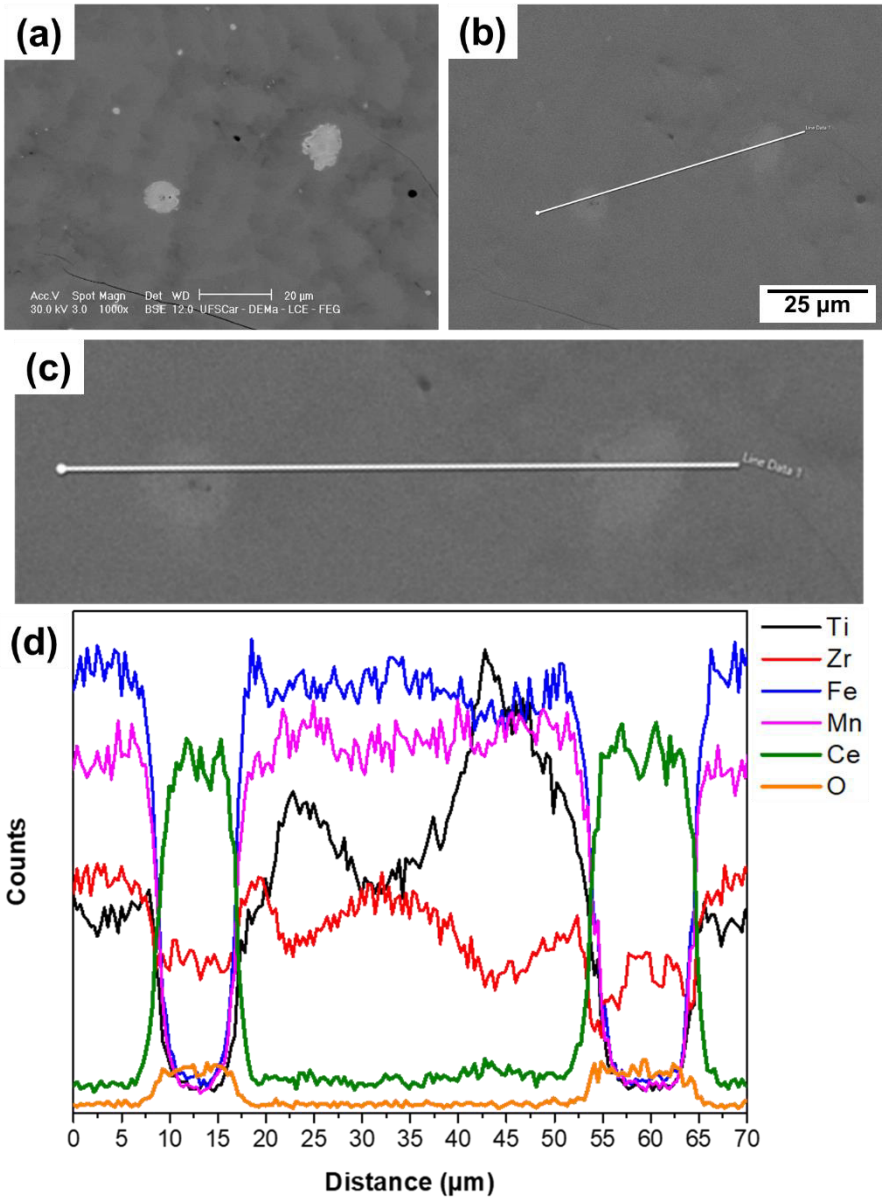


Figure 5. 65 - (a) SEM-BSE image and (b) corresponding line mapping measurement of the as-cast $(Ti_{0.5}Zr_{0.5})_1(Fe_{0.5}Mn_{0.5})_2$+Ce alloy. (c) Line mapping and the (d) corresponding graph with the count of elements in the line region.

Following the comprehensive structural analysis of the alloy, the investigation of the hydrogen storage properties of the Ce-doped alloy was carried out. The hydrogen storage performance of the $(Ti_{0.5}Zr_{0.5})_1(Fe_{0.5}Mn_{0.5})_2$+Ce alloy was first investigated by absorption kinetic measurement at room temperature. Initially, the alloy was not subjected to other

activation procedures, such as temperature or dynamic vacuum, except the addition of Ce.

Figure 5.66 shows the four measurements of hydrogen absorption kinetics at 25 °C in H/M of the $(Ti_{0.5}Zr_{0.5})_1(Fe_{0.5}Mn_{0.5})_2$+Ce alloy.

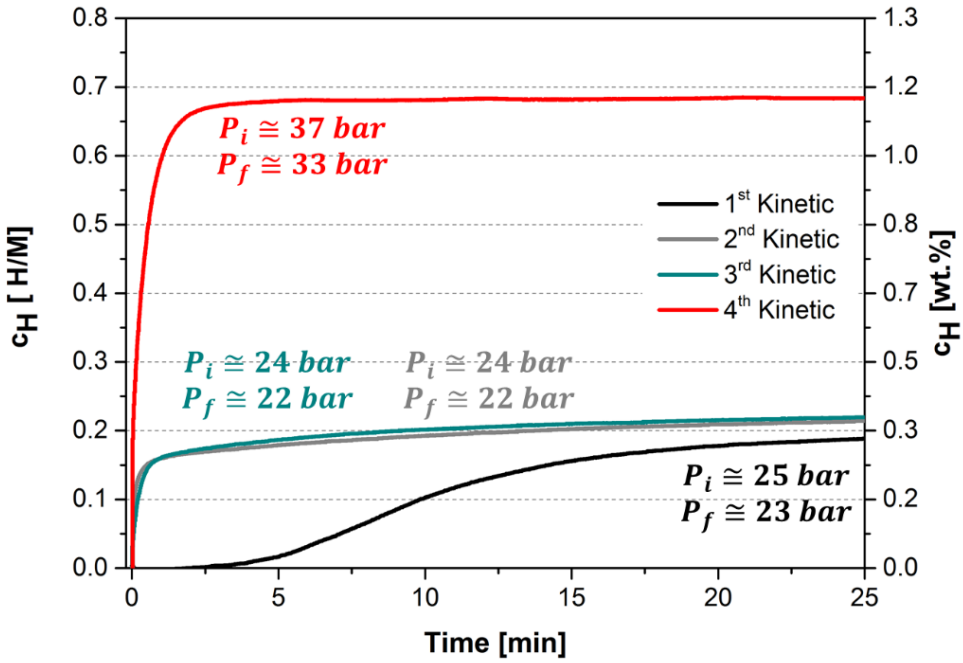


Figure 5. 66 - Measurement of hydrogen absorption kinetics at 25 °C in H/M of the $(Ti_{0.5}Zr_{0.5})_1(Fe_{0.5}Mn_{0.5})_2$+Ce alloy under an initial hydrogen pressure $P_i$ = 25 bar (1st kinetic – black curve), $P_i$ = 24 bar (2nd kinetic – grey curve), $P_i$ = 24 bar (3rd kinetic – blue curve), and $P_i$ = 37 bar (4th kinetic – red curve).

The first kinetic measurement (black curve) was carried out under an initial hydrogen pressure $P_i$ = 25 bar. One can see that the alloy presented a short incubation time (approximately 3 min) before start absorbing hydrogen. In addition, it took approximately 25 minutes to absorb approximately H/M = 0.2. Whereas, in the second kinetic measurement (grey curve), carried out under an initial hydrogen pressure $P_i$ = 24 bar, the alloy did not present an incubation time, and started to absorb hydrogen when in contact with the gas. It is worth mentioning that prior to the second measurement, the same sample was exposed to a dynamic vacuum for 15 minutes. Moreover, it took approximately 10 min to

reach the hydrogen absorption capacity of approximately H/M = 0.2. The same exact behavior was observed in the third kinetic measurement, as can be seen in the blue curve. As a fourth attempt to enhance the hydrogen absorption capacity, the sample was subjected to a high hydrogen pressure. As illustrated by the red curve, the sample reached a hydrogen storage capacity of approximately H/M = 0.7 in less than 2 min under an initial hydrogen pressure $P_i$ = 37 bar. It is important to mention that a dynamic vacuum was also applied to the sample for 15 minutes between the second and third measurements, as well as between the third and fourth measurements.

Hence, based on the capacity observed in the fourth measurement, we can infer that in the preceding measurements (second and third kinetics), the alloy reached its maximum absorption capacity under the applied equilibrium pressure of 24 bar. By subjecting the alloy to a higher pressure (37 bar), it demonstrated an increased absorption capacity. These capacities are also observed in the PCI measurements shown in Figure 5.67.

The hydrogen absorption and desorption performance of the $(Ti_{0.5}Zr_{0.5})_1(Fe_{0.5}Mn_{0.5})_2$+Ce alloy was further evaluated by PCI measurements. Figure 5.67 shows the PCI measurements at 30 °C up to the maximum hydrogen pressure of 80 bar. Figure 5.67 (b) shows the PCI curves with the x-axis (equilibrium pressure) in linear scale. This scale provides a clearer visualization of the pronounced hysteresis observed in this alloy.

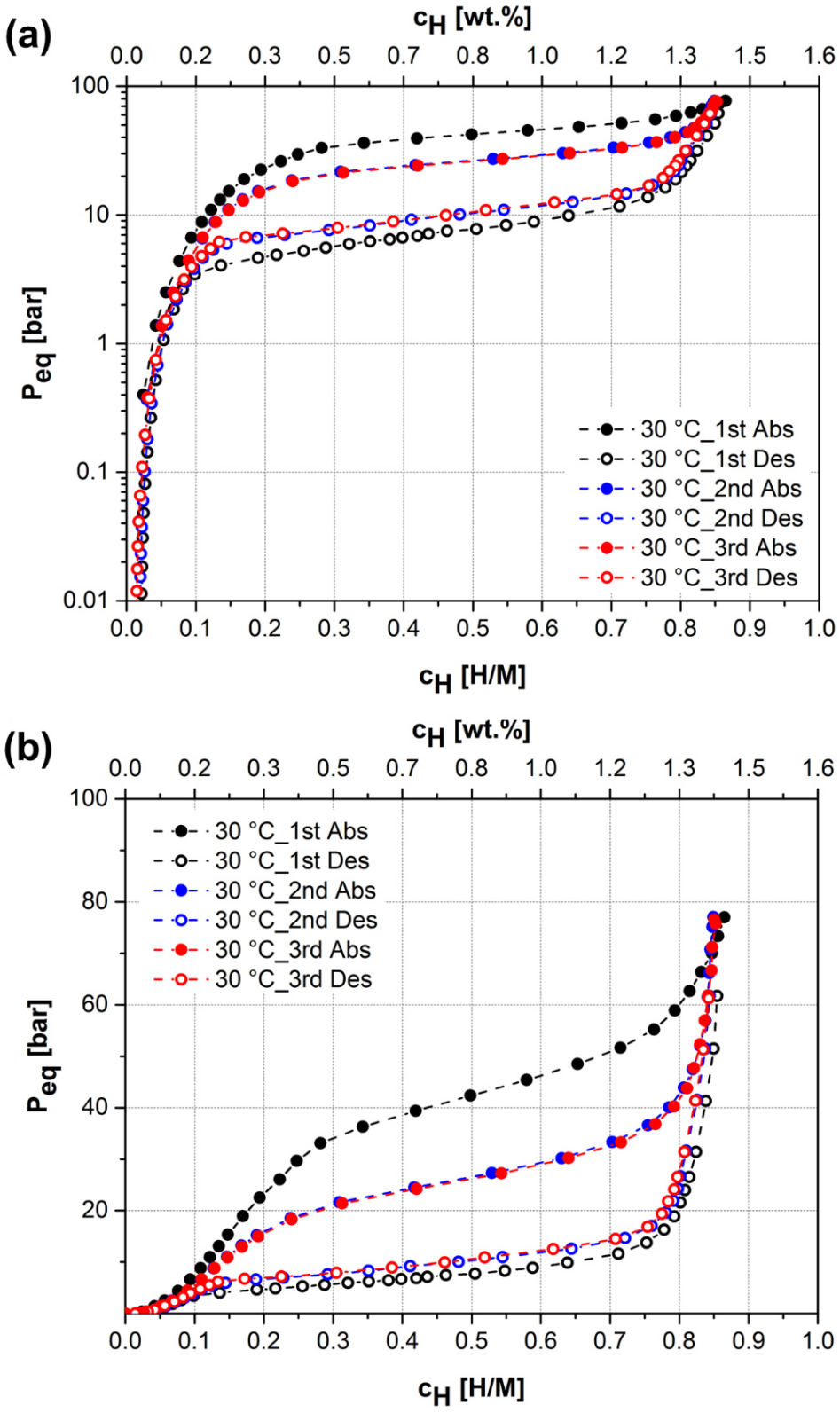


Figure 5. 67 - PCIs of the $(Ti_{0.5}Zr_{0.5})_1(Fe_{0.5}Mn_{0.5})_2$+Ce alloy at 30 °C (a) with x-axis in logarithmic scale and (b) in linear scale.

As shown in the first PCI measurement at 30 °C (black curve), the maximum hydrogen uptake at 80 bar was H/M = 0.86 (1.43 wt.%). For these temperature, the observed hydrogen equilibrium pressures for the alloy having H/M = 0.5 was approximately 42.4 bar. Since a pronounced hysteresis was observed (the equilibrium pressure during the desorption was 7.8 bar) a new PCI at 30 °C was acquired. The second PCI, illustrated in blue color in Figure 5.64, shows that the hydrogen capacity remained the same: H/M = 0.85 (1.40 wt.%). However, the equilibrium pressure during absorption was 27.3 bar, and during desorption was 11.0 bar. In means that the difference between absorption and desorption equilibrium pressures decrease from 34.6 bar to 16.3 bar. A third PCI measurement was performed to check whether there would be a further reduction in equilibrium pressure or whether this condition had stabilized. As noticed in the red curve, the behavior during absorption and desorption was notable the same as the previously measurement. Therefore, this alloy presented a high equilibrium pressure of approximately 27 bar with and a total hydrogen capacity of H/M = 0.85 (1.40 wt.%) at 80 bar.

A comparison between the experimental equilibrium pressure of the Ce-doped and the Ce-free alloy has not been possible since the alloy without Ce did not absorbed hydrogen. Additionally, the comparison between experimental and calculated values for the Ce-doped alloy was not possible. This is primarily because the Ce remained in the $CeO_2$ form, which means it doesn't occupy any sublattice of the C14 Laves phase structure and therefore isn't accounted in the thermodynamic model.

In comparison to the calculated equilibrium pressure for the $(Ti_{0.5}Zr_{0.5})_1(Fe_{0.5}Mn_{0.5})_2$ base alloy, without Ce addition, calculated equilibrium pressure using the thermodynamic model proposed here was considerably underestimated, as illustrated in Figure 5.68. Notably, the Ce-doped alloy presented an equilibrium pressure exceeding that of the base alloy by one order of magnitude. The calculated equilibrium pressure for the $(Ti_{0.5}Zr_{0.5})_1(Fe_{0.5}Mn_{0.5})_2$ alloy was 2.22 bar. Since most of the Ce is in the form of cerium oxide, the higher equilibrium pressure could be attributed to the remaining oxygen dissolved in the C14-Laves phase. However, a deeper investigation regarding the effect of

oxygen and deoxidizing elements in the equilibrium pressure of C14-Laves phase alloys must be carried out.

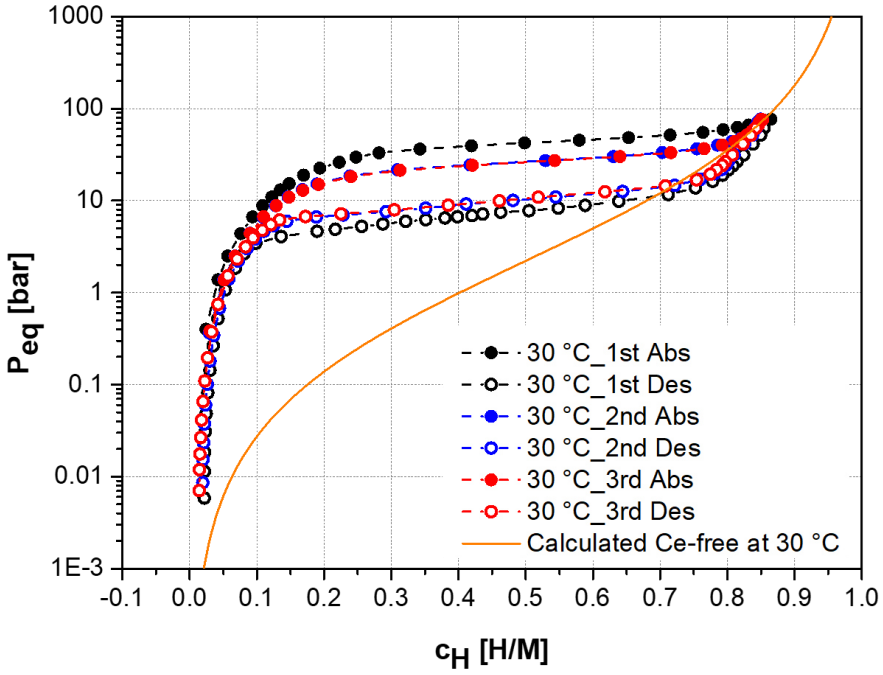


Figure 5. 68 - PCIs of the $(Ti_{0.5}Zr_{0.5})_1(Fe_{0.5}Mn_{0.5})_2$+Ce alloy at 30 °C compared to the calculated PCI for the base composition without Ce ($(Ti_{0.5}Zr_{0.5})_1(Fe_{0.5}Mn_{0.5})_2$).

Moreover, the absence of a well-defined plateau pressure was observed in the PCI curves, as seen for the previously alloys without any activation procedure. In addition, the PCI curves showed that the sample could be desorbed almost entirely (H/M < 0.05) by reducing the hydrogen pressure to approximately 1 bar. Even with almost entirely (H/M < 0.05) desorption of hydrogen by the sample by reducing the hydrogen pressure to approximately 1 bar, after each PCI measurement, the sample was exposed to a dynamic vacuum for a few minutes at the current temperature to ensure no remaining hydrogen was in the lattice.

The hydrogen absorption/desorption performance of the alloy was further evaluated by measuring the cycling hydrogen absorption capacity over 40 cycles. The results of the cycling test are shown in Figure 5.69.

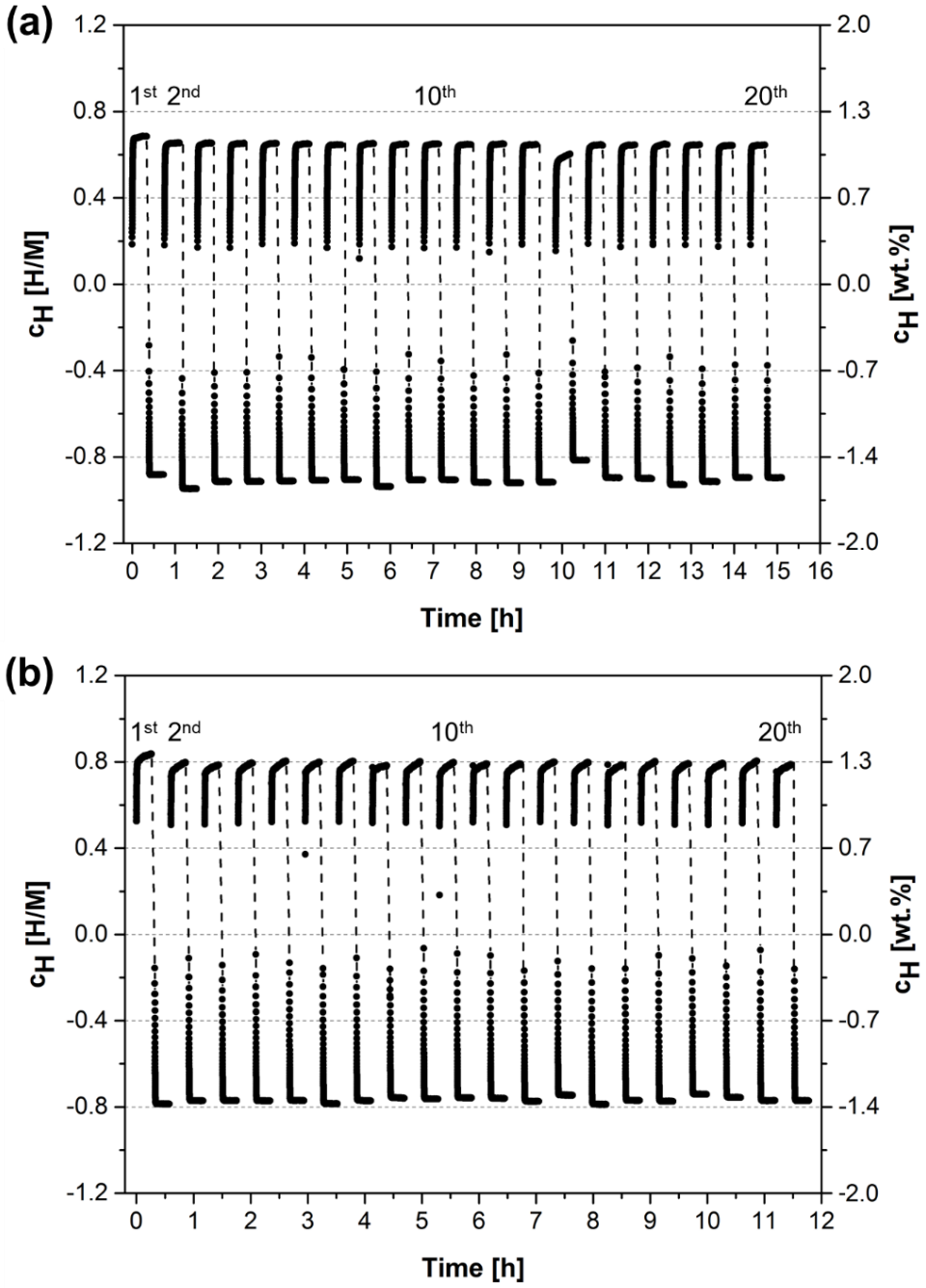


Figure 5. 69 – Hydrogen absorption capacity in H/M of the $(Ti_{0.5}Zr_{0.5})_1(Fe_{0.5}Mn_{0.5})_2$+Ce alloy over the 40th cycles of absorption and desorption at 30 °C. (a) During the absorption cycles, the initial hydrogen pressure was 37 bar, and the final pressure was 33 bar, approximately. (b) During the absorption cycles, the initial hydrogen pressure was 50 bar, and the final pressure was 49 bar, approximately. The desorption was carried out without vacuum exposure.

Figure 5.69 (a) and (b) presented 20 cycles of absorption and desorption each one and the only difference between them is the initial hydrogen pressure to which the sample was subjected. During the cycling test illustrated in Figure 5.69 (a) the hydrogen absorption behavior was performed at 30 °C under an initial pressure of 37 bar for 20 min, while the hydrogen desorption was carried out at the same temperature under an initial pressure of approximately 0.5 bar for 20 min (the sample was not subjected to dynamic vacuum). The hydrogen absorption capacity in the first cycle was H/M = 0.68 (1.13 wt.%), decreased in the second cycle to H/M = 0.65 (1.09 wt.%). After the second cycle, a slight decrease in hydrogen absorption was observed during the subsequent cycles to a 0.64 H/M (1.07 wt.%), which indicates that the alloy can store 94 % of its initial capacity over 20 cycles.

It is important to emphasize that the sample was not exposed to a dynamic vacuum during the dehydrogenation kinetics measurements. Therefore, the decrease in the hydrogen absorption capacity should be related to the remaining hydrogen in the alloy under cycling measurements. Moreover, this slight decrease in the hydrogen storage capacity can be attributed to the size refinement of the alloy particles, which takes place during the hydrogenation. This refinement could lead to an increase in crystalline defects, known to reduce the hydrogen storage capacity of metal hydrides, as previously discussed.

The hydrogen storage capacity observed in the first cycle of the test is equal to the capacity observed in the fourth kinetic measurement (Figure 5.66), conducted under comparable hydrogen pressure and temperature conditions. However, aiming for higher storage capacity, as observed in the PCI measurement, a new cycling test was carried out applying an elevated hydrogen pressure to the sample (50 bar). The new cycling test is illustrated in Figure 5.69 (b). The hydrogen absorption capacity in the first cycle was H/M = 0.84 (1.39 wt.%), decreased in the second cycle to H/M = 0.80 (1.32 wt.%). After the second cycle, a slight decrease in hydrogen absorption was observed during the subsequent cycles to a 0.79 H/M (1.30 wt.%), which indicates that the alloy can store again 94 % of its initial capacity over more 20 cycles.

In the initial cycle, the hydrogen absorption capacity was H/M = 0.84 (1.39 wt.%), a slightly decreased to H/M = 0.80 (1.32 wt.%) in the second cycle was seen. Following this, a slight decline in hydrogen absorption was noted in the subsequent cycles, reaching 0.79 H/M (1.30 wt.%). Nonetheless, the alloy demonstrated that can retaining approximately 94% of its initial capacity over the additional 20 cycles.

In order to have deeper insights into the hydrogen storage characteristics of the alloys, XRD characterization was performed on samples following both the initial and final cycles of absorption and desorption. Figure 5.70 shows the XRD patterns of these samples and the XRD pattern of the as-cast $(Ti_{0.5}Zr_{0.5})_1(Fe_{0.5}Mn_{0.5})_2$+Ce sample.

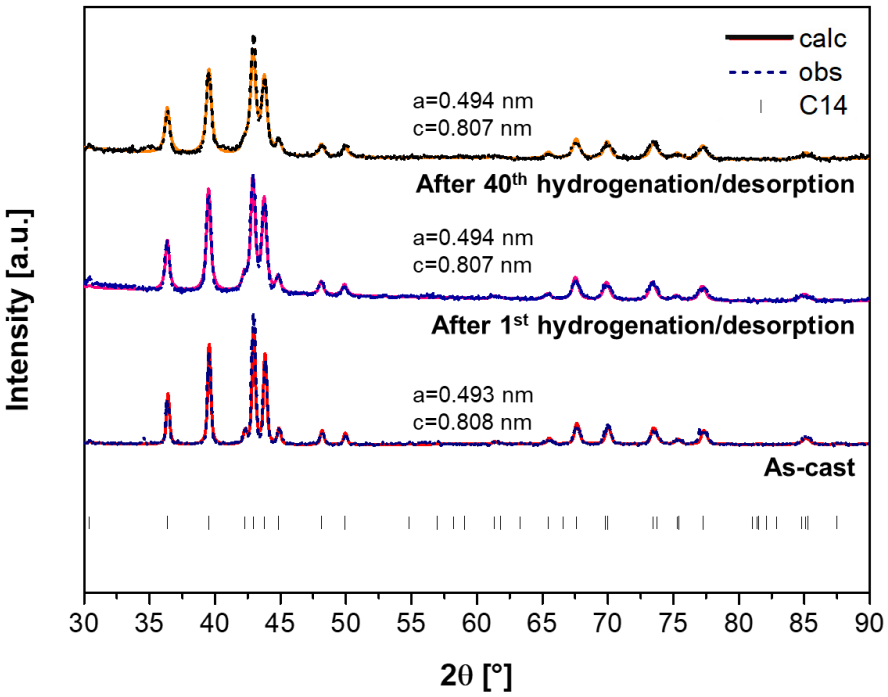


Figure 5. 70 - XRD patterns of the $(Ti_{0.5}Zr_{0.5})_1(Fe_{0.5}Mn_{0.5})_2$+Ce alloy. (a) as-cast, (b) after one absorption/desorption cycle, and (c) after forty absorption/desorption cycles (measured with KαCu radiation).

The lattice parameters determined through Rietveld refinement for the C14 Laves phase in these three samples are also illustrated in Figure 5.70. One can see that even after several hydrogenation cycles, there were no changes in the

constituent phases. Following one and forty hydrogenation cycles, the samples maintained a single C14 Laves phase, with no evident changes in lattice parameters. These XRD observations, along with the PCI curves (Figure 5.67) and cycling test curves (Figure 5.68), show that the $(Ti_{0.5}Zr_{0.5})_1(Fe_{0.5}Mn_{0.5})_2$+Ce alloy efficiently releases most of its hydrogen content as the pressure decreases to 1 bar. In addition, the hydrogen remaining in the alloy structure was released during the evacuation of the sample prior to the further characterization of the alloy. Thus, the characterization of the hydrogenated phase by XRD was not possible after the hydrogenation tests.

Figure 5.71 shows the microstructural characteristics of the $(Ti_{0.5}Zr_{0.5})_1(Fe_{0.5}Mn_{0.5})_2$+Ce alloy in two conditions.

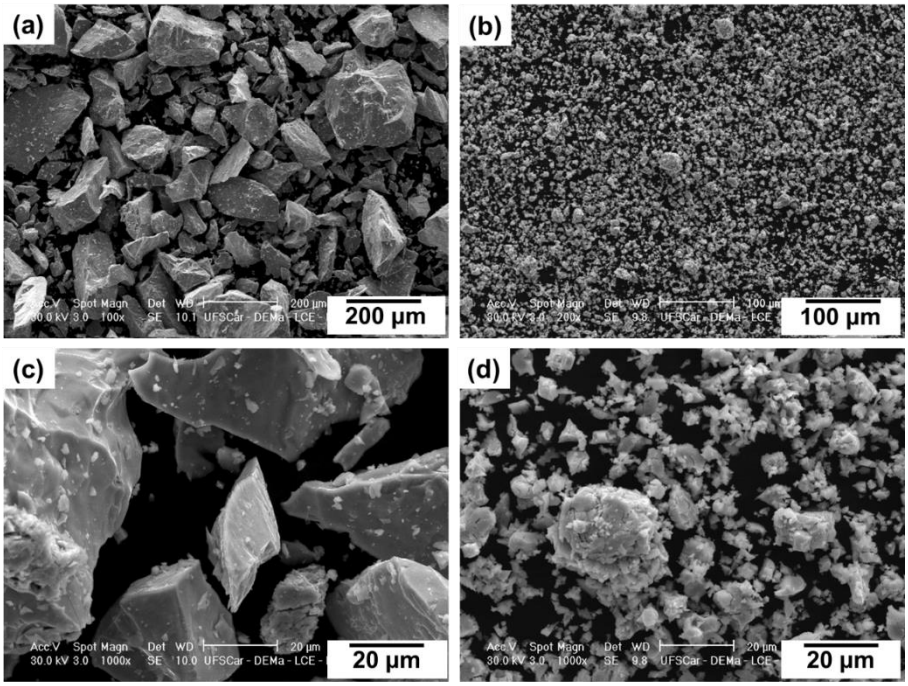


Figure 5. 71 - SEM images of the $(Ti_{0.5}Zr_{0.5})_1(Fe_{0.5}Mn_{0.5})_2$+Ce alloy in as cast (a) and (c), and after 40th cycles of hydrogenation/dehydrogenation (b) and (d).

Figures (a) and (c) show the as-cast sample after being crushed into powder (used to load into a Sieverts-type apparatus) in two different magnifications. The particle size of the alloy is in the range of about 200 µm. Figures (b) and (d) corresponding to the sample after 40 cycles of hydrogen

absorption and desorption. The decrease in alloy particle size is evident, accompanied by the development of surface cracks on the particles. Previous studies have also noted comparable behavior, which was attributed to the volume expansion of the C14 Laves phase after hydrogen absorption. This expansion creates significant internal stress concentration within the host metal, causing embrittlement after absorption. Consequently, the result is a powder characterized by fine particle sizes ranging from 10 to 100 μm [5,19,66]. Additionally, the slight reduction of capacity during cycling tests and the reflection broadening in the XRD patterns observed, can be attributed to this particle size reduction.

### 5.3.3 Oxygen content

Since only the addition of Ce resulted in a successful activation, a further study on the oxygen concentration in the samples was carried out. This study was performed because the oxygen concentration in alloys designated for hydrogen absorption tests is considered a critical factor for proper absorption, and for most of these alloys. Generally, the surface is easily contaminated by the formation of oxides during an exposure to air, moreover, a contamination of the bulk can also occur during the alloy processing, even with a rigorous controlling of the atmosphere of the melting chamber during arc melting.

Initially the $(Ti_{0.5}Zr_{0.5})_1(Fe_{0.5}Mn_{0.5})_2$ and $(Ti_{0.5}Zr_{0.5})_1(Fe_{0.5}Mn_{0.5})_2$+Ce alloys had their oxygen concentration quantified by the inert gas fusion infrared detection method (LECO® equipment). The results are shown in Table 5.19.

Table 5. 19 - Oxygen content of the as-cast $(Ti_{0.5}Zr_{0.5})_1(Fe_{0.5}Mn_{0.5})_2$ and $(Ti_{0.5}Zr_{0.5})_1(Fe_{0.5}Mn_{0.5})_2$+Ce alloys.

| Alloy | Oxygen average ± Std. Dev [%] |
|---|---|
| **$(Ti_{0.5}Zr_{0.5})_1(Fe_{0.5}Mn_{0.5})_2$** | 0.097 ± 0.005 |
| **$(Ti_{0.5}Zr_{0.5})_1(Fe_{0.5}Mn_{0.5})_2$+Ce** | 0.123 ± 0.001 |

As can be seen, the average oxygen content in both alloys are quite similar (approximately 0.1 %). This result is somehow expected since the

$(Ti_{0.5}Zr_{0.5})_1(Fe_{0.5}Mn_{0.5})_2$+Ce alloy also contains oxygen, however it is in the $CeO_2$ form, as presented in the previous topic. Thus, the critical aspect governing hydrogen absorption by the alloy should not rely on the oxygen concentration, but rather on the distribution of oxygen in the alloy structure. In the $(Ti_{0.5}Zr_{0.5})_1(Fe_{0.5}Mn_{0.5})_2$+Ce alloy the Ce removed oxygen from C14 Laves phase by forming $CeO_2$, while for the Ce-free alloy, the oxygen must be dissolved in the C14 Laves phase.

Table 5.20 shows the oxygen content of the other alloys that absorbed hydrogen without any activation or doping procedure. As can be seen, the alloys contain similar oxygen levels.

Table 5. 20 - Oxygen content of the as-cast alloys that absorbed hydrogen.

| Alloy | Oxygen average ± Std. Dev [%] |
|---|---|
| $(Ti_{0.5}Zr_{0.5})_1(Mn_{0.5}Cr_{0.5})_2$ | 0.091 ± 0.004 |
| $(Ti_{0.5}Zr_{0.5})_1(Fe_{0.33}Mn_{0.33}Cr_{0.33})_2$ | 0.078 ± 0.001 |
| $(Ti_{0.33}Zr_{0.33}Nb_{0.33})_1(Mn_{0.5}Cr_{0.5})_2$ | 0.178 ± 0.002 |
| $(Ti_{0.5}Zr_{0.5})_1(Fe_{0.25}Mn_{0.25}Cr_{0.25}Ni_{0.25})_2$ | 0.071 ± 0.001 |

Finally, the alloys that did not absorb hydrogen, even after activation attempts, had their oxygen concentration quantified by LECO measurements, as shown in Table 5.21. As observed, the oxygen level of these samples presented similar order of magnitude as the previous ones.

Table 5. 21 - Oxygen content of the as-cast alloys that did not absorbed hydrogen.

| Alloy | Oxygen average ± Std. Dev [%] |
|---|---|
| $(Ti_{0.5}Zr_{0.5})_1Mn_2$ | 0.102 ± 0.005 |
| $(Ti_{0.5}Zr_{0.5})_1(Fe_{0.5}Mn_{0.5})_2$ | 0.097 ± 0.005 |
| $(Ti_{0.33}Zr_{0.33}Nb_{0.33})_1(Fe_{0.5}Mn_{0.5})_2$ | 0.058 ± 0.005 |
| $(Ti_{0.5}Nb_{0.5})_1(Fe_{0.5}Mn_{0.5})_2$ | 0.039 ± 0.001 |

The oxygen content values presented in Tables 5.19, 5.20, and 5.21 are graphically represented in Figure 5.72. The alloys that absorbed hydrogen: $(Ti_{0.5}Zr_{0.5})_1(Mn_{0.5}Cr_{0.5})_2$, $(Ti_{0.5}Zr_{0.5})_1(Fe_{0.33}Mn_{0.33}Cr_{0.33})_2$, $(Ti_{0.33}Zr_{0.33}Nb_{0.33})_1(Mn_{0.5}Cr_{0.5})_2$, $(Ti_{0.5}Zr_{0.5})_1(Fe_{0.25}Mn_{0.25}Cr_{0.25}Ni_{0.25})_2$, and $(Ti_{0.5}Zr_{0.5})_1(Fe_{0.5}Mn_{0.5})_2$+Ce, are highlighted in blue color, and the alloys that did not absorb hydrogen (after the trials of activation): $(Ti_{0.5}Zr_{0.5})_1Mn_2$, $(Ti_{0.5}Zr_{0.5})_1(Fe_{0.5}Mn_{0.5})_2$, $(Ti_{0.33}Zr_{0.33}Nb_{0.33})_1(Fe_{0.5}Mn_{0.5})_2$, and $(Ti_{0.5}Nb_{0.5})_1(Fe_{0.5}Mn_{0.5})_2$ are highlighted in red color.

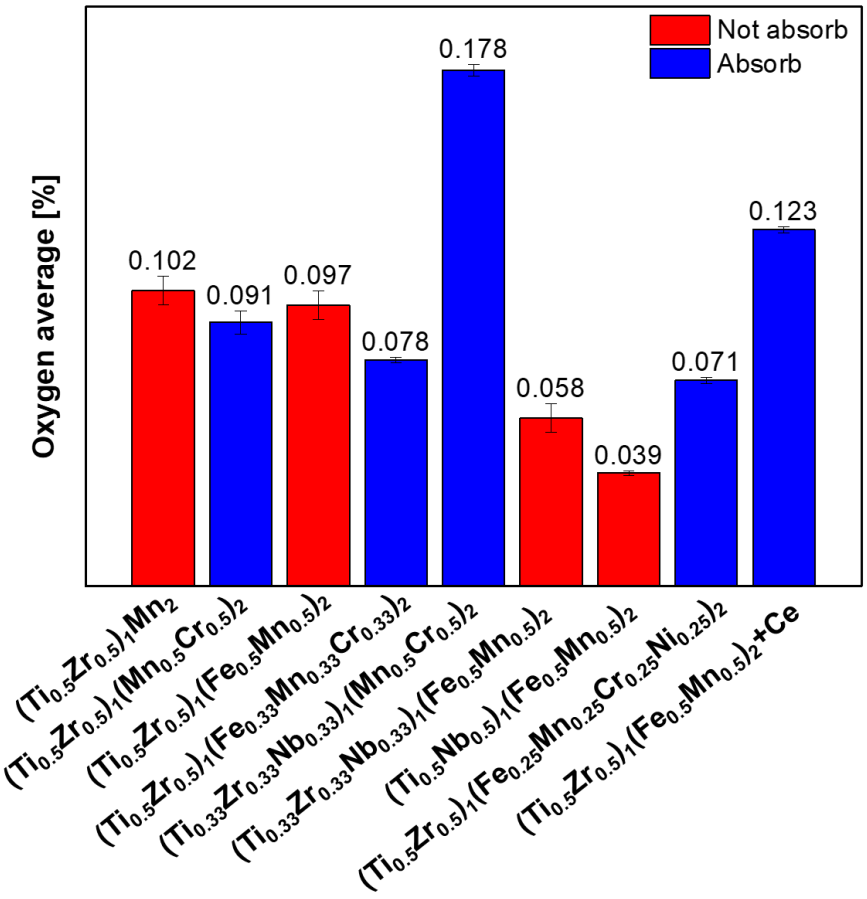


Figure 5. 72 - Oxygen content of the as-cast samples of the alloys.

As mentioned, there was no discernible correlation between the oxygen content in the samples and the distinction between absorbing and non-absorbing alloys, since all alloys have oxygen concentrations in the same value range (400-1000 ppm). We can discuss this observation based not only on the oxygen content of the alloy itself, but on the distribution of oxygen in the alloy structure.

The difference between the hydrogen-absorbing and non-absorbing alloys might be a consequence of one of the alloying elements acting as a deoxidizing agent, leading to the formation of oxides in the microstructure. In this case, these oxides would probably be nanometric, so it could not be seen in the SEM analysis. Remarkably, all alloys capable of absorbing hydrogen contain Cr, whereas those not able of absorbing hydrogen do not contain Cr. Consequently, one could infer that Cr probably act as the deoxidizer in these alloys. Furthermore, it is worth mentioning that the oxygen content in some of the Cr-free alloys is lower than that in alloys containing Cr. However, Cr acting as a deoxidizing agent in these alloys is counterintuitive, since Cr has a less negative standard Gibbs free energy of oxide formation than other alloying elements such as Ti, Zr, and Mn, as illustrated in the Ellingham Diagram (Figure 5.59), which could act as even stronger deoxidizers.

The structural characterizations used in this study were not able to assess these hypotheses. Therefore, a more comprehensive investigation on the presence or not of oxides in the microstructure and oxide composition presented in the alloys should be carried out to establish any correlations between the oxygen content and distribution in the alloys and their hydrogen absorption capabilities. These studies may include other structural characterization techniques such transmission electron microscopy (TEM) and X-ray photoelectron spectroscopy (XPS) techniques, as discussed in the study conducted by Silva et al. [55].

## 6 DISCUSSIONS

Given that the primary objective of this doctoral thesis was to use computational methodologies and thermodynamic modeling to identify multicomponent alloys with the C14 Laves phase tailored for diverse hydrogen storage applications, as well as to investigate the activation processes for these alloys, we can outline some of the discoveries of this work.

Knowing that the thermodynamic model proposed predicted that the equilibrium pressures for the C14 Laves phase can vary widely, from $10^{-4}$ up to $10^{5}$ bar, the design methods with predictive properties modeling proposed here may play a crucial role in minimizing the need for numerous experiments when navigating through the vast compositional space of multicomponent alloys. Therefore, by combining the CALPHAD method and the thermodynamic model to calculate the PCT diagram for the C14 Laves phase, we were able to design alloys compositions with the equilibrium pressure in two order of magnitude, which would allow the use in specific hydrogen storage applications.

In terms of applicability, alloys with high hydrogen storage capacity and equilibrium pressures varying between 2 and 20 atm, so they can absorb hydrogen at moderate pressures and desorb at room temperature in atmospheric pressure, are promising options for room temperature hydrogen storage tank. Therefore, the $(Ti_{0.5}Zr_{0.5})_1(Fe_{0.33}Mn_{0.33}Cr_{0.33})_2$ and $(Ti_{0.33}Zr_{0.33}Nb_{0.33})_1(Mn_{0.5}Cr_{0.5})_2$ alloys that presented equilibrium pressures equal to 6 and 10 bar at 30 °C, respectively, are good candidates for this kind of application.

The transportation sector indubitably holds the greatest promise for advancing the utilization of hydrogen-based energy systems. With growing concerns over dwindling conventional energy resources and environmental issues associated with fossil fuels, there has been a concerted effort to develop systems facilitating hydrogen-powered vehicles.

In 2006, Toyota's research group demonstrated the utilization of $Ti_{1.1}MnCr$ alloys in a high-pressure metal hydride tank, exhibiting a very high hydrogen absorption plateau pressure. However, for achieve the maximum storage capacity of 1.9 wt.% it required a hydrogen pressure of approximately 350 bar at room temperature [68]. Subsequently, in 2015, Toyota introduced a hydrogen

fuel-cell-driven vehicle equipped with two 700 bar high-pressure hydrogen storage tanks, presenting a hydrogen density of 5.7 wt.% [69]. Nonetheless, the elevated operating pressure of these hydrogen storage tanks raises concerns regarding safety and cost. More recently, an $AB_2$-type Ti–Zr–Cr-based alloy was optimized for a hybrid hydrogen storage tank in a fuel cell bicycle, presenting a hydrogen storage capacity of 1.82 wt.% under a hydrogen pressure of around 11 bar at room temperature [44].

In this context, the development of hydrogen storage tanks operable at room temperature holds significant promise in facilitating the safe and cost-effective utilization of hydrogen-based energy systems in stationary and mobile applications. Then, this comprehensive study identified a set of crucial properties that an alloy must have to be suitable for use in a solid-state hydrogen storage tank operating under room temperature and mild pressure conditions. These properties include high hydrogen storage capacity, favorable absorption and desorption kinetics, cycling stability, reversibility, and equilibrium pressure above atmospheric pressure. The study conclusively demonstrated that alloys such as $(Ti_{0.5}Zr_{0.5})_1(Fe_{0.33}Mn_{0.33}Cr_{0.33})_2$ and $(Ti_{0.33}Zr_{0.33}Nb_{0.33})_1(Mn_{0.5}Cr_{0.5})_2$, designed using computational thermodynamic tools are excellent options for this particular application.

Further, the $(Ti_{0.5}Zr_{0.5})_1(Mn_{0.5}Cr_{0.5})_2$, which presented an equilibrium pressure of 0.4 bar at 30 °C, is a promising option for Ni-MH batteries. For instance, for batteries application, the equilibrium pressure must be between 0.1 and 1 atm so the self-discharging is minimized and the pressure inside the battery does not reach pressure levels above the atmospheric one [70].

Concerning the reversibility and cycling performance study, the acquisition of absorption kinetics data is essential for understanding how a material transforms into a hydride, including the effects of time, temperature, and pressure. However, the investigation of these parameters in reverse, when the hydride reverts to its metallic state, is equally important yet often reported. Therefore, this study investigated desorption kinetics, providing insights on this critical aspect from an application point of view. In terms of hydrogen absorption capacity, the alloy under examination demonstrates excellent performance,

similar to the calculated theoretical capacity for the $AB_2H_3$ hydrides. These alloys performance can be considered comparable or superior to those reported for many C14 Laves phase alloys, which are often observed to be close to H/M = 1 [10,11,13,41,43–45,66]. For example, Edalati et al. [10] reported that the equiatomic $(TiZr)_1(CrMnFeNi)_2$ multicomponent alloy exhibits a hydrogen absorption capacity of 1.70 wt.% (H/M = 1) in its initial cycle. Floriano et al. [11] demonstrated that the $Ti_{20}Zr_{20}Nb_5Fe_{40}Ni_{15}$ alloy absorbs 1.38 wt.% (H/M = 0.95) in its first cycle.

Additionally, regarding cyclability, the three studied alloys presented exceptional performance is comparable to the limited studies available on the cycling of C14 Laves phase alloys. Li et al. [66] found that the $Ti_{0.8}Zr_{0.2}Mn_{0.9}Cr_{0.6}V_{0.3}Fe_{0.2}$ alloy achieved a maximum hydrogen absorption of 1.80 wt.%, with a slight decrease in initial cycles, stabilizing at 1.71 wt.% over ten cycles. Notably, desorption in this case involved raising the temperature to 400°C under dynamic vacuum for 30 minutes. Chen et al. [71] noted a maximum hydrogen absorption capacity of 1.80 wt.% for the first cycle in their study of the equiatomic TiZrFeMnCrV alloy, which decreased to 1.76 wt.% in the second cycle and remained constant over the subsequent 50 cycles. Desorption was conducted at high temperatures (350 °C) under dynamic vacuum for 30 minutes.

Therefore, the temperature-induced reversible hydrogen storage in the $(Ti_{0.5}Zr_{0.5})_1(Mn_{0.5}Cr_{0.5})_2$ alloy without the need of vacuum application is an important characteristic of the alloy. The alloy exhibited a good reversible hydrogen storage property and could store at least 89% of its initial capacity after ten cycles. The desorption behavior without dynamic vacuum application is a facilitating factor for the practical use of the alloy. Moreover, the room-temperature cycling stability of the $(Ti_{0.5}Zr_{0.5})_1(Fe_{0.33}Mn_{0.33}Cr_{0.33})_2$ is very impressive since practically the total hydrogen storage capacity of the alloy can be cycled without the need of increasing temperature or applying vacuum for hydrogen release. Lastly, the $(Ti_{0.33}Zr_{0.33}Nb_{0.33})_1(Mn_{0.5}Cr_{0.5})_2$ alloy also exhibited a good cycling result, indicating that the alloy could store at least 93 % from the second cycle to the $50^{th}$ cycle.

In addition, $(Ti_{0.5}Zr_{0.5})_1(Mn_{0.5}Cr_{0.5})_2$, $(Ti_{0.5}Zr_{0.5})_1(Fe_{0.33}Mn_{0.33}Cr_{0.33})_2$, and $(Ti_{0.33}Zr_{0.33}Nb_{0.33})_1(Mn_{0.5}Cr_{0.5})_2$ compositions can be produced at a relatively low cost because of their high fraction of Mn, Cr, and Fe, which are relatively cheap elements. The $(Ti_{0.5}Zr_{0.5})_1(Mn_{0.5}Cr_{0.5})_2$ alloy have 31.13 wt.% of Mn, 29.46 wt.% of Cr, $(Ti_{0.5}Zr_{0.5})_1(Fe_{0.33}Mn_{0.33}Cr_{0.33})_2$ alloy have 20.90 wt.% of Fe, 20.57 wt.% of Mn, and 19.47 wt.% of Cr, and $(Ti_{0.33}Zr_{0.33}Nb_{0.33})_1(Mn_{0.5}Cr_{0.5})_2$ alloy have 29.82 wt.% Mn and 28.22 wt.% of Cr.

As observed in this study regarding the activation procedures, the Ce addition of 0.4 wt.% proved to be the fastest and efficient option for making a sample capable of absorbing hydrogen. As it is a rare earth metal, it oxidizes very readily at room temperature. Due to this, Ce doping was used aiming at a possible reduction of oxygen/oxides in the alloy, which may have been the factor that induced the absorption of hydrogen by the alloy. Figure 5.63 and 5.64 showed that the oxygen is concentrated in Ce particles ($CeO_2$). However, this procedure is also the more expensive. The rare earth elements are known for their high cost, primarily due to the challenges associated with their mining and extraction processes. Unlike transition metals, rare earth elements are not typically found in concentrated forms, making their extraction more complex and resource-intensive.

Furthermore, the resulting Ce-doped alloy, with a hydrogen equilibrium pressure equal to 40 bar, showed to be also a promising candidate for room hydrogen storage applications, since can absorb hydrogen at relatively moderate pressures and completely desorb at room temperature in atmospheric pressure. Moreover, the $(Ti_{0.5}Zr_{0.5})_1(Fe_{0.5}Mn_{0.5})_2$+Ce alloy presented an excellent cycling stability over several cycles, exhibiting superb reversible hydrogen storage properties.

## 7 CONCLUSIONS

In this thesis, a method to design multicomponent alloys with single C14-type Laves phase based on based on computational thermodynamics was proposed and validated.

The method to design C14 Laves phase multicomponent alloys for hydrogen storage assisted by computational thermodynamic, combining high-throughput calculations of VEC, $r_A/r_B$, and δ with CALPHAD method allowed us to find 440 multicomponent alloys prone to form C14 Laves phase structure.

The developed thermodynamic model to calculate PCT diagrams for C14 Laves phase alloys was suitable for predicting the order of magnitude for hydrogen absorption pressure.

With this design method, seven alloy compositions were selected, produced and experimentally characterized. All the alloys presented C14 Laves phase, validating the method to design C14 Laves phase multicomponent alloys.

$(Ti_{0.5}Zr_{0.5})_1(Mn_{0.5}Cr_{0.5})_2$, $(Ti_{0.5}Zr_{0.5})_1(Fe_{0.33}Mn_{0.33}Cr_{0.33})_2$, and $(Ti_{0.33}Zr_{0.33}Nb_{0.33})_1(Mn_{0.5}Cr_{0.5})_2$, alloys absorbed hydrogen without the need for activation, demonstrating fast absorption kinetics, high absorption capacity, reversibility, and excellent cycling stability over several cycles in different conditions.

The $(Ti_{0.5}Zr_{0.5})_1(Mn_{0.5}Cr_{0.5})_2$, $(Ti_{0.5}Zr_{0.5})_1(Fe_{0.33}Mn_{0.33}Cr_{0.33})_2$, and $(Ti_{0.33}Zr_{0.33}Nb_{0.33})_1(Mn_{0.5}Cr_{0.5})_2$ alloys reached a total hydrogen storage capacity equal to H/M = 1.14 (1.92 wt.%), H/M = 1.04 (1.75 wt.%), and H/M = 0.92 (1.50 wt.%), respectively, in less than one minute, demonstrating fast absorption kinetics.

In addition, The PCT diagrams demonstrated that the alloy could reversibly absorb and desorb significant amounts of hydrogen under moderate temperatures and pressure range. The $(Ti_{0.5}Zr_{0.5})_1(Mn_{0.5}Cr_{0.5})_2$, $(Ti_{0.5}Zr_{0.5})_1(Fe_{0.33}Mn_{0.33}Cr_{0.33})_2$, and $(Ti_{0.33}Zr_{0.33}Nb_{0.33})_1(Mn_{0.5}Cr_{0.5})_2$ alloys presented an equilibrium pressure of 0.4 bar, 6.0 and 9.6 bar at 30 °C, respectively

The addition of Ce proved highly effective in making $(Ti_{0.5}Zr_{0.5})_1(Fe_{0.5}Mn_{0.5})_2$ alloy capable of absorbing hydrogen. The Ce-doped alloy,

which exhibited a hydrogen equilibrium pressure of 27 bar, demonstrated promising potential for room-temperature hydrogen storage applications. Notably, it could absorb hydrogen at relatively moderate pressures and completely desorb at room temperature under atmospheric pressure. Furthermore, the $(Ti_{0.5}Zr_{0.5})_1$ $(Fe_{0.5}Mn_{0.5})_2$+Ce alloy demonstrated outstanding cycling stability over numerous cycles, highlighting its excellent reversible hydrogen storage properties.

Finally, it was shown that the design method developed here can play a crucial role in minimizing the need for numerous experiments when navigating through the vast compositional space of multicomponent alloys.

## 8 SUGGESTIONS FOR FUTURE WORKS

- To work on improving the predictability of the thermodynamic to calculated PCT diagram for C14 Laves phase alloys (description of the $\Delta G_m(c_H)$);
- To evaluate the formation or not of plateau pressure on the PCT diagrams during the hydrogenation of C14 Laves phase alloys;
- To evaluate different activation procedures of the C14 Laves phase alloys;
- To evaluate the Ce addition in other compositions that was unsuccessfully activated by the other procedures in this work;
- To conduct a more comprehensive investigation into the oxide composition presented in the samples via X-ray photoelectron spectroscopy (XPS) and TEM;

## 9 REFERENCES

[1] K.T. Møller, T.R. Jensen, E. Akiba, H. wen Li, Hydrogen - A sustainable energy carrier, Prog. Nat. Sci. Mater. Int. 27 (2017) 34–40. https://doi.org/10.1016/j.pnsc.2016.12.014.

[2] M. Marinelli, M. Santarelli, Hydrogen storage alloys for stationary applications, J. Energy Storage. 32 (2020) 101864. https://doi.org/10.1016/j.est.2020.101864.

[3] L. Schlapbach, A. Züttel, Hydrogen-storage materials for mobile applications, Nature. 414 (2001) 353–358. https://doi.org/10.1038/35104634.

[4] M. Hirscher, V.A. Yartys, M. Baricco, J. Bellosta von Colbe, D. Blanchard, R.C. Bowman, D.P. Broom, C.E. Buckley, F. Chang, P. Chen, Y.W. Cho, J.C. Crivello, F. Cuevas, W.I.F. David, P.E. de Jongh, R. V. Denys, M. Dornheim, M. Felderhoff, Y. Filinchuk, G.E. Froudakis, D.M. Grant, E.M.A. Gray, B.C. Hauback, T. He, T.D. Humphries, T.R. Jensen, S. Kim, Y. Kojima, M. Latroche, H.W. Li, M. V. Lototskyy, J.W. Makepeace, K.T. Møller, L. Naheed, P. Ngene, D. Noréus, M.M. Nygård, S. ichi Orimo, M. Paskevicius, L. Pasquini, D.B. Ravnsbæk, M. Veronica Sofianos, T.J. Udovic, T. Vegge, G.S. Walker, C.J. Webb, C. Weidenthaler, C. Zlotea, Materials for hydrogen-based energy storage – past, recent progress and future outlook, J. Alloys Compd. 827 (2020). https://doi.org/10.1016/j.jallcom.2019.153548.

[5] A. Züttel, Materials for hydrogen storage, Mater. Today. 6 (2003) 24–33. https://doi.org/10.1016/S1369-7021(03)00922-2.

[6] D.B. Miracle, O.N. Senkov, A critical review of high entropy alloys and related concepts, Acta Mater. 122 (2017) 448–511. https://doi.org/10.1016/j.actamat.2016.08.081.

[7] F. Marques, M. Balcerzak, F. Winkelmann, G. Zepon, M. Felderhoff, Review and outlook on high-entropy alloys for hydrogen storage, Energy Environ. Sci. (2021). https://doi.org/10.1039/d1ee01543e.

[8] F. Stein, A. Leineweber, Laves phases: a review of their functional and structural applications and an improved fundamental understanding of

stability and properties, J. Mater. Sci. 56 (2021) 5321–5427. https://doi.org/10.1007/s10853-020-05509-2.

[9] H. Kohlmann, Hydrogen order in hydrides of Laves phases, Zeitschrift Fur Krist. - Cryst. Mater. 235 (2020) 319–332. https://doi.org/10.1515/zkri-2020-0043.

[10] P. Edalati, R. Floriano, A. Mohammadi, Y. Li, G. Zepon, H.W. Li, K. Edalati, Reversible room temperature hydrogen storage in high-entropy alloy TiZrCrMnFeNi, Scr. Mater. 178 (2020) 387–390. https://doi.org/10.1016/j.scriptamat.2019.12.009.

[11] R. Floriano, G. Zepon, K. Edalati, G.L.B.G. Fontana, A. Mohammadi, Z. Ma, H.W. Li, R.J. Contieri, Hydrogen storage in TiZrNbFeNi high entropy alloys, designed by thermodynamic calculations, Int. J. Hydrogen Energy. 45 (2020) 33759–33770. https://doi.org/10.1016/j.ijhydene.2020.09.047.

[12] E. Akiba, H. Iba, Hydrogen absorption by Laves phase related BCC solid solution, Intermetallics. 6 (1998) 461–470. https://doi.org/10.1016/S0966-9795(97)00088-5.

[13] V. Charbonnier, H. Enoki, K. Asano, H. Kim, K. Sakaki, Tuning the hydrogenation properties of Ti1+Cr2-Mn laves phase compounds for high pressure metal-hydride compressors, Int. J. Hydrogen Energy. (2021) 1–12. https://doi.org/10.1016/j.ijhydene.2021.08.143.

[14] S.K. Chen, P.H. Lee, H. Lee, H.T. Su, Hydrogen storage of C14-CruFevMnwTixVyZrz alloys, Mater. Chem. Phys. 210 (2018) 336–347. https://doi.org/10.1016/j.matchemphys.2017.08.008.

[15] F. Stein, Consequences of crystal structure differences between C14, C15, and C36 Laves phase polytypes for their coexistence in transition-metal-based systems, Mater. Res. Soc. Symp. Proc. 1295 (2011) 299–310. https://doi.org/10.1557/opl.2011.211.

[16] S.B. Gesari, M.E. Pronsato, A. Visintin, A. Juan, Hydrogen storage in AB2 Laves phase (A = Zr, Ti; B = Ni, Mn, Cr, V): Binding energy and electronic structure, J. Phys. Chem. C. 114 (2010) 16832–16836. https://doi.org/10.1021/jp106036v.

[17] N. Yurchenko, N. Stepanov, G. Salishchev, Laves-phase formation

criterion for high-entropy alloys, Mater. Sci. Technol. (United Kingdom). 33 (2017) 17–22. https://doi.org/10.1080/02670836.2016.1153277.

[18] G. Zepon, B.H. Silva, C. Zlotea, W.J. Botta, Y. Champion, Thermodynamic modelling of hydrogen-multicomponent alloy systems: Calculating pressure-composition-temperature diagrams, Acta Mater. 215 (2021) 117070. https://doi.org/10.1016/j.actamat.2021.117070.

[19] M. Dornheim, Thermodynamics of Metal Hydrides: Tailoring Reaction Enthalpies of Hydrogen Storage Materials, Thermodyn. - Interact. Stud. - Solids, Liq. Gases. (2011). https://doi.org/10.5772/21662.

[20] T.B. Flanagan, W.A. Oates, Some thermodynamic aspects of metal hydrogen systems, J. Alloys Compd. 404–406 (2005) 16–23. https://doi.org/10.1016/j.jallcom.2004.11.108.

[21] P.J. Linstrom and W.G. Mallard, Nist Chem. Webb. 69 (2017).

[22] T.B. Flanagan, W.A. Oates, L. Schlapbach (Ed.), Thermodynamics of Intermetallic Compound-Hydrogen Systems. Topics in Applied Physics 63, Springer, Berlin, Heidelberg, 1988, doi:10.1007/3540183337_10.

[23] Q. Lai, Y. Sun, T. Wang, P. Modi, C. Cazorla, U.B. Demirci, J.R. Ares Fernandez, F. Leardini, K.F. Aguey-Zinsou, How to Design Hydrogen Storage Materials? Fundamentals, Synthesis, and Storage Tanks, Adv. Sustain. Syst. 3 (2019) 1–64. https://doi.org/10.1002/adsu.201900043.

[24] G. Sandrock, Panoramic overview of hydrogen storage alloys from a gas reaction point of view, J. Alloys Compd. 293 (1999) 877–888. https://doi.org/10.1016/S0925-8388(99)00384-9.

[25] R.L. Johnston', R. Hoffmann, Structure-Bonding Relationships in the Laves Phases, Z. Anorg. Allg. Chem. 616 (1992) 105–120.

[26] K.H. Young, S. Chang, X. Lin, C14 laves phase metal hydride alloys for Ni/Mh batteries applications, Batteries. 3 (2017) 1–33. https://doi.org/10.3390/batteries3030027.

[27] S. Guo, C.T. Liu, Phase stability in high entropy alloys: Formation of solid-solution phase or amorphous phase, Prog. Nat. Sci. Mater. Int. 21 (2011) 433–446. https://doi.org/10.1016/S1002-0071(12)60080-X.

[28] V.F. Gorban', N.A. Krapivka, S.A. Firstov, High-entropy alloys: Interrelations between electron concentration, phase composition, lattice parameter, and properties, Phys. Met. Metallogr. 118 (2017) 970–981. https://doi.org/10.1134/S0031918X17080051.

[29] J.H. Zhu, P.K. Liaw, C.T. Liu, Effect of electron concentration on the phase stability of NbCr2-based Laves phase alloys, Mater. Sci. Eng. A. 239–240 (1997) 260–264. https://doi.org/10.1016/s0921-5093(97)00590-x.

[30] F. Stein, M. Palm, G. Sauthoff, Structure and stability of Laves phases . Part I . Critical assessment of factors controlling Laves phase stability, 12 (2004) 713–720. https://doi.org/10.1016/j.intermet.2004.02.010.

[31] S.S. Mishra, T.P. Yadav, O.N. Srivastava, N.K. Mukhopadhyay, K. Biswas, Formation and stability of C14 type Laves phase in multi component high-entropy alloys, J. Alloys Compd. 832 (2020) 153764. https://doi.org/10.1016/j.jallcom.2020.153764.

[32] D. Xiaoming, M. Ping, W. Erdong, Ab initio investigation of ScMn 2 -H system, Optoelectronics and Advanced Materials 8 (2014) 292–299.

[33] K. Sun, X. Guo, E. Wu, Y. Liu, H. Wang, Neutron diffraction study of the deuterides of Zr0.9Ti0.1MnCr Laves phase alloy, Phys. B Condens. Matter. 385-386 I (2006) 137–140. https://doi.org/10.1016/j.physb.2006.05.302.

[34] J. Bodega, J.F. Fernández, F. Leardini, J.R. Ares, C. Sánchez, Synthesis of hexagonal C14/C36 and cubic C15 ZrCr2 Laves phases and thermodynamic stability of their hydrides, J. Phys. Chem. Solids. 72 (2011) 1334–1342. https://doi.org/10.1016/j.jpcs.2011.08.004.

[35] S.F. Matar, Progress in Solid State Chemistry Intermetallic hydrides : A review with ab initio aspects, Prog. Solid State Chem. 38 (2010) 1–37. https://doi.org/10.1016/j.progsolidstchem.2010.08.003.

[36] A.R. Merlino, C.R. Luna, A. Juan, M.E. Pronsato, ScienceDirect Laves phase, Int. J. Hydrogen Energy. (2015) 1–11. https://doi.org/10.1016/j.ijhydene.2015.10.077.

[37] S.A. Lushnikov, V.N. Verbetsky, V.P. Glazkov, V.A. Somenkov, Structure of deuterided NbVCo, Inorganic Materials 42 (2006) 733–738. https://doi.org/10.1134/S0020168506070089.

[38] A. V Skripov, Hydrogen jump motion in Laves-phase hydrides : Two frequency scales, J. Alloys Compd 404–406 (2005) 224–229. https://doi.org/10.1016/j.jallcom.2004.12.160.

[39] S. V Mitrokhin, Regularities of hydrogen interaction with multicomponent Ti ( Zr )– Mn – V Laves phase alloys, J. Alloys Compd 404–406 (2005) 384–387. https://doi.org/10.1016/j.jallcom.2005.02.078.

[40] I. Kunce, M. Polanski, J. Bystrzycki, Structure and hydrogen storage properties of a high entropy ZrTiVCrFeNi alloy synthesized using Laser Engineered Net Shaping (LENS), Int. J. Hydrogen Energy. 38 (2013) 12180–12189. https://doi.org/10.1016/j.ijhydene.2013.05.071.

[41] K.H. Young, J. Nei, C. Wan, R. V. Denys, V.A. Yartys, Comparison of C14- and C15-predomiated AB 2 metal hydride alloys for electrochemical applications, Batteries. 3 (2017). https://doi.org/10.3390/batteries3030022.

[42] B.H. Liu, Hydrogen – Metal Systems : Hydride Forming Alloys ( Properties and Characteristics , Database Information) (2021). doi: 10.1016/B0-08-043152-6/00697-5

[43] B. Sarac, V. Zadorozhnyy, E. Berdonosova, Y.P. Ivanov, S. Klyamkin, S. Gumrukcu, A.S. Sarac, A. Korol, D. Semenov, M. Zadorozhnyy, A. Sharma, A.L. Greer, J. Eckert, Hydrogen storage performance of the multi-principal-component CoFeMnTiVZr alloy in electrochemical and gas-solid reactions, RSC Adv. 10 (2020) 24613–24623. https://doi.org/10.1039/d0ra04089d.

[44] B. Tu, H. Wang, Y. Wang, R. Li, L. Ouyang, R. Tang, Optimizing Ti–Zr–Cr–Mn–Ni–V alloys for hybrid hydrogen storage tank of fuel cell bicycle, Int. J. Hydrogen Energy. 47 (2022) 14952–14960. https://doi.org/10.1016/j.ijhydene.2022.03.018.

[45] L. Zhou, W. Li, H. Hu, H. Zeng, Q. Chen, Ce-Doped TiZrCrMn Alloys for Enhanced Hydrogen Storage, Energy and Fuels. 36 (2022) 3997–4005. https://doi.org/10.1021/acs.energyfuels.2c00011.

[46] J. Garcés, The configurational entropy of mixing of interstitials solid solutions, Appl. Phys. Lett. 96 (2010) 67–70. https://doi.org/10.1063/1.3400221.

[47] I. Kunce, M. Polanski, J. Bystrzycki, Microstructure and hydrogen storage

properties of a TiZrNbMoV high entropy alloy synthesized using Laser Engineered Net Shaping (LENS), Int. J. Hydrogen Energy. 39 (2014) 9904–9910. https://doi.org/10.1016/j.ijhydene.2014.02.067.

[48] C. Zhang, Y. Wu, L. You, X. Cao, Z. Lu, X. Song, Investigation on the activation mechanism of hydrogen absorption in TiZrNbTa high entropy alloy, J. Alloys Compd. 781 (2019) 613–620. https://doi.org/10.1016/j.jallcom.2018.12.120.

[49] M.M. Nygård, G. Ek, D. Karlsson, M. Sahlberg, M.H. Sørby, B.C. Hauback, Hydrogen storage in high-entropy alloys with varying degree of local lattice strain, Int. J. Hydrogen Energy. 44 (2019) 29140–29149. https://doi.org/10.1016/j.ijhydene.2019.03.223.

[50] J. Montero, G. Ek, L. Laversenne, V. Nassif, G. Zepon, M. Sahlberg, C. Zlotea, Hydrogen storage properties of the refractory Ti–V–Zr–Nb–Ta multi-principal element alloy, J. Alloys Compd. 835 (2020) 155376. https://doi.org/10.1016/j.jallcom.2020.155376.

[51] S.K. Chen, P.H. Lee, H. Lee, H.T. Su, Hydrogen storage of C14-CruFevMnwTixVyZrz alloys, Mater. Chem. Phys. 210 (2018) 336–347. https://doi.org/10.1016/j.matchemphys.2017.08.008.

[52] V. A. Yartys and M. V. Lototskyy, Laves Type Intermetallic Compounds As Hydrogen Storage Materials: A Review, J. Alloys Compd. 916 (2022) 165219. https://doi.org/10.1016/j.jallcom.2022.165219.

[53] S. Dangwal, K. Edalati, Significance of interphase boundaries on activation of high-entropy alloys for room-temperature hydrogen storage, Int. J. Hydrogen Energy. 50 (2024) 626–636. https://doi.org/10.1016/j.ijhydene.2023.07.327.

[54] A.K. Patel, D. Siemiaszko, J. Dworecka-Wójcik, M. Polański, Just shake or stir. About the simplest solution for the activation and hydrogenation of an FeTi hydrogen storage alloy, Int. J. Hydrogen Energy. 47 (2022) 5361–5371. https://doi.org/10.1016/j.ijhydene.2021.11.136.

[55] B. H. Silva, J.M.P. Almeida, A.C. Hernandes, R. V. Gonçalves, G. Zepon, Pulsed laser activation method for hydrogen storage alloys, Int. J. Hydrogen Energy. 53 (2024) 885–890.

https://doi.org/10.1016/j.ijhydene.2023.12.143.

[56] H. Liu, J. Zhang, P. Sun, C. Zhou, Y. Liu, Z.Z. Fang, The mechanistic role of Ti4Fe2O1-x phases in the activation of TiFe alloys for hydrogen storage, Int. J. Hydrogen Energy. 48 (2023) 32011–32024. https://doi.org/10.1016/j.ijhydene.2023.05.016.

[57] V. Zadorozhnyy, B. Sarac, E. Berdonosova, T. Karazehir, A. Lassnig, C. Gammer, M. Zadorozhnyy, S. Ketov, S. Klyamkin, J. Eckert, Evaluation of hydrogen storage performance of ZrTiVNiCrFe in electrochemical and gas-solid reactions, Int. J. Hydrogen Energy. 45 (2020) 5347–5355. https://doi.org/10.1016/j.ijhydene.2019.06.157.

[58] B. H. Toby and R. B. Von Dreele, GSAS-II: the genesis of a modern open-source all purpose crystallography software package, J. Appl. Crystallogr., 2013, 46, 544–549. https://doi.org/10.1107/S0021889813003531

[59] ASTM E1409-13, Standard Test Method for Determination of Oxygen and Nitrogen in Titanium and Titanium Alloys by Inert Gas Fusion. American Society for Testing and Materials (2021).

[60] B. Hessel, C. Zlotea, G. Vaughan, Y. Champion, Hydrogen absorption/desorption reactions of the (TiVNb)85Cr15 multicomponent alloy, J. Alloys Compd. 901 (2022) 163620. https://doi.org/10.1016/j.jallcom.2022.163620.

[61] B.H. Silva, C. Zlotea, Y. Champion, W.J. Botta, G. Zepon, valence electron concentration for hydrogen storage, J. Alloys Compd. 865 (2021) 158767. https://doi.org/10.1016/j.jallcom.2021.158767.

[62] B. Hessel, W. J. Botta, G. Zepon, Design of a Ti e V e Nb e Cr alloy with room temperature hydrogen absorption / desorption reversibility, Int. J. of Hydrogen Energy. 48 (2023) 32813-32825. https://doi.org/10.1016/j.ijhydene.2023.05.032.

[63] R.B. Strozi, B.H. Silva, D.R. Leiva, C. Zlotea, W.J. Botta, G. Zepon, Tuning the hydrogen storage properties of Ti-V-Nb-Cr alloys by controlling the Cr/(TiVNb) ratio, J. Alloys Compd. 932 (2023) 167609. https://doi.org/10.1016/j.jallcom.2022.167609.

[64] R. Griessen, T. Riesterer, Heat of formation models, (1988) 219–284.

https://doi.org/10.1007/3540183337_13.

[65] Y.F. Kao, S.K. Chen, J.H. Sheu, J.T. Lin, W.E. Lin, J.W. Yeh, S.J. Lin, T.H. Liou, C.W. Wang, Hydrogen storage properties of multi-principal-component CoFeMnTi xVyZrz alloys, Int. J. Hydrogen Energy. 35 (2010) 9046–9059. https://doi.org/10.1016/j.ijhydene.2010.06.012.

[66] Z. Li, Y. Yan, H. Huang, B. Liu, Y. Lv, B. Zhang, W. Lv, J. Yuan, Y. Wu, Effects of the different element substitution on hydrogen storage properties of Ti0.8Zr0.2Mn0.9Cr0.6V0.3M0.2 (M = Fe, Ni, Co), J. Alloys Compd. 908 (2022) 164605. https://doi.org/10.1016/j.jallcom.2022.164605.

[67] H. Peisl, Lattice strains due to hydrogen in metals, in: G. Alefeld, J. Völkl (Eds.), Hydrog. Met. I. Top. Appl. Physics, 28 Springer, Berlin, Heidelberg, 1978, pp. 53–74, https://doi.org/10.1007/3540087052_42

[68] Y. Kojima, Y. Kawai, S. Towata, T. Matsunaga, T. Shinozawa, M. Kimbara, Development of metal hydride with high dissociation pressure, 419 (2006) 256–261. https://doi.org/10.1016/j.jallcom.2005.08.078.

[69] S.G. and N.O. A. Yamashita, M. Kondo, Development of High-Pressure Hydrogen Storage System for the Toyota “Mirai,” SAE Tech. Pap. 2015-01–11 (2015). doi: https://doi.org/10.4271/2015-01-1169.

[70] P.H.L. Notten, Rechargeable nickel-metalhydride batteries: a successful new concept, Interstitial Intermet. Alloy. (1995) 151–195. https://doi.org/10.1007/978-94-011-0295-7_7.

[71] J. Chen, Z. Li, H. Huang, Y. Lv, B. Liu, Y. Li, Y. Wu, J. Yuan, Y. Wang, Superior cycle life of TiZrFeMnCrV high entropy alloy for hydrogen storage, Scr. Mater. 212 (2022) 114548. https://doi.org/10.1016/j.scriptamat.2022.114548.

## APPENDIX A

Table A1 – Non-equiatomic compositions predicted to form C14 Laves phase by CALPHAD calculations. The alloys were named as number 87 to 440. The atomic fraction of the elements and their $r_A/r_B$, VEC, and δ parameter are presented.

| Alloy number | Concentration atomic fraction | | | | | | | | | | | $r_A/r_B$ | VEC | δ |
|---|---|---|---|---|---|---|---|---|---|---|---|---|---|---|
| | Ti | Zr | Nb | Fe | Mn | V | Cr | Ni | Co | Zn | Cu | | | |
| 87 | 0.3333 | | 0.0011 | | | | | | | 0.6656 | | 1.054 | 9.3 | 2.3 |
| 88 | 0.3333 | | | 0.5373 | | | | 0.1294 | | | | 1.159 | 6.9 | 6.9 |
| 89 | 0.3323 | | | | 0.6427 | | | | | | 0.0250 | 1.150 | 6.1 | 7.1 |
| 90 | | 0.3855 | | | 0.6143 | 0.0002 | | | | | | 1.226 | 5.8 | 11.9 |
| 91 | | 0.2436 | | | 0.7549 | | | 0.0016 | | | | 1.275 | 6.3 | 10.9 |
| 92 | | | 0.3363 | | 0.6635 | 0.0002 | | | | | | 1.126 | 6.3 | 7.5 |
| 93 | | | 0.3356 | | 0.4326 | | | 0.2318 | | | | 1.157 | 7.0 | 7.6 |
| 94 | | | 0.3382 | | 0.6615 | | | | | | 0.0003 | 1.159 | 6.3 | 7.5 |
| 95 | 0.3287 | 0.0027 | | 0.3193 | | 0.3493 | | | | | | 1.168 | 5.6 | 5.7 |
| 96 | 0.3333 | | | 0.3002 | | | | | | 0.3665 | | 1.098 | 8.1 | 5.5 |
| 97 | 0.1097 | 0.2239 | | 0.6664 | | | | | | | | 1.205 | 6.7 | 10.2 |
| 98 | 0.0810 | 0.3311 | | | 0.5878 | | | | | | | 1.214 | 5.8 | 11.4 |
| 99 | 0.0508 | 0.2825 | | | 0.3837 | | | | 0.2830 | | | 1.219 | 6.6 | 11.4 |
| 100 | 0.3334 | | | | 0.2089 | | | | | 0.4576 | | 1.102 | 8.3 | 5.2 |

| | | | | | | | | | | | | | | |
|---|---|---|---|---|---|---|---|---|---|---|---|---|---|---|
| 101 | 0.0331 | 0.3000 | | | 0.6669 | | | | | | | 1.214 | 6.0 | 11.4 |
| 102 | 0.1451 | 0.1906 | | | 0.6637 | | | | | | | 1.214 | 6.0 | 10.2 |
| 103 | 0.3334 | | | | | | 0.1197 | | | 0.5469 | | 1.094 | 8.6 | 3.9 |
| 104 | 0.3275 | | 0.0028 | 0.3885 | | 0.2812 | | | | | | 1.118 | 5.8 | 5.9 |
| 105 | 0.1147 | | 0.2186 | 0.5712 | | | | 0.0954 | | | | 1.163 | 7.1 | 7.1 |
| 106 | 0.3333 | | | 0.1989 | | | | | | 0.4678 | | 1.098 | 8.5 | 4.8 |
| 107 | 0.1120 | | 0.2516 | | 0.6353 | 0.0010 | | | | | | 1.123 | 6.2 | 7.5 |
| 108 | 0.0042 | | 0.3265 | | 0.6370 | | | 0.0323 | | | | 1.167 | 6.4 | 7.4 |
| 109 | 0.0559 | | 0.2775 | | 0.3763 | | | | 0.2904 | | | 1.167 | 6.9 | 7.6 |
| 110 | 0.0023 | | 0.3314 | | 0.6663 | | | | | | | 1.163 | 6.3 | 7.4 |
| 111 | 0.3333 | | 0.0007 | | 0.0547 | | | | | 0.6113 | | 1.106 | 9.1 | 3.4 |
| 112 | 0.0133 | | 0.3289 | | 0.6576 | | | | | | 0.0003 | 1.154 | 6.3 | 7.5 |
| 113 | 0.3333 | | 0.0047 | | | 0.0189 | | | | 0.6430 | | 1.069 | 9.2 | 2.4 |
| 114 | 0.3333 | | 0.0005 | | | | 0.0412 | | | 0.6250 | | 1.097 | 9.1 | 3.0 |
| 115 | | 0.0399 | 0.2934 | 0.2642 | 0.4024 | | | | | | | 1.213 | 6.6 | 8.0 |
| 116 | | 0.0002 | 0.3332 | 0.5932 | | | | 0.0733 | | | | 1.218 | 7.1 | 7.2 |
| 117 | | 0.3244 | 0.0479 | | 0.6275 | 0.0015 | | | | | | 1.176 | 5.9 | 11.5 |
| 118 | | 0.0211 | 0.3105 | | 0.6142 | | | 0.0543 | | | | 1.223 | 6.5 | 7.9 |
| 119 | | 0.0112 | 0.3225 | | 0.6662 | | | | | | | 1.218 | 6.3 | 7.7 |
| 120 | | 0.1478 | 0.1973 | | 0.6549 | | | | | | | 1.218 | 6.2 | 9.8 |

| | | | | | | | | | | | | | | |
|---|---|---|---|---|---|---|---|---|---|---|---|---|---|---|
| 121 | 0.2097 | 0.0183 | 0.1054 | 0.6667 | | | | | | | | 1.189 | 6.8 | 7.2 |
| 122 | 0.3334 | | | 0.4097 | 0.2227 | | | 0.0342 | | | | 1.159 | 6.5 | 6.9 |
| 123 | 0.3333 | | | 0.3854 | 0.1283 | | | | 0.1529 | | | 1.159 | 6.7 | 7.0 |
| 124 | 0.3338 | | | 0.2265 | 0.4254 | | | | | | 0.0143 | 1.150 | 6.6 | 7.0 |
| 125 | 0.3334 | | | 0.2136 | | 0.1085 | | | | 0.3445 | | 1.092 | 7.7 | 5.0 |
| 126 | 0.3247 | | | 0.3574 | | 0.3152 | | | | | 0.0041 | 1.123 | 5.8 | 5.8 |
| 127 | 0.3333 | | | 0.4981 | | | 0.0462 | 0.1224 | | | | 1.153 | 6.8 | 6.9 |
| 128 | 0.3333 | | | 0.3485 | | | 0.1241 | | 0.1941 | | | 1.153 | 6.6 | 6.9 |
| 129 | 0.3317 | | | 0.4516 | | | | 0.0435 | 0.1732 | | | 1.162 | 6.9 | 7.0 |
| 130 | 0.3333 | | | 0.5232 | | | | 0.0691 | | 0.0744 | | 1.120 | 7.1 | 6.7 |
| 131 | 0.3334 | | | 0.5712 | | | | 0.0949 | | | 0.0005 | 1.153 | 6.9 | 6.8 |
| 132 | 0.3333 | | | 0.4981 | | | | | 0.1673 | | 0.0013 | 1.153 | 6.8 | 6.9 |
| 133 | 0.3337 | | | | 0.4359 | | 0.2303 | 0.0001 | | | | 1.156 | 5.8 | 6.9 |
| 134 | 0.3337 | | | | 0.4129 | | 0.2307 | | | | 0.0227 | 1.147 | 5.9 | 6.8 |
| 135 | 0.3309 | | | | 0.6288 | | | | 0.0251 | | 0.0152 | 1.156 | 6.1 | 7.1 |
| 136 | 0.3343 | | | | 0.5364 | | | | | 0.1087 | 0.0205 | 1.115 | 6.6 | 6.9 |
| 137 | 0.3335 | | | | | | 0.4971 | | | 0.1517 | 0.0176 | 1.109 | 6.3 | 6.1 |
| 138 | | 0.3359 | | 0.2072 | 0.4567 | 0.0001 | | | | | | 1.237 | 6.2 | 11.6 |
| 139 | | 0.3335 | | 0.2080 | 0.4585 | | | | | | | 1.265 | 6.2 | 11.6 |
| 140 | | 0.3404 | | | 0.6512 | 0.0001 | 0.0084 | | | | | 1.234 | 6.0 | 11.7 |

| | | | | | | | | | | | | |
|---|---|---|---|---|---|---|---|---|---|---|---|---|
| 141 | 0.3375 | | | 0.6615 | 0.0001 | | 0.0009 | | | 1.244 | 6.0 | 11.7 |
| 142 | 0.3453 | | | 0.6162 | 0.0001 | | | 0.0334 | | 1.244 | 6.0 | 11.8 |
| 143 | 0.3288 | | | 0.6473 | | 0.0132 | 0.0107 | | | 1.266 | 6.0 | 11.6 |
| 144 | 0.3335 | | | 0.6579 | | 0.0085 | | | | 1.260 | 6.0 | 11.7 |
| 145 | 0.3349 | | | 0.6480 | | 0.0171 | | | | 1.260 | 6.0 | 11.7 |
| 146 | 0.3333 | | | 0.3405 | | | 0.0365 | 0.2896 | | 1.277 | 6.7 | 11.9 |
| 147 | 0.3335 | | | 0.4902 | | | | 0.1764 | | 1.275 | 6.4 | 11.8 |
| 148 | 0.3334 | | | 0.4305 | | | | 0.2361 | | 1.275 | 6.5 | 11.8 |
| 149 | | 0.3395 | 0.2040 | 0.4563 | 0.0002 | | | | | 1.137 | 6.5 | 7.4 |
| 150 | | 0.3435 | 0.1769 | 0.4793 | | | | | 0.0003 | 1.157 | 6.5 | 7.4 |
| 151 | | 0.3346 | 0.2987 | | 0.0001 | 0.3666 | | | | 1.131 | 6.3 | 6.9 |
| 152 | | 0.3348 | 0.2838 | | | 0.3812 | | | 0.0002 | 1.151 | 6.3 | 6.8 |
| 153 | | 0.3337 | 0.3253 | | | | 0.0903 | 0.2507 | | 1.170 | 7.4 | 7.5 |
| 154 | | 0.3343 | | 0.3956 | 0.0002 | 0.2699 | | | | 1.134 | 6.1 | 7.2 |
| 155 | | 0.3364 | | 0.5895 | 0.0002 | | 0.0739 | | | 1.142 | 6.5 | 7.5 |
| 156 | | 0.3368 | | 0.4609 | | | | 0.2020 | | 1.171 | 6.7 | 7.6 |
| 157 | | 0.3359 | | 0.4501 | | | 0.2140 | | | 1.171 | 7.0 | 7.6 |
| 158 | | 0.3388 | | 0.5277 | | | 0.1332 | | 0.0002 | 1.164 | 6.7 | 7.5 |
| 159 | | 0.3410 | | 0.5348 | | | | 0.1239 | 0.0003 | 1.164 | 6.6 | 7.6 |
| 160 | | 0.3341 | | | 0.0001 | 0.4067 | | 0.2591 | | 1.137 | 6.4 | 7.2 |

| | | | | | | | | | | | | | |
|---|---|---|---|---|---|---|---|---|---|---|---|---|---|
| 161 | | | 0.3342 | | | | 0.4315 | | 0.2341 | | 0.0002 | 1.157 | 6.4 | 7.1 |
| 162 | 0.0349 | 0.3171 | | 0.2110 | 0.4368 | 0.0001 | | | | | | 1.183 | 6.2 | 11.3 |
| 163 | 0.0694 | 0.2640 | | 0.2743 | 0.3923 | | | | | | | 1.209 | 6.3 | 10.9 |
| 164 | 0.1331 | 0.2014 | | 0.2466 | 0.4187 | | | | | | 0.0001 | 1.205 | 6.2 | 10.2 |
| 165 | 0.3320 | 0.0004 | | 0.3193 | | 0.3443 | 0.0040 | | | | | 1.177 | 5.6 | 5.7 |
| 166 | 0.1538 | 0.1886 | | 0.5004 | | 0.0023 | | 0.1549 | | | | 1.186 | 6.9 | 10.0 |
| 167 | 0.3230 | 0.0003 | | 0.3836 | | 0.2930 | | | | | | 1.186 | 5.8 | 5.9 |
| 168 | 0.3237 | 0.0051 | | 0.3707 | | 0.3043 | | | | | 0.0007 | 1.177 | 5.8 | 6.0 |
| 169 | 0.3333 | | | 0.2880 | | | 0.0520 | | | 0.3266 | | 1.112 | 7.9 | 5.7 |
| 170 | 0.1560 | 0.1774 | | 0.3851 | | | | 0.2814 | | 0.0001 | | 1.174 | 7.2 | 10.0 |
| 171 | 0.1748 | 0.1586 | | 0.4376 | | | | 0.2289 | | | | 1.214 | 7.1 | 9.7 |
| 172 | 0.1380 | 0.2246 | | | 0.6042 | 0.0005 | 0.0327 | | | | | 1.180 | 5.9 | 10.5 |
| 173 | 0.1064 | 0.2326 | | | 0.6529 | 0.0003 | | 0.0079 | | | | 1.189 | 6.0 | 10.7 |
| 174 | 0.0221 | 0.3203 | | | 0.6405 | 0.0001 | | | 0.0170 | | | 1.189 | 6.0 | 11.5 |
| 175 | 0.0289 | 0.3107 | | | 0.6603 | 0.0001 | | | | | | 1.172 | 6.0 | 11.5 |
| 176 | 0.0907 | 0.2412 | | | 0.6578 | 0.0021 | | | | | | 1.172 | 5.9 | 10.9 |
| 177 | 0.2686 | 0.0648 | | | 0.5490 | | 0.1170 | 0.0006 | | | | 1.211 | 5.9 | 8.2 |
| 178 | 0.1129 | 0.2201 | | | 0.6392 | | 0.0278 | | | | | 1.205 | 6.0 | 10.5 |
| 179 | 0.3342 | 0.0001 | | | 0.3542 | | 0.0310 | | | 0.2814 | | 1.168 | 7.4 | 6.3 |
| 180 | 0.2489 | 0.0852 | | | 0.5652 | | 0.0975 | | | | 0.0032 | 1.202 | 5.9 | 8.6 |

| | | | | | | | | | | | | | | |
|---|---|---|---|---|---|---|---|---|---|---|---|---|---|---|
| 181 | 0.0789 | 0.2098 | | | 0.7084 | | | 0.0029 | | | | 1.219 | 6.1 | 10.5 |
| 182 | 0.0426 | 0.2903 | | | 0.5351 | | | | 0.1320 | | | 1.219 | 6.3 | 11.4 |
| 183 | 0.0537 | 0.2789 | | | 0.5646 | | | | 0.1028 | | | 1.219 | 6.2 | 11.2 |
| 184 | 0.0431 | 0.2927 | | | 0.6642 | | | | | | | 1.155 | 6.0 | 11.3 |
| 185 | 0.1076 | 0.2257 | | | | | | 0.2751 | 0.3916 | | | 1.224 | 7.6 | 11.0 |
| 186 | 0.3328 | | 0.0048 | 0.3549 | 0.0337 | 0.2738 | | | | | | 1.133 | 5.8 | 6.0 |
| 187 | 0.0435 | | 0.3041 | 0.1559 | 0.4961 | 0.0005 | | | | | | 1.133 | 6.4 | 7.4 |
| 188 | 0.1234 | | 0.2099 | 0.3734 | 0.2658 | | | 0.0274 | | | | 1.163 | 6.7 | 7.1 |
| 189 | 0.3333 | | 0.0001 | 0.1396 | 0.0530 | | | | | 0.4740 | | 1.121 | 8.5 | 4.8 |
| 190 | 0.0617 | | 0.2748 | 0.3027 | 0.3604 | | | | | | 0.0004 | 1.154 | 6.6 | 7.2 |
| 191 | 0.0269 | | 0.3077 | 0.2469 | | 0.0002 | 0.4182 | | | | | 1.127 | 6.1 | 6.8 |
| 192 | 0.3233 | | 0.0016 | 0.4326 | | 0.2384 | | 0.0041 | | | | 1.136 | 6.0 | 6.1 |
| 193 | 0.3336 | | 0.0050 | 0.1420 | | 0.0655 | | | | 0.4541 | | 1.096 | 8.3 | 4.4 |
| 194 | 0.1199 | | 0.2134 | 0.4167 | | | 0.2060 | 0.0440 | | | | 1.157 | 6.6 | 6.9 |
| 195 | 0.0204 | | 0.3129 | 0.2983 | | | 0.3684 | | | | | 1.149 | 6.2 | 6.8 |
| 196 | 0.0641 | | 0.2694 | 0.3073 | | | 0.3590 | | | | 0.0002 | 1.148 | 6.2 | 6.8 |
| 197 | 0.0857 | | 0.2476 | 0.3563 | | | | 0.0217 | 0.2887 | | | 1.166 | 7.2 | 7.4 |
| 198 | 0.1236 | | 0.2101 | 0.5974 | | | | 0.0688 | | 0.0001 | | 1.124 | 7.0 | 7.0 |
| 199 | 0.1400 | | 0.1937 | 0.5959 | | | | 0.0701 | | | 0.0003 | 1.157 | 7.0 | 7.0 |
| 200 | 0.0518 | | 0.2818 | 0.4095 | | | | | 0.2569 | | | 1.163 | 7.2 | 7.3 |

| | | | | | | | | | | | | |
|---|---|---|---|---|---|---|---|---|---|---|---|---|
| 201 | 0.0691 | 0.2646 | 0.4602 | | | | | 0.2059 | | 0.0001 | 1.157 | 7.1 | 7.3 |
| 202 | 0.1057 | 0.2420 | | 0.3641 | 0.0004 | 0.2878 | | | | | 1.130 | 5.9 | 7.1 |
| 203 | 0.0448 | 0.2962 | | 0.6563 | 0.0003 | | 0.0024 | | | | 1.139 | 6.3 | 7.4 |
| 204 | 0.0034 | 0.3337 | | 0.5078 | 0.0002 | | | 0.1549 | | | 1.139 | 6.6 | 7.6 |
| 205 | 0.3335 | 0.0137 | | 0.1350 | 0.0378 | | | | 0.4800 | | 1.099 | 8.3 | 4.6 |
| 206 | 0.0195 | 0.3223 | | 0.6579 | 0.0003 | | | | | | 1.123 | 6.3 | 7.5 |
| 207 | 0.0176 | 0.3230 | | 0.6588 | 0.0003 | | | | | | 1.123 | 6.3 | 7.5 |
| 208 | 0.1086 | 0.2248 | | 0.3970 | | 0.2674 | 0.0022 | | | | 1.160 | 6.0 | 7.1 |
| 209 | 0.3333 | 0.0002 | | 0.0936 | | 0.0892 | | | 0.4837 | | 1.118 | 8.3 | 4.7 |
| 210 | 0.0251 | 0.3083 | | 0.3315 | | 0.3351 | | | | | 1.154 | 6.0 | 7.1 |
| 211 | 0.0836 | 0.2499 | | 0.3331 | | 0.3331 | | | | 0.0004 | 1.151 | 5.9 | 7.0 |
| 212 | 0.0106 | 0.3228 | | 0.3679 | | | 0.0221 | 0.2767 | | | 1.169 | 6.9 | 7.6 |
| 213 | 0.0026 | 0.3311 | | 0.6453 | | | 0.0211 | | | | 1.167 | 6.4 | 7.5 |
| 214 | 0.0041 | 0.3296 | | 0.6501 | | | 0.0161 | | | 0.0001 | 1.160 | 6.4 | 7.5 |
| 215 | 0.1780 | 0.2520 | | 0.5699 | | | | | | | 1.163 | 6.0 | 7.6 |
| 216 | 0.0031 | 0.3387 | | 0.5317 | | | | 0.1261 | | 0.0003 | 1.160 | 6.6 | 7.6 |
| 217 | 0.0143 | 0.3298 | | 0.6558 | | | | | | 0.0001 | 1.154 | 6.3 | 7.5 |
| 218 | 0.0226 | 0.3114 | | | 0.0002 | 0.4105 | | 0.2553 | | | 1.133 | 6.4 | 7.1 |
| 219 | 0.3336 | 0.0066 | | | 0.0365 | 0.1345 | | | 0.4888 | | 1.093 | 8.2 | 4.1 |
| 220 | 0.0507 | 0.2825 | | | | 0.3131 | 0.0116 | 0.3420 | | | 1.163 | 6.7 | 7.3 |

| | | | | | | | | | | | | | |
|---|---|---|---|---|---|---|---|---|---|---|---|---|---|
| 221 | 0.0366 | | 0.2968 | | | | 0.3952 | | 0.2714 | | | 1.158 | 6.4 | 7.2 |
| 222 | 0.0187 | | 0.3153 | | | | 0.4674 | | 0.1983 | | 0.0003 | 1.154 | 6.2 | 7.0 |
| 223 | | 0.3159 | 0.0435 | 0.3235 | 0.3170 | | | | | | | 1.213 | 6.3 | 11.3 |
| 224 | | 0.1255 | 0.2197 | 0.1726 | 0.4821 | 0.0001 | | | | | | 1.187 | 6.4 | 9.4 |
| 225 | | 0.0098 | 0.3235 | 0.2822 | 0.3534 | | | 0.0310 | | | | 1.218 | 6.7 | 7.5 |
| 226 | | 0.0091 | 0.3243 | 0.2342 | 0.4323 | | | | | | | 1.213 | 6.6 | 7.5 |
| 227 | | 0.3168 | 0.0400 | 0.3299 | 0.3133 | | | | | | | 1.213 | 6.3 | 11.3 |
| 228 | | 0.1196 | 0.2242 | 0.1762 | 0.4800 | | | | | | | 1.213 | 6.4 | 9.3 |
| 229 | | 0.0001 | 0.3334 | 0.3785 | | | 0.2546 | 0.0334 | | | | 1.212 | 6.6 | 7.0 |
| 230 | | | 0.3334 | 0.3839 | | | 0.2826 | | | | | 1.153 | 6.4 | 6.9 |
| 231 | | 0.0002 | 0.3335 | 0.6024 | | | | 0.0638 | | | | 1.218 | 7.1 | 7.1 |
| 232 | | 0.1540 | 0.1854 | | 0.6178 | 0.0001 | 0.0428 | | | | | 1.184 | 6.1 | 9.8 |
| 233 | | 0.0026 | 0.3334 | | 0.5853 | 0.0002 | | 0.0785 | | | | 1.193 | 6.6 | 7.6 |
| 234 | | 0.1279 | 0.2115 | | 0.4178 | 0.0001 | | | 0.2427 | | | 1.193 | 6.7 | 9.6 |
| 235 | | 0.1341 | 0.2055 | | 0.6603 | 0.0001 | | | | | | 1.176 | 6.2 | 9.6 |
| 236 | | 0.2423 | 0.1047 | | 0.6529 | 0.0001 | | | | | | 1.176 | 6.1 | 10.8 |
| 237 | | 0.0050 | 0.3284 | | 0.4387 | | 0.1818 | 0.0461 | | | | 1.215 | 6.3 | 7.4 |
| 238 | | 0.0019 | 0.3315 | | 0.4548 | | 0.2117 | | | | | 1.209 | 6.1 | 7.3 |
| 239 | | 0.0542 | 0.2828 | | 0.5526 | | 0.1102 | | | | 0.0001 | 1.205 | 6.2 | 8.3 |
| 240 | | 0.0418 | 0.2916 | | 0.4081 | | | 0.0443 | 0.2142 | | | 1.225 | 6.9 | 8.4 |

| | | | | | | | | | | | | | | |
|---|---|---|---|---|---|---|---|---|---|---|---|---|---|---|
| 241 | | 0.0075 | 0.3263 | | 0.6285 | | | 0.0377 | | | | 1.223 | 6.4 | 7.6 |
| 242 | | 0.0017 | 0.3370 | | 0.5247 | | | 0.1363 | | | 0.0002 | 1.215 | 6.7 | 7.6 |
| 243 | | 0.0174 | 0.3163 | | 0.4223 | | | | 0.2441 | | | 1.223 | 6.8 | 7.9 |
| 244 | | 0.1159 | 0.2255 | | 0.3985 | | | | 0.2600 | | | 1.223 | 6.7 | 9.5 |
| 245 | | 0.0911 | 0.2506 | | 0.6583 | | | | | | | 1.218 | 6.2 | 9.0 |
| 246 | | 0.0017 | 0.3319 | | | | 0.3141 | | 0.3523 | | | 1.213 | 6.4 | 7.4 |
| 247 | 0.32871 | 0.0007 | 0.0034 | 0.3810 | | 0.2861 | | | | | | 1.153 | 6.4 | 5.9 |
| 248 | 0.16152 | 0.1717 | 0.0001 | 0.2901 | | | | 0.3765 | | | | 1.198 | 7.4 | 10.0 |
| 249 | 0.00915 | | 0.3247 | 0.5372 | | | | 0.1290 | | | | 1.163 | 7.2 | 7.2 |
| 250 | 0.02975 | 0.0002 | 0.3037 | 0.6664 | | | | | | | | 1.189 | 7.0 | 7.0 |
| 251 | 0.16645 | 0.0055 | 0.1627 | 0.6648 | | | | | | | 0.0006 | 1.184 | 6.8 | 7.0 |
| 252 | 0.05669 | 0.2420 | 0.0791 | | 0.6220 | 0.0002 | | | | | | 1.157 | 5.9 | 10.7 |
| 253 | 0.00024 | 0.0062 | 0.3258 | | 0.5953 | | | 0.0724 | | | | 1.203 | 6.5 | 7.6 |
| 254 | 0.0111 | 0.0710 | 0.2512 | | 0.6667 | | | | | | | 1.198 | 6.3 | 8.7 |
| 255 | 0.3333 | 0.0000 | 0.0003 | | 0.1210 | | | | | 0.5454 | | 1.140 | 8.7 | 4.3 |
| 256 | 0.0563 | 0.0660 | 0.2194 | | 0.6582 | | | | | | 0.0001 | 1.189 | 6.2 | 8.6 |
| 257 | 0.1252 | 0.2079 | 0.0002 | | | | 0.2827 | 0.3839 | | | | 1.194 | 6.9 | 10.3 |
| 258 | 0.3333 | | 0.0005 | | | | 0.0351 | | | 0.6311 | | 1.097 | 9.1 | 2.9 |
| 259 | 0.0443 | 0.1762 | 0.1367 | 0.1952 | 0.4474 | 0.0002 | | | | | | 1.168 | 6.3 | 10.0 |
| 260 | 0.0478 | 0.2401 | 0.0743 | 0.2553 | 0.3824 | 0.0002 | | | | | | 1.168 | 6.2 | 10.6 |

| | | | | | | | | | | | | | | |
|---|---|---|---|---|---|---|---|---|---|---|---|---|---|---|
| 261 | 0.1630 | 0.1705 | | 0.2959 | 0.0319 | | | 0.3388 | | | | 1.214 | 7.3 | 10.0 |
| 262 | 0.0170 | 0.0032 | 0.3128 | 0.0889 | 0.5679 | | | 0.0102 | | | | 1.198 | 6.4 | 7.4 |
| 263 | 0.0460 | 0.0336 | 0.2538 | 0.2219 | 0.4447 | | | | | | | 1.194 | 6.5 | 7.9 |
| 264 | 0.0616 | 0.0756 | 0.2066 | 0.2551 | 0.4010 | | | | | | 0.0001 | 1.189 | 6.4 | 8.6 |
| 265 | 0.3307 | 0.0001 | 0.0039 | 0.3821 | | 0.2758 | 0.0074 | | | | | 1.162 | 5.8 | 6.0 |
| 266 | 0.1616 | 0.1718 | 0.0001 | 0.3545 | | 0.0001 | | 0.3118 | | | | 1.171 | 7.3 | 10.0 |
| 267 | 0.3334 | | 0.0038 | 0.1668 | | 0.0755 | | | | 0.4205 | | 1.096 | 8.1 | 4.7 |
| 268 | 0.3277 | 0.0006 | 0.0030 | 0.3870 | | 0.2808 | | | | | 0.0008 | 1.162 | 5.8 | 5.9 |
| 269 | 0.1650 | 0.1683 | 0.0001 | 0.2116 | | | 0.1271 | 0.3279 | | | | 1.192 | 7.1 | 9.9 |
| 270 | 0.0066 | | 0.3266 | 0.2431 | | | 0.4068 | 0.0169 | | | | 1.157 | 6.2 | 6.8 |
| 271 | 0.0189 | 0.0002 | 0.3143 | 0.3697 | | | 0.2969 | | | | | 1.184 | 6.4 | 6.9 |
| 272 | 0.0410 | 0.0002 | 0.2926 | 0.3370 | | | 0.3290 | | | | 0.0002 | 1.183 | 6.3 | 6.8 |
| 273 | 0.1555 | 0.1778 | | 0.2569 | | | | 0.3649 | 0.0449 | | | 1.218 | 7.4 | 10.1 |
| 274 | 0.1546 | 0.1788 | 0.0001 | 0.3355 | | | | 0.3310 | | | | 1.198 | 7.3 | 10.1 |
| 275 | 0.1561 | 0.1772 | 0.0001 | 0.3106 | | | | 0.3560 | | | | 1.198 | 7.4 | 10.1 |
| 276 | 0.0930 | 0.0694 | 0.1962 | | 0.5553 | 0.0006 | 0.0856 | | | | | 1.165 | 6.0 | 8.5 |
| 277 | 0.0019 | 0.0031 | 0.3301 | | 0.6580 | 0.0002 | | 0.0067 | | | | 1.174 | 6.3 | 7.5 |
| 278 | 0.0022 | 0.0693 | 0.2648 | | 0.5937 | 0.0001 | | | 0.0698 | | | 1.174 | 6.4 | 8.7 |
| 279 | 0.3335 | 0.0007 | 0.0125 | | 0.1358 | 0.0451 | | | | 0.4724 | | 1.133 | 8.2 | 4.6 |
| 280 | 0.0207 | 0.1011 | 0.2221 | | 0.6560 | 0.0002 | | | | | | 1.157 | 6.2 | 9.1 |

| | | | | | | | | | | | | | | |
|---|---|---|---|---|---|---|---|---|---|---|---|---|---|---|
| 281 | 0.0375 | 0.0472 | 0.2603 | | 0.6546 | 0.0003 | | | | | 0.0001 | 1.165 | 6.2 | 8.3 |
| 282 | 0.0045 | 0.0035 | 0.3253 | | 0.4216 | | 0.2375 | 0.0076 | | | | 1.195 | 6.1 | 7.3 |
| 283 | 0.0239 | 0.0108 | 0.2987 | | 0.4899 | | 0.1768 | | | | | 1.189 | 6.1 | 7.4 |
| 284 | 0.3333 | | 0.0002 | | 0.1306 | | 0.0465 | | | 0.4894 | | 1.118 | 8.4 | 4.8 |
| 285 | 0.0873 | 0.0204 | 0.2266 | | 0.4823 | | 0.1830 | | | | 0.0003 | 1.186 | 6.0 | 7.6 |
| 286 | 0.0023 | 0.0200 | 0.3111 | | 0.3076 | | | 0.0346 | 0.3245 | | | 1.205 | 7.1 | 8.0 |
| 287 | 0.0008 | 0.0093 | 0.3233 | | 0.6563 | | | 0.0103 | | | | 1.203 | 6.4 | 7.6 |
| 288 | 0.0001 | 0.0009 | 0.3324 | | 0.6051 | | | 0.0613 | | | 0.0001 | 1.195 | 6.5 | 7.5 |
| 289 | 0.0142 | 0.0522 | 0.2670 | | 0.4848 | | | | 0.1819 | | | 1.203 | 6.6 | 8.5 |
| 290 | 0.0095 | 0.0712 | 0.2527 | | 0.4966 | | | | 0.1699 | | | 1.203 | 6.6 | 8.8 |
| 291 | 0.0151 | 0.0756 | 0.2576 | | 0.6516 | | | | | | 0.0001 | 1.189 | 6.2 | 8.8 |
| 292 | 0.0294 | 0.0021 | 0.3016 | | | | 0.2444 | 0.0140 | 0.4085 | | | 1.198 | 6.9 | 7.5 |
| 293 | 0.0634 | 0.0017 | 0.2682 | | | | 0.3340 | | 0.3326 | | | 1.194 | 6.6 | 7.3 |
| 294 | 0.0282 | 0.0010 | 0.3045 | | | | 0.3833 | | 0.2829 | | 0.0002 | 1.189 | 6.5 | 7.2 |
| 295 | 0.0918 | 0.2537 | | 0.0984 | 0.5330 | 0.0003 | 0.0228 | | | | | 1.186 | 6.0 | 10.8 |
| 296 | 0.1209 | 0.2168 | | 0.2728 | 0.3334 | 0.0006 | | 0.0554 | | | | 1.193 | 6.4 | 10.4 |
| 297 | 0.3318 | 0.0002 | | 0.3573 | 0.0455 | 0.2651 | | 0.0001 | | | | 1.193 | 5.8 | 6.0 |
| 298 | 0.0266 | 0.3086 | | 0.2874 | 0.3502 | 0.0001 | | | 0.0270 | | | 1.193 | 6.3 | 11.3 |
| 299 | 0.0259 | 0.3096 | | 0.1602 | 0.5042 | 0.0001 | | | | | | 1.183 | 6.2 | 11.4 |
| 300 | 0.0487 | 0.2872 | | 0.2294 | 0.4345 | 0.0001 | | | | | | 1.183 | 6.2 | 11.1 |

| | | | | | | | | | | | | | |
|---|---|---|---|---|---|---|---|---|---|---|---|---|---|
| 301 | 0.3317 | 0.0003 | 0.3479 | 0.0377 | 0.2809 | | | | | 0.0015 | 1.186 | 5.8 | 6.0 |
| 302 | 0.3333 | | 0.1606 | 0.2535 | | 0.0254 | | | 0.2272 | | 1.123 | 7.3 | 6.4 |
| 303 | 0.2319 | 0.1025 | 0.1801 | 0.4147 | | 0.0692 | | | | 0.0015 | 1.202 | 6.1 | 8.8 |
| 304 | 0.1375 | 0.1958 | 0.3120 | 0.0614 | | | 0.1901 | 0.1032 | | | 1.217 | 7.1 | 10.3 |
| 305 | 0.1362 | 0.1973 | 0.2779 | 0.1956 | | | 0.1929 | | 0.0001 | | 1.184 | 6.9 | 10.2 |
| 306 | 0.1555 | 0.1779 | 0.3056 | 0.2492 | | | 0.1116 | | | 0.0001 | 1.209 | 6.6 | 9.9 |
| 307 | 0.1005 | 0.2328 | 0.2356 | 0.2865 | | | | 0.1446 | | | 1.214 | 6.5 | 10.6 |
| 308 | 0.3333 | | 0.1422 | 0.1257 | | | | 0.1061 | 0.2927 | | 1.130 | 7.8 | 6.2 |
| 309 | 0.1053 | 0.2281 | 0.2898 | 0.2799 | | | | 0.0969 | | | 1.214 | 6.5 | 10.5 |
| 310 | 0.0427 | 0.2914 | 0.2393 | 0.4265 | | | | | | | 1.209 | 6.2 | 11.1 |
| 311 | 0.1763 | 0.1600 | 0.4067 | | 0.0011 | 0.0659 | 0.1901 | | | | 1.188 | 6.9 | 9.6 |
| 312 | 0.3295 | | 0.4107 | | 0.2504 | 0.0091 | 0.0003 | | | | 1.134 | 5.9 | 6.0 |
| 313 | 0.3305 | 0.0001 | 0.3480 | | 0.3120 | 0.0074 | | | | 0.0019 | 1.181 | 5.7 | 5.8 |
| 314 | 0.1367 | 0.1966 | 0.3636 | | | | 0.2172 | 0.0858 | | | 1.218 | 7.2 | 10.2 |
| 315 | 0.1663 | 0.1673 | 0.4501 | | 0.0005 | | 0.2156 | | 0.0001 | | 1.163 | 7.1 | 9.8 |
| 316 | 0.3333 | | 0.2129 | | 0.0588 | | | | 0.3949 | | 1.092 | 8.1 | 5.0 |
| 317 | 0.1709 | 0.1630 | 0.5153 | | 0.0015 | | 0.1492 | | | 0.0001 | 1.188 | 7.0 | 9.6 |
| 318 | 0.3204 | 0.0001 | 0.4367 | | 0.2417 | | 0.0001 | | | 0.0009 | 1.188 | 6.0 | 6.1 |
| 319 | 0.1700 | 0.1634 | 0.2813 | | | 0.1340 | 0.2512 | | 0.0001 | | 1.179 | 6.9 | 9.7 |
| 320 | 0.1908 | 0.1427 | 0.3367 | | | 0.1523 | 0.1775 | | | 0.0001 | 1.205 | 6.7 | 9.3 |

| | | | | | | | | | | | | | |
|---|---|---|---|---|---|---|---|---|---|---|---|---|---|
| 321 | 0.1543 | 0.1790 | 0.3944 | | | | 0.1931 | 0.0791 | | | 1.218 | 7.1 | 10.0 |
| 322 | 0.1394 | 0.1939 | 0.3330 | | | | 0.2018 | 0.1319 | | | 1.218 | 7.2 | 10.3 |
| 323 | 0.1639 | 0.1699 | 0.4983 | | | | 0.1678 | | 0.0001 | | 1.174 | 7.0 | 9.8 |
| 324 | 0.2010 | 0.1378 | | 0.5866 | 0.0017 | 0.0690 | 0.0040 | | | | 1.191 | 5.9 | 9.4 |
| 325 | 0.3397 | 0.3153 | | 0.0025 | | 0.0180 | 0.3245 | | | | 1.211 | 6.0 | 10.0 |
| 326 | 0.0492 | 0.2896 | | 0.6260 | 0.0001 | 0.0210 | | 0.0142 | | | 1.191 | 6.0 | 11.2 |
| 327 | 0.1045 | 0.2371 | | 0.6356 | 0.0003 | 0.0225 | | | | | 1.180 | 6.0 | 10.7 |
| 328 | 0.1451 | 0.1950 | | 0.6152 | 0.0006 | 0.0440 | | | | 0.0002 | 1.184 | 5.9 | 10.2 |
| 329 | 0.0263 | 0.3058 | | 0.6642 | | | 0.0036 | | | | 1.219 | 6.0 | 11.4 |
| 330 | 0.0962 | 0.2365 | | 0.6646 | 0.0001 | | 0.0027 | | | 0.0001 | 1.191 | 6.0 | 10.7 |
| 331 | 0.0106 | 0.3234 | | 0.6214 | | | | 0.0446 | | | 1.219 | 6.1 | 11.6 |
| 332 | 0.0252 | 0.3107 | | 0.6417 | 0.0001 | | | 0.0223 | | | 1.189 | 6.0 | 11.5 |
| 333 | 0.0167 | 0.3228 | | 0.6604 | 0.0001 | | | | | | 1.172 | 6.0 | 11.6 |
| 334 | 0.0884 | 0.2428 | | 0.6291 | | 0.0193 | 0.0204 | | | | 1.211 | 6.0 | 10.8 |
| 335 | 0.3333 | | | 0.2934 | | 0.0171 | 0.0000 | | 0.3562 | | 1.127 | 7.8 | 5.9 |
| 336 | 0.0557 | 0.2764 | | 0.5889 | | 0.0111 | | 0.0679 | | | 1.211 | 6.1 | 11.2 |
| 337 | 0.1265 | 0.2064 | | 0.5833 | | 0.0445 | | 0.0392 | | 0.0001 | 1.207 | 6.0 | 10.4 |
| 338 | 0.1172 | 0.2181 | | 0.6308 | | 0.0339 | | | | 0.0001 | 1.168 | 6.0 | 10.5 |
| 339 | 0.0679 | 0.2589 | | 0.6640 | | | 0.0092 | | | | 1.219 | 6.0 | 11.0 |
| 340 | 0.0168 | 0.3168 | | 0.6122 | | | | 0.0543 | | | 1.219 | 6.1 | 11.6 |

| | | | | | | | | | | | | | |
|---|---|---|---|---|---|---|---|---|---|---|---|---|---|
| 341 | 0.0610 | 0.2778 | 0.1128 | 0.2986 | 0.0006 | 0.2493 | | | | | 1.136 | 6.1 | 7.1 |
| 342 | 0.0429 | 0.2942 | 0.2183 | 0.4383 | 0.0004 | | 0.0059 | | | | 1.142 | 6.5 | 7.3 |
| 343 | 0.3300 | 0.0017 | 0.3912 | 0.0292 | 0.2457 | | 0.0022 | | | | 1.142 | 5.9 | 6.1 |
| 344 | 0.0144 | 0.3216 | 0.2407 | 0.3669 | 0.0002 | | | 0.0563 | | | 1.142 | 6.7 | 7.3 |
| 345 | 0.3334 | 0.0062 | 0.1268 | 0.0475 | 0.0550 | | | | 0.4310 | | 1.112 | 8.2 | 4.8 |
| 346 | 0.0122 | 0.3292 | 0.2172 | 0.4412 | 0.0002 | | | | | | 1.133 | 6.5 | 7.3 |
| 347 | 0.3303 | 0.0037 | 0.3809 | 0.0218 | 0.2602 | | | | | 0.0031 | 1.136 | 5.9 | 6.0 |
| 348 | 0.0348 | 0.3100 | 0.2402 | 0.4143 | 0.0004 | | | | | 0.0003 | 1.136 | 6.5 | 7.3 |
| 349 | 0.1344 | 0.1989 | 0.2511 | 0.2088 | | 0.1960 | 0.0107 | | | | 1.158 | 6.3 | 7.0 |
| 350 | 0.0456 | 0.2878 | 0.1938 | 0.2274 | | 0.2455 | | | | | 1.154 | 6.2 | 7.0 |
| 351 | 0.3333 | 0.0001 | 0.1296 | 0.0830 | | 0.0575 | | | 0.3966 | | 1.127 | 8.1 | 5.4 |
| 352 | 0.0989 | 0.2347 | 0.1995 | 0.2318 | | 0.2347 | | | | 0.0004 | 1.151 | 6.2 | 7.0 |
| 353 | 0.0497 | 0.2836 | 0.2851 | 0.2044 | | | 0.0201 | 0.1570 | | | 1.165 | 6.9 | 7.3 |
| 354 | 0.0153 | 0.3186 | 0.3185 | 0.3261 | | | 0.0216 | | | | 1.163 | 6.7 | 7.3 |
| 355 | 0.0311 | 0.3026 | 0.3268 | 0.3225 | | | 0.0170 | | | 0.0001 | 1.158 | 6.7 | 7.2 |
| 356 | 0.0361 | 0.2972 | 0.2315 | 0.2709 | | | | 0.1642 | | | 1.163 | 6.9 | 7.4 |
| 357 | 0.0174 | 0.3178 | 0.2719 | 0.3304 | | | | 0.0622 | | 0.0002 | 1.158 | 6.7 | 7.3 |
| 358 | 0.0210 | 0.3289 | 0.1923 | 0.4576 | | | | | | 0.0002 | 1.154 | 6.5 | 7.4 |
| 359 | 0.0309 | 0.3029 | 0.3565 | | 0.0002 | 0.3017 | 0.0079 | | | | 1.138 | 6.4 | 6.9 |
| 360 | 0.0106 | 0.3237 | 0.2684 | | 0.0001 | 0.3380 | | 0.0592 | | | 1.138 | 6.4 | 6.9 |

| | | | | | | | | | | | | | |
|---|---|---|---|---|---|---|---|---|---|---|---|---|---|
| 361 | 0.3334 | 0.0064 | 0.0985 | | 0.0405 | 0.0242 | | | 0.4971 | | 1.108 | 8.5 | 4.2 |
| 362 | 0.0055 | 0.3292 | 0.3025 | | 0.0001 | 0.3627 | | | 0.0000 | | 1.108 | 6.3 | 6.8 |
| 363 | 0.3320 | 0.0044 | 0.3777 | | 0.2690 | 0.0141 | | | | 0.0027 | 1.131 | 5.8 | 6.0 |
| 364 | 0.0219 | 0.3131 | 0.3005 | | 0.0002 | 0.3641 | | | | 0.0001 | 1.131 | 6.2 | 6.8 |
| 365 | 0.0185 | 0.3152 | 0.3289 | | 0.0000 | | 0.0391 | 0.2984 | | | 1.145 | 7.4 | 7.5 |
| 366 | 0.0602 | 0.2729 | 0.2841 | | | 0.1844 | 0.0205 | 0.1778 | | | 1.160 | 6.8 | 7.2 |
| 367 | 0.0117 | 0.3217 | 0.3208 | | | 0.3312 | 0.0146 | | | | 1.157 | 6.4 | 6.9 |
| 368 | 0.0207 | 0.3126 | 0.3255 | | | 0.3255 | 0.0156 | | | | 1.157 | 6.4 | 6.9 |
| 369 | 0.0444 | 0.2889 | 0.2319 | | | 0.2547 | | 0.1801 | | | 1.157 | 6.6 | 7.1 |
| 370 | 0.0124 | 0.3216 | 0.2774 | | | 0.3217 | | 0.0667 | | 0.0002 | 1.154 | 6.4 | 7.0 |
| 371 | 0.0104 | 0.3247 | 0.2813 | | | 0.3835 | | | | 0.0001 | 1.148 | 6.2 | 6.8 |
| 372 | 0.0215 | 0.3121 | 0.3864 | | | | 0.0328 | 0.2472 | | | 1.166 | 7.3 | 7.4 |
| 373 | 0.0204 | 0.3133 | 0.3830 | | | | 0.0430 | 0.2402 | | 0.0001 | 1.160 | 7.3 | 7.4 |
| 374 | 0.0444 | 0.2912 | | 0.4200 | 0.0003 | 0.2416 | 0.0026 | | | | 1.140 | 6.1 | 7.2 |
| 375 | 0.0100 | 0.3249 | | 0.3679 | 0.0002 | 0.2606 | | 0.0363 | | | 1.140 | 6.1 | 7.2 |
| 376 | 0.3339 | 0.0121 | | 0.1150 | 0.0458 | 0.0737 | | | 0.4196 | | 1.110 | 7.9 | 4.9 |
| 377 | 0.0316 | 0.3049 | | 0.3777 | 0.0003 | 0.2855 | | | | | 1.130 | 6.0 | 7.1 |
| 378 | 0.0163 | 0.3193 | | 0.3985 | 0.0002 | 0.2655 | | | | 0.0002 | 1.133 | 6.0 | 7.1 |
| 379 | 0.0015 | 0.3321 | | 0.4011 | 0.0001 | | 0.0355 | 0.2298 | | | 1.147 | 6.9 | 7.6 |
| 380 | 0.0018 | 0.3331 | | 0.6534 | 0.0002 | | 0.0115 | | | | 1.139 | 6.4 | 7.5 |

| | | | | | | | | | | | | | |
|---|---|---|---|---|---|---|---|---|---|---|---|---|---|
| 381 | 0.0024 | | 0.3332 | | 0.5042 | 0.0002 | | | 0.1600 | | | 1.139 | 6.6 | 7.5 |
| 382 | 0.0047 | | 0.3333 | | 0.6030 | 0.0002 | | | 0.0585 | | 0.0003 | 1.140 | 6.4 | 7.5 |
| 383 | 0.0242 | | 0.3194 | | 0.6560 | 0.0003 | | | | | 0.0002 | 1.130 | 6.3 | 7.5 |
| 384 | 0.0123 | | 0.3210 | | 0.1929 | | 0.2028 | 0.0257 | 0.2453 | | | 1.163 | 6.7 | 7.4 |
| 385 | 0.0065 | | 0.3269 | | 0.3250 | | 0.3251 | 0.0166 | | | | 1.160 | 6.1 | 7.1 |
| 386 | 0.0081 | | 0.3252 | | 0.3342 | | 0.3176 | 0.0148 | | | | 1.160 | 6.1 | 7.1 |
| 387 | 0.0265 | | 0.3068 | | 0.2738 | | 0.2417 | | 0.1512 | | | 1.160 | 6.4 | 7.3 |
| 388 | 0.0233 | | 0.3102 | | 0.2953 | | 0.3102 | | 0.0609 | | 0.0002 | 1.156 | 6.1 | 7.1 |
| 389 | 0.0144 | | 0.3208 | | 0.3277 | | 0.3370 | | | | 0.0002 | 1.151 | 6.0 | 7.1 |
| 390 | 0.0013 | | 0.3323 | | 0.4000 | | | 0.0345 | 0.2319 | | | 1.169 | 6.9 | 7.6 |
| 391 | 0.0015 | | 0.3320 | | 0.3808 | | | 0.0406 | 0.2450 | | 0.0001 | 1.163 | 6.9 | 7.6 |
| 392 | 0.0035 | | 0.3307 | | 0.6532 | | | 0.0126 | | | | 1.167 | 6.4 | 7.5 |
| 393 | 0.0022 | | 0.3395 | | 0.5284 | | | | 0.1298 | 0.0000 | 0.0001 | 1.131 | 6.6 | 7.6 |
| 394 | 0.0249 | | 0.3085 | | | 0.0000 | 0.2156 | 0.0130 | 0.4380 | | | 1.142 | 7.0 | 7.5 |
| 395 | 0.0137 | | 0.3204 | | | 0.0001 | 0.4031 | | 0.2626 | | | 1.133 | 6.4 | 7.2 |
| 396 | 0.0197 | | 0.3141 | | | 0.0001 | 0.4755 | | 0.1902 | | 0.0003 | 1.136 | 6.2 | 7.0 |
| 397 | 0.0146 | | 0.3188 | | | | 0.3643 | 0.0136 | 0.2887 | | | 1.163 | 6.6 | 7.2 |
| 398 | 0.0165 | | 0.3168 | | | | 0.3928 | 0.0170 | 0.2569 | | 0.0001 | 1.158 | 6.5 | 7.2 |
| 399 | 0.0109 | | 0.3230 | | | | 0.4936 | | 0.1725 | | 0.0001 | 1.154 | 6.2 | 7.0 |
| 400 | | 0.0840 | 0.2560 | 0.1266 | 0.4845 | 0.0001 | 0.0487 | | | | | 1.190 | 6.3 | 8.8 |

| | | | | | | | | | | | | |
|---|---|---|---|---|---|---|---|---|---|---|---|---|
| 401 | 0.0063 | 0.3292 | 0.2781 | 0.3807 | 0.0001 | | 0.0056 | | | 1.197 | 6.6 | 7.4 |
| 402 | 0.2666 | 0.0772 | 0.1649 | 0.2895 | | | | 0.2017 | | 1.218 | 6.6 | 11.1 |
| 403 | 0.0554 | 0.2860 | 0.1475 | 0.5110 | 0.0002 | | | | | 1.187 | 6.4 | 8.4 |
| 404 | 0.3152 | 0.0463 | 0.3189 | 0.3196 | | | | | | 1.213 | 6.3 | 11.2 |
| 405 | 0.1298 | 0.2165 | 0.1702 | 0.4833 | 0.0001 | | | | | 1.187 | 6.3 | 9.4 |
| 406 | 0.0056 | 0.3278 | 0.2177 | 0.3289 | | 0.1045 | 0.0155 | | | 1.213 | 6.5 | 7.3 |
| 407 | 0.0030 | 0.3304 | 0.2122 | 0.3300 | | 0.1245 | | | | 1.209 | 6.4 | 7.2 |
| 408 | 0.0374 | 0.3041 | 0.1675 | 0.4112 | | 0.0797 | | | 0.0001 | 1.206 | 6.4 | 8.0 |
| 409 | 0.0170 | 0.3164 | 0.1819 | 0.3389 | | | 0.0285 | 0.1174 | | 1.221 | 6.8 | 7.8 |
| 410 | 0.3343 | 0.0009 | 0.2806 | 0.3335 | | | 0.0507 | | | 1.218 | 6.4 | 11.5 |
| 411 | 0.0038 | 0.3296 | 0.3296 | 0.3133 | | | 0.0237 | | | 1.218 | 6.7 | 7.3 |
| 412 | 0.0097 | 0.3237 | 0.2039 | 0.3234 | | | | 0.1394 | | 1.218 | 6.8 | 7.6 |
| 413 | 0.1924 | 0.1435 | 0.1566 | 0.2909 | | | | 0.2166 | | 1.218 | 6.7 | 10.3 |
| 414 | 0.0705 | 0.2777 | 0.1517 | 0.5001 | | | | | 0.0001 | 1.209 | 6.4 | 8.6 |
| 415 | 0.0001 | 0.3341 | 0.3171 | | 0.0001 | 0.3369 | 0.0117 | | | 1.192 | 6.3 | 6.9 |
| 416 | 0.0006 | 0.3330 | 0.2726 | | | 0.1982 | 0.0239 | 0.1717 | | 1.216 | 6.8 | 7.2 |
| 417 | 0.0001 | 0.3339 | 0.3543 | | | 0.2616 | 0.0502 | | | 1.212 | 6.6 | 7.0 |
| 418 | 0.0001 | 0.3334 | 0.3280 | | | 0.3046 | 0.0338 | | 0.0001 | 1.209 | 6.5 | 6.9 |
| 419 | 0.0005 | 0.3329 | 0.2599 | | | 0.2107 | | 0.1960 | | 1.212 | 6.8 | 7.2 |
| 420 | 0.0045 | 0.3299 | | 0.4024 | 0.0002 | 0.2541 | 0.0089 | | | 1.195 | 6.1 | 7.3 |

| | | | | | | | | | | | |
|---|---|---|---|---|---|---|---|---|---|---|---|
| 421 | 0.1002 | 0.2379 | 0.4569 | 0.0001 | 0.0573 | | 0.1476 | | 1.195 | 6.5 | 9.1 |
| 422 | 0.0272 | 0.3087 | 0.5834 | 0.0002 | 0.0806 | | | | 1.184 | 6.2 | 7.9 |
| 423 | 0.1427 | 0.1963 | 0.6140 | 0.0001 | 0.0468 | | | | 1.184 | 6.1 | 9.6 |
| 424 | 0.0270 | 0.3084 | 0.3570 | 0.0001 | | 0.0152 | 0.2922 | | 1.202 | 6.9 | 8.1 |
| 425 | 0.0087 | 0.3263 | 0.6464 | 0.0002 | | 0.0184 | | | 1.193 | 6.4 | 7.6 |
| 426 | 0.0024 | 0.3349 | 0.5921 | 0.0002 | | 0.0702 | | 0.0002 | 1.195 | 6.5 | 7.5 |
| 427 | 0.0619 | 0.2773 | 0.4918 | 0.0002 | | | 0.1689 | | 1.193 | 6.6 | 8.6 |
| 428 | 0.1207 | 0.2199 | 0.4150 | 0.0001 | | | 0.2443 | | 1.193 | 6.7 | 9.5 |
| 429 | 0.1578 | 0.1833 | 0.6588 | 0.0001 | | | | | 1.176 | 6.2 | 9.9 |
| 430 | 0.0167 | 0.3167 | 0.3196 | | 0.1332 | 0.0195 | 0.1943 | | 1.218 | 6.6 | 7.8 |
| 431 | 0.0020 | 0.3320 | 0.4017 | | 0.1901 | 0.0742 | | | 1.215 | 6.4 | 7.3 |
| 432 | 0.0026 | 0.3309 | 0.3367 | | 0.2780 | 0.0518 | | 0.0001 | 1.211 | 6.2 | 7.2 |
| 433 | 0.0085 | 0.3248 | 0.3245 | | 0.1555 | | 0.1866 | | 1.215 | 6.5 | 7.6 |
| 434 | 0.0560 | 0.2827 | 0.3932 | | 0.1010 | | 0.1670 | 0.0001 | 1.211 | 6.5 | 8.5 |
| 435 | 0.0189 | 0.3173 | 0.5378 | | 0.1259 | | | 0.0001 | 1.205 | 6.2 | 7.7 |
| 436 | 0.0098 | 0.3253 | 0.3980 | | | 0.0391 | 0.2278 | | 1.225 | 6.9 | 7.8 |
| 437 | 0.0199 | 0.3141 | 0.3141 | | | 0.0376 | 0.3141 | 0.0001 | 1.218 | 7.1 | 8.0 |
| 438 | 0.0031 | 0.3362 | 0.6208 | | | 0.0398 | | 0.0001 | 1.215 | 6.4 | 7.6 |
| 439 | 0.1022 | 0.2431 | 0.4456 | | | | 0.2091 | 0.0001 | 1.215 | 6.6 | 9.3 |
| 440 | 0.0019 | 0.3320 | | | 0.3100 | 0.0300 | 0.3261 | | 1.218 | 6.8 | 7.4 |

Table A2 – Equiatomic compositions predicted to form C15 Laves phase by CALPHAD calculations. For each composition, the atomic fraction of the elements and their $r_A/r_B$, VEC, and δ parameter are presented.

| Concentration atomic fraction | | | | | | | | | | | $r_A/r_B$ | VEC | δ |
|---|---|---|---|---|---|---|---|---|---|---|---|---|---|
| **Ti** | **Zr** | **Nb** | **Fe** | **Mn** | **V** | **Cr** | **Ni** | **Co** | **Zn** | **Cu** | | | |
| | 0.3333 | | 0.6667 | | | | | | | | 1.260 | 6.7 | 11.3 |
| | 0.3333 | | | | | | | 0.6667 | | | 1.280 | 7.3 | 12.1 |
| | 0.3333 | | | | | | | | 0.6667 | | 1.151 | 9.3 | 6.8 |
| | | 0.3333 | | | | | | 0.6667 | | | 1.176 | 7.7 | 7.8 |
| 0.1667 | 0.1667 | | | | | | | 0.6667 | | | 1.224 | 7.3 | 10.3 |
| 0.1667 | | 0.1667 | | | | | | 0.6667 | | | 1.172 | 7.5 | 7.7 |
| 0.1667 | | 0.1667 | 0.6667 | | | | | | | | 1.209 | 6.8 | 9.6 |
| | 0.1667 | 0.1667 | | | | | | 0.6667 | | | 1.228 | 7.5 | 10.4 |
| 0.3333 | | | | | | 0.3333 | | 0.3333 | | | 1.154 | 6.3 | 7.0 |
| | 0.3333 | | 0.3333 | | 0.3333 | | | | | | 1.221 | 5.7 | 10.0 |
| | 0.3333 | | 0.3333 | | | 0.3333 | | | | | 1.255 | 6.0 | 11.1 |
| | 0.3333 | | 0.3333 | | | | 0.3333 | | | | 1.270 | 7.3 | 11.7 |
| | 0.3333 | | 0.3333 | | | | | 0.3333 | | | 1.270 | 7.0 | 11.7 |
| | 0.3333 | | 0.3333 | | | | | | 0.3333 | | 1.203 | 8.0 | 9.6 |
| | 0.3333 | | | | 0.3333 | 0.3333 | | | | | 1.217 | 5.0 | 9.7 |
| | 0.3333 | | | | 0.3333 | | | | 0.3333 | | 1.168 | 7.0 | 7.6 |

| | | | | | | | | | | | | |
|---|---|---|---|---|---|---|---|---|---|---|---|---|
| | 0.3333 | | | | | 0.3333 | | 0.3333 | | 1.265 | 6.3 | 11.5 |
| | 0.3333 | | | | | 0.3333 | | | 0.3333 | 1.199 | 7.3 | 9.3 |
| | 0.3333 | | | | | | 0.3333 | 0.3333 | | 1.280 | 7.7 | 12.1 |
| | | 0.3333 | | | | | 0.3333 | 0.3333 | | 1.176 | 8.0 | 7.8 |
| 0.1667 | 0.1667 | | 0.3333 | | | | | 0.3333 | | 1.214 | 7.0 | 9.9 |
| 0.1667 | 0.1667 | | | | | 0.3333 | | 0.3333 | | 1.209 | 6.3 | 9.7 |
| | 0.1667 | 0.1667 | | 0.3333 | | 0.3333 | | | | 1.204 | 6.2 | 9.4 |
| | 0.1667 | 0.1667 | | 0.3333 | | | | 0.3333 | | 1.218 | 7.2 | 10.0 |
| | 0.1667 | 0.1667 | | | | | 0.3333 | 0.3333 | | 1.228 | 7.8 | 10.4 |
| 0.1111 | 0.1111 | 0.1111 | | | | | | 0.6667 | | 1.208 | 7.4 | 9.6 |
| | 0.3333 | | 0.2222 | | 0.2222 | 0.2222 | | | | 1.231 | 5.6 | 10.3 |
| | 0.3333 | | 0.2222 | | 0.2222 | | | 0.2222 | | 1.240 | 6.2 | 10.8 |
| | 0.3333 | | 0.2222 | | 0.2222 | | | | 0.2222 | 1.197 | 6.9 | 9.2 |
| | 0.3333 | | 0.2222 | | | 0.2222 | | 0.2222 | | 1.263 | 6.4 | 11.4 |
| | 0.3333 | | 0.2222 | | | 0.2222 | | | 0.2222 | 1.218 | 7.1 | 10.1 |
| | 0.3333 | | 0.2222 | | | | 0.2222 | 0.2222 | | 1.273 | 7.3 | 11.8 |
| | 0.3333 | | 0.2222 | | | | 0.2222 | | 0.2222 | 1.228 | 8.0 | 10.6 |
| | 0.3333 | | 0.2222 | | | | | 0.2222 | 0.2222 | 1.228 | 7.8 | 10.6 |
| | 0.3333 | | | | 0.2222 | 0.2222 | | | 0.2222 | 1.194 | 6.4 | 9.0 |
| | 0.3333 | | | | | 0.2222 | | 0.2222 | 0.2222 | 1.224 | 7.3 | 10.4 |

| | | | | | | | | | | | |
|---|---|---|---|---|---|---|---|---|---|---|---|
| | 0.3333 | | | | | 0.2222 | 0.2222 | 0.2222 | 1.234 | 8.2 | 10.9 |
| 0.1667 | 0.1667 | | 0.2222 | | 0.2222 | | 0.2222 | | 1.208 | 6.4 | 9.7 |
| | 0.1667 | 0.1667 | 0.2222 | | 0.2222 | | 0.2222 | | 1.212 | 6.6 | 9.8 |
| | 0.1667 | 0.1667 | 0.2222 | | | 0.2222 | 0.2222 | | 1.221 | 7.5 | 10.1 |
| 0.1111 | 0.1111 | 0.1111 | 0.3333 | | | | 0.3333 | | 1.198 | 7.1 | 9.2 |

Table A3 **–** Equiatomic compositions predicted to form BCC phase by CALPHAD calculations. For each composition, the atomic fraction of the elements and their $r_A/r_B$, VEC, and δ parameter are presented.

| **Concentration atomic fraction** | | | | | | | | | | | $r_A/r_B$ | **VEC** | **δ** |
|---|---|---|---|---|---|---|---|---|---|---|---|---|---|
| **Ti** | **Zr** | **Nb** | **Fe** | **Mn** | **V** | **Cr** | **Ni** | **Co** | **Zn** | **Cu** | | | |
| **0.3333** | | | | | 0.6667 | | | | | | 1.081 | 4.7 | 3.7 |
| | | 0.3333 | | | 0.6667 | | | | | | 1.089 | 5.0 | 4.1 |
| **0.1667** | | 0.1667 | | | 0.6667 | | | | | | 1.085 | 4.8 | 3.9 |
| **0.3333** | | | | 0.3333 | 0.3333 | | | | | | 1.119 | 5.3 | 6.0 |
| **0.3333** | | | | | 0.3333 | 0.3333 | | | | | 1.110 | 5.0 | 5.4 |
| **0.3333** | | | | | | | | | 0.3333 | 0.3333 | 1.094 | 9.0 | 5.4 |
| | | 0.3333 | | 0.3333 | 0.3333 | | | | | | 1.126 | 5.7 | 6.3 |
| | | 0.3333 | | | 0.3333 | 0.3333 | | | | | 1.118 | 5.3 | 5.7 |
| **0.1667** | 0.1667 | | | | | | | | 0.3333 | 0.3333 | 1.146 | 9.0 | 7.9 |
| **0.1667** | | 0.1667 | | 0.3333 | 0.3333 | | | | | | 1.123 | 5.5 | 6.2 |

| | | | | | | | | | | |
|---|---|---|---|---|---|---|---|---|---|---|
| **0.1667** | | 0.1667 | | | 0.3333 | 0.3333 | | | 1.114 | 5.2 | 5.6 |
| **0.1111** | 0.1111 | 0.1111 | | | 0.6667 | | | | 1.119 | 4.8 | 6.0 |
| **0.3333** | | | | 0.2222 | 0.2222 | 0.2222 | | | 1.126 | 5.3 | 6.2 |

**Table A4:** Atomic fraction of element $i$ in the sublattice A and sublattice B for each one of the 354 non-equiatomic alloys with tendency to form single C14 Laves phase. For each composition are also presented the $h_{C14}$, molar weight (M), maximum theoretical hydrogen content (considering H/M=1), and equilibrium pressure at $c_H$ = 0.5.

| Alloy number | Site fraction sublattice A | | | | | | Site fraction sublattice B | | | | | | | | | | | $h_{C14}$ | M alloy [g/mol] | $c_{H_{MAX}}$ [wt.%] | P ($c_H$=0.5) [bar] |
|---|---|---|---|---|---|---|---|---|---|---|---|---|---|---|---|---|---|---|---|---|---|
| | Ti | Zr | Nb | Mn | V | Cr | Ti | Zr | Nb | Fe | Mn | V | Cr | Ni | Co | Zn | Cu | | | | |
| **87** | 1 | | | | | | | | 0.002 | | | | | | | 0.998 | | -18.54 | 59.58 | 1.67 | 2.12 |
| **88** | 1 | | | | | | | | | 0.806 | | | | 0.194 | | | | -13.34 | 53.56 | 1.85 | 140.40 |
| **89** | 1 | | | 0.005 | | | 0.001 | | | | 0.962 | | | | | | 0.037 | -24.55 | 52.81 | 1.88 | 0.02 |
| **90** | | 1 | | | | | | 0.078 | | | 0.921 | | | | | | | -27.58 | 68.92 | 1.44 | 0.00 |
| **91** | | 0.731 | | 0.269 | | | | | | | 0.998 | | | 0.002 | | | | -18.35 | 63.78 | 1.56 | 2.46 |
| **92** | | | 1 | | | | | | 0.004 | | 0.995 | | | | | | | -17.08 | 67.71 | 1.47 | 6.86 |
| **93** | | | 1 | | | | | | 0.003 | | 0.649 | | | 0.348 | | | | -15.50 | 68.55 | 1.45 | 24.67 |
| **94** | | | 1 | | | | | | 0.007 | | 0.992 | | | | | | | -17.12 | 67.78 | 1.47 | 6.65 |
| **95** | 0.976 | | | | 0.024 | | 0.005 | 0.004 | | 0.479 | | 0.512 | | | | | | -25.63 | 51.61 | 1.92 | 0.01 |
| **96** | 1 | | | | | | | | | 0.450 | | | | | | 0.550 | | -15.35 | 56.69 | 1.75 | 27.82 |
| **97** | 0.328 | 0.672 | | | | | | | | 1 | | | | | | | | -11.52 | 62.89 | 1.58 | 614.28 |
| **98** | 0.045 | 0.955 | | | | | 0.099 | 0.019 | | | 0.882 | | | | | | | -28.63 | 66.38 | 1.50 | 0.00 |
| **99** | 0.153 | 0.847 | | | | | | | | | 0.576 | | | | 0.424 | | | -21.25 | 65.96 | 1.51 | 0.24 |
| **100** | 1 | | | | | | | | | | 0.313 | | | | | 0.686 | | -20.70 | 57.37 | 1.73 | 0.37 |

| | | | | | | | | | | | | | | | | | | | |
|---|---|---|---|---|---|---|---|---|---|---|---|---|---|---|---|---|---|---|---|
| **101** | 0.098 | 0.900 | | 0.002 | | 0.001 | | | | 0.999 | | | | | | | -25.47 | 65.59 | 1.52 | 0.01 |
| **102** | 0.428 | 0.572 | | 0.001 | | 0.004 | | | | 0.995 | | | | | | | -25.59 | 60.82 | 1.63 | 0.01 |
| **103** | 1 | | | | | | | | | | | 0.180 | | | 0.820 | | -17.34 | 57.94 | 1.71 | 5.59 |
| **104** | 0.981 | | 0.001 | | 0.018 | 0.001 | | 0.004 | 0.583 | | 0.413 | | | | | | -22.76 | 51.96 | 1.91 | 0.07 |
| **105** | 0.344 | | 0.656 | | | | | | 0.857 | | | | 0.143 | | | | -7.29 | 63.31 | 1.57 | 18685.63 |
| **106** | 1 | | | | | | | | 0.298 | | | | | | 0.702 | | -16.41 | 57.65 | 1.72 | 11.78 |
| **107** | 0.260 | | 0.740 | | | 0.038 | | 0.008 | | 0.953 | 0.002 | | | | | | -20.37 | 63.70 | 1.56 | 0.48 |
| **108** | 0.013 | | 0.979 | 0.008 | | | | | | 0.951 | | | 0.048 | | | | -16.75 | 67.43 | 1.48 | 9.00 |
| **109** | 0.168 | | 0.832 | | | | | | | 0.564 | | | | 0.436 | | | -14.07 | 66.24 | 1.50 | 78.22 |
| **110** | 0.007 | | 0.993 | | | | | 0.001 | | 0.999 | | | | | | | -17.07 | 67.50 | 1.47 | 6.94 |
| **111** | 1 | | | | | | | 0.001 | | 0.082 | | | | | 0.917 | | -19.10 | 58.99 | 1.68 | 1.35 |
| **112** | 0.027 | | 0.973 | | | 0.006 | | 0.007 | | 0.986 | | | | | | | -17.51 | 67.33 | 1.48 | 4.85 |
| **113** | 1 | | | | | | | 0.007 | | | 0.028 | | | | 0.965 | | -19.26 | 59.40 | 1.67 | 1.19 |
| **114** | 1 | | | | | | | 0.001 | | | | 0.062 | | | 0.937 | | -18.12 | 59.01 | 1.68 | 2.98 |
| **115** | | 0.120 | 0.880 | | | | | | 0.396 | 0.604 | | | | | | | -12.47 | 67.77 | 1.47 | 284.13 |
| **116** | | 0.001 | 0.999 | | | | | | 0.890 | | | | 0.110 | | | | -4.05 | 68.41 | 1.45 | 253509.89 |
| **117** | | 0.920 | 0.080 | | | | 0.027 | 0.032 | | 0.941 | | | | | | | -26.10 | 68.60 | 1.45 | 0.00 |
| **118** | | 0.063 | 0.931 | 0.005 | | | | | | 0.919 | | | 0.081 | | | | -17.07 | 67.69 | 1.47 | 6.92 |
| **119** | | 0.034 | 0.966 | | | | | 0.001 | | 0.999 | | | | | | | -17.30 | 67.59 | 1.47 | 5.77 |
| **120** | | 0.439 | 0.561 | | | | 0.002 | 0.015 | | 0.982 | | | | | | | -21.06 | 67.79 | 1.47 | 0.28 |
| **121** | 0.629 | 0.055 | 0.316 | | | | | | 1 | | | | | | | | -8.81 | 58.73 | 1.69 | 5462.79 |
| **122** | 1 | | | | | | | | 0.615 | 0.334 | | | 0.051 | | | | -16.67 | 53.09 | 1.87 | 9.61 |
| **123** | 1 | | | | | | | | 0.578 | 0.193 | | | | 0.229 | | | -15.11 | 53.55 | 1.85 | 33.70 |
| **124** | 1 | | | | | 0.001 | | | 0.340 | 0.638 | | | | | | 0.021 | -20.28 | 52.91 | 1.87 | 0.52 |
| **125** | 1 | | | | | | | | 0.320 | | 0.163 | | | | 0.517 | | -19.59 | 55.94 | 1.77 | 0.90 |
| **126** | 0.971 | | | | 0.029 | 0.001 | | | 0.536 | | 0.458 | | | | | 0.004 | -23.75 | 51.82 | 1.91 | 0.03 |
| **127** | 1 | | | | | 0.000 | | | 0.747 | | | 0.069 | 0.184 | | | | -13.28 | 53.36 | 1.86 | 147.99 |

| | | | | | | | | | | | | | | | | | | | |
|---|---|---|---|---|---|---|---|---|---|---|---|---|---|---|---|---|---|---|---|
| **128** | 1 | | | | | | | 0.523 | | 0.186 | | 0.291 | | | -12.75 | 53.31 | 1.86 | 226.25 |
| **129** | 0.995 | | | | | | | 0.675 | | | 0.065 | 0.259 | | | -12.96 | 53.86 | 1.84 | 191.55 |
| **130** | 1 | | | | | | | 0.785 | | | 0.104 | | 0.112 | | -13.26 | 54.10 | 1.83 | 149.65 |
| **131** | 1 | | | | | | | 0.857 | | | 0.142 | | | 0.001 | -12.85 | 53.47 | 1.85 | 209.67 |
| **132** | 1 | | | | | | | 0.747 | | | | 0.251 | | 0.002 | -12.48 | 53.72 | 1.85 | 281.43 |
| **133** | 1 | | | | 0.001 | | | | 0.654 | 0.345 | | | | | -20.85 | 51.91 | 1.91 | 0.33 |
| **134** | 1 | | | | 0.001 | | | | 0.619 | 0.346 | | | | 0.034 | -20.08 | 52.10 | 1.90 | 0.61 |
| **135** | 0.992 | | 0.008 | | | | | | 0.939 | | | 0.038 | | 0.023 | -24.41 | 52.83 | 1.88 | 0.02 |
| **136** | 1 | | | | 0.002 | | | | 0.805 | | | | 0.163 | 0.031 | -23.70 | 53.89 | 1.84 | 0.03 |
| **137** | 1 | | | | | | | | | 0.746 | | | 0.228 | 0.026 | -13.25 | 52.86 | 1.87 | 151.14 |
| **138** | | 1 | | | | 0.004 | | 0.311 | 0.685 | | | | | | -21.25 | 67.31 | 1.48 | 0.24 |
| **139** | | 1 | | | | | | 0.312 | 0.688 | | | | | | -21.14 | 67.23 | 1.48 | 0.26 |
| **140** | | 1 | | | | 0.011 | | | 0.977 | 0.013 | | | | | -25.61 | 67.27 | 1.48 | 0.01 |
| **141** | | 1 | | | | 0.006 | | | 0.992 | | 0.001 | | | | -25.66 | 67.19 | 1.48 | 0.01 |
| **142** | | 1 | | | | 0.018 | | | 0.924 | | | 0.058 | | | -25.40 | 67.33 | 1.48 | 0.01 |
| **143** | | 0.986 | 0.014 | | | | | | 0.964 | 0.020 | 0.016 | | | | -24.80 | 66.87 | 1.49 | 0.01 |
| **144** | | 1 | | | | | | | 0.987 | 0.013 | | | | | -25.33 | 67.01 | 1.48 | 0.02 |
| **145** | | 1 | | | | 0.002 | | | 0.972 | 0.026 | | | | | -25.22 | 67.04 | 1.48 | 0.01 |
| **146** | | 1 | | | | | | | 0.511 | | 0.055 | 0.434 | | | -20.91 | 68.33 | 1.46 | 0.31 |
| **147** | | 1 | | | | | | | 0.735 | | | 0.265 | | | -22.86 | 67.74 | 1.47 | 0.06 |
| **148** | | 1 | | | | | | | 0.646 | | | 0.354 | | | -21.96 | 67.98 | 1.46 | 0.13 |
| **149** | | | 1 | | | | 0.009 | 0.306 | 0.684 | | | | | | -12.89 | 68.01 | 1.46 | 203.20 |
| **150** | | | 1 | | | | 0.015 | 0.265 | 0.719 | | | | | | -13.55 | 68.14 | 1.46 | 118.93 |
| **151** | | | 1 | | | | 0.002 | 0.448 | | 0.550 | | | | | -3.34 | 66.83 | 1.49 | 451693.92 |
| **152** | | | 1 | | | | 0.002 | 0.426 | | 0.572 | | | | | -3.36 | 66.79 | 1.49 | 445826.70 |
| **153** | | | 1 | | | | 0.001 | 0.488 | | | 0.135 | 0.376 | | | -5.81 | 69.24 | 1.44 | 61584.22 |
| **154** | | | 1 | | | | 0.001 | | 0.593 | 0.405 | | | | | -11.56 | 66.84 | 1.49 | 590.56 |

| | | | | | | | | | | | | | | | | | | |
|---|---|---|---|---|---|---|---|---|---|---|---|---|---|---|---|---|---|---|
| **155** | | | 1 | | | | 0.005 | | 0.884 | | | 0.111 | | | -16.59 | 67.99 | 1.46 | 10.25 |
| **156** | | | 1 | | | | 0.005 | | 0.691 | | | | 0.303 | | -14.07 | 68.53 | 1.45 | 78.31 |
| **157** | | | 1 | | | | 0.004 | | 0.675 | | | 0.321 | | | -15.63 | 68.49 | 1.45 | 22.27 |
| **158** | | | 1 | | | | 0.008 | | 0.792 | | | 0.200 | | | -16.24 | 68.31 | 1.46 | 13.54 |
| **159** | | | 1 | | | | 0.011 | | 0.802 | | | | 0.186 | | -15.34 | 68.38 | 1.46 | 28.09 |
| **160** | | | 1 | | | | 0.001 | | | 0.610 | | | 0.389 | | -4.90 | 67.46 | 1.48 | 127802.42 |
| **161** | | | 1 | | | | 0.001 | | | 0.647 | | | 0.351 | | -4.77 | 67.30 | 1.48 | 142579.64 |
| **162** | 0.051 | 0.949 | | | 0.027 | 0.001 | | 0.317 | 0.655 | | | | | | -21.81 | 66.39 | 1.50 | 0.15 |
| **163** | 0.208 | 0.792 | | | | | | 0.411 | 0.588 | | | | | | -19.74 | 64.28 | 1.55 | 0.80 |
| **164** | 0.396 | 0.604 | | | 0.002 | | | 0.370 | 0.628 | | | | | | -20.36 | 61.53 | 1.61 | 0.49 |
| **165** | 0.983 | | | 0.017 | 0.007 | 0.001 | | 0.479 | | 0.508 | 0.006 | | | | -25.54 | 51.51 | 1.92 | 0.01 |
| **166** | 0.434 | 0.566 | | | 0.014 | | | 0.751 | | 0.003 | | 0.232 | | | -14.35 | 61.72 | 1.61 | 62.17 |
| **167** | 0.968 | 0.001 | | 0.032 | 0.001 | | | 0.575 | | 0.424 | | | | | -22.77 | 51.85 | 1.91 | 0.07 |
| **168** | 0.969 | 0.001 | | 0.030 | 0.001 | 0.001 | | 0.556 | | 0.441 | | | | 0.001 | -23.30 | 52.22 | 1.90 | 0.05 |
| **169** | 1 | | | | | | | 0.432 | | | 0.078 | | 0.490 | | -14.97 | 56.11 | 1.77 | 37.81 |
| **170** | 0.468 | 0.532 | | | | | | 0.578 | | | | 0.422 | | | -15.52 | 61.68 | 1.61 | 24.29 |
| **171** | 0.524 | 0.476 | | | | | | 0.656 | | | | 0.343 | | | -14.77 | 60.72 | 1.64 | 44.47 |
| **172** | 0.329 | 0.671 | | | 0.042 | 0.001 | | | 0.906 | 0.001 | 0.049 | | | | -26.01 | 62.02 | 1.60 | 0.01 |
| **173** | 0.303 | 0.697 | | | 0.008 | | | | 0.979 | | | 0.012 | | | -25.67 | 62.65 | 1.59 | 0.01 |
| **174** | 0.043 | 0.957 | | | 0.012 | 0.002 | | | 0.961 | | | | 0.025 | | -25.61 | 66.47 | 1.50 | 0.01 |
| **175** | 0.069 | 0.930 | | | 0.009 | 0.001 | | | 0.990 | | | | | | -25.75 | 66.01 | 1.51 | 0.01 |
| **176** | 0.247 | 0.753 | | | 0.012 | | | | 0.987 | | | | | | -25.84 | 62.60 | 1.59 | 0.01 |
| **177** | 0.805 | 0.194 | 0.001 | | 0.001 | | | | 0.823 | | 0.175 | 0.001 | | | -23.12 | 55.05 | 1.80 | 0.05 |
| **178** | 0.337 | 0.660 | 0.003 | | 0.001 | | | | 0.958 | | 0.042 | | | | -24.89 | 62.05 | 1.60 | 0.01 |
| **179** | 1 | | | | | | | | 0.531 | | 0.047 | | 0.422 | | -21.92 | 55.47 | 1.79 | 0.14 |
| **180** | 0.744 | 0.256 | 0.001 | | 0.001 | | | | 0.847 | | 0.146 | | | 0.005 | -23.44 | 56.01 | 1.77 | 0.04 |
| **181** | 0.236 | 0.630 | 0.134 | | | | | | 0.996 | | 0.004 | | | | -21.89 | 62.01 | 1.60 | 0.14 |

| | | | | | | | | | | | | | | | | | | |
|---|---|---|---|---|---|---|---|---|---|---|---|---|---|---|---|---|---|---|
| **182** | 0.128 | 0.871 | | 0.001 | | | | | 0.802 | | | | 0.198 | | | -23.49 | 65.70 | 1.51 | 0.04 |
| **183** | 0.161 | 0.837 | | 0.002 | | | | | 0.846 | | | | 0.154 | | | -23.90 | 65.09 | 1.53 | 0.03 |
| **184** | 0.122 | 0.878 | | | | 0.004 | | | 0.996 | | | | | | | -25.59 | 65.25 | 1.52 | 0.01 |
| **185** | 0.323 | 0.677 | | | | | | | | | | 0.413 | 0.587 | | | -17.77 | 64.97 | 1.53 | 3.94 |
| **186** | 0.993 | | 0.001 | | 0.005 | 0.003 | 0.007 | 0.532 | 0.051 | 0.408 | | | | | | -23.66 | 52.00 | 1.91 | 0.03 |
| **187** | 0.109 | | 0.891 | | | 0.011 | 0.011 | 0.234 | 0.744 | 0.001 | | | | | | -15.14 | 66.32 | 1.50 | 32.95 |
| **188** | 0.370 | | 0.630 | | | | | 0.560 | 0.399 | | | 0.041 | | | | -12.12 | 62.48 | 1.59 | 377.07 |
| **189** | 1 | | | | | | | 0.209 | 0.080 | | | | | 0.711 | | -17.59 | 57.66 | 1.72 | 4.55 |
| **190** | 0.181 | | 0.819 | | | 0.002 | 0.003 | 0.454 | 0.541 | | | | | | 0.001 | -12.28 | 65.22 | 1.53 | 332.32 |
| **191** | 0.079 | | 0.921 | | | 0.001 | 0.001 | 0.370 | | | 0.627 | | | | | -4.07 | 65.43 | 1.52 | 251035.07 |
| **192** | 0.970 | | 0.004 | | 0.027 | | 0.001 | 0.649 | | 0.344 | | 0.006 | | | | -20.67 | 52.17 | 1.90 | 0.38 |
| **193** | 1 | | | | | | 0.008 | 0.213 | | 0.098 | | | | 0.681 | | -19.21 | 57.40 | 1.73 | 1.23 |
| **194** | 0.360 | | 0.640 | | | | | 0.625 | | | 0.309 | 0.066 | | | | -6.84 | 62.13 | 1.60 | 26840.83 |
| **195** | 0.061 | | 0.939 | | | | | 0.447 | | | 0.553 | | | | | -3.79 | 65.86 | 1.51 | 312680.19 |
| **196** | 0.192 | | 0.808 | | | | | 0.461 | | | 0.539 | | | | | -4.90 | 63.94 | 1.56 | 127644.99 |
| **197** | 0.257 | | 0.743 | | | | | 0.534 | | | | 0.033 | 0.433 | | | -7.22 | 65.29 | 1.52 | 19639.39 |
| **198** | 0.371 | | 0.629 | | | | 0.001 | 0.896 | | | | 0.103 | | | | -7.15 | 62.84 | 1.58 | 20818.07 |
| **199** | 0.420 | | 0.580 | | | | 0.001 | 0.894 | | | | 0.105 | | | | -7.58 | 62.11 | 1.60 | 14668.91 |
| **200** | 0.155 | | 0.845 | | | | | 0.614 | | | | | 0.385 | | | -5.88 | 66.67 | 1.49 | 58275.89 |
| **201** | 0.207 | | 0.793 | | | | | 0.690 | | | | | 0.309 | | | -6.01 | 65.74 | 1.51 | 52235.05 |
| **202** | 0.284 | | 0.716 | | | 0.017 | 0.005 | | 0.546 | 0.001 | 0.432 | | | | | -14.12 | 62.53 | 1.59 | 74.83 |
| **203** | 0.116 | | 0.884 | | | 0.009 | 0.003 | | 0.984 | 0.001 | | 0.004 | | | | -18.26 | 65.88 | 1.51 | 2.65 |
| **204** | 0.009 | | 0.991 | | | | 0.005 | | 0.762 | | | | 0.232 | | | -14.86 | 68.20 | 1.46 | 41.16 |
| **205** | 1 | | | | | | 0.021 | | 0.202 | 0.057 | | | | 0.720 | | -21.60 | 57.97 | 1.71 | 0.18 |
| **206** | 0.043 | | 0.957 | | | 0.008 | 0.005 | | 0.987 | | | | | | | -17.67 | 67.04 | 1.48 | 4.28 |
| **207** | 0.040 | | 0.960 | | | 0.006 | 0.005 | | 0.988 | | | | | | | -17.59 | 67.08 | 1.48 | 4.56 |
| **208** | 0.325 | | 0.674 | | | | | | 0.595 | | 0.401 | 0.003 | | | | -14.34 | 61.93 | 1.60 | 62.81 |

| | | | | | | | | | | | | | | | | | | | |
|---|---|---|---|---|---|---|---|---|---|---|---|---|---|---|---|---|---|---|---|
| **209** | 1 | | | | | | | | 0.140 | | 0.134 | | | 0.726 | | -18.62 | 57.38 | 1.73 | 1.99 |
| **210** | 0.075 | | 0.925 | | | | | | 0.497 | | 0.503 | | | | | -10.85 | 65.48 | 1.52 | 1047.58 |
| **211** | 0.250 | | 0.750 | | | | | | 0.500 | | 0.500 | | | | 0.001 | -12.38 | 62.86 | 1.58 | 306.13 |
| **212** | 0.032 | | 0.968 | | | | | | 0.552 | | | 0.033 | 0.415 | | | -12.97 | 68.31 | 1.46 | 189.88 |
| **213** | 0.007 | | 0.993 | | | | | | 0.968 | | | 0.032 | | | | -16.93 | 67.57 | 1.47 | 7.77 |
| **214** | 0.012 | | 0.988 | | | | | | 0.975 | | | 0.024 | | | | -17.00 | 67.49 | 1.47 | 7.32 |
| **215** | 0.302 | | 0.698 | | | 0.116 | | 0.029 | 0.855 | | | | | | | -23.17 | 63.25 | 1.57 | 0.05 |
| **216** | 0.007 | | 0.993 | 0.007 | | 0.001 | | 0.012 | 0.798 | | | | 0.189 | | | -15.39 | 68.28 | 1.46 | 26.85 |
| **217** | 0.027 | | 0.973 | | | | | 0.008 | 0.984 | | | | | | | -17.58 | 67.36 | 1.48 | 4.59 |
| **218** | 0.068 | | 0.932 | | | | | 0.001 | | | 0.616 | | 0.383 | | | -5.46 | 66.41 | 1.50 | 81647.61 |
| **219** | 1 | | | | | | | 0.010 | | 0.055 | 0.202 | | | 0.733 | | -18.57 | 57.40 | 1.73 | 2.06 |
| **220** | 0.152 | | 0.847 | | | | | | | | 0.470 | 0.017 | 0.513 | | | -6.73 | 65.79 | 1.51 | 29131.87 |
| **221** | 0.110 | | 0.890 | | | | | | | | 0.593 | | 0.407 | | | -5.86 | 65.87 | 1.51 | 59078.62 |
| **222** | 0.056 | | 0.944 | | | | | 0.001 | | | 0.701 | | 0.297 | | | -5.04 | 66.20 | 1.50 | 114152.42 |
| **223** | | 0.948 | 0.052 | | | | | 0.039 | 0.485 | 0.476 | | | | | | -18.97 | 68.35 | 1.46 | 1.50 |
| **224** | | 0.375 | 0.625 | | | | 0.001 | 0.017 | 0.259 | 0.723 | | | | | | -16.89 | 67.99 | 1.46 | 7.99 |
| **225** | | 0.030 | 0.970 | | | | | | 0.423 | 0.530 | | 0.046 | | | | -11.11 | 67.95 | 1.46 | 849.89 |
| **226** | | 0.027 | 0.973 | | | | | | 0.351 | 0.648 | | | | | | -12.32 | 67.80 | 1.47 | 321.52 |
| **227** | | 0.950 | 0.050 | | | | | 0.035 | 0.495 | 0.470 | | | | | | -18.79 | 68.25 | 1.46 | 1.73 |
| **228** | | 0.358 | 0.642 | | | | 0.001 | 0.015 | 0.264 | 0.720 | | | | | | -16.63 | 67.95 | 1.46 | 9.90 |
| **229** | | | 1 | | | | | | 0.568 | | 0.382 | 0.050 | | | | -3.68 | 67.32 | 1.48 | 343286.37 |
| **230** | | | 1 | | | | | | 0.576 | | 0.424 | | | | | -3.22 | 67.12 | 1.48 | 496922.89 |
| **231** | | 0.001 | 0.999 | | | | | 0.001 | 0.904 | | | 0.096 | | | | -3.93 | 68.39 | 1.46 | 280311.43 |
| **232** | | 0.459 | 0.541 | | | | 0.002 | 0.007 | | 0.927 | 0.064 | | | | | -20.21 | 67.44 | 1.48 | 0.55 |
| **233** | | 0.008 | 0.992 | | | | | 0.004 | | 0.878 | | 0.118 | | | | -16.61 | 67.98 | 1.46 | 10.06 |
| **234** | | 0.383 | 0.617 | | | | | 0.009 | | 0.627 | | | 0.364 | | | -16.78 | 68.58 | 1.45 | 8.73 |
| **235** | | 0.400 | 0.600 | | | | 0.001 | 0.008 | | 0.990 | | | | | | -20.58 | 67.61 | 1.47 | 0.41 |

| | | | | | | | | | | | | | | | | | | | |
|---|---|---|---|---|---|---|---|---|---|---|---|---|---|---|---|---|---|---|---|
| **236** | | 0.718 | 0.282 | | | | 0.004 | 0.016 | | 0.979 | | | | | | -23.51 | 67.70 | 1.47 | 0.04 |
| **237** | | 0.015 | 0.985 | | | | | | | 0.658 | | 0.273 | 0.069 | | | -13.14 | 67.23 | 1.48 | 165.88 |
| **238** | | 0.006 | 0.994 | | | | | | | 0.682 | | 0.318 | | | | -12.77 | 66.97 | 1.49 | 223.99 |
| **239** | | 0.162 | 0.838 | | | | 0.001 | 0.005 | | 0.829 | | 0.165 | | | | -16.25 | 67.32 | 1.48 | 13.50 |
| **240** | | 0.125 | 0.875 | | | | | | | 0.612 | | | 0.067 | 0.321 | | -14.55 | 68.55 | 1.45 | 52.93 |
| **241** | | 0.022 | 0.978 | | | | | 0.001 | | 0.943 | | | 0.057 | | | -16.95 | 67.74 | 1.47 | 7.66 |
| **242** | | 0.005 | 0.995 | | | | | 0.008 | | 0.787 | | | 0.204 | | | -16.26 | 68.31 | 1.46 | 13.31 |
| **243** | | 0.052 | 0.948 | | | | | | | 0.633 | | | | 0.366 | | -13.79 | 68.55 | 1.45 | 97.96 |
| **244** | | 0.347 | 0.653 | | | | | 0.012 | | 0.598 | | | | 0.390 | | -16.27 | 68.75 | 1.45 | 13.21 |
| **245** | | 0.271 | 0.729 | | | | 0.001 | 0.011 | | 0.987 | | | | | | -19.54 | 67.76 | 1.47 | 0.95 |
| **246** | | 0.005 | 0.995 | | | | | 0.000 | | | | 0.471 | | 0.528 | | -5.40 | 68.08 | 1.46 | 85378.40 |
| **247** | 0.983 | 0.001 | 0.001 | | 0.015 | 0.001 | | 0.005 | 0.572 | | 0.422 | | | | | -23.13 | 51.98 | 1.91 | 0.05 |
| **248** | 0.485 | 0.515 | | | | | | | 0.435 | | | | 0.565 | | | -16.86 | 61.71 | 1.61 | 8.19 |
| **249** | 0.027 | 0.973 | | | | | | 0.001 | 0.806 | | | | 0.194 | | | -13.36 | 68.17 | 1.46 | 138.46 |
| **250** | 0.089 | 0.001 | 0.910 | | | | | | 1 | | | | | | | -3.78 | 66.87 | 1.49 | 317067.28 |
| **251** | 0.498 | 0.016 | 0.485 | | | | | 0.002 | 0.997 | | | | | | 0.001 | -7.44 | 60.75 | 1.64 | 16539.54 |
| **252** | 0.074 | 0.716 | 0.210 | | | 0.048 | 0.005 | 0.014 | | 0.933 | | | | | | -25.37 | 66.32 | 1.50 | 0.01 |
| **253** | 0.001 | 0.019 | 0.978 | 0.003 | | | | | | 0.891 | | | 0.109 | | | -16.62 | 67.80 | 1.47 | 9.99 |
| **254** | 0.033 | 0.213 | 0.753 | 0.001 | | | | | | 1 | | | | | | -19.08 | 66.97 | 1.49 | 1.36 |
| **255** | 1 | | | | | | | | | 0.182 | | | | 0.818 | | -19.78 | 58.29 | 1.70 | 0.78 |
| **256** | 0.149 | 0.197 | 0.653 | | | 0.010 | | 0.002 | | 0.987 | | | | | | -20.25 | 65.26 | 1.52 | 0.53 |
| **257** | 0.376 | 0.624 | 0.001 | | | | | | | | | 0.424 | 0.576 | | | -17.18 | 62.22 | 1.60 | 6.36 |
| **258** | 1 | | | | | | | 0.001 | | | | 0.053 | | 0.947 | | -18.18 | 59.09 | 1.68 | 2.84 |
| **259** | 0.117 | 0.528 | 0.356 | | | 0.008 | | 0.027 | 0.293 | 0.671 | | | | | | -19.10 | 66.38 | 1.50 | 1.35 |
| **260** | 0.131 | 0.720 | 0.150 | | | 0.006 | | 0.037 | 0.383 | 0.574 | | | | | | -19.70 | 66.36 | 1.50 | 0.83 |
| **261** | 0.489 | 0.511 | | | | | | | 0.444 | 0.048 | | | 0.508 | | | -17.00 | 61.51 | 1.62 | 7.32 |
| **262** | 0.051 | 0.010 | 0.938 | 0.001 | | | | | 0.133 | 0.851 | | | 0.015 | | | -15.56 | 66.93 | 1.49 | 2.19 |

| | | | | | | | | | | | | | | | | | | |
|---|---|---|---|---|---|---|---|---|---|---|---|---|---|---|---|---|---|---|
| **263** | 0.138 | 0.101 | 0.761 | | | | | 0.333 | 0.667 | | | | | | -14.37 | 65.67 | 1.51 | 61.23 |
| **264** | 0.175 | 0.226 | 0.599 | | 0.005 | | 0.011 | 0.383 | 0.602 | | | | | | -15.37 | 65.32 | 1.52 | 27.27 |
| **265** | 0.989 | | 0.001 | 0.010 | 0.002 | | 0.005 | 0.573 | | 0.409 | 0.011 | | | | -22.84 | 51.98 | 1.91 | 0.07 |
| **266** | 0.484 | 0.516 | | | | | | 0.532 | | | | 0.468 | | | -15.96 | 61.53 | 1.62 | 17.00 |
| **267** | 1 | | | | | | 0.006 | 0.250 | | 0.113 | | | | 0.631 | -19.22 | 56.97 | 1.74 | 1.23 |
| **268** | 0.981 | 0.001 | 0.001 | 0.017 | 0.001 | | 0.004 | 0.581 | | 0.413 | | | | 0.001 | -22.80 | 52.00 | 1.91 | 0.07 |
| **269** | 0.495 | 0.505 | | | | | | 0.317 | | | 0.191 | 0.492 | | | -16.27 | 60.93 | 1.63 | 13.23 |
| **270** | 0.020 | | 0.980 | | | | | 0.365 | | | 0.610 | 0.025 | | | -3.70 | 66.38 | 1.50 | 337525.71 |
| **271** | 0.057 | | 0.943 | | | | | 0.555 | | | 0.445 | | | | -3.71 | 66.21 | 1.50 | 335042.64 |
| **272** | 0.122 | 0.001 | 0.877 | | | | | 0.506 | | | 0.493 | | | | -4.32 | 65.11 | 1.53 | 205367.19 |
| **273** | 0.466 | 0.533 | | | | | | 0.385 | | | | 0.547 | 0.067 | | -16.97 | 62.08 | 1.60 | 7.53 |
| **274** | 0.464 | 0.536 | | | | | | 0.503 | | | | 0.497 | | | -16.22 | 61.88 | 1.61 | 13.73 |
| **275** | 0.468 | 0.532 | | | | | | 0.466 | | | | 0.534 | | | -16.58 | 61.89 | 1.61 | 10.34 |
| **276** | 0.216 | 0.207 | 0.577 | | 0.031 | 0.001 | 0.006 | | 0.833 | 0.001 | 0.128 | | | | -19.83 | 64.00 | 1.55 | 0.75 |
| **277** | 0.005 | 0.009 | 0.986 | | | | 0.002 | | 0.987 | | | 0.010 | | | -17.13 | 67.60 | 1.47 | 6.61 |
| **278** | 0.006 | 0.207 | 0.787 | | | | 0.004 | | 0.891 | | | | 0.105 | | -17.85 | 67.77 | 1.47 | 3.69 |
| **279** | 1 | | | | | 0.001 | 0.019 | | 0.204 | 0.068 | | | | 0.709 | -21.83 | 57.84 | 1.72 | 0.15 |
| **280** | 0.044 | 0.302 | 0.654 | | 0.009 | | 0.006 | | 0.984 | | | | | | -20.31 | 66.89 | 1.49 | 0.51 |
| **281** | 0.088 | 0.141 | 0.771 | | 0.012 | | 0.005 | | 0.982 | | | | | | -19.37 | 66.27 | 1.50 | 1.08 |
| **282** | 0.014 | 0.010 | 0.976 | | | | | | 0.632 | | 0.356 | 0.011 | | | -12.34 | 66.71 | 1.49 | 314.89 |
| **283** | 0.072 | 0.032 | 0.896 | | | | | | 0.735 | | 0.265 | | | | -14.30 | 65.98 | 1.51 | 64.64 |
| **284** | 1 | | | | | | | | 0.196 | | 0.070 | | | 0.734 | -19.43 | 57.57 | 1.72 | 1.04 |
| **285** | 0.259 | 0.061 | 0.680 | | 0.001 | | | | 0.723 | | 0.275 | | | | -16.05 | 63.13 | 1.57 | 15.82 |
| **286** | 0.007 | 0.060 | 0.933 | | | | | | 0.461 | | | 0.052 | 0.487 | | -12.47 | 68.88 | 1.45 | 285.16 |
| **287** | 0.002 | 0.028 | 0.970 | | | | | | 0.984 | | | 0.015 | | | -17.19 | 67.58 | 1.47 | 6.31 |
| **288** | | 0.003 | 0.997 | | | | | | 0.908 | | | 0.092 | | | -16.61 | 67.82 | 1.47 | 10.02 |
| **289** | 0.042 | 0.157 | 0.801 | | | | | | 0.727 | | | | 0.273 | | -15.96 | 67.60 | 1.47 | 16.93 |

| | | | | | | | | | | | | | | | | | | | |
|---|---|---|---|---|---|---|---|---|---|---|---|---|---|---|---|---|---|---|---|
| **290** | 0.028 | 0.214 | 0.758 | | | | | | 0.745 | | | | 0.255 | | | -16.51 | 67.73 | 1.47 | 10.92 |
| **291** | 0.026 | 0.225 | 0.749 | | | 0.010 | 0.001 | 0.012 | 0.977 | | | | | | | -19.63 | 67.36 | 1.48 | 0.88 |
| **292** | 0.088 | 0.006 | 0.905 | | | | | | | | 0.366 | 0.021 | 0.613 | | | -6.61 | 67.22 | 1.48 | 32138.50 |
| **293** | 0.190 | 0.005 | 0.805 | | | | | | | | 0.501 | | 0.499 | | | -6.91 | 65.08 | 1.53 | 25331.62 |
| **294** | 0.084 | 0.003 | 0.912 | | | | | | | | 0.575 | | 0.424 | | | -5.74 | 66.34 | 1.50 | 64916.70 |
| **295** | 0.240 | 0.760 | | | | 0.018 | | 0.148 | 0.799 | | 0.034 | | | | | -23.46 | 63.52 | 1.57 | 0.04 |
| **296** | 0.350 | 0.650 | | | | 0.007 | | 0.409 | 0.500 | 0.001 | | 0.083 | | | | -19.59 | 62.40 | 1.59 | 0.91 |
| **297** | 0.993 | | | 0.007 | | 0.001 | | 0.536 | 0.068 | 0.394 | | | | | | -23.27 | 51.87 | 1.91 | 0.05 |
| **298** | 0.074 | 0.926 | | | | 0.003 | | 0.431 | 0.525 | | | | 0.041 | | | -19.14 | 66.32 | 1.50 | 1.31 |
| **299** | 0.072 | 0.928 | | | | 0.003 | | 0.240 | 0.756 | | | | | | | -22.22 | 66.13 | 1.50 | 0.11 |
| **300** | 0.138 | 0.862 | | | | 0.004 | | 0.344 | 0.652 | | | | | | | -20.79 | 65.22 | 1.52 | 0.35 |
| **301** | 0.991 | | | 0.008 | | 0.002 | | 0.522 | 0.057 | 0.417 | | | | | 0.002 | -23.72 | 51.81 | 1.91 | 0.03 |
| **302** | 1 | | | | | | | 0.241 | 0.380 | | 0.038 | | | 0.341 | | -19.23 | 55.03 | 1.80 | 1.21 |
| **303** | 0.693 | 0.307 | | | | 0.002 | | 0.270 | 0.622 | | 0.104 | | | | 0.002 | -20.31 | 56.99 | 1.74 | 0.51 |
| **304** | 0.412 | 0.588 | | | | | | 0.468 | 0.092 | | | 0.285 | 0.155 | | | -16.12 | 62.48 | 1.59 | 14.96 |
| **305** | 0.408 | 0.592 | | | | | | 0.417 | 0.293 | | | 0.289 | | | | -18.37 | 62.11 | 1.60 | 2.44 |
| **306** | 0.466 | 0.534 | | | | | | 0.458 | 0.374 | | | 0.167 | | | | -18.33 | 60.99 | 1.63 | 2.51 |
| **307** | 0.302 | 0.698 | | | | | | 0.353 | 0.430 | | | | 0.217 | | | -18.38 | 63.47 | 1.57 | 2.40 |
| **308** | 1 | | | | | | | 0.213 | 0.189 | | | | 0.159 | 0.439 | | -17.85 | 56.19 | 1.77 | 3.70 |
| **309** | 0.316 | 0.684 | | | | | | 0.435 | 0.420 | | | | 0.145 | | | -17.96 | 63.12 | 1.57 | 3.38 |
| **310** | 0.126 | 0.874 | | | | 0.001 | | 0.359 | 0.640 | | | | | | | -20.51 | 65.43 | 1.52 | 0.43 |
| **311** | 0.520 | 0.480 | | | | 0.004 | | 0.610 | | 0.002 | 0.099 | 0.285 | | | | -14.48 | 60.38 | 1.65 | 56.27 |
| **312** | 0.987 | | | 0.012 | | 0.001 | | 0.616 | | 0.369 | 0.014 | | | | | -21.53 | 51.96 | 1.91 | 0.19 |
| **313** | 0.986 | | | 0.014 | | 0.003 | | 0.522 | | 0.461 | 0.011 | | | | 0.003 | -24.09 | 51.67 | 1.92 | 0.02 |
| **314** | 0.410 | 0.590 | | | | | | 0.545 | | | | 0.326 | 0.129 | | | -15.11 | 62.60 | 1.59 | 33.73 |
| **315** | 0.498 | 0.502 | | | | | | 0.675 | | 0.001 | | 0.323 | | | | -14.61 | 61.05 | 1.63 | 50.34 |
| **316** | 1 | | | | | | | 0.319 | | 0.088 | | | | 0.592 | | -18.07 | 56.67 | 1.75 | 3.08 |

| | | | | | | | | | | | | | | | | | | | |
|---|---|---|---|---|---|---|---|---|---|---|---|---|---|---|---|---|---|---|---|
| **317** | 0.511 | 0.489 | | | | 0.001 | | | 0.773 | | 0.002 | | 0.224 | | | | -13.72 | 60.67 | 1.64 | 103.55 |
| **318** | 0.961 | | | 0.038 | | | | | 0.655 | | 0.343 | | | | | 0.001 | -20.43 | 52.12 | 1.90 | 0.46 |
| **319** | 0.510 | 0.490 | | | | | | | 0.422 | | | 0.201 | 0.377 | | | | -15.19 | 60.47 | 1.64 | 31.73 |
| **320** | 0.572 | 0.428 | | | | | | | 0.505 | | | 0.228 | 0.266 | | | | -14.15 | 59.29 | 1.67 | 73.22 |
| **321** | 0.463 | 0.537 | | | | | | | 0.592 | | | | 0.290 | 0.119 | | | -14.73 | 61.74 | 1.61 | 45.96 |
| **322** | 0.418 | 0.582 | | | | | | | 0.499 | | | | 0.303 | 0.198 | | | -15.17 | 62.58 | 1.59 | 32.23 |
| **323** | 0.490 | 0.510 | | | | 0.001 | | | 0.747 | | | | 0.252 | | | | -13.92 | 61.03 | 1.63 | 88.27 |
| **324** | 0.587 | 0.413 | | | | 0.008 | | | | 0.880 | 0.003 | 0.103 | 0.006 | | | | -24.33 | 58.32 | 1.70 | 0.02 |
| **325** | 0.001 | 0.946 | | | 0.053 | 0.509 | | | | 0.004 | | | 0.487 | | | | -34.67 | 65.15 | 1.53 | 0.00 |
| **326** | 0.132 | 0.868 | | | | 0.008 | 0.001 | | | 0.939 | | 0.031 | | 0.021 | | | -25.08 | 65.09 | 1.53 | 0.01 |
| **327** | 0.289 | 0.711 | | | | 0.012 | | | | 0.953 | | 0.034 | | | | | -25.38 | 62.74 | 1.58 | 0.01 |
| **328** | 0.415 | 0.584 | | | | 0.010 | | | | 0.923 | 0.001 | 0.066 | | | | | -24.88 | 60.86 | 1.63 | 0.01 |
| **329** | 0.079 | 0.917 | | 0.004 | | | | | | 0.994 | | | 0.005 | | | | -25.38 | 65.86 | 1.51 | 0.01 |
| **330** | 0.287 | 0.709 | | 0.004 | | 0.001 | | | | 0.995 | | | 0.004 | | | | -25.41 | 62.85 | 1.58 | 0.01 |
| **331** | 0.030 | 0.970 | | | | 0.001 | | | | 0.932 | | | | 0.067 | | | -24.86 | 66.78 | 1.49 | 0.01 |
| **332** | 0.068 | 0.931 | | | | 0.004 | | | | 0.962 | | | | 0.033 | | | -25.27 | 66.12 | 1.50 | 0.01 |
| **333** | 0.035 | 0.965 | | | | 0.008 | 0.002 | | | 0.991 | | | | | | | -25.75 | 66.53 | 1.50 | 0.01 |
| **334** | 0.265 | 0.728 | | 0.007 | | | | | | 0.940 | | 0.029 | 0.031 | | | | -24.80 | 63.14 | 1.57 | 0.01 |
| **335** | 1 | | | | | | | | | 0.440 | | 0.026 | | | 0.534 | | -21.42 | 56.25 | 1.76 | 0.21 |
| **336** | 0.167 | 0.829 | | 0.004 | | | | | | 0.881 | | 0.017 | | 0.102 | | | -24.16 | 64.81 | 1.53 | 0.02 |
| **337** | 0.379 | 0.619 | | 0.002 | | | | | | 0.874 | | 0.067 | | 0.059 | | | -23.97 | 61.56 | 1.61 | 0.03 |
| **338** | 0.345 | 0.654 | | 0.001 | | 0.003 | | | | 0.946 | | 0.051 | | | | | -24.88 | 61.92 | 1.60 | 0.01 |
| **339** | 0.203 | 0.777 | | 0.020 | | | | | | 0.986 | | | 0.014 | | | | -24.92 | 63.89 | 1.56 | 0.01 |
| **340** | 0.050 | 0.950 | | | | | | | | 0.918 | | | | 0.081 | | | -24.69 | 66.53 | 1.50 | 0.01 |
| **341** | 0.172 | | 0.828 | | | 0.006 | | 0.002 | 0.169 | 0.448 | 0.001 | 0.374 | | | | | -11.25 | 64.42 | 1.54 | 763.44 |
| **342** | 0.124 | | 0.876 | | | 0.002 | | 0.003 | 0.328 | 0.658 | 0.001 | | 0.009 | | | | -13.55 | 66.03 | 1.51 | 118.43 |
| **343** | 0.989 | | 0.002 | 0.009 | | 0.001 | | 0.002 | 0.587 | 0.044 | 0.364 | | 0.003 | | | | -22.09 | 52.06 | 1.90 | 0.12 |

| | | | | | | | | | | | | | | | | |
|---|---|---|---|---|---|---|---|---|---|---|---|---|---|---|---|---|
| **344** | 0.042 | 0.958 | | 0.001 | 0.003 | 0.361 | 0.550 | | | 0.084 | | -11.54 | 67.49 | 1.47 | 602.52 |
| **345** | 1 | | | | 0.009 | 0.190 | 0.071 | 0.083 | | | 0.647 | -19.59 | 57.22 | 1.73 | 0.90 |
| **346** | 0.032 | 0.968 | | 0.002 | 0.010 | 0.326 | 0.662 | | | | | -12.95 | 67.55 | 1.47 | 192.75 |
| **347** | 0.989 | 0.002 | 0.009 | 0.001 | 0.004 | 0.571 | 0.033 | 0.386 | | | | 0.005 | -22.58 | 52.08 | 1.90 | 0.08 |
| **348** | 0.093 | 0.907 | | 0.006 | 0.012 | 0.360 | 0.621 | 0.001 | | | | | -13.10 | 66.68 | 1.49 | 170.37 |
| **349** | 0.403 | 0.597 | | | | 0.377 | 0.313 | | 0.294 | 0.016 | | | -11.11 | 61.23 | 1.62 | 849.28 |
| **350** | 0.137 | 0.863 | | | | 0.291 | 0.341 | | 0.368 | | | | -9.12 | 65.00 | 1.53 | 4242.47 |
| **351** | 1 | | | | | 0.194 | 0.124 | | 0.086 | | 0.595 | | -17.45 | 56.68 | 1.75 | 5.09 |
| **352** | 0.296 | 0.704 | | | | 0.299 | 0.348 | | 0.352 | | | 0.001 | -10.57 | 62.65 | 1.59 | 1318.95 |
| **353** | 0.149 | 0.851 | | | | 0.428 | 0.307 | | | 0.030 | 0.236 | | -9.79 | 66.32 | 1.50 | 2475.75 |
| **354** | 0.046 | 0.954 | | | 0.001 | 0.478 | 0.489 | | | 0.032 | | | -10.57 | 67.30 | 1.48 | 1320.82 |
| **355** | 0.093 | 0.907 | | | | 0.490 | 0.484 | | | 0.026 | | | -10.82 | 66.57 | 1.49 | 1077.99 |
| **356** | 0.108 | 0.892 | | | | 0.347 | 0.406 | | | | 0.246 | | -10.60 | 66.83 | 1.49 | 1288.72 |
| **357** | 0.052 | 0.948 | | | 0.003 | 0.408 | 0.496 | | | | 0.093 | | -10.84 | 67.38 | 1.48 | 1056.25 |
| **358** | 0.050 | 0.950 | | 0.007 | 0.018 | 0.288 | 0.686 | | | | | | -13.88 | 67.45 | 1.48 | 90.92 |
| **359** | 0.092 | 0.908 | | | 0.001 | 0.535 | | | 0.453 | 0.012 | | | -4.16 | 65.69 | 1.51 | 233538.13 |
| **360** | 0.032 | 0.968 | | | 0.001 | 0.403 | | | 0.507 | | 0.089 | | -3.93 | 66.64 | 1.49 | 280028.07 |
| **361** | 1 | | | | 0.010 | 0.148 | | 0.061 | 0.036 | | | 0.746 | -18.72 | 57.87 | 1.72 | 1.84 |
| **362** | 0.016 | 0.984 | | | 0.002 | 0.454 | | | 0.544 | | | | -3.48 | 66.61 | 1.49 | 402148.67 |
| **363** | 0.992 | 0.001 | 0.007 | 0.002 | 0.006 | 0.567 | | 0.400 | 0.021 | | | 0.004 | -22.65 | 52.01 | 1.90 | 0.08 |
| **364** | 0.065 | 0.935 | | 0.001 | 0.002 | 0.451 | | | 0.546 | | | | -3.92 | 65.87 | 1.51 | 283604.52 |
| **365** | 0.055 | 0.945 | | | | 0.493 | | | | 0.059 | 0.448 | | -5.83 | 68.41 | 1.45 | 60321.09 |
| **366** | 0.181 | 0.819 | | | | 0.426 | | | 0.277 | 0.031 | 0.267 | | -6.01 | 65.38 | 1.52 | 52137.04 |
| **367** | 0.035 | 0.965 | | | | 0.481 | | | 0.497 | 0.022 | | | -3.75 | 66.44 | 1.50 | 323077.72 |
| **368** | 0.062 | 0.938 | | | | 0.488 | | | 0.488 | 0.023 | | | -3.99 | 66.06 | 1.51 | 267278.30 |
| **369** | 0.133 | 0.867 | | | | 0.348 | | | 0.382 | | 0.270 | | -5.40 | 65.78 | 1.51 | 85442.53 |
| **370** | 0.037 | 0.963 | | | 0.001 | 0.416 | | | 0.483 | | 0.100 | | -3.99 | 66.64 | 1.49 | 267951.69 |

| | | | | | | | | | | | | | | | |
|---|---|---|---|---|---|---|---|---|---|---|---|---|---|---|---|
| **371** | 0.030 | 0.970 | | | 0.002 | 0.422 | | | 0.575 | | | | -3.63 | 66.32 | 1.50 | 357023.93 |
| **372** | 0.065 | 0.935 | | | | 0.580 | | | | 0.049 | 0.371 | | -5.51 | 68.10 | 1.46 | 78151.10 |
| **373** | 0.061 | 0.939 | | | | 0.575 | | | | 0.065 | 0.360 | | -5.59 | 68.16 | 1.46 | 73564.38 |
| **374** | 0.128 | 0.872 | | 0.003 | 0.001 | | 0.630 | | 0.362 | 0.004 | | | -13.27 | 64.98 | 1.53 | 149.50 |
| **375** | 0.029 | 0.971 | | 0.001 | 0.002 | | 0.552 | | 0.391 | | 0.054 | | -11.47 | 66.58 | 1.49 | 635.01 |
| **376** | 1 | | | 0.001 | 0.018 | | 0.173 | 0.069 | 0.110 | | | 0.629 | -20.88 | 57.02 | 1.74 | 0.32 |
| **377** | 0.088 | 0.912 | | 0.003 | 0.002 | | 0.567 | | 0.428 | | | | -12.09 | 65.45 | 1.52 | 386.58 |
| **378** | 0.045 | 0.955 | | 0.002 | 0.002 | | 0.598 | | 0.398 | | | | -12.08 | 66.17 | 1.50 | 389.14 |
| **379** | 0.004 | 0.996 | | | | | 0.602 | | | 0.053 | 0.345 | | -13.36 | 68.59 | 1.45 | 138.70 |
| **380** | 0.004 | 0.995 | | | 0.002 | | 0.980 | | | 0.017 | | | -17.01 | 67.62 | 1.47 | 7.28 |
| **381** | 0.007 | 0.993 | | | 0.003 | | 0.756 | | | | 0.240 | | -14.73 | 68.21 | 1.46 | 191.55 |
| **382** | 0.011 | 0.989 | | 0.001 | 0.006 | | 0.904 | | | | 0.088 | | -16.35 | 67.79 | 1.47 | 12.39 |
| **383** | 0.053 | 0.947 | | 0.010 | 0.006 | | 0.984 | | | | | | -17.81 | 66.89 | 1.49 | 3.81 |
| **384** | 0.037 | 0.963 | | | | | 0.289 | | 0.304 | 0.039 | 0.368 | | -9.35 | 67.52 | 1.47 | 3516.46 |
| **385** | 0.019 | 0.981 | | | | | 0.488 | | 0.488 | 0.025 | | | -10.47 | 66.41 | 1.50 | 1427.77 |
| **386** | 0.024 | 0.976 | | | | | 0.501 | | 0.476 | 0.022 | | | -10.67 | 66.35 | 1.50 | 1212.75 |
| **387** | 0.079 | 0.920 | | | | | 0.411 | | 0.363 | | 0.227 | | -10.51 | 66.29 | 1.50 | 1378.65 |
| **388** | 0.070 | 0.930 | | | | | 0.443 | | 0.465 | | 0.091 | | -10.40 | 65.88 | 1.51 | 1516.80 |
| **389** | 0.041 | 0.959 | | 0.001 | 0.001 | | 0.491 | | 0.506 | | | | -10.57 | 66.03 | 1.51 | 1314.86 |
| **390** | 0.004 | 0.996 | | | | | 0.600 | | | 0.052 | 0.348 | | -13.33 | 68.60 | 1.45 | 142.02 |
| **391** | 0.005 | 0.995 | | | | | 0.571 | | | 0.061 | 0.367 | | -13.09 | 68.66 | 1.45 | 171.99 |
| **392** | 0.010 | 0.990 | | | 0.001 | | 0.980 | | | 0.019 | | | -17.02 | 67.52 | 1.47 | 7.21 |
| **393** | 0.005 | 0.995 | | | 0.012 | | 0.793 | | | | 0.195 | | -15.32 | 68.33 | 1.46 | 28.39 |
| **394** | 0.075 | 0.925 | | | | | | | 0.323 | 0.019 | 0.657 | | -6.61 | 67.64 | 1.47 | 32136.86 |
| **395** | 0.041 | 0.959 | | | 0.001 | | | | 0.605 | | 0.394 | | -5.27 | 66.87 | 1.49 | 94931.10 |
| **396** | 0.059 | 0.941 | | | 0.001 | | | | 0.713 | | 0.285 | | -5.03 | 66.09 | 1.51 | 115648.57 |
| **397** | 0.044 | 0.956 | | | | | | | 0.546 | 0.020 | 0.433 | | -5.57 | 67.07 | 1.48 | 74498.00 |

| | | | | | | | | | | | | | | | |
|---|---|---|---|---|---|---|---|---|---|---|---|---|---|---|---|
| **398** | 0.049 | | 0.950 | | | | | | 0.589 | 0.025 | 0.385 | | -5.49 | 66.79 | 1.49 | 79308.40 |
| **399** | 0.033 | | 0.967 | | 0.001 | | | | 0.740 | | 0.259 | | -4.71 | 66.36 | 1.50 | 149813.22 |
| **400** | | 0.251 | 0.749 | 0.001 | 0.009 | 0.190 | 0.727 | | 0.073 | | | | -15.67 | 67.68 | 1.47 | 21.39 |
| **401** | | 0.019 | 0.981 | | 0.003 | 0.417 | 0.571 | | | 0.008 | | | -11.35 | 67.94 | 1.46 | 704.53 |
| **402** | | 0.799 | 0.201 | | 0.016 | 0.247 | 0.434 | | | | 0.303 | | -17.59 | 68.50 | 1.45 | 4.56 |
| **403** | | 0.165 | 0.835 | 0.001 | 0.011 | 0.221 | 0.766 | | | | | | -15.53 | 67.94 | 1.46 | 24.00 |
| **404** | | 0.945 | 0.055 | | 0.042 | 0.478 | 0.479 | | | | | | -19.10 | 68.42 | 1.45 | 1.35 |
| **405** | | 0.388 | 0.612 | 0.001 | 0.019 | 0.255 | 0.725 | | | | | | -17.08 | 68.02 | 1.46 | 6.87 |
| **406** | | 0.017 | 0.983 | | | 0.327 | 0.493 | | 0.157 | 0.023 | | | -10.35 | 67.53 | 1.47 | 1573.47 |
| **407** | | 0.009 | 0.991 | | | 0.318 | 0.495 | | 0.187 | | | | -10.10 | 67.42 | 1.48 | 1927.23 |
| **408** | | 0.111 | 0.889 | 0.001 | 0.011 | 0.251 | 0.617 | | 0.120 | | | | -13.03 | 67.76 | 1.47 | 180.29 |
| **409** | | 0.051 | 0.949 | | | 0.273 | 0.508 | | | 0.043 | 0.176 | | -11.66 | 68.31 | 1.46 | 547.32 |
| **410** | | 0.003 | 0.997 | | 0.003 | 0.421 | 0.500 | | | 0.076 | | | -10.84 | 67.55 | 1.47 | 1063.17 |
| **411** | | 0.012 | 0.988 | | | 0.494 | 0.470 | | | 0.036 | | | -10.02 | 67.98 | 1.46 | 2058.07 |
| **412** | | 0.029 | 0.971 | | | 0.306 | 0.485 | | | | 0.209 | | -10.87 | 68.32 | 1.46 | 1030.48 |
| **413** | | 0.577 | 0.423 | | 0.004 | 0.235 | 0.436 | | | | 0.325 | | -15.44 | 68.37 | 1.46 | 25.89 |
| **414** | | 0.209 | 0.791 | 0.001 | 0.021 | 0.227 | 0.750 | | | | | | -16.00 | 68.18 | 1.46 | 16.41 |
| **415** | | | 1 | | 0.001 | 0.476 | | | 0.505 | 0.017 | | | -3.47 | 66.97 | 1.49 | 406570.07 |
| **416** | | 0.002 | 0.998 | | | 0.409 | | | 0.297 | 0.036 | 0.258 | | -4.55 | 68.04 | 1.46 | 170222.94 |
| **417** | | | 1 | | 0.001 | 0.532 | | | 0.392 | 0.075 | | | -3.94 | 67.36 | 1.48 | 277831.32 |
| **418** | | | 1 | | | 0.492 | | | 0.457 | 0.051 | | | -3.72 | 67.13 | 1.48 | 331504.04 |
| **419** | | 0.001 | 0.998 | | | 0.390 | | | 0.316 | | 0.294 | | -4.35 | 67.99 | 1.46 | 200156.00 |
| **420** | | 0.014 | 0.986 | | 0.002 | | 0.604 | | 0.381 | 0.013 | | | -11.94 | 66.91 | 1.49 | 434.90 |
| **421** | | 0.300 | 0.700 | | 0.007 | | 0.685 | | 0.086 | | 0.221 | | -16.31 | 68.02 | 1.46 | 12.84 |
| **422** | | 0.081 | 0.919 | | 0.004 | | 0.875 | | 0.121 | | | | -16.13 | 67.41 | 1.48 | 14.78 |
| **423** | | 0.425 | 0.575 | 0.001 | 0.007 | | 0.921 | | 0.070 | | | | -19.83 | 67.43 | 1.48 | 0.75 |
| **424** | | 0.081 | 0.919 | | 0.003 | | 0.536 | | | 0.023 | 0.438 | | -13.26 | 68.85 | 1.45 | 150.44 |

| | | | | | | | | | | | | |
|---|---|---|---|---|---|---|---|---|---|---|---|---|
| **425** | 0.026 | 0.974 | | 0.003 | 0.970 | | 0.028 | | -17.15 | 67.71 | 1.47 | 6.52 |
| **426** | 0.007 | 0.993 | | 0.006 | 0.888 | | 0.105 | | -16.69 | 68.00 | 1.46 | 9.42 |
| **427** | 0.185 | 0.815 | | 0.009 | 0.738 | | | 0.253 | -16.20 | 68.38 | 1.46 | 13.96 |
| **428** | 0.361 | 0.639 | | 0.011 | 0.623 | | | 0.366 | -16.61 | 68.64 | 1.45 | 10.09 |
| **429** | 0.470 | 0.530 | 0.002 | 0.010 | 0.988 | | | | -21.22 | 67.62 | 1.47 | 0.24 |
| **430** | 0.050 | 0.950 | | | 0.479 | 0.200 | 0.029 | 0.291 | -11.68 | 68.03 | 1.46 | 535.75 |
| **431** | 0.006 | 0.994 | | 0.001 | 0.603 | 0.285 | 0.111 | | -12.72 | 67.34 | 1.48 | 232.33 |
| **432** | 0.008 | 0.992 | | | 0.505 | 0.417 | 0.078 | | -11.09 | 66.97 | 1.49 | 867.58 |
| **433** | 0.026 | 0.974 | | | 0.487 | 0.233 | | 0.280 | -11.27 | 67.87 | 1.47 | 749.16 |
| **434** | 0.168 | 0.832 | | 0.008 | 0.590 | 0.152 | | 0.251 | -14.02 | 68.08 | 1.46 | 81.32 |
| **435** | 0.056 | 0.944 | | 0.004 | 0.807 | 0.189 | | | -15.00 | 67.30 | 1.48 | 36.78 |
| **436** | 0.029 | 0.971 | | 0.003 | 0.597 | | 0.059 | 0.342 | -13.62 | 68.70 | 1.45 | 112.62 |
| **437** | 0.060 | 0.940 | | 0.001 | 0.471 | | 0.056 | 0.471 | -12.56 | 68.98 | 1.44 | 264.43 |
| **438** | 0.009 | 0.991 | | 0.009 | 0.931 | | 0.060 | | -16.97 | 67.97 | 1.46 | 7.52 |
| **439** | 0.306 | 0.694 | | 0.017 | 0.668 | | | 0.314 | -16.79 | 68.71 | 1.45 | 8.72 |
| **440** | 0.006 | 0.994 | | | | 0.465 | 0.045 | 0.489 | -5.69 | 68.11 | 1.46 | 67763.10 |

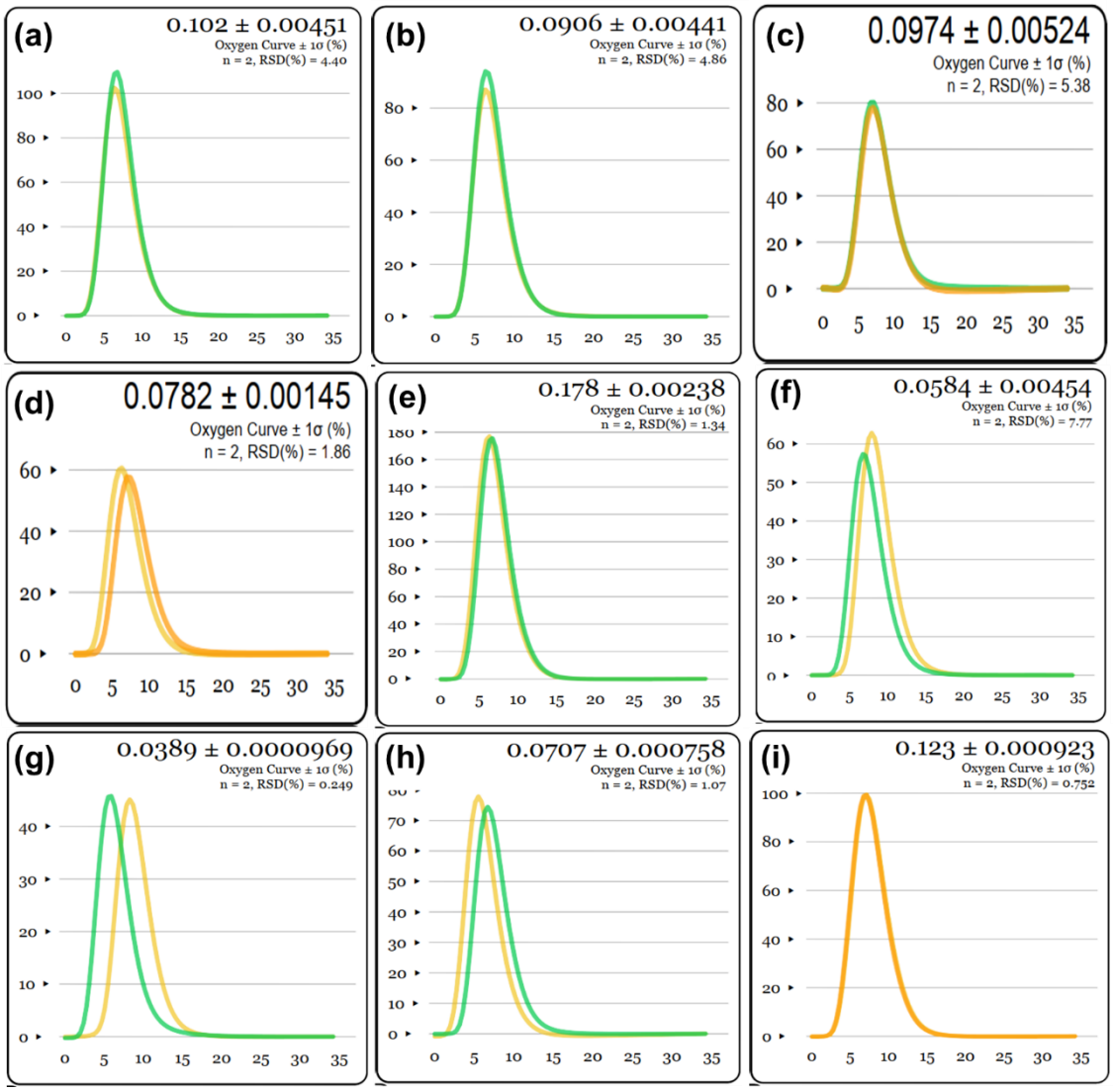


Figure A1 – Oxygen curve and standard deviation for the (a) $(Ti_{0.5}Zr_{0.5})_1Mn_2$, (b) $(Ti_{0.5}Zr_{0.5})_1(Mn_{0.5}Cr_{0.5})_2$, (c) $(Ti_{0.5}Zr_{0.5})_1(Fe_{0.5}Mn_{0.5})_2$, (d) $(Ti_{0.5}Zr_{0.5})_1(Fe_{0.33}Mn_{0.33}Cr_{0.33})_2$, (e) $(Ti_{0.33}Zr_{0.33}Nb_{0.33})_1(Mn_{0.5}Cr_{0.5})_2$, (f) $(Ti_{0.33}Zr_{0.33}Nb_{0.33})_1(Fe_{0.5}Mn_{0.5})_2$, (g) $(Ti_{0.5}Nb_{0.5})_1(Fe_{0.5}Mn_{0.5})_2$, (h) $(Ti_{0.5}Zr_{0.5})_1(Fe_{0.25}Mn_{0.25}Cr_{0.25}Ni_{0.25})_2$, and (i) $(Ti_{0.5}Zr_{0.5})_1(Fe_{0.5}Mn_{0.5})_2$+Ce.